NON-SLAGGING ENTRAINED FLOW GASIFICATION OF PYROLYSIS OIL FROM RADIATA PINE WOODY BIOMASS

by

Muhamad Fazly Abdul Patah

(fazly.abdulpatah@pg.canterbury.ac.nz)

A THESIS SUBMITTED IN PARTIAL FULFILLMENT OF THE REQUIREMENTS FOR THE DEGREE OF

DOCTOR OF PHILOSOPHY

CHEMICAL AND PROCESS ENGINEERING DEPARTMENT

UNIVERSITY OF CANTERBURY

NEW ZEALAND

November 2016

ABSTRACT

A pilot scale non-slagging entrained flow (EF) gasification system was developed to gasify biomass pyrolysis oil using oxygen as the gasification agent. The pyrolysis oil was derived from New Zealand radiata pine wood chips through a fast pyrolysis process. The oil was fed into the system through an external mix twin-fluid atomizer which is capable of generating fine oil droplets after impact with the oxygen gas. Gasification was conducted at atmospheric pressure while the operation temperatures were dependent on the heat generated from partial combustion of pyrolysis oil with oxygen upon leaving the atomizer.

Cold model experiments were first performed to investigate the effect of pyrolysis oil and gas flow rates on atomization performance. The use of external mix atomizer in this work is advantageous as it allows superior control of atomization performance by independent adjustments of pyrolysis oil and oxygen flow rates. Results from this cold model experiments show both flow rates of pyrolysis oil and oxygen gas have distinct influence on the resulted spray characteristics and consequently gasification performance. Increase in pyrolysis oil flow rate has negative influence on spray characteristics as larger droplet size and less uniform spray are generated. On the other hand, atomization at high gas flow rate substantially improves spray characteristics by production of more uniform spray and smaller droplets. The combined effect of pyrolysis oil and gas flow rates is reflected by the gas-to-fuel ratio (GFR) where higher GFR values indicate higher atomization performance and therefore better spray characteristics.

After the cold model experiments, entrained flow gasification of pyrolysis oil were conducted to investigate effects of different gasification conditions on producer gas composition, gas yield, tar species distributions and total tar content in the producer gas. When equivalence ratio (ER) was increased during gasification at constant oxygen flow rate, concentrations of H_2, CO and CO_2 in the producer gas changed in parabolic trends, which is unique compared to linear relationships usually reported in the literature. Below the critical ER value, the H_2 and CO concentrations increase while the CO_2 concentration decreases with increasing equivalence ratio. However when the equivalence ratio exceeds the critical value, the opposite trends are observed. The critical ER during gasification at oxygen feeding rate of 900 L/h occurred at equivalence ratio of 0.3. At this condition, the maximum concentrations of H_2 and CO were at 22 vol% and 36 vol% respectively while the minimum concentration of CO_2 was measured at 33 vol%.

The changes in producer gas trends with equivalence ratio relates to the continuous improvements in the spray characteristics and increase in the process residence time as the equivalence ratio increases. At

constant oxygen flow rate, higher ER value is obtained by decreasing pyrolysis oil feeding into the system, which corresponds to higher GFR value thus better spray characteristics. The decline in pyrolysis oil feeding also results production of less producer gas which reduces its velocity and consequently increases the process residence time.

Investigation on influence of increasing oxygen flow rate during gasification at constant ER was also performed in which the oxygen flow rate was varied between 600 L/h, 900 L/h, 1500 L/h and 3000 L/h in separate sets of experiments. Results from these experiments proved that at a given ER, gasification with high oxygen flow rate is highly desirable due to the substantial improvements in the oil spray characteristics and mixing behaviour that consequently leads to better overall reaction kinetics in the system. In addition to that, increase in the gasification temperature during gasification at high oxygen flow rates also help drive the system closer to equilibrium state which favours H_2 and CO concentrations in the product.

Increase of oxygen flow rate from 900 L/h to 1500L/h during gasification was observed to shift the critical ER value from 0.3 to 0.5 at which the maximum H_2 and CO concentrations were also increased from 22 vol% to 28 vol% and from 36 vol% to 41 vol% respectively. On the other hand CO_2 concentration declined from 33 vol% to 27 vol% when the oxygen flow rate was increased. In general, at high ER values, higher oxygen and pyrolysis oil flow rates favour producer gas quality with higher concentrations of H_2 and CO but lower concentrations of CO_2. However, at low ER values, the producer gas from gasification at higher oxygen and pyrolysis oil flow rates consists of lower concentrations of H_2 and CO but higher concentration of CO_2. As the residence time increases at increasing equivalence ratio, pyrolysis oil conversion improves more rapidly during gasification at 1500 L/h than that at 900 L/h thus giving more rapid growth in H_2 and CO concentrations in the producer gas. These results are related to the effects of varying oxygen and pyrolysis oil flow rates on both spay characteristics and residence time.

From analysis of tar in the producer gas, it was found that the total tar content in the producer gas decreased as the equivalence ratio was increased. In all cases investigated in this work, light polyaromatic hydrocarbon (PAH) compounds form the largest fractions of the tar components which accounts up to 78 wt% of the total tar in the producer gas. Detailed investigation into the tar individual species revealed naphthalene as the single most abundant tar species in the system which contributed as much as 36 wt% of the total tar in the producer gas. Results from this analysis also confirm that the methods used for tar sampling and analyses adopted in this work are capable of capturing and analysing tar compounds in the producer gas.

ACKNOWLEDGMENTS

First and foremost I would like to thank God for His blessing of good health and for giving me the strength and perseverance to reach this stage of my PhD journey.

The completion of this thesis is a shared accomplishment for everyone that has been working hard and contributing in this project. Above all, I would like to express my sincere appreciations to my senior supervisor, Professor Shusheng Pang for his patience, guidance and valuable time assisting me from the very beginning of my studies. This journey would have been extremely difficult without his assistance and support. Special thanks to my co-supervisor, Dr. Aaron Marshall for his interest, insightful advices, critical comments and feedbacks at various stages of my studies.

Not to forget all technical staffs in the Chemical and Process Engineering Department at the University of Canterbury, most importantly Leigh Richardson, Stephen Beuzenberg and Michael Sandridge for sharing their knowledge and experience as well as for continuously providing technical supports in making this project a success. Their willingness to take part and help in this challenging journey is highly appreciated. I am also thankful to Dr. Woei Lean Saw and Dr. Lim Mook Tzeng for their contributions at the early stages of this project.

I also wish to thank Ministry of Higher Education Malaysia for the scholarship and various financial supports throughout my study period. Similar goes to Ministry of Business, Innovation and Employment New Zealand and the University of Canterbury for every form of financial support given in this project particularly for that spent on the development of the Entrained Flow Gasification system. Furthermore, I am thankful to the University of Malaya for supporting my family financially throughout their stay in New Zealand.

I would like to take this opportunity to express my deepest gratitude and appreciation to my parents, Abdul Patah Abdul Rahman and Rabiah Awang, who continuously praying for my success and tirelessly encouraging me to do my very best in life. Their endless words of comfort and wisdom have been very inspiring. Thank you to my lovely wife, Nornazahie Zulkifli for all the sacrifices that she has made, from accompanying me living in New Zealand, giving birth to our first child and now being separated; only so I could complete my PhD journey successfully. Her sacrifices have been very great that I will never able to be thankful enough for.

Last but not least, thank you to all my siblings, colleagues and friends for their encouragements and supports towards the completion of my studies.

TABLE OF CONTENTS

1 INTRODUCTION

1.1 Global Energy and Renewable Energy Alternative

The world's dependence on fossil fuel as a major source of transportation fuel has created various concerns around the world mainly due to negative impacts it has caused on the environment. Combustion of fossil fuels has been proven as one of the major contributors to emissions of greenhouse gas (GHG) and other pollutants such as sulphur oxides, nitrogen oxides and carbon oxides to the atmosphere. In fact increase in fossil fuel consumption has been reported as the main reason for drastic rise of carbon dioxide content in the atmosphere, which has led to serious environmental issues like global warming, rise of sea level and extreme weather changes around the world [1]. Sulphur oxides and nitrogen oxides on the other hand lead to acid rain that could harm aquatic animals and plants, damages building surfaces, monuments and statues, as well as cause negative impacts on human health.

From economical point of view, fossil fuels are depleting due to limited fossil resources available to be utilized. It is believed that the world supply of fossil fuel has reached its peak and soon will be unable to meet the requirement [2] as a result of drastic increase in the world human population and energy demand. Based on the current energy trend, the world primary energy consumption is expected to double from that recorded in 2011 when the human population grows from 7 billion to 10 billion by the end of this century [1]. If the current dependency on fossil fuel derived energy remain unchanged, its demand is predicted to escalate dramatically; which as the consequence would shrink the reserve lifetimes of oil, gas and coal, respectively, to just another 43 years, 62 years and slightly above 100 years [1].

Fossil fuel also does not guarantee the best energy security solution in most countries around the world. This is because many countries unwillingly depend on fossil fuel imports due to absence of their own resources. Taking petroleum as an example, there are currently only a limited number of countries around the world that have self-sufficient oil reserves, either in the sea or on land to sustain their domestic energy demand. From political point of views, such strong dependence is undesirable since any unexpected world crisis in the future will directly distress supplies of these resources, hence will lead to much greater problems for the affected nations.

In response to these perturbing issues and trends, many studies have been conducted to find possible energy alternatives that could ease our current dependence on fossil fuel derived energy [3]. This effort includes progressive shifts towards energy production from renewable resources such as hydro-power, biomass, solar, ocean tides, geothermal and wind. Unlike fossil fuels, the apparent advantage of using

renewable resources is that they are naturally regenerative and therefore theoretically unlimited. Development of renewable energy options around the world has been encouraging and the trend was reported to have become more significant in recent years. In 2014, renewable energy contributed as much as 19.2% [4] of the total 13800 million tonnes of oil equivalent (Mtoe) of global energy consumption [5]. Between 2014 and 2015 alone, global renewable energy generation has increased by around 150GW from 1700GW, hence is the largest annual growth of renewable energy ever recorded in history. The increase was mainly contributed by significant addition in wind and solar power generation during this period, which account for around 77% of the total increase. Hydropower, on the other hand continued to be the largest renewable energy sector in 2015 with energy production of 1064GW globally (58%), followed by wind (23%), solar (12%) and bio-power (6%) [4].

Besides power generation, renewable resources are also used as alternative fuels in transportation sector as well as for heating and cooling services (heating sector). In heating sector as an example, renewable energy contributed to 25% of the total thermal energy used in 2015, where the vast majority of the energy produced was derived from biomass, followed by small fractions from solar thermal and geothermal energy. The contribution of renewable energy as transportation fuel is relatively less compared to power and heating sectors due to competition with low fossil fuel prices. In 2015, 128 billion litres of liquid biofuels (bio-ethanol and bio-diesel) were consumed globally, which accounts for around 4% of the total transportation fuel used during this period [4].

The positive shift towards renewable energy alternative has driven rapid development of relevant conversion technologies such as hydropower, wind turbines, solar photovoltaic panels, biomass gasification systems and photo-bioreactors to fulfil the increasing energy demand. Such progression has consequently improved renewable resources conversions into higher energy yield and catalyses on-going advancement of the process efficiencies; thus help resolve major challenges associated with renewable energy production and commercialization at present.

1.2 Biomass Gasification and Its Challenges

Biomass is abundant on earth and thus has a promising potential to be a reliable source of renewable energy in the future. Biomass is a general term used for carbonaceous matters and commonly refers to lignocellulosic plant, which is the most abundant and renewable biomass material on earth [6, 7]. Lignocellulosic biomass is built of three main components, which are cellulose, hemicellulose and lignin. Compositions of each component of the biomass may vary significantly from one biomass species to

another as well as when different parts of the biomass are considered, for example between hardwoods, softwoods and leaves [7].

In countries where forest and agriculture activities are major industries, utilization of biomass as an alternative source of energy holds a bright potential considering large biomass harvesting residues and processing wastes available to be utilized; such as sawdust, off-cuts, branches, leaves, barks, roots, stoves, husks and straws. Besides lignocellulosic biomass, municipal solid wastes are also considered as a potential biomass resources for energy generation due to its abundance and continuous supply. Presently biomass resources has already been contributing to approximately 14% of the total energy consumption in the world [8] and is expected to account for 20% of the total energy by the end of this century [9]. The biomass-derived energy is considered as carbon neutral where with strategic re-plantation of forest and harvested trees, there will be no net addition of carbon in the atmosphere, since CO_2 released during energy production or consumption is recycled during plant growth via photosynthesis [3, 9-12].

There are two major approaches for turning biomass into useful energy output, which are through thermal or biological process. Combustion, co-firing, pyrolysis and gasification are examples of thermochemical processes that convert biomass into energy products. Aerobic and anaerobic digestions, on the other hands, are examples of biological approach for converting biomass into energy products. Biological conversion of biomass is generally a slow process where it utilizes microorganisms to break down biomass complex structure into simpler molecules such as alcohol, methane, carbon monoxide, carbon dioxide and organic acids. In contrast, thermochemical conversion utilizes heat to break down chemical bonds in the biomass following complex reaction mechanisms within short residence times. The rapid conversion of biomass during thermochemical conversion process makes this approach often more favourable in the industries, particularly at large operation scales [13].

Gasification is a process that decomposes carbonaceous materials into useful gas products at high temperatures (600-1200°C) through a series of chemical reactions with different gasification agents. The gas products are generally referred to as ‘producer gas’ and contain combustible gas species such as H_2, CO, CH_4, C_2H_4 and C_2H_6. Producer gas is generally a preferred form of product as its applications are flexible in comparison to the products from other biomass-to-energy conversion approaches. The producer gas from biomass gasification can be compressed, stored or transported when required, and may be used as the primary feedstock in production of liquid fuel, synthetic natural gas (SNG) or other chemicals. Producer gas may also be combusted directly to generate heat and for power generations.

Besides the flexible product utilization, gasification is a mature technology as it has been widely used in coal processing industry to generate heat and gas lights for over hundred years [8].

However, gasification of biomass is relatively new. The biggest challenges when using biomass for energy production through gasification are associated with biomass properties, particularly, its high moisture content and low density, which lead to undesirable high costs for handling, transportation and storage [8, 12, 14-16]. In addition, biomass properties are generally not uniform and could vary largely even within a same species and supply. Certain types of biomass could also have high ash content and other undesirable contaminants that may be harmful to downstream equipment and processes.

Another hurdle to biomass gasification is related to fibrous nature of woody biomass species, which makes biomass grinding into small particle size difficult to be achieved and energy extensive [14]. While this may not be a concern to most gasification operations, there are selected gasification technologies such as entrained flow gasification that require the feedstock size to be below 0.1 mm [17], in order to achieve the required conversion performance.

1.3 Biomass Densification through Fast Pyrolysis

In order to increase the density of biomass and thus to reduce the costs, the biomass can be densified into liquid form through a thermal pre-treatment process called pyrolysis [8, 12, 15, 18], in an environment with absence of oxygen [19]. Pyrolysis process can takes place in several different modes depending on the operation temperature, heating rate and residence time. 'Fast pyrolysis' at high temperature and fast heating rate generates higher fraction of liquid product than other modes of pyrolysis [9] hence is more relevant for biomass densification purpose. During fast pyrolysis, biomass is rapidly heated at 500^{o}C with fast quenching of product vapour thus achieve high liquid yield of up to 75 wt% [7, 20, 21]. The liquid product from biomass pyrolysis is commonly referred to as 'pyrolysis oil' or 'bio-oil'. In addition to liquid, the fast pyrolysis also produces small fraction of char (largely carbon) and non-condensable gas. In terms of energy content, pyrolysis oil stores up to 2/3 of the initial energy stored in the solid biomass input [1]. Most importantly, pyrolysis oil has density of 4 to 5 times that of the original solid biomass feedstock, thus help reduces high costs associated with solid biomass transportation, handling and storage [1, 7, 12, 22, 23].

In some cases, pyrolysis oil is mixed with char by-products from the pyrolysis process to produce pyrolysis slurry. The main advantage of this approach is that it significantly increases the product's total

energy content to as high as 90% of the original solid feedstock. Besides that, addition of char to pyrolysis oil is also claimed to improve the oil stability [1, 9, 24]. Nevertheless, major drawbacks of using pyrolysis slurry are the significant increase in its viscosity that restricts flow-ability and limitation on the choice of atomizer that can be used since the atomizer should be able to tolerate char particles. In addition, a colloidal mixer is needed to keep the char and oil suspension uniform before feeding to the downstream operation.

Biomass pyrolysis oil or slurry of biomass pyrolysis oil and char also has an advantage in integration with high pressure downstream operations [23]. This is because feeding liquid/slurry into a pressurized system is much simpler and less problematic compared to feeding solid, since it could be done conveniently using a pump. Moreover, liquid feedstock can be atomized into fine oil droplets, as small as 10μm, thus the fine droplets significantly enhance reaction kinetics, feed conversions and the overall efficiency of the gasification system.

1.4 Biomass Fast Pyrolysis Followed by Central Gasification

The idea of biomass densification prior to gasification is also regarded as a two stages biomass-to-energy process. This approach has been studied and reported in literature, and it allows more economical management of biomass material from harvesting ground to the gasification plant; by making sure the density of material transported in every trip is maximized. In practice, this approach can be implemented by pre-treating raw biomass materials in many mobile fast pyrolysis units in the forests or farm lands and then the pyrolysis oil or slurry of pyrolysis oil and char is transported to a central gasification unit to be gasified into producer gas. Figure 1–1 represents the concept of two stages biomass-to-energy process to illustrate the magnitude of operational scale relevant to this approach.

The benefits of transporting high density liquid pyrolysis oil or slurry become most apparent at large scale plants and when the biomass resources are widely distributed in a large area. In these cases, intensive transportation from harvesting grounds to the central gasification plant is required hence creates a huge difference in terms of the capital and operational costs if the biomass density is first maximized prior to being transported.

In addition to saving the biomass transportation-related cost, the proposed use of mobile fast pyrolysis units is also more economical since the units can be shifted and shared between different harvesting grounds across a large plantation or forest areas. This is important because installation of fix biomass pre-

treatment plants is less practical due to a need to frequently shift to a new harvesting ground once the biomass resources being collected in an area has depleted.

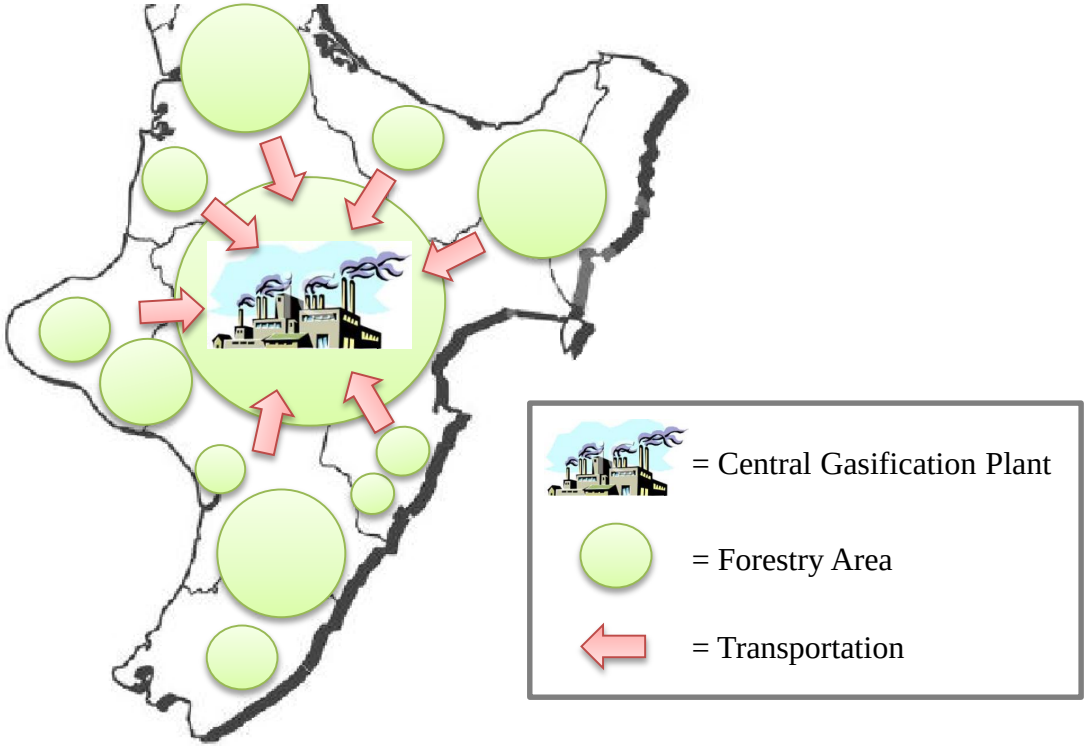

Figure 1–1**:** Illustrations of two stages biomass-to-energy process.

1.5 Research Motivation and Objectives

As discussed in the previous section, gasification of biomass pyrolysis oil has a great potential as an economical route to convert biomass into energy in the future. However, this approach is relatively new and due to the lack of information on this approach, many key aspects of its operations remain unexplored. Following this situation, important questions have been raised on whether or not it is feasible and practical to be implemented. Therefore, the objectives of this study were to develop a new entrained flow gasification system at pilot scale for gasifying biomass pyrolysis oil; and to investigate effects of different operation conditions on producer gas composition and gasification performance.

Different aspects of the entrained flow gasification operation were investigated in this work, with the main research goals being subdivided and summarized as follows:

i. To modify and test the operability of the gasification system developed in this work.

ii. To investigate influences of pyrolysis oil and oxygen gas flow rates on gasification temperature and producer gas yield.
iii. To investigate influences of equivalence ratio and oxygen flow rate on producer gas composition, tar species distribution and concentrations.
iv. To determine the optimum operating condition for the entrained flow gasification system.

Each of these goals was explored experimentally while the findings are discussed in more details in the subsequent chapters. This research will contribute to fundamental understanding of entrained flow gasification process for biomass pyrolysis oil and identify technical challenges that should be resolved for improved gasification operations in the future.

1.6 Thesis Scope and Overview

The introduction, background information and motivation of this work, as given in this section, are considered as **Chapter 1** of the thesis.

Chapter 2 provides a literature review of important topics related to entrained flow gasification of biomass pyrolysis oil to be investigated in this work. This chapter is structured in a way that it provides comprehensive information on fundamental aspects of entrained flow gasification operation such as pyrolysis oil properties, types of reactions involved during gasification and relationship between pyrolysis oil atomization and gasification performance (producer gas yield and composition). Recent research and development of entrained flow gasification system for biomass pyrolysis oil will also be reviewed in this chapter.

Chapter 3 presents detailed descriptions of the entrained flow gasification system developed in this work. This chapter highlights the system's major design characteristics that make it different from entrained flow gasification systems reported in literature. Other aspects of the system's operation such as the operation procedures, safety consideration and controls, lists of challenges encountered and modifications performed on the system during commissioning stage are also included in this chapter.

Chapter 4 describes various calculation methods used for data analysis. It provides relevant formula and step-by-step calculations on how data were collected during experiments, analysed and interpreted to provide more useful information about the system's behaviour, producer gas yield and composition.

Chapter 5 discusses pyrolysis oil atomization at room temperature at different flow rates of gas and pyrolysis oil. The chapter starts by describing the cold model atomization experimental setup and methodology, followed by analysis and discussion on the experimental results. Findings from this section are vital to help explain effects of pyrolysis oil and oxygen gas feeding rates on the entrained flow gasification performance.

In **Chapter 6**, a mathematical model for entrained flow gasification is developed based on thermodynamically equilibrium reactions. This chapter provides an introduction to the equilibrium model and presents derivations of all the equations used for the model development. Validation of the model is also discussed in this chapter. This model will be used extensively in predicting equilibrium products for entrained flow gasification experiments in Chapter 7.

Chapter 7 presents detailed plan and results for entrained flow gasification experiments from which the effects of various gasification parameters on the producer gas yield and gas composition are analysed. The operating conditions, test materials and experimental methods are described in details. Results from the gasification experiments are compared with those predicted by the equilibrium model, and deviation from the theoretical results are also analysed. Based on the results and achievements presented in this chapter, four journal articles have been prepared and will be submitted to selected journal publishers for publication.

Chapter 8 gives conclusion to highlight the major findings and contributions of this research towards optimization of entrained flow gasification operations. Recommendations are also presented in **Chapter 9** to further explore potentials of the entrained flow gasification of biomass pyrolysis oil and possible improvements in the future. **Chapter 10** of this thesis contains compilation of various documents related to the entrained flow gasification development and operations as well as other additional information relevant to this work.

1.7 References

1. Dahmen, N., et al., *The bioliq® bioslurry gasification process for the production of biosynfuels, organic chemicals, and energy*. Energy, Sustainability and Society, 2012. **2**(1): p. 1-44.
2. McKinnon, H., *Improved Hydrogen Production from Biomass Gasification in a Dual Fluidized Bed Reactor*, in *Department of Chemical and Process Engineering*. 2009, University of Canterbury: Christchurch.

3. Qin, K., et al., *High-temperature entrained flow gasification of biomass.* Fuel, 2012. **93**(0): p. 589-600.
4. REN21, *Renewables 2016 Global Status Report*. 2016, REN21 Secretariat: Paris.
5. International Energy Agency, I., *Key World Energy Trends - Statistics*. 2016, International Energy Agency (IEA).
6. Isikgor, F.H. and C.R. Becer, *Lignocellulosic biomass: a sustainable platform for the production of bio-based chemicals and polymers.* Polymer Chemistry, 2015. **6**(25): p. 4497-4559.
7. Chhiti, Y., *Non catalytic steam gasification of wood bio-oil*. 2011.
8. Xiao, R., et al., *Pyrolysis pretreatment of biomass for entrained-flow gasification.* Applied Energy, 2010. **87**(1): p. 149-155.
9. Raffelt, K., et al., *The BTL2 process of biomass utilization entrained-flow gasification of pyrolyzed biomass slurries.* Applied Biochemistry and Biotechnology, 2006. **129**(1-3): p. 153-64.
10. Carlsson, P., et al., *Experimental investigation of an industrial scale black liquor gasifier. 1. The effect of reactor operation parameters on product gas composition.* Fuel, 2010. **89**(12): p. 4025-4034.
11. Zhou, J., et al., *Biomass–oxygen gasification in a high-temperature entrained-flow gasifier*. Biotechnology Advances, 2009. **27**(5): p. 606-611.
12. Henrich, E., N. Dahmen, and E. Dinjus, *Cost estimate for biosynfuel production via biosyncrude gasification.* Biofuels, Bioproducts and Biorefining, 2009. **3**(1): p. 28-41.
13. Bridgwater, T., *Biomass for energy.* Journal of the Science of Food and Agriculture, 2006. **86**(12): p. 1755-1768.
14. Abdullah, H., et al., *Bioslurry as a Fuel. 3. Fuel and Rheological Properties of Bioslurry Prepared from the Bio-oil and Biochar of Mallee Biomass Fast Pyrolysis.* Energy & Fuels, 2010. **24**(10): p. 5669-5676.
15. Abdullah, H. and H. Wu, *Bioslurry as a Fuel. 4. Preparation of Bioslurry Fuels from Biochar and the Bio-oil-Rich Fractions after Bio-oil/Biodiesel Extraction.* Energy & Fuels, 2011. **25**(4): p. 1759-1771.
16. Manzer, L. *Recent developments in the conversion of biomass to renewable fuels and chemicals*. 2009.
17. Samiran, N.A., et al., *Progress in biomass gasification technique – With focus on Malaysian palm biomass for syngas production.* Renewable and Sustainable Energy Reviews, 2016. **62**: p. 1047-1062.

18. Sarkar, S. and A. Kumar, *Large-scale biohydrogen production from bio-oil.* Bioresource Technology, 2010. **101**(19): p. 7350-7361.
19. Ricketts, B., et al. *Technology status review of waste/biomass co-gasification with coal*. in *IChemE Fifth European Gasification Conference*. 2002.
20. Johansson, D., P.T. Franck, and T. Berntsson, *Hydrogen production from biomass gasification in the oil refining industry - A system analysis.* Energy, 2012. **38**(1): p. 212-227.
21. Bridgwater, A.V., *Review of fast pyrolysis of biomass and product upgrading.* Biomass and Bioenergy, 2012. **38**(0): p. 68-94.
22. Sakaguchi, M., *Gasification of bio-oil and bio-oil/char slurry*, in *Chemical and Biological Engineering*. 2010, The University of British Columbia: Vancouver.
23. Van der Drift, A., et al. (2004) *Entrained flow gasification of biomass*.
24. Dahmen, N., et al., *State of the art of the bioliq® process for synthetic biofuels production.* Environmental Progress & Sustainable Energy, 2012. **31**(2): p. 176-181.

2 LITERATURE REVIEW ON ENTRAINED FLOW GASIFICATION OF BIOMASS PYROLYSIS OIL

2.1 Biomass Pyrolysis Oil and Its Properties

Pyrolysis oil is a viscous, dark coloured liquid with a distinctive smoky odour [1]. Pyrolysis oil is produced when major components of the original biomass structure are de-polymerized into smaller molecules when subjected to high temperatures. Biomass in general consists of cellulose, hemicelluloses and lignin which, exposed to high temperatures, are broken down into complex mixtures of chemical compounds including acids, esters, alcohols, ketones, aldehydes, phenols, alkenes, furans, sugars and various oxygenates [2, 3]. Once cooled down, these vapours condense to form pyrolysis oil which has much higher mass and energy densities than the original biomass. Pyrolysis oil density is reported to be 1000 to 1200kg/m^3 [4, 5], which is up to 4-6 times higher than the original biomass density in solid form.

Pyrolysis oil could contain more than 300 organic compounds in a single sample [6, 7], thus characterization of every individual components of the oil is very challenging. In fact, pyrolytic lignins existing in the pyrolysis oil cannot be determined by gas chromatography or high performance liquid chromatography (HPLC) [2]. In addition, the species and compositions of the pyrolysis oil may also vary largely from one processing plant to another since these are affected by many factors including feedstock species, properties (such as moisture content, ash contents and particle size), pyrolysis process heating rate, temperature and total residence time [8].

Pyrolysis oil also contains significant water and carboxylic acid molecules, hence is highly acidic. Water in pyrolysis oil is not readily separable as it mixes well with polar components of the oil [8]. Too much water in pyrolysis oil is not desirable since it dilutes the pyrolysis oil and consumes substantial amount of heat for water evaporation during gasification, therefore, responsible for significant reduction of pyrolysis oil's heating value. However, moderate amount of water in pyrolysis oil (5-10 wt%) helps lower the oil viscosity thus improves pyrolysis oil atomization and pumping during gasification. Water content of pyrolysis oil depends strongly on the original moisture of the biomass feedstock used and the operation conditions of the pyrolysis process.

Solid and ash particles in pyrolysis oil are undesirable although their contents are usually low when woody biomass is used as feedstock. In many fast pyrolysis processes, particulates are removed from

pyrolysis vapour using high temperature filters so solid content in the pyrolysis oil is minimized. The removal of solids from pyrolysis oil is an important step in pyrolysis oil production because solid particles, particularly char, has been proven to catalyse undesirable secondary reactions between molecules in the oil during storage [8].

Table 2-1 presents summary of typical properties of biomass pyrolysis oil derived from wood, forest residues and straw, as reported in the literature.

Table 2-1: Key properties of pyrolysis oil derived from various biomass species

Physical Properties	Wood [1, 5, 6, 9-12]	Forest Residues [10]	Straw [10, 13]
Moisture content (wt %)	15 – 44	26 – 27	51
pH	2.0 – 3.1	3.2	3.7
Ash content (wt %)	0 – 0.2	0.1 – 0.3	0.07
Viscosity at 40-50^{o}C (cSt or mm^{2}/s)	14 – 100	17 – 24	17.6
Solid Content (wt %)	0.01 – 1	0.09 – 0.17	0.43
LHV (MJ/kg)	15.3 – 17.3	15.2 – 15.3	9.1 – 11.5
HHV (MJ/kg)	16.9 – 17.0	16.7 – 16.9	11.1 – 13.3
Elemental Composition			
C (wt %)	30 – 58	41	27
H (wt %)	5.5 – 8.3	7.4 – 8.0	9.0
O (wt %)	35 – 62	50 – 51	63
N (wt %)	0 – 0.3	0.3	0.9

It is important to emphasize that pyrolysis oil is a product of non-equilibrium process thus is chemically unstable. During thermal treatment of biomass feedstock in fast pyrolysis, there are three types of products including vapour, non-condensable gas and solid char. Once being cooled down, the vapour condenses rapidly into liquid oil thus further reactions are forcefully stopped and consequently molecules in the pyrolysis oil are not at equilibrium [1]. Although the liquid compounds are not as reactive as when they were in the vapour form at high pyrolysis temperatures, secondary reactions are still expected to take place gradually to form compounds with better stability and the reactions eventually reach equilibrium.

Pyrolysis oil's instability could also be explained considering complex co-existence of hundreds of chemical compounds in the pyrolysis oil. Although pyrolysis oil is physically a single phase liquid mixture, it exhibits complex multi-phase structure characteristics as a result of the diverse building components. Pyrolysis oil microscopically contains multi-phase components such as waxy materials, heavy compound micelles, aqueous droplets and char particles; which co-exist as a form of micro-emulsion by hydrogen bonding and micelle formations [8]. Figure 2–1 shows drawings of different building components of pyrolysis oil that leads to its complex multiphase characteristics and ultimately contributes to the oil poor stability.

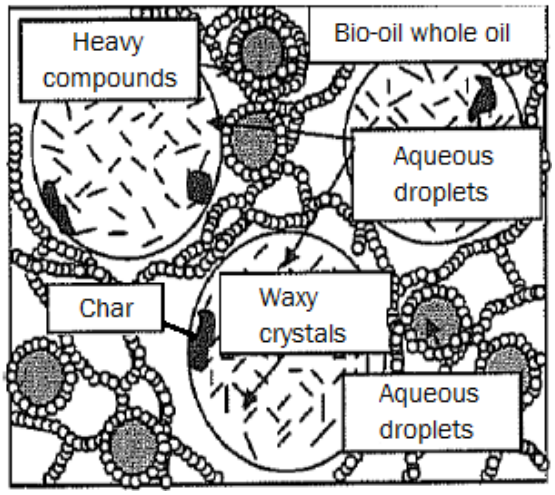

Figure 2–1: Illustration of building components of wood derived pyrolysis oil as [adapted from [14]]

The phenomenon of changes of pyrolysis oil composition and physicochemical properties with elapsed time is termed as 'ageing'. Pyrolysis oil ageing could occur following many reaction pathways which can be generalized into several main categories as follows [8, 15]:

i. Aldehydes reactions with alcohols, water, phenolics, proteins and other aldehydes. Products of these reactions are water, hydrates, hemiacetals, acetals, resin, dimmers and oligomers.
ii. Acids reactions with alcohols and olefins to form water and esters.
iii. Polymerization of olefins into polymers and oligomers.
iv. Pyrolysis oil oxidation into acidic compounds and peroxides, which in turn enhance polymerization of unsaturated compounds in the oil.

During the storage of pyrolysis oil, its water content and acidity usually increase due to the aging effect [8]. Pyrolysis oil viscosity, on the other hand, could either increase or decrease depending on whether water content increase or formation of compounds due to polymerization is more dominant. In the case where polymerization effects dominate, the oil viscosity is expected to increase correspondingly while the opposite is true for water content.

Phase separation is another challenge associated with pyrolysis oil, particularly after storage for an extended period of time. Phase separation occurs due to increase of large polymer molecules in the oil that poorly co-exists with other components of the oil. Similarly, increase of water content alters the overall polarity of the oil where the highly polar water molecules separate from other less polar components of the oil and appear as distinct layers [8]. The polarity differences between the two layers then promotes molecular segregation based on their polarity, forming more prominent separations between polar and non-polar components of the oil.

Pyrolysis oil is also thermally unstable; therefore, the oil properties also change when being exposed to varying temperatures. In this case the most obvious change in pyrolysis oil properties is its viscosity, where the oil viscosity is usually high at low temperature and decreases rapidly as the temperature increases. These changes were reported to have occurred due to the presence of waxy compounds in the oil (such as fatty acids, sterols, aliphatic hydrocarbons and fatty alcohols); as well as pyrolytic lignin and solids, which form viscous three-dimensional networks at low temperatures. At high temperatures, these networks disintegrate into individual compounds hence reducing the overall viscosity of the oil [16]. Besides affecting pyrolysis oil viscosity, the waxy compounds is also responsible for promoting crystallization of various compounds in the oil [14] thus contributing to changes of pyrolysis oil properties. Increase of oil temperature prevents crystallization of compounds in the oil thus help minimizes problems of pyrolysis oil filter blinding and liquid outlet blockage.

Pyrolysis oil could be stabilized with addition of methanol or ethanol in the oil. The rate of increase in pyrolysis oil viscosity has been reported to decline by a factor of 17 by addition of 10% of methanol into the oil. Besides that, the oil can be hydrogenated to remove oxygen, saturate olefins and convert aldehydes into alcohol; however this method consequently increases the oil viscosity. Addition of antioxidant helps reduce effects of ageing by minimizing absorption of oxygen into the oil thus prevents polymerization of compounds. Char, which contains various elements that are responsible for catalysing many ageing reactions, may also be removed from pyrolysis oil to improve its stability particularly upon storage for an extended period of time [15].

2.2 Pyrolysis Oil Conversion at High Temperatures

Conversion of pyrolysis oil at high temperature behaves differently from that of traditional liquid fuels such as gasoline and diesel. Instead of continuously releasing volatile compounds and burns quiescently throughout its lifetime, pyrolysis oil's transformation takes place in several distinct stages before eventually forms 'cenosphere', which is a term used to describe the residue of pyrolysis oil to gas conversion [17, 18]. The multi-stages conversion of pyrolysis oil upon exposure at high temperature was reported thoroughly by Wornat et al. [17] based on comparative studies between biomass pyrolysis oil and traditional fuel oil droplets in excess air environment (combustion).

To help highlight pyrolysis oil unique conversion behaviour, each transformation stage of the oil is elaborated separately as follows [17]:

i. Stage 1 – Evaporation of water and light hydrocarbons

Pyrolysis oil conversion starts with release of water and light hydrocarbon components of the oil. While water in the oil is expected to completely vaporize at around 100^{o}C, release of hydrocarbon from the oil is more gradual as a result of hydrocarbon's wide volatility range. Analysis on species of hydrocarbon released at this stage indicated high concentrations of oxygenated volatiles compounds, which with presence of oxygen, burn in quiescent blue flame enveloping the droplet.

ii. Stage 2 – Swelling and micro-explosion of pyrolysis oil

While pyrolysis oil droplet continues to burn on the outside from oxidation of volatile compounds, temperature of the oil continues to rise and consequently causes more volatiles to be released. Rapid release of volatile at high temperature has been reported to cause build-up of vapour pockets inside pyrolysis oil that distorts the original shape of the droplet and make it appears swelling. At the same time, heat from the flame surrounding the droplet also causes heavy components on the droplet's surface to polymerize into a shell-like layer, thus resisting further change of the droplet size.

As the oil internal vapour pressure continues to grow, there is a point where the pressure is sufficient to rupture the droplet's shell structure, bursting the vapours previously accumulated in the droplet and therefore appear as a micro-explosion. In many occasions, this phenomenon is also regarded as a secondary atomization where it further reduces pyrolysis oil droplet's size and improves the overall conversion for the system. Similar to the parent oil droplet, fragments resulted from the micro-explosion also continue to release volatiles but burn in faint blue flames with presence of oxygen. At this stage the

flame size was reported to shrink closer to the oil surface, indicating decline in the amount of combustible vapour released during this stage [18].

In events where pyrolysis oil conversion is limited by kinetics and residence time, the droplets may end its transformation course at this stage. This situation has been shown in experimental studies reported by Wornat et al. [17] where at short residence time and low oxygen atmosphere, pyrolysis oil droplets failed to vaporize completely while leaving solid residues after the experiments. The residues are characterized by dense and glassy sphere appearance with low carbon-oxygen mass ratio (4:1). Further analysis of the residues showed similarities in its properties with pyrolysis oil, hence proving its origin from incomplete conversion of pyrolysis oil droplets due to the process short residence time.

iii. Stage 3 – Cenospheres formation and combustion

The dense, glassy solid residues formed in Stage 2 could be regarded as a precursor to formation of cenospheres in this final stage. During the transition from solid residues to cenosphere, the solid residues continue to swell and occasionally burst due to sudden release of volatiles build-up; but in a less pronounce magnitude compared to before the main micro-explosion occurrence. Cenospheres could be characterized by its porous, fragile and oxygen deficient structure (carbon-mass ratio of 9:1) as opposed to the dense solid residue. Its high carbon content indicated effects of severe carbonization; and further investigations of its properties did not show any resemblance of this material to pyrolysis oil. The cenospheres mostly consist of non-evaporative components leftovers from the oil, and burns in a yellow flame indicating the presence of soot during the combustion.

Although the pyrolysis oil conversion information gathered here are based on combustion and not gasification environment, pyrolysis oil conversion behaviour is believed to still follow the same principle since in both conditions, the oil are subjected to high temperature environment. However, the types reactions involved during the conversion are expected to be different, due to absence or lack of oxygen gas in gasification environment. In this case instead of reaction with oxygen to produce flame, the volatile vapours, steam, solid residues and cenospheres are expected to react with each other to form more useful gasification products such as H_2, CO, CO_2 and CH_4 gases.

2.3 Gasification Technologies for Biomass Pyrolysis Oil

There is a wide range of gasification technologies available at present to be used for converting biomass and biomass pyrolysis oil into energy. These technologies are classified into three main categories which are fixed bed, fluidized bed and entrained flow gasification. Each of these technologies is different in many ways particularly in terms of its operation principles, gasification conditions, feedstock requirements, product distributions and performance. Due to these differences, some approaches are more appropriate than others for an application to a given feedstock, making selection of suitable gasification approach critical for successful operations.

Gasification requires addition of air, oxygen or steam as the gasification agent during conversion of feedstock into producer gas. Gasification with air is relatively simple and less expensive but results in excessive dilution of the gas product with nitrogen hence reducing its heating value. Gasification with oxygen gas solves the dilution problem as with air but oxygen is more costly due to the need of pure oxygen gas supply. Steam as a gasification agent attracts interests since it helps improve the quality of the gas product while costs less than oxygen. However, additional heat supply is required in the gasification as the steam gasification reactions are endothermal overall.

Description of different gasification technologies and how gasification agent is involved in the operations are summarized in the following subsections:

i. Fixed bed gasifier

This type of gasifier is characterized by a stationary grate inside the gasifier where the feedstock is fed from the top. During gasification, the bed slowly moves downwards as gasification takes place in the lower part of the bed where the feedstock is consumed. Fresh feedstock is added to maintain the depth of the bed during gasification [19, 20]. Fixed bed gasifier is also known as ‘moving bed’ gasifier since the bed is moving slowly during the operation [20]. There are four zones in fixed bed gasifiers including drying zone, pyrolysis zone, reduction zone and combustion zone, from the top to the bottom of the bed.

Fixed bed gasifier is available in two configurations, which are updraft and downdraft gasifiers. Updraft fixed bed gasification is the most basic approach to gasification process where biomass feedstock is introduced into the gasifier from the top while gasification agent flows upwards from the bottom through the bed material. With this configuration, producer gas exits the gasifier from the top. As the ash and char descend towards gasifier bottom section, they come into contact with gasification agent thus promoting

gasification reactions and more gas products [20]. Due to opposite flows between feedstock and gas product, updraft gasifier is also commonly known as counter-current gasifier [19].

Main advantages for using this type of gasifier are its simple operation and ability to gasify high moisture content feedstock. Moreover, updraft fixed bed gasifier is also popular for its high energy efficiently since most heat energy stored in the producer gas is used to dry the incoming feedstock on its way to the top of the gasifier [19, 20]. However, updraft fixed bed gasification system exhibits risk of explosion during its operation due to potential interactions between combustible producer gas and any unreacted gasification agent in the top section of the gasifier. Common problems with updraft gasification system associate with feedstock high residence time inside the reactor, which causes severe plugging of the bed material when operated for a long time [21]. The producer gas also requires extensive cleaning stage due to high concentrations of tars in the producer gas, between 10-20 wt% [19], which otherwise causes problems for downstream equipment and applications.

In the downdraft gasifier, gasification agent enters the gasifier from the middle while the producer gas leaves the system from the bottom section of the gasifier. Drying and pyrolysis take place as feedstock slowly move to the bottom before coming into contact with gasification agent at the 'throat' section, where gasification reactions begin to take place. In this section, unconverted char, tars and pyrolysis gas react to form higher concentrations of H_2 and CO in the product gas [22]. The producer gas generated from this type of gasifier contains little solid since it passes through the bed material during exiting the system, which helps filter solid contaminants from the products. In addition tar concentration in the producer gas is also significantly less than that in updraft gasifier as the producer gas flows through the high temperature oxidation zones, before exits, which cracks the tars into producer gas [19]. Figure 2–2 shows simple configurations of both updraft and downdraft gasification systems for comparison.

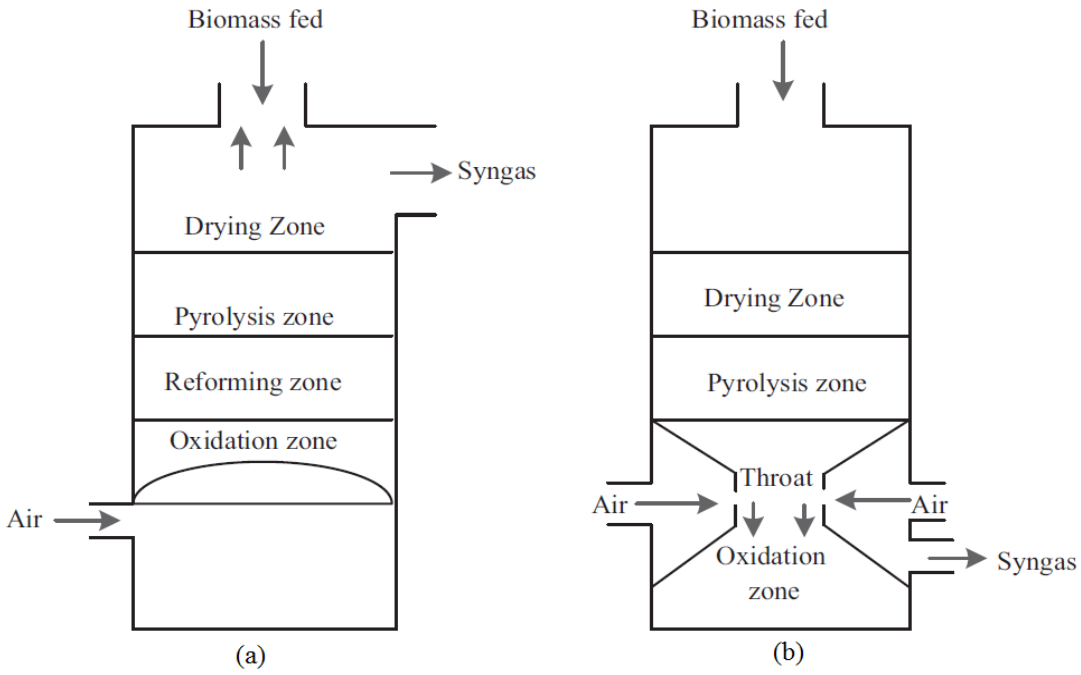

Figure 2–2: Configurations of fixed bed (a) updraft gasifier and (b) downdraft gasifier [adapted from [19]].

ii. Fluidized bed gasifier

Fluidized bed gasifier utilizes a bed of solid particles to improve heat transfer to feedstock. The bed material is fluidized with a gasification agent (air or steam) at sufficiently high velocities so it remains in a state of suspension. In this condition, uniform temperature distribution can be achieved within the bed. In general fluidized bed gasifiers are operated at temperature between 800-1200^{o}C [19, 22].

There are two types of fluidized bed which are bubbling and circulating fluidized bed gasifiers as shown in Figure 2–3. In both cases, feedstock is converted into gasification products through contact with the hot bed material. In bubbling fluidized bed, mixing between feedstock and bed material is obtained by bubbling the mixture at relatively low velocity. When feedstock is introduced into the system, it rapidly mixes with the bed material and pyrolyzes into vapours, gas and char. Subsequently reactions occur both among the gases (including gasification agent and producer gas) and between gases and solid char. Tar yield during the operation is low considering good heat transfer between materials in the system. Producer gas exits the system from the top of the system while the remaining unconverted char stays in the bed

material until near complete conversion. The conversion cycle is repeated by addition of fresh feedstock into the system [19, 20].

Similar principle applies to circulating fluidized bed gasifier except that in the circulating fluidized bed gasifier, the gas velocity is sufficiently high so that part or all of the solid materials are entrained in the gas leaving the system. Due to this reason, a cyclone is required to be installed at the exit of the gasifier to separate producer gas from the solids (bed material, char and ash). The solids are then returned to the reactor for the next conversion cycle [19].

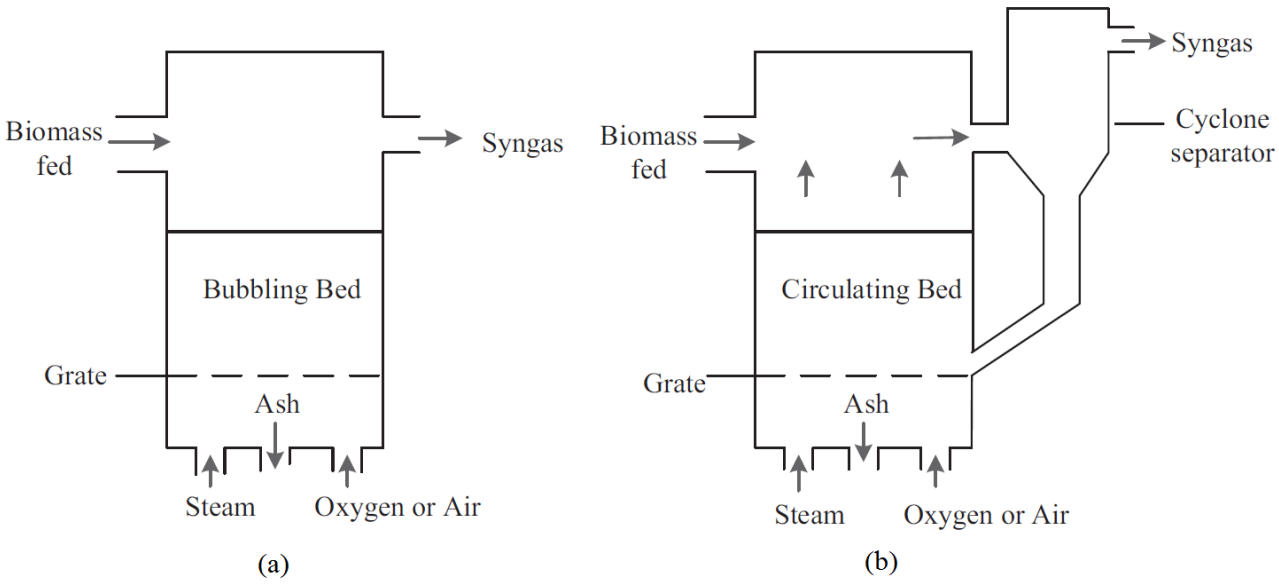

Figure 2–3: Illustration of (a) bubbling fluidized bed gasifier and (b) circulating fluidized bed gasifier [adapted from [19]].

iii. Entrained flow gasifier

Typical configuration of an entrained flow gasifier is shown in Figure 2–4. This technology is suitable for processing fine particles and liquid feedstocks. In the entrained flow gasifier, feedstock and gasification agent enter the gasifier from the top at high velocities, which are sufficiently high to create high turbulence thus uniform distribution of the feedstock in the upper part of the gasifier. Operational temperature for entrained flow gasification is high which could reach up to 1500^{o}C. Due to the gasifier high reaction temperature and fast reaction rates, reaction residence time in this type of gasifier is significantly short [23-25], between 1-5 seconds.

This type of gasifier is known for its ability to achieve near 100% carbon conversion mainly due to its high operation temperature [19, 23-25]. It is due to such high gasification temperature that tar, which has been a major issue in most gasification operations, is mostly cracked hence the producer gas is much cleaner than that in other types of gasifiers [19, 25].

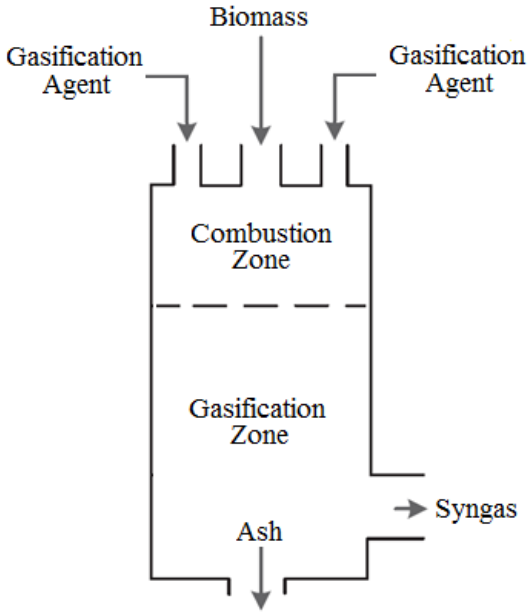

Figure 2–4: Schematic diagram of the entrained flow gasifier [adapted from [19]]

Entrained flow gasification has been widely used in coal gasification. It is also used in petrochemical processing industries to convert bottom-of-barrel fractions of the process into more useful gas products. However, its potential for biomass feedstock has just been explored relatively recently [1, 23].

Entrained flow gasification application for woody biomass is challenging due to its feedstock size requirement, where very fine particles are required in order to achieve maximum conversion at a short residence time [1, 26-28]. It is reported that entrained flow gasification operation requires feed particles smaller than 1 mm [28, 29], which is difficult to be fulfilled with woody biomass due to its fibrous nature [28]. In addition, grinding woody biomass into such fine size consumes extensive amount of energy hence is not economically feasible especially in large scale operations.

It is reported that the entrained flow gasification has recently been applied for black liquor, which is a by-product during wood cooking process in paper and pulp industries [30-36]. Entrained flow gasification is also studied for application on other types of liquid from biomass and it is believed that this technology holds promising potentials in the future. An example is the gasification of biomass pyrolysis oil which is

used as a way of biomass densification, as well as to overcome challenges related to entrained flow gasification stringent feedstock size requirements. In this case, biomass pyrolysis oil is atomized into fine spray droplets to enhance reaction rates, thus enables maximum conversion within gasification short residence time.

2.4 Review of Works Performed on Biomass Pyrolysis Oil Gasification

Table 2-2 summarizes various gasification systems designed for biomass pyrolysis oil along with their operation conditions as reported in literature.

Table 2-2: Summary of various gasification systems that use pyrolysis oil as feedstocks.

#	Process	Reactor Type	Fuel	Fuel Feed Rate	Gasif. Agent	Agent Feed Rate/Ratio	Operating Temp	Operating Pressure	Reactor Dimensions	Reference
Entrained Flow Gasification System										
1	GASIF.	Entrained flow gasifier	Pyrolysis oil derived from pine wood chips	10-70 g/min	Oxygen	ER: 0.1-0.9	600-1000ºC	1 atm	120mm (ID) x 800mm (H)	*This work*
2	GASIF.	Entrained flow gasifier	Pyrolysis oil derived from whole pine wood	10 mL/min	Oxygen	ER: 0.25	850ºC	1 atm & 6.8 atm	33mm (ID) x 1000mm (H)	*[37]*
3	GASIF.	Entrained flow gasifier	Pyrolysis oil derived from wood and straw	1330 g/min	Oxygen	ER: 0.42	1200-1400ºC	4 atm	520mm (ID) x 1670mm (H)	*[38]*

Table 2-2: Summary of various gasification systems that use pyrolysis oil as feedstocks (continued)

4	GASIF.	Entrained flow gasifier	Pyrolysis oil	0.3 g/min	<u>Case 1:</u> Steam <u>Case 2:</u> Oxygen	<u>Case 1:</u> Steam/C: 0-8.3 <u>Case 2:</u> ER: 0.08-0.53	1000-1400ºC	1 atm	75mm (ID) x 1000mm (H)	*[39]*
5	GASIF.	Entrained flow gasifier	Pyrolysis oil	0.3 g/min	Steam	Steam/C: 8.3	1000-1400ºC	1 atm	75mm (ID) x 1000mm (H)	*[40, 41]*
6	GASIF.	Partial oxidation reactor	50:50 wt% methanol and pyrolysis oil (derived from poplar)	0.1 – 10 mL/min	Oxygen	ER: 0-0.35	625-850ºC	1 atm	11 mm (ID) X 320mm (H)	*[42]*
7	GASIF.	Partial oxidation reactor	Pyrolysis oil derived from rice husk	1.2 g/min	Air	ER: 0.18	700-1100ºC	1 atm	30mm (ID) x 1100mm (H)	*[43]*
8	PYRO LYSIS	Entrained flow gasifier	Pyrolysis oil	0.3 g/min	Not applicable	Not applicable	550-1000ºC	1 atm	75mm (ID) x 1000mm (H)	*[44]*

Table 2-2: Summary of various gasification systems that use pyrolysis oil as feedstocks (continued)

Fluidized Bed Gasification System										
9	GASIF.	Fluidized bed gasifier	Pyrolysis oil derived from pine wood	3.3-42 g/min	Steam & Air	Case 1 ER: 0 Steam/C: 1.9 Case 2 ER: 0.23 Steam/C: 1.0	Case 1: 790ºC Case 2: 840ºC	1 atm	108mm (ID) x 720mm (H)	*[12]*
10	GASIF.	Fluidized bed gasifier	Case 1: Pyrolysis oil Case 2: Pyrolysis oil & char slurry	Case 1: 7.5 g/min Case 2: 6.6 g/min	Steam & Air	ER: 0.1-0.5 & Steam/C: 2.1	790-850ºC	1 atm	78 mm (ID) x 800 mm (H)	*[45]*
11	GASIF.	Fluidized bed gasifier	Case 1: Pyrolysis oil Case 2: Pyrolysis oil & char slurry	Case 1: 2.7-5.3 g/min Case 2: 3.3-3.5 g/min	Steam	Steam/C: 2.7, 5.6, 7.5	800ºC	1 atm	78 mm (ID) x 800 mm (H)	*[46]*
12	GASIF.	Fluidized bed gasifier	Pyrolysis oil	2 mL/min	Steam	Not given	500-700ºC	1 atm	78 mm (ID) x 520 mm (H)	*[47]*

Table 2-2: Summary of various gasification systems that use pyrolysis oil as feedstocks (continued)

13	PYRO LYSIS	Fluidized bed gasifier	Pyrolysis oil	1.6 g/min	Not applicable	Not applicable	500-850ºC	1 atm	108mm (ID) x 720mm (H)	*[48]*
Fixed Bed Gasification System										
14	GASIF.	Fixed bed gasifier	Pyrolysis oil	Not given	Steam	Steam/C: 0.66 - 4.0	1000-1200ºC	1 atm	27mm (ID) x 600mm (H)	*[49]*
15	GASIF.	Fixed bed gasifier	Pyrolysis oil	0.08 g/min	Steam	Steam/C: 0.5-2.5	800ºC	1 atm	13mm (ID) x 500mm (H)	*[50]*
16	PYRO LYSIS	Fixed bed gasifier	Pyrolysis oil	0.46 g/min	Not applicable	Not applicable	600-1000ºC	1 atm	16mm (ID) x 500mm (H)	*[51]*
Packed Bed Gasification System										
17	CATA LYTIC GASIF.	Packed bed reactor	Pyrolysis oil derived from pine wood	25 g/min	Steam & Air	Steam/C: 1.2-2.0 & ER: 0.25-0.42	790-890ºC	1 atm	108mm (ID) x 1600mm (H)	*[52, 53]*

Table 2-2: Summary of various gasification systems that use pyrolysis oil as feedstocks (continued)

18	CATALYTIC GASIF.	Packed bed reactor	Pyrolysis oil mixed with methanol	0.6-1.2 g/min	Air	Steam/C: 0-6.3 & ER: 0.37-0.84	700-800ºC	Not given	32mm (ID) x 450mm (H)	*[54]*
19	CATALYTIC GASIF.	Packed bed reactor	Pyrolysis oil mixed with old engine oil	0.3-1.0 g/min	Steam & Air	Steam/C: 0-0.5 & ER: 0.15-0.45	1050-1100ºC	1 atm	26mm (ID) x 1000mm (H)	*[55]*

Note that the term 'ER' in the table refers to equivalence ratio which is defined as the ratio of oxygen feeding rate into the system during gasification over that required for theoretical stoichiometric combustion [56]. In practice, equivalence ratio of 1 represents sufficient supply of oxygen for stoichiometric combustion to take place while equivalence ratio of 0 represents no supply of oxygen into the system. Equivalence ratio could be represented by the following equation:

$$\underset{Ratio}{Equivalence}\ (ER) = \frac{\left(M_{oxygen}/M_{pyrolysis\ oil}\right)_{experimental}}{\left(M_{oxygen}/M_{pyrolysis\ oil}\right)_{stoichiometry}} = \frac{AFR_{experimental}}{AFR_{stiochiometry}}$$

M_{oxygen} and $M_{pyrolysis\ oil}$ represent flow rates of oxygen gas and pyrolysis oil feed into a system respectively. The stoichiometric ratio could be calculated based on the feedstock empirical composition or formula such as that presented in the following equation:

$$C_xH_yO_z + \left(\frac{\boldsymbol{\frac{y}{2} + 2x - z}}{\mathbf{2}}\right)O_2 \rightarrow xCO_2 + \frac{y}{2}H_2O$$

The From Table 2-2, it is clear that most of the gasification systems for biomass pyrolysis oil use entrained flow gasifier, with oxygen gas as the preferred gasification agent [37-39]. It is worth noting that Marda et al. [42] and Li et al. [43] gasify biomass pyrolysis oil in partial oxidation reactors, which operation principles are identical to entrained flow gasifier hence are grouped in a similar gasification

category. Fluidized bed gasifiers were also used for gasification of pyrolysis oil with both steam and air as the gasification agent [4, 12, 50]. Gasification of pyrolysis oil were conducted in fixed bed gasifiers [49, 51, 57] and packed bed (catalytic) gasifiers [52-55] where steam and air were used as the gasification agent, however, this is not common.

In this work, entrained flow gasification was chosen as the most appropriate approach to gasify biomass pyrolysis oil for production of producer gas. Subsequent discussions in this chapter will focus on this gasification technology and relevant topics.

2.5 Atomization of Pyrolysis Oil and Its Influence on Gasification

Atomization is a process where liquid stream is disintegrated into fine droplets to maximize the liquid active surface area to enhance mass and heat transfers within a system. To put this process into a simple term, the liquid is sprayed into fine droplets. This technology was originally used to improve combustion of non-volatile liquid fuels such as heavy oil [58]. Atomization has also been used in other applications such as in automotive fuel injection system, painting industries, spray drying and gasification. Particularly for gasification, atomization is often used even with volatile liquid fuel in order to achieve the maximum conversion efficiency hence improving the overall process performance [59].

Fuel spray combustions can be categorized into two modes which are heterogeneous combustion and homogeneous combustion [58, 60]. Heterogeneous combustion mode takes place when individual spray droplets enter combustion zone and burn as discrete droplets in yellow colour flames. This combustion mode could be further separated into four different sub-modes depending on the spray combustion characteristics, as illustrated in Figure 2–5 [60].

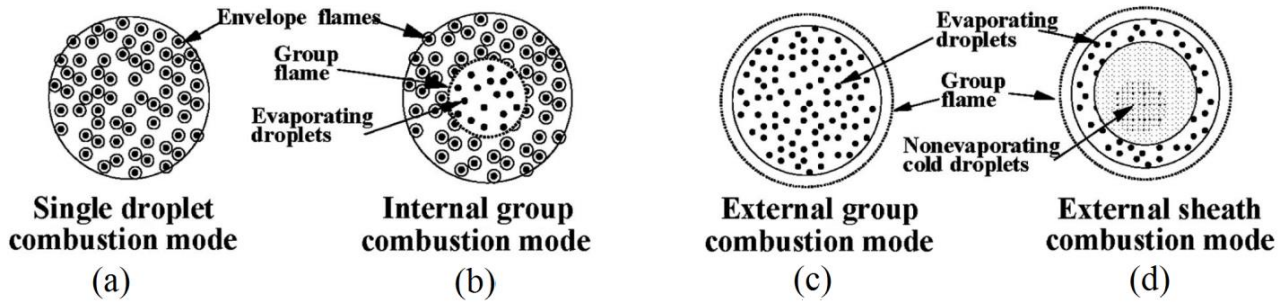

Figure 2–5: Spray droplets heterogeneous combustion modes [60].

Homogeneous combustion, on the other hand usually takes place during combustion of highly volatile liquid or when the droplets sizes are sufficiently small to rapidly evaporate into vapour clouds prior to entering the combustion zone. In practice homogeneous and heterogeneous combustion modes could occur simultaneously within a spray, where large spray droplets burn heterogeneously while smaller droplets burn homogeneously at different sections of the spray [58].

These combustion categories and modes also apply to the combustion zone in the entrained flow gasification process as indicated in the Chapter 2.3 (Figure 2–4). Williams [58] explained three major factors that affect the spray combustion behaviour. These factors were summarized as follows:

i) The characteristics of the spray.
ii) The rate of combustion of each droplet in the spray and its products.
iii) The inter-droplets interactions during spray combustion.

Among these three factors, the characteristics of spray generated during atomization are the most important. In general spray characteristics refer to various aspects of a spray including the spray pattern, spray dimensions, droplets size, droplets spatial distribution, spray propagation and droplet velocities. Examples of spray patterns that are usually reported during liquid atomization are hollow cone, full cone, solid and flat patterns [58, 61]. Characteristics of a spray are determined by many factors including atomizer types, nozzle design and atomization mechanism, therefore, the spray characteristics vary substantially from one operation to another.

There are various atomization technologies that could be selected to fulfil different process requirements. Nevertheless the most commonly used atomization technologies include pressure jet atomizer, twin-fluid atomizer and ultrasonic atomizer. Brief descriptions of each of these atomizers are given as follows:

a) Pressure jet atomizer

This atomization approach works by forcing liquid through an orifice at high pressure, thus accelerating the liquid at high velocity upon leaving the orifice. As the liquid jet exits the nozzle, the pressure difference between the ambient and that in the nozzle causes the liquid to become highly instable hence disintegrates into spray droplets. For this type of atomizer, the resulted spray characteristics are mainly dictated by liquid flow rate and diameter of the discharge orifice [58].

b) Twin-fluid atomizer

As suggested by its name, this twin-fluid atomization involves two streams of fluids, one liquid and one gas. This type of atomizer is also known as air-assisted atomizer. With this atomization approach, spray characteristics are strongly determined by flow rates of both fluids.

One of the major advantages of using twin-fluid atomizers is its ability to generate finer droplets in comparison to that by pressure jet atomizers. In addition, twin-fluid atomizer is most suitable when it is used in operations where gas-liquid reactions are expected. In these cases, the reactant gas can be used as the gas stream for enhancing liquid atomization, and both the liquid and gas streams are forced to interact with one another during spray formation process. Such interaction is beneficial as it helps improve mixing between liquid droplets and gas thus enhancing kinetics of reactions.

Twin-fluid atomizers are available in two different configurations, internal mix and external mix, depending on where the two fluids come into contact. Internal mix atomizers blend liquid and gas inside the atomizer prior to exiting the nozzle, while external mix atomizers keep the two streams separate inside the atomizer body, and the gas and liquid only come into contact as soon as both streams exit the nozzle.

In comparison to the internal mixing atomizer, the external mixing atomization provides a much safer combustion environment by minimizing risk of internal combustion within the atomizer and flame flashback during operation at elevated temperatures [58]. In addition, the impact of high velocity gas on liquid jet during external mix atomizer also promotes secondary atomization, resulting in finer spray droplets in comparison to that in an internal mix atomizer. Nevertheless, internal mix atomizer is more efficient as it promotes better liquid-gas mixing within the spray while requiring smaller gas flow rate to achieve similar atomization performance compared to that required by external mix atomizer [62].

c) Ultrasonic atomizer (nebulizer)

Unlike pressure jet and twin-fluid atomizers, ultrasonic atomizer generates fine droplets by breaking the liquid stream using high frequency vibrations. In this atomization system, liquid is passed through piezoelectric transducers and a stepped horn that vibrate at ultrasonic frequencies to produce short wavelength sounds and disintegrate the liquid into droplets. Major advantage of the ultrasonic atomizer is that it allows atomization at low spray velocities as well as it does not depend on liquid or gas flow rates in determining its atomization performance [62].

In addition to atomization performance, liquid properties also have significant influence on spray combustion behaviour. In general, high viscosity liquid is more difficult to atomize since it requires high flow rates or pressure of the atomizing gas [63], or high vibration strength in the ultrasonic atomizer, to destabilize the liquid stream into fine droplets.

Highly volatile liquid, on the other hand is desirable as it enhances release of volatile vapours into its surrounding, thus improving spray combustion behaviour dramatically. Rapid volatile release from the liquid also means less time taken for individual spray droplets to completely evaporate into vapour and combust homogeneously. Therefore, volatile liquid is expected to have better spray combustion behaviour by enhancing droplets combustion rate while at the same time minimizing interactions between droplets in the spray, as outlined earlier by Williams [58]. However, spray combustion behaviour of a liquid may also affected by other factors such as the flow dynamics, mixing pattern, non-uniformity of droplets sizes as well as uneven heat and mass transfers during operation [58].

In literature, investigations on pyrolysis oil spray behaviour and its influence on combustion are very limited. In most cases, model liquids were used as a substitution to the actual pyrolysis oil due to the oil hazardous nature, which consequently may results in some unknown differences in spray behaviour between these two liquids. Ethylene glycol has been used as the model liquid for pyrolysis oil due to its comparable physical properties and relatively non-toxic nature [64-66]. Ethylene glycol has also been used in oxidative entrained flow gasification as reported by Kolb et al. [64] where influences of atomization quality and fuel composition on entrained flow gasification performance between 1200-1500^{o}C were investigated.

Useful information on pyrolysis oil combustion behaviour was reported by Wornat et al. [17] who studied combustion of individual pyrolysis oil droplet upon exposure to combustion environment at high temperatures. This work provided critical insight into pyrolysis oil physical transformations which was found to occur in several distinct stages, as has been discussed earlier in Chapter 2.2. Although the findings provided in-depth understanding of pyrolysis oil conversion at high temperatures, it did not represent the actual behaviour of pyrolysis oil spray and the spay combustion, unfortunately, since the tests were conducted using a single droplet at a time.

2.6 Reactions during Pyrolysis Oil Entrained Flow Gasification

Conversion of carbonaceous feedstock into producer gas via gasification, can be divided into two main stages which are devolatilization and gasification following an initial short period of drying [67]. Devolatilization typically starts once the feedstock is dried and exposed to high temperatures, from which a wide range of hydrocarbon compounds are released from the feedstock decomposition as the intermediate products. These products initially include light molecular compounds such as aldehydes, organic carboxylic acid and alcohols [51]. Solid char and non-condensable gases (H_2, CO and CO_2) are also generated from this devolatilization stage. As the feedstock temperature increases with time continuing, more volatile compounds are generated and eventually leaving behind char and solid ash as residues. In this context, products of devolatilization could be grouped as 'primary volatile' compounds [44].

Following the devolatilization stage, gasification reactions takes place which include reactions among the gases (the primary volatile compounds and gasification agent) and reactions between the gases and char. The former reactions are termed as homogeneous reactions and the latter as heterogeneous reactions. Examples of reactions involved during gasification include Water-Gas Shift, Boudouard and cracking reactions which result in production of more non-condensable gases and secondary and tertiary volatile compounds. At sufficiently high temperatures, the products may also undergo Reforming reactions between methane and steam to produce more non-condensable gas products in the system [44].

Higman et al. [67] suggested that the feedstock heating rate has significant influence on the transition from devolatilization to gasification stages during the gasification operation. In one extreme situation such as in the entrained flow gasifier where heating rate is very high, the rapid release of volatile compounds during devolatilization is consumed by efficient gasification reactions, thus minimizes build-up of volatiles compounds in the gasification environment. The low concentration of volatiles subsequently limits the undesirable secondary reactions in the system, resulting in cleaner gas product even when the system is operated at short residence time. On the other extreme situation, when devolatilization occurs slowly at low heating rate, accumulation of volatile compounds in the system becomes highly dominant thus some of the volatiles may leave the system [68] in the form of tar or unconverted feedstock, thus resulting producer gas with low quality, as has been observed during many gasification operations at low temperatures.

In practice heating rate of feedstock in entrained flow gasifiers is usually very high, owing the system strict feed size requirements. Feedstock heating rate in entrained flow gasification system was reported to

have reached as high as 2000°C/s when pyrolysis oil was used as the feedstock and atomized into the system [44]. Therefore, there are potentially significant advantages of using pyrolysis oil in entrained flow gasification system in order to achieve the maximum feedstock-gas conversion and high quality producer gas during the operation.

In order to understand and predict the composition of producer gas from gasification of biomass pyrolysis oil, various homogeneous reactions and heterogeneous reactions have been considered which are listed as follows [67, 69-72].

Homogeneous gas phase reactions:

Combustion/Oxidation reactions:

$CO + {}^{1}/_{2}\, O_2 \rightarrow CO_2$ ΔH_r = -283 kJ/mol Reaction 1

$H_2 + {}^{1}/_{2}\, O_2 \rightarrow H_2O$ ΔH_r = -242 kJ/mol Reaction 2

$CH_4 + {}^{1}/_{2}\, O_2 \rightarrow CO + 2H_2$ ΔH_r = -36 kJ/mol Reaction 3

Hydrogasification/methanation reaction:

$CO + 3H_2 \leftrightarrow CH_4 + H_2O$ ΔH_r = -206 kJ/mol Reaction 4

Water-Gas Shift reaction:

$CO + H_2O \leftrightarrow CO_2 + H_2$ ΔH_r = -41.0 kJ/mol Reaction 5

Steam/Methane Reforming reactions:

$CH_4 + H_2O \leftrightarrow CO + 3H_2$ ΔH_r = +206 kJ/mol Reaction 6

$CH_4 + CO_2 \leftrightarrow 2CO + 2H_2$ ΔH_r = +247 kJ/mol Reaction 7

Simultaneously, solid char generated from the initial devolatilization of feedstock conversions also reacts with steam and other gases in the system, heterogeneously, during gasification. This includes reactions with O_2 (oxidation reaction), CO_2 (Boudouard reaction), H_2O (char-steam reforming or water gas reactions) and H_2 (hydrogenation reaction). Heterogeneous reactions are slower than the homogeneous reactions in general, thus are dominant in the overall conversion rate.

The lists of heterogeneous reactions that may take place during gasification are presented below [67, 69-72], in which char is represented by pure carbon.

Heterogeneous solid-gas phase reactions:

Combustion/oxidation reactions:

$C + O_2 \rightarrow CO_2$ ΔH_r = -394 kJ/mol Reaction 8

$C + {}^1/_2\, O_2 \rightarrow CO$ ΔH_r = -111 kJ/mol Reaction 9

Hydrogasification/hydrogenation/methanation reaction:

$C + 2H_2 \leftrightarrow CH_4$ ΔH_r = -75 kJ/mol Reaction 10

Boudouard reaction:

$C + CO_2 \leftrightarrow 2CO$ ΔH_r = +172 kJ/mol Reaction 11

Char-steam reforming/water gas reactions:

$C + H_2O \leftrightarrow CO + H_2$ ΔH_r = +131 kJ/mol Reaction 12

$C + 2H_2O \leftrightarrow CO_2 + 2H_2$ ΔH_r = +90.1 kJ/mol Reaction 13

$C + H_2O \leftrightarrow {}^1/_2\, CH_4 + {}^1/_2\, CO_2$ ΔH_r = +7.6 kJ/mol Reaction 14

Like all chemical reactions, the homogeneous and heterogeneous reactions involved during gasification are influenced by kinetics and thermodynamics factors. Reaction kinetics is a measure of how fast a chemical reaction progress towards equilibrium given sufficient activation energy for the reactions to take place. Reaction thermodynamics, on the other hand, associates with the energy stored in the reactants and products, thus relates strongly to the stability and favourability of the reactions to occur [73]. Following these factors, some reactions may be more favourable than others at a given reaction environments, thus the final products are expected to vary accordingly. In general, exothermic reactions, as denoted by

negative enthalpy (ΔH_r) values are more favourable at lower temperature while endothermic reactions, as denoted by positive enthalpy (ΔH_r) values are more favourable at higher temperature.

It is reported that char reactivity can be enhanced if the feedstock is subjected to a high heating rate during devolatilization stage in gasification. This has been proven to be true for gasification of biomass pyrolysis oil as the feedstock, where rapid heating of pyrolysis oil droplets during gasification has resulted in less char in the producer gas [44, 74] in comparison to that at low heating rate. Besides heating rate, char reactivity is also influenced by gasification temperature. However, the char reactivity becomes less sensitive to temperature when the gasification temperature is higher than 1000^{o}C since at such high temperatures, char reactions are controlled by gas diffusion rather than surface reactions [74].

2.7 Slagging and Non-Slagging Approaches for Entrained Flow Gasification

Entrained flow gasification operations can be subdivided into two categories which are slagging and non-slagging gasification. Major difference between the slagging and non-slagging processes is the formation of slags during the gasification which is controlled by gasification conditions, gasifier design and feedstock properties. Slagging entrained flow gasification requires ash and inorganic compounds in the feedstock to melt into liquid slag during gasification at very high temperatures, above the ash melting point. Non-slagging entrained flow gasification, on the other hand, operates at lower gasification temperatures, well below the ash melting point so that ash and inorganic compounds remain as solid and finally exit the system [27, 75] to be filtered and collected.

Slagging entrained flow gasification is a complex process at very high temperatures and, in many cases, at elevated pressures [76]. Despite that, slagging gasification is widely employed for gasification of feedstocks with high ash content such as coal and black liquor. Information on the slagging entrained flow gasification is available in literature as it has been well studied and scaled-up to demonstration and commercial scales. In contrast, studies on non-slagging entrained flow gasification are limited in literature and its potentials have not been fully explored. The non-slagging entrained flow gasification avoids production of slags during the gasification and its operation temperature is much lower than the slagging entrained flow gasification. The non-slagging entrained flow gasification system is more suitable for low ash content feedstocks.

The aim of this section is to review the potentials and challenges of the non-slagging entrained flow gasification based on theoretical and experimental evidences. Review of the slagging gasification approach was also conducted in this section for comparison.

2.7.1 Slagging entrained flow gasification

2.7.1.1 Advantages of slagging entrained flow gasification

1. Protection of reactor material from deterioration at high temperatures

One of the challenges for entrained flow gasification operation is the selection of suitable reactor materials that can withstand high operating temperatures and are inert to the gasification environment. While there are a number of materials that can withstand the high temperature, many of them are not resistant to chemical attack or, in other words, are reactive to the gasification environment. In the gasification reactor, the feedstock and the products normally contains high alkaline, chlorine and other organic compounds which cause leaching or corrosion [77], particularly at high temperatures, and thus reduce the life time of the reactor wall.

The main advantage for using slagging entrained flow gasification is the formation of protective layers of slag on the reactor walls against gasification harsh environment. At operating temperatures above ash melting point, slag will be formed and flows down the reactor wall into a slag collection tank. The initial batch of liquid slag impacting the reactor wall normally solidifies on the wall and act as a protective barrier from corrosion and chemical attack. This protective slag layer is also self-repairing thus very robust and has extended lifetime of up to 20 years of operation [76].

Slag is considered to be inert to gasification environment. In addition, slag also helps to minimize heat loss through gasifier walls by the formation of additional layers with low thermal conductivity on the reactor wall [78].

2. Feed flexibility

Slagging entrained flow gasifier is designed for feedstocks with high ash content compared to those for non-slagging gasifier. In generally, the minimum ash content required for the slagging entrained flow gasifier is 6 wt% of the total fuel feed into the system [27, 79]. When the feed ash content is lower than 6%, modification of the feedstock is needed for successful slagging entrained flow gasifier operations.

Low ash content feedstock can be mixed with other higher ash content feedstocks such as char or coal to achieve the minimum ash requirement for its operation [80].

However, if the feedstock has a very high ash melting temperature, fluxing agent such as clay and silica are added to the feed to lower the ash melting temperature. Adding fluxing agent is particularly useful for gasification of wood and wood derived feedstocks as the ash in almost all of wood species melts at higher temperatures than normal slagging gasification operating temperature of 1300-1500^{o}C [27]. It was reported that addition of silica to the woody biomass feedstock at the right ratio can reduce its ash melting point from 1560^{o}C to 1260^{o}C [27].

3. Application in coal gasification plants

The slagging entrained flow gasification has been widely applied in conversion of coal and black liquor into producer gas or other chemical products. For entrained flow gasification of biomass, the biomass is commonly blended with coal to meet the requirements of ash content and melting temperatures for slagging entrained flow gasification. This provides a bright potential for using existing gasification plants designed for coal without major plant modifications [27].

4. Environmental friendly slag waste

Slag in nature is less hazardous to the environment compared to ash. This is because it does not cause heavy metal leaching due to its intertwined structure as the result of high gasification temperature [75].

2.7.1.2 Disadvantages of slagging entrained flow gasifier

1. High temperature operation

The operating temperature of a slagging entrained flow gasification process is determined by ash melting characteristics and feed reactivity. Thus, one of the main disadvantages of slagging entrained flow gasification is the high operation temperature, particularly when gasifying feedstocks with high ash melting temperatures. As an example, typical gasification temperature of slagging entrained flow gasification of coal and woody biomass are around 1400^{o}C [67, 75] and 1600^{o}C [78], respectively. The high melting temperature of biomass ash is mainly contributed by its high calcium oxide (CaO) content [29, 79, 81]. Without addition of fluxing agent, the ash may require temperature of up to 1800^{o}C before it could melt and form liquid slag [27].

At very high operating temperature for slagging gasification, deterioration of refractory lining of the reactor wall may be accelerated which reduces the material life time [78]. The result could be detrimental if formation of protective slag layer on the reactor surfaces is not successful or the protective layer is not fully distributed over the reactor wall surfaces as desired. Other than that, high gasification temperature also means higher oxygen and fuel requirements [67] in order to raise and maintain the operation temperature. At such high operation temperature, heat loss from slag leaving the gasification system is also significant [78, 80], hence lead to substantial reduction in overall energy efficiency [67].

2. Excessive slag formation during operation

Although slagging entrained flow gasifiers are designed for feedstocks with relatively high ash content, in practice feedstock with moderate ash content is always recommended. Too high ash content in a feedstock means more energy is required to melt the ash and rapid slag build-up inside the reactor. In addition to reduction of gasification overall efficiencies, high slag deposition also increases the risk of plugging and fouling of gasifier and producer gas cleaning device [78, 82].

Gasification operations with rapid slag formation also requires sophisticated system for slag removal and disposal [78]. At present, slag residues have limited utilization and commercial value as it is not well accepted in industry. Although it was claimed that the slag could be used as construction material or as additive for construction bricks, the potential is still not clear [75].

3. Complex slag properties and deposition behaviour

Successful application of slagging entrained flow gasification requires in-depth understanding on slagging properties of the feedstocks such as chemical composition, ash melting point, critical viscosity and flow behaviour. In fact, in most coal gasification operations, ash melting point and slag viscosity of the coal are of more importance than carbon conversion performance due to their significant influence on the operational success [82].

Slag viscosity is important because the optimum slag velocity is closely related to the success of protective deposit formation on the reactor surfaces during the gasification [78]. Without the right slag viscosity, the slag may not form sufficient deposition across the gasifier surfaces or, in another extreme, could cause severe blockage to the system.

In general, slag viscosity is inversely proportional to gasification temperature. Higher operating temperature usually reduces slag viscosity thus allowing slag to flow more easily, solidify and cover the

gasifier wall during gasification. The minimum temperature where slag viscosity is sufficient to start flowing is known as the temperature of critical viscosity. Another factor that affects slag viscosity is the slag chemical composition [78]. In order to characterize slag behaviour successfully, good understanding of the relation between slag viscosity and slag composition is required. Characterization of slag behaviour from mixing different feedstocks is necessary but is complex.

Mixing different feedstock is required when the ash content of a particular feed is below the minimum operation limit such as that in woody biomass. Woody biomass, which usually contains approximately 0.4–2.1 wt% of ash [83], would require addition of another feedstock which has higher ash content, most commonly coal, in order to raise the feed ash content to the desired operational values. In practice, this process requires careful consideration by taking into account the variability of biomass ash content and other physicochemical properties. When a fluxing agent is added to the feedstock, other properties of the ash may also be changed, resulting in variation in slag properties.

In the slagging entrained flow gasifiers, the slagging performance is also affected by other factors including ash molten percentage, slag surface stickiness, impact angle and surface tension [82]. All of these factors contribute to complex slagging behaviour thus making it very challenging to form an evenly distributed slag deposit during the operation start-up stage.

While slagging entrained flow gasification of coal and black liquor has been well studied and reported in literature, slag properties of biomass species are still not thoroughly investigated [80]. Comprehensive studies are required in the future to fully understand biomass slagging behaviour of the biomass feedstock at different operating conditions.

2.7.2 Non-slagging entrained flow gasification

2.7.2.1 Advantages of non-slagging entrained flow gasification

Non-slagging entrained flow gasification has been used since 1950 for gasifying viscous vis-breaking and de-asphalting residues from petroleum refinery plants. Vis-breaking is a process after vacuum distillation of crude oil in which high viscosity distillation residues are thermally broken down to less viscous liquid products as well as small quantity of light hydrocarbons such as LPG and gasoline. The vis-breaking liquid products in some cases then undergo solvent de-asphalting process where asphalt is removed from the liquid before these are fed into a gasifier. Vis-breaking and de-asphalting residues are noxious, low value products of refinery process that can be upgraded to producer gas through gasification. Non-

slagging entrained flow gasification technology has been used widely by Shell, known as the Shell Gasification Process (SGP) unit, which are integrated into petroleum refinery complexes to convert bottom-of-the-barrel refinery residues into valuable gas products [76].

There are a number of advantages for the non-slagging entrained flow gasification although its application is not as common as the slagging entrained flow gasification. The most important advantage of using the non-slagging entrained flow gasification is the low operation temperature; therefore, the reactor design and operation are simpler than those of slagging entrained flow gasification. As no slag deposition is required in the non-slagging gasification, comprehensive characterization of slag properties of the feedstock is no longer necessary. In addition, absence of slag in the system also reduces risks of fouling and plugging during the operation. In comparison to slagging approach, non-slagging entrained flow gasification is expected to encounters less problems during its operations particularly during the start-up stage. Slag collection, slag disposal and maintenance are also consequently simplified.

The operation temperature for the non-slagging gasification only considers the needs for gasification reactions, producer gas quality and carbon conversion efficiency. In fact, the gasification temperature should not exceed the ash melting point of the feedstock to prevent ash deposits or slag formation on the reactor wall. Non-slagging entrained flow gasification systems are usually operated at temperature range between 600^{o}C and 1100^{o}C [37, 42, 43, 84], although some non-slagging gasification systems are operated at temperature as high 1400^{o}C for enhanced gasification performance [23, 38-40, 85]. In the case when high temperature is used for non-slagging gasification operation, the risk of undesirable slag formation increases dramatically thus may lead to fouling or blockage to the process equipment when appropriate slag handling measures are failed to be considered. Table 2-3 shows ash softening and melting points of several biomass species for reference.

Table 2-3: Softening and melting temperature of ash in several biomass species

Number	Biomass Species	Ash Softening Point (°C)	Ash Melting Point (°C)	Reference
1	50% bark 50% wood chips	1000-1200	1470	[86]
2	60% bark 40% wood chips	1000-1200	1480	[86]
4	Wood	Not given	1200	[69]
5	Wood	Not given	≥ 1450	[27]
3	Barley straw	700	970	[86]
6	Straw	Not given	850	[69]

From the above discussion, the non-slagging entrained flow gasification is suitable for feedstocks with low ash content or high ash melting point. Many biomass species fall into this category thus has bright potential to benefit from non-slagging gasification operations. Table 2-4 summarizes typical ash contents of various biomass species in which coal species are also included for comparison.

Table 2-4: Elemental components and ash contents of different biomass and coal species [adapted from [83]]

#	Feedstock	Ash %	#	Feedstock	Ash %
1	Beans	4.7	7	Miscanthus	2.7
2	Corn	1.5	8	Switchgrass	5.7
3	Canola	4.5	9	Wheat straw	7.7
4	Wood Bark	1.5	10	Corn stover	5.1
5	Willow	2.1	11	Lignite coal	22
6	Hardwood	0.4	12	Low sulphur sub-bituminous coal	6

Nevertheless, non-slagging entrained flow gasification system can also process feedstocks with high ash contents because the gasification operating temperature is maintained well below the ash melting point, thus minimum or no slag is expected to be formed. Solid ash in the producer gas can be filtered in the downstream unit of the gasifier which can then be used as cement fillers [75]. Therefore, there is no strict requirement of the maximum ash content allowed for feedstocks to be used in this gasification system.

Non-slagging gasification does not require feedstock blending or fluxing agent addition in order to increase ash content or reduce the ash melting temperature as required in the slagging entrained flow gasification [27, 78], thus makes the design and operation much simpler than that of the slagging gasification. It is also believed that the non-slagging entrained flow gasification is more cost effective to operate compared to slagging gasification [27].

2.7.2.2 Challenges for non-slagging entrained flow gasification

The major challenge for non-slagging entrained flow gasification is the selection of suitable material for the gasifier. Material corrosion is an intrinsic problem in many gasification processes as a result of high operation temperatures as well as corrosive environment within the gasifier. Therefore selection of a suitable reactor material is critical to ensure the durability and reliability of the reactor for this application.

From literature review, it is found that high temperature reactors are commonly constructed using ceramic materials such as corundum tube, alumina refractory and silicon carbide [23, 84, 87, 88]. Nevertheless, limited information is available on the performance of these materials at high temperatures and corrosive environment as encountered under the non-slagging entrained flow gasification operation. In addition, ceramic materials are less durable and have limited ability to fulfil various engineering requirements in comparison to steels and alloys.

It is apparent that the application of entrained flow gasification for biomass resources is relatively new compared to gasification of coal and refinery residues. Limited information is also available on the non-slagging entrained flow gasification approach; therefore, there are clear knowledge gaps in the non-slagging entrained flow gasification of biomass feedstocks. These include fundamental understanding of the gasification process, quantification of effects of operation conditions and feedstock properties on the gasification performance; and material selections for the reactor construction.

2.8 References

1. Svoboda, K., et al., *Pretreatment and feeding of biomass for pressurized entrained flow gasification.* Fuel Processing Technology, 2009. **90**(5): p. 629-635.
2. Lu, Q., W.-Z. Li, and X.-F. Zhu, *Overview of fuel properties of biomass fast pyrolysis oils.* Energy Conversion and Management, 2009. **50**(5): p. 1376-1383.

3. Zhang, Q., et al., *Review of biomass pyrolysis oil properties and upgrading research.* Energy Conversion and Management, 2007. **48**(1): p. 87-92.
4. Sakaguchi, M., *Gasification of bio-oil and bio-oil/char slurry*, in *Chemical and Biological Engineering*. 2010, The University of British Columbia: Vancouver.
5. Bridgwater, A.V., *Review of fast pyrolysis of biomass and product upgrading.* Biomass and Bioenergy, 2012. **38**(0): p. 68-94.
6. Hassan, E.-b., P. Steele, and L. Ingram, *Characterization of Fast Pyrolysis Bio-oils Produced from Pretreated Pine Wood.* Applied Biochemistry and Biotechnology, 2009. **154**(1-3): p. 3-13.
7. Vispute, T., *Pyrolysis oils: Characterization, stability analysis and catalytic upgrading to fuels and chemicals*. 2011, University of Massachusetts: Amherst.
8. Chhiti, Y., *Non catalytic steam gasification of wood bio-oil*. 2011.
9. Czernik, S. and A.V. Bridgwater, *Overview of Applications of Biomass Fast Pyrolysis Oil.* Energy & Fuels, 2004. **18**(2): p. 590-598.
10. Oasmaa, A., et al., *Fast Pyrolysis Bio-Oils from Wood and Agricultural Residues.* Energy & Fuels, 2009. **24**(2): p. 1380-1388.
11. Oasmaa, A. and C. Peacocke, *Properties and fuel use of biomass-derived fast pyrolysis liquids.* VTT, Finland, 2010.
12. Van Rossum, G., S.R.A. Kersten, and W.P.M. Van Swaaij, *Catalytic and noncatalytic gasification of pyrolysis oil.* Industrial and Engineering Chemistry Research, 2007. **46**(12): p. 3959-3967.
13. Li, H., et al., *Stability evaluation of fast pyrolysis oil from rice straw.* Chemical Engineering Science, 2015. **135**: p. 258-265.
14. Garcia-Perez, M., et al., *Multiphase structure of bio-oils.* Energy & Fuels, 2006. **20**(1): p. 364-375.
15. Diebold, J.P., *A review of the chemical and physical mechanisms of the storage stability of fast pyrolysis bio-oils*. 2000: Citeseer.
16. Ba, T., et al., *Colloidal Properties of Bio-Oils Obtained by Vacuum Pyrolysis of Softwood Bark. Storage Stability.* Energy & Fuels, 2004. **18**(1): p. 188-201.
17. Wornat, M.J., B.G. Porter, and N.Y.C. Yang, *Single Droplet Combustion of Biomass Pyrolysis Oils.* Energy & Fuels, 1994. **8**(5): p. 1131-1142.
18. Lehto, J., A. Oasmaa, and Y. Solantausta, *Fuel oil quality and combustion of fast pyrolysis bio-oils.*

19. Samiran, N.A., et al., *Progress in biomass gasification technique – With focus on Malaysian palm biomass for syngas production.* Renewable and Sustainable Energy Reviews, 2016. **62**: p. 1047-1062.
20. Ruiz, J.A., et al., *Biomass gasification for electricity generation: Review of current technology barriers.* Renewable and Sustainable Energy Reviews, 2013. **18**(0): p. 174-183.
21. NETL. *Commercial Gasifiers - Types of Gasifiers*. 2016 3/10/2016]; Available from: https://www.netl.doe.gov/research/coal/energy-systems/gasification/gasifipedia/types-gasifiers.
22. Zhang, L., C. Xu, and P. Champagne, *Overview of recent advances in thermo-chemical conversion of biomass.* Energy Conversion and Management, 2010. **51**(5): p. 969-982.
23. Qin, K., et al., *High-temperature entrained flow gasification of biomass.* Fuel, 2012. **93**(0): p. 589-600.
24. Xiao, R., et al., *Pyrolysis pretreatment of biomass for entrained-flow gasification.* Applied Energy, 2010. **87**(1): p. 149-155.
25. Zhou, J., et al., *Biomass–oxygen gasification in a high-temperature entrained-flow gasifier.* Biotechnology Advances, 2009. **27**(5): p. 606-611.
26. Kirkels, A.F. and G.P.J. Verbong, *Biomass gasification: Still promising? A 30-year global overview.* Renewable and Sustainable Energy Reviews, 2011. **15**(1): p. 471-481.
27. Van der Drift, A., et al. (2004) *Entrained flow gasification of biomass*.
28. Abdullah, H., et al., *Bioslurry as a Fuel. 3. Fuel and Rheological Properties of Bioslurry Prepared from the Bio-oil and Biochar of Mallee Biomass Fast Pyrolysis.* Energy & Fuels, 2010. **24**(10): p. 5669-5676.
29. Basu, P., *Chapter 6 - Design of Biomass Gasifiers*, in *Biomass Gasification and Pyrolysis*, P. Basu, Editor. 2010, Academic Press: Boston. p. 167-228.
30. Järvinen, M., et al., *Black liquor devolatilization and swelling—a detailed droplet model and experimental validation.* Biomass and Bioenergy, 2003. **24**(6): p. 495-509.
31. Whitty, K., *Investigation of Pressurized Entrained-Flow Kraft Black Liquor Gasification in an Industrially Relevant Environment - Annual Topical Report - Year 1*. 2006, University of Utah.
32. Whitty, K., R. Backman, and M. Hupa, *Influence of pressure on pyrolysis of black liquor: 1. Swelling.* Bioresource Technology, 2008. **99**(3): p. 663-670.
33. Whitty, K., et al., *Influence of pressure on pyrolysis of black liquor: 2. Char yields and component release.* Bioresource Technology, 2008. **99**(3): p. 671-679.

34. Kankkunen, A., et al., *Spraying characteristics of mixed black liquor - Two different spraying cases.* The Swedish and Finnish National Committees of the International Flame Research Foundation.
35. Carlsson, P., et al., *Experimental investigation of an industrial scale black liquor gasifier. 1. The effect of reactor operation parameters on product gas composition.* Fuel, 2010. **89**(12): p. 4025-4034.
36. Wiinikka, H., et al., *Experimental investigation of an industrial scale black liquor gasifier. Part 2: Influence of quench operation on product gas composition.* Fuel, 2012. **93**(0): p. 117-129.
37. Creager, N. and R.C. Brown. *High pressure, oxygen blown entrained-flow gasification of bio-oil*. in *AIChE 2012 - 2012 AIChE Annual Meeting, Conference Proceedings*. 2012.
38. Leijenhorst, E.J., et al., *Entrained flow gasification of straw- and wood-derived pyrolysis oil in a pressurized oxygen blown gasifier.* Biomass and Bioenergy, 2015. **79**: p. 166-176.
39. Chhiti, Y., M. Peyrot, and S. Salvador, *Soot formation and oxidation during bio-oil gasification: experiments and modeling*. Journal of Energy Chemistry, 2013. **22**(5): p. 701-709.
40. Chhiti, Y., et al., *Wood Bio-Oil Noncatalytic Gasification: Influence of Temperature, Dilution by an Alcohol and Ash Content.* Energy & Fuels, 2010. **25**(1): p. 345-351.
41. Chhiti, Y. and S. Salvador, *Gasification of Wood Bio-Oil*. Gasification for Practical Applications. 2012.
42. Marda, J.R., et al., *Non-catalytic partial oxidation of bio-oil to synthesis gas for distributed hydrogen production.* International Journal of Hydrogen Energy, 2009. **34**(20): p. 8519-8534.
43. Li, J., et al., *Preparation of syngas from partial oxidation of bio-oil.* Ranliao Huaxue Xuebao/Journal of Fuel Chemistry and Technology, 2012. **40**(7): p. 816-821.
44. Chhiti, Y., et al., *Thermal decomposition of bio-oil: Focus on the products yields under different pyrolysis conditions.* Fuel, 2012. **102**(0): p. 274-281.
45. Sakaguchi, M., *Chapter 4: Partial Oxidation of Bio-oil and Bio-oil/Char Slurry in a Fluidized Bed Reactor*, in *Gasification of bio-oil and bio-oil/char slurry (PhD Thesis)*. 2010, Chemical and Biological Engineering, The University of British Columbia: Vancouver.
46. Sakaguchi, M., *Chapter 3: Steam Gasification of Bio-Oil and Bio-oil/Char Slurry in a Fluidized Bed Reactor*, in *Gasification of bio-oil and bio-oil/char slurry (PhD Thesis)*. 2010, Chemical and Biological Engineering, The University of British Columbia: Vancouver.
47. Latifi, M., *Gasification of Bio-oils to Syngas in Fluidized Bed Reactors*, in *Department of Chemical and Biochemical Engineering*. 2012, University of Western Ontario: Ontario.

48. Van Rossum, G., et al., *Evaporation of pyrolysis oil: Product distribution and residue char analysis.* AIChE Journal, 2010. **56**(8): p. 2200-2210.
49. Wang, Y., et al., *Experimental study of bio-oil gasification with steam.* Journal of Fuel Chemistry and Technology, 2012. **40** (2): p. 170-176.
50. Panigrahi, S., et al., *Synthesis Gas Production from Steam Gasification of Biomass-Derived Oil.* Energy & Fuels, 2003. **17**(3): p. 637-642.
51. Zhang, M., et al., *Experimental study on bio-oil pyrolysis/gasification.* BioResources, 2010. **5**(1): p. 135-146.
52. Leijenhorst, E.J., et al., *Autothermal Catalytic Reforming of Pine-Wood-Derived Fast Pyrolysis Oil in a 1.5 kg/h Pilot Installation: Performance of Monolithic Catalysts.* Energy & Fuels, 2014. **28**(8): p. 5212-5221.
53. Leijenhorst, E.J., et al., *Autothermal catalytic reforming of pine wood derived fast pyrolysis-oil in a 1.5kg/h pilot installation: Aspects of adiabatic operation.* Fuel Processing Technology, 2013. **115**(0): p. 164-173.
54. Rennard, D., et al., *Production of synthesis gas by partial oxidation and steam reforming of biomass pyrolysis oils.* International Journal of Hydrogen Energy, 2010. **35**(9): p. 4048-4059.
55. Guo, H., et al., *Production of hydrogen rich bio-oil derived syngas from co-gasification of bio-oil and waste engine oil as feedstock for lower alcohols synthesis in two-stage bed reactor.* International Journal of Hydrogen Energy, 2014. **39**(17): p. 9200-9211.
56. Abdoulmoumine, N., A. Kulkarni, and S. Adhikari, *Effects of Temperature and Equivalence Ratio on Pine Syngas Primary Gases and Contaminants in a Bench-Scale Fluidized Bed Gasifier.* Industrial & Engineering Chemistry Research, 2014. **53**(14): p. 5767-5777.
57. Wang, Y., et al., *Experimental study of rheological behavior and steam gasification of coal bio-oil slurry.* Energy and Fuels, 2010. **24**(9): p. 5210-5214.
58. Williams, A., *Combustion of Liquid Fuel Sprays*. 1990, London: Butterworth & Co (Publishers) Ltd.
59. Broniarz-Press, L., et al., *The atomization of water–oil emulsions.* Experimental Thermal and Fluid Science, 2009. **33**(6): p. 955-962.
60. Nakamura, M., et al., *Combustion mechanism of liquid fuel spray in a gaseous flame.* Physics of Fluids, 2005. **17**(12): p. 123301.
61. *Industrial Spray Products Catalogue 70-M*, S.S. Co., Editor. 2007: Wheaton, USA.
62. Lefebvre, A.H., *General Considerations - Atomizers*, in *Atomization and Sprays*, T. Francis, Editor. 1988, Combustion (Hemisphere Publishing Corporation). p. 4-9.

63. Schick, R.J., *Spray Technology Reference Guide: Understanding Drop Size*. 2008, Spray Analysis and Research Services - Spraying Systems Co.: Illinois, USA.
64. Kolb, T., T. Jakobs, and N. Zarzalis, *Syngas from biomass-based slurry entrained flow gasification*, in *10th Conference on Energy for a clean Environment*. 2009.
65. Wiemer, H.J., et al., *Spray characteristics for the gasification of pyrolysis oil slurries*. 2006.
66. Jakobs, T., et al., *Gasification of high viscous slurry R&D on atomization and numerical simulation.* Applied Energy, 2012. **93**(0): p. 449-456.
67. Higman, C. and M. van der Burgt, *Chapter 2 - The Thermodynamics of Gasification*, in *Gasification (Second Edition)*, C. Higman and M.v.d. Burgt, Editors. 2008, Gulf Professional Publishing: Burlington. p. 11-31.
68. Higman, C. and M. van der Burgt, *Chapter 3 - The Kinetics of Gasification and Reactor Theory*, in *Gasification (Second Edition)*, C. Higman and M.v.d. Burgt, Editors. 2008, Gulf Professional Publishing: Burlington. p. 33-45.
69. Ricketts, B., et al. *Technology status review of waste/biomass co-gasification with coal*. in *IChemE Fifth European Gasification Conference*. 2002.
70. Kunze, C. and H. Spliethoff, *Modelling, comparison and operation experiences of entrained flow gasifier.* Energy Conversion and Management, 2011. **52**(5): p. 2135-2141.
71. Hernández, J.J., et al., *Effect of steam content in the air–steam flow on biomass entrained flow gasification.* Fuel Processing Technology, 2012. **99**(0): p. 43-55.
72. Basu, P., *Chapter 1 - Introduction*, in *Biomass Gasification and Pyrolysis*, P. Basu, Editor. 2010, Academic Press: Boston. p. 1-25.
73. Ozery, G. *Chemistry: Kinetics vs Thermodynamics*. 2016 30/11/2016]; Available from: http://chem.libretexts.org/Core/Physical_and_Theoretical_Chemistry/Equilibria/Chemical_Equilibria/Principles_of_Chemical_Equilibria/Kinetically_vs_Thermodynamically_Stable.
74. Sakaguchi, M., A.P. Watkinson, and N. Ellis, *Steam gasification reactivity of char from rapid pyrolysis of bio-oil/char slurry.* Fuel, 2010. **89**(10): p. 3078-3084.
75. Yun, Y., S.J. Lee, and S.W. Chung, *Considerations for the Design and Operation of Pilot-Scale Coal Gasifiers*. Gasification for Practical Applications. 2012.
76. Higman, C. and M. van der Burgt, *Chapter 5 - Gasification Processes*, in *Gasification (Second Edition)*. 2008, Gulf Professional Publishing: Burlington. p. 91-191.
77. Raffelt, K., et al., *The BTL2 process of biomass utilization entrained-flow gasification of pyrolyzed biomass slurries.* Applied Biochemistry and Biotechnology, 2006. **129**(1-3): p. 153-64.

78. Collot, A.-G., *Matching gasification technologies to coal properties.* International Journal of Coal Geology, 2006. **65**(3–4): p. 191-212.
79. Coda, B., et al., *Slagging Behavior of Wood Ash under Entrained-Flow Gasification Conditions.* Energy & Fuels, 2007. **21**(6): p. 3644-3652.
80. Dahmen, N., et al., *The bioliq® bioslurry gasification process for the production of biosynfuels, organic chemicals, and energy.* Energy, Sustainability and Society, 2012. **2**(1): p. 1-44.
81. Coda, B., M.K. Cieplik, and J.H.A. Kiel. *Slagging behaviour of wood ash upon entrained-flow gasification conditions: Preliminary studies*. 2004.
82. Wang, P. and M. Massoudi, *Slag Behavior in Gasifiers Part I: Influence of Coal Properties and Gasification Conditions.* Energies, 2013. **6**(2): p. 784-806.
83. Clarke, S. and F. Preto. *Biomass Burn Characteristics: Fact Sheet*. 2011 [cited 2013 25 March]; Available from: http://www.omafra.gov.on.ca/english/engineer/facts/11-033.htm#5.
84. Zhao, Y., et al., *Characteristics of rice husk gasification in an entrained flow reactor.* Bioresource Technology, 2009. **100**(23): p. 6040-6044.
85. Qin, K., et al., *Biomass Gasification Behavior in an Entrained Flow Reactor: Gas Product Distribution and Soot Formation.* Energy & Fuels, 2012. **26**(9): p. 5992-6002.
86. Olanders, B. and B.-M. Steenari, *Characterization of ashes from wood and straw.* Biomass and Bioenergy, 1995. **8**(2): p. 105-115.
87. Senapati, P.K. and S. Behera, *Experimental investigation on an entrained flow type biomass gasification system using coconut coir dust as powdery biomass feedstock.* Bioresource Technology, 2012. **117**(0): p. 99-106.
88. Ouyang, S., H. Yeasmin, and J. Mathews, *A pressurized drop-tube furnace for coal reactivity studies.* Review of Scientific Instruments, 1998. **69**(8): p. 3036-3041.

3 DEVELOPMENT OF NON-SLAGGING ENTRAINED FLOW GASIFICATION SYSTEM

3.1 Selection of Non-slagging Gasification Technology

In this work, non-slagging entrained flow gasification system was developed for gasification of biomass pyrolysis oil. The selection of the non-slagging gasification technology was based on consideration that the biomass pyrolysis oil has low ash content and high ash melting point.

Non-slagging gasification operation also eliminates the risk of aggressive molten ash formation in the system thus avoiding potential technical operational issues related to slagging behaviour during gasification operation. Moreover it allows gasification to be conducted at reasonably low temperatures.

Recent advancement on material science and discoveries of various high temperature resistance materials such as refractory metals and heat resistant alloys has made it possible to select the required materials for construction of non-slagging gasifiers. This advancement reduces dependency on slag formation during gasification operations and consequently widens the potential of non-slagging gasification system.

3.2 Entrained Flow Gasifier Design

The entrained flow gasification system designed and developed in this work is capable of gasification or combustion of liquid fuel at operation conditions of atmospheric pressure and temperatures of up to 1100^{o}C. The gasifier consists of two concentric cylinders with inner diameters of 120 mm and 248 mm, respectively. The inner cylinder is the gasification reactor and its walls are made of two layers of 2 mm high temperature resistant 253MA (micro-alloyed) stainless steel. Justification for the selection of this material will be discussed in detailed in Chapter 3.4 of this thesis.

The inner layer of the reactor wall functions as a sacrificial layer for replacement, when required, from chemical attack by corrosive gasification environment. The outer cylinder, on the other hand, was made of 316 grade stainless steel due to less extreme reaction environment requirements. The hollow space between the two cylinders is used for preheating at the start-up stage and for heat insulation during normal gasification operation.

The gasifier was designed to have separable top and bottom sections to allow easy access for inspection, maintenance and material replacement when required. These two sections are connected by two flanges and are sealed by carbon gaskets to ensure gas tight connection between the two sections. The total height of both sections combined is 850 mm.

Figure 3–1 illustrates simplified version of the entrained flow gasifier design with emphasis on the gasifier main sections and important components for clarification.

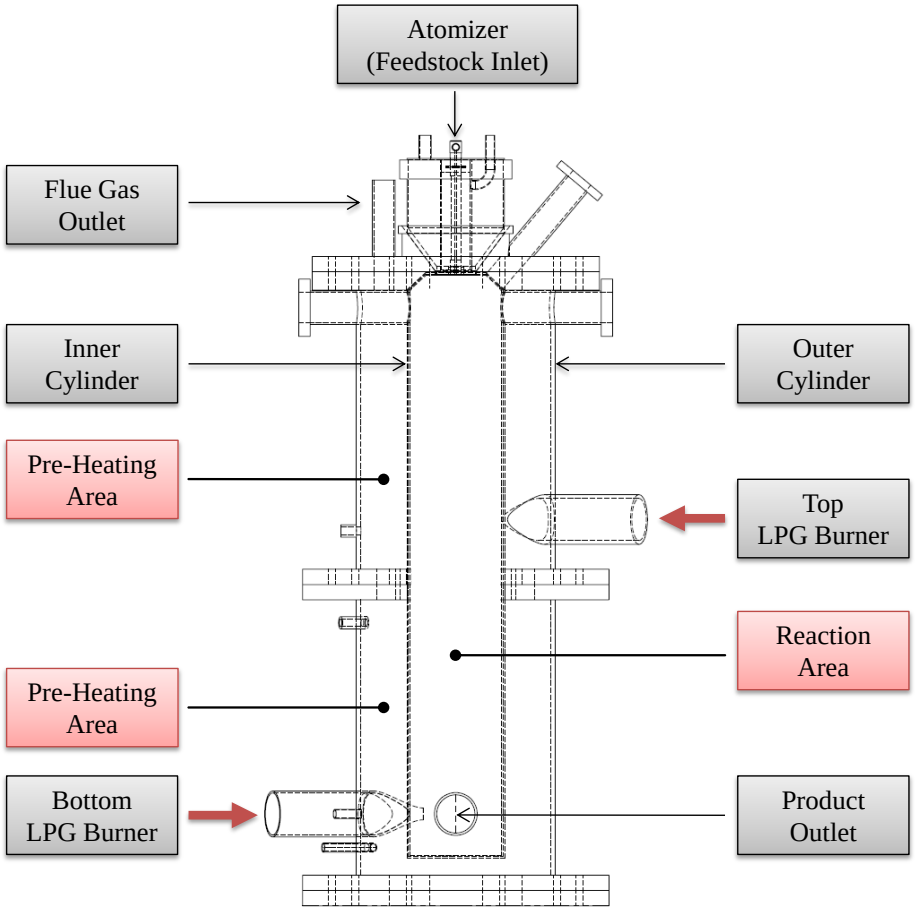

Figure 3–1: Simplified drawing of the entrained flow gasifier developed in this work and its main components

The gasifier inner cylinder (gasification reactor) has a total volume of 9 litres to accommodate rapid gasification reactions during its operation. This volume was chosen based on the goal of achieving 1–3 seconds reaction residence time during gasification with pyrolysis oil average feeding rate of around 40

mL/min. As shown in Figure 3–2, the reactor fulfils the minimum requirement for the specified conditions although larger reactor volume will be required for operations at higher oil feeding rates.

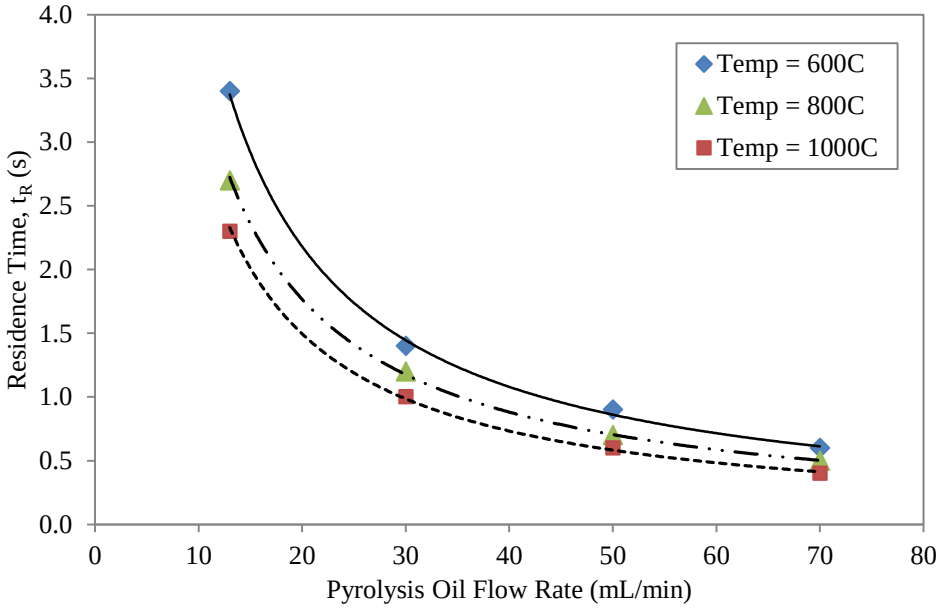

Figure 3–2: The relationship between pyrolysis oil flow rate and gasification residence time for reactor volume of 9 litres and temperatures between 600-1000°C.

The reactor diameter is 120mm, which is sufficiently large to provide horizontal clearance for pyrolysis oil spray formation during gasification. This is important to prevent direct impact of the atomized oil spray droplets on gasifier hot surfaces which could lead to undesirable char accumulation in the system. Based on the volume and diameter selections, the reactor height was then calculated. The ratio between the reactor height and diameter is around 6.5, which is reasonably large to ensure good mixing between reactants in the system, as well as to allow efficient transfer of heat from the pre-heating region towards the centre of the gasifier.

There are a number of ports dedicated on the gasifier for gas sampling, temperature and pressure measurements, and observation. To measure temperature profile across the inner gasifier reactor length, two thermocouple probes were installed at the middle and bottom part of the gasifier. The temperature at the top part of the reactor was not measured since it sits too close to the pyrolysis oil inlet and was found to interfere with the oil spray formation and combustion during operation. To resolve this limitation, a specially designed surface thermocouple was installed to measure surface temperature of the reactor wall as well as part of the system's safety requirements. This pair of thermocouples monitors the reactor wall

temperature during operation to ensure it remains below the material melting point. In order to monitor the temperature increase in the heat-up stage, two pairs of thermocouples are positioned in the hollow space between the inner and outer cylinders (pre-heating area). All thermocouples used in this work are K-type thermocouples.

Besides thermocouples, pressure sensors are also installed in the system to monitor pressure profiles both in the cavity and in the gasifier reactor during operation. Producer gas outlet port is located close to the gasifier floor and is connected to a pipework that leads to an after-burner. Two more ports are dedicated as a safety valve and an observation/viewing glass.

Engineering drawing of the entrained flow gasifier design is shown in Figure 3–3.

Figure 3–4 shows selected photos of the entrained flow gasifier during its construction to highlight important features of the gasifier design described in this section.

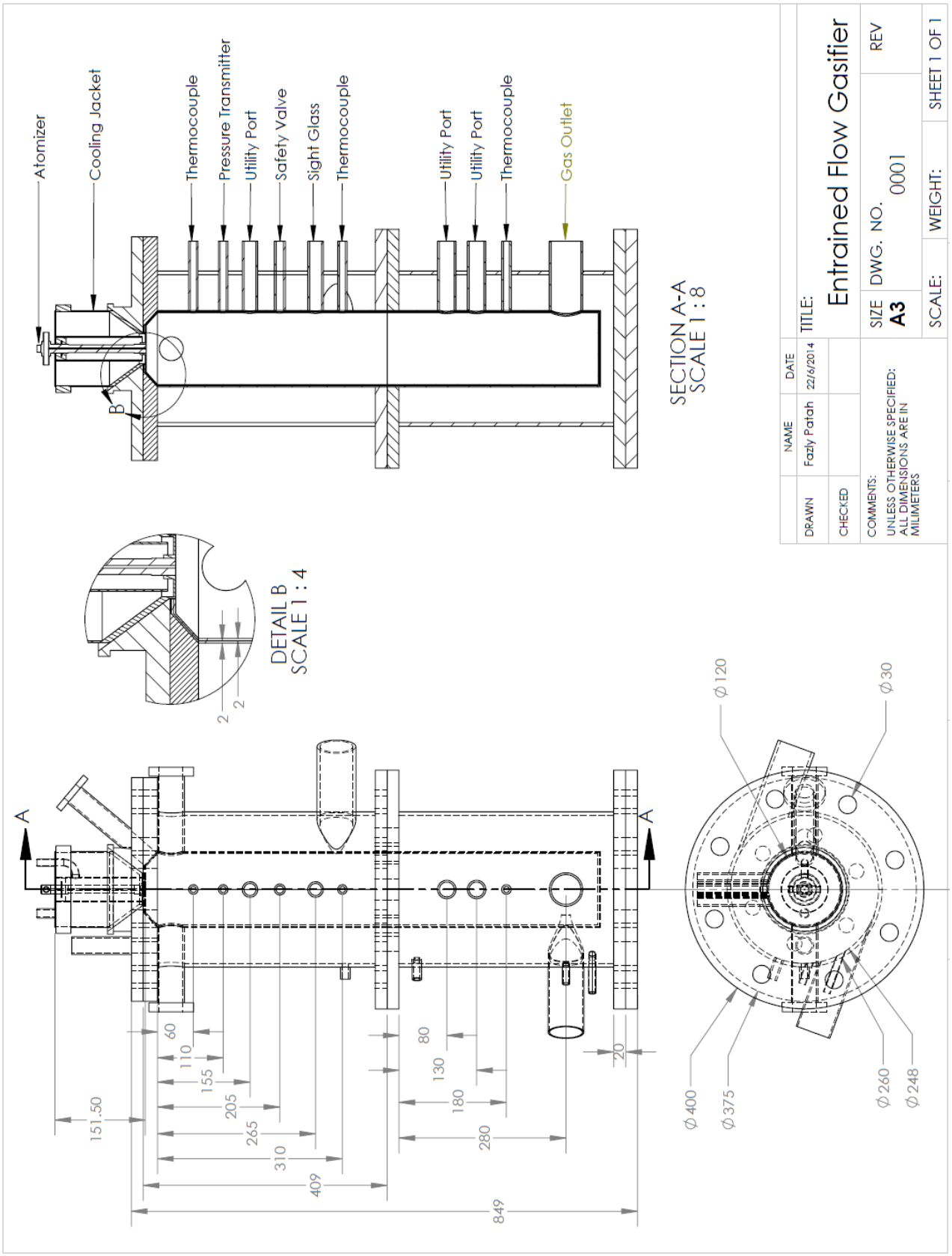

Figure 3–3: Engineering drawing of the entrained flow gasifier developed in this work

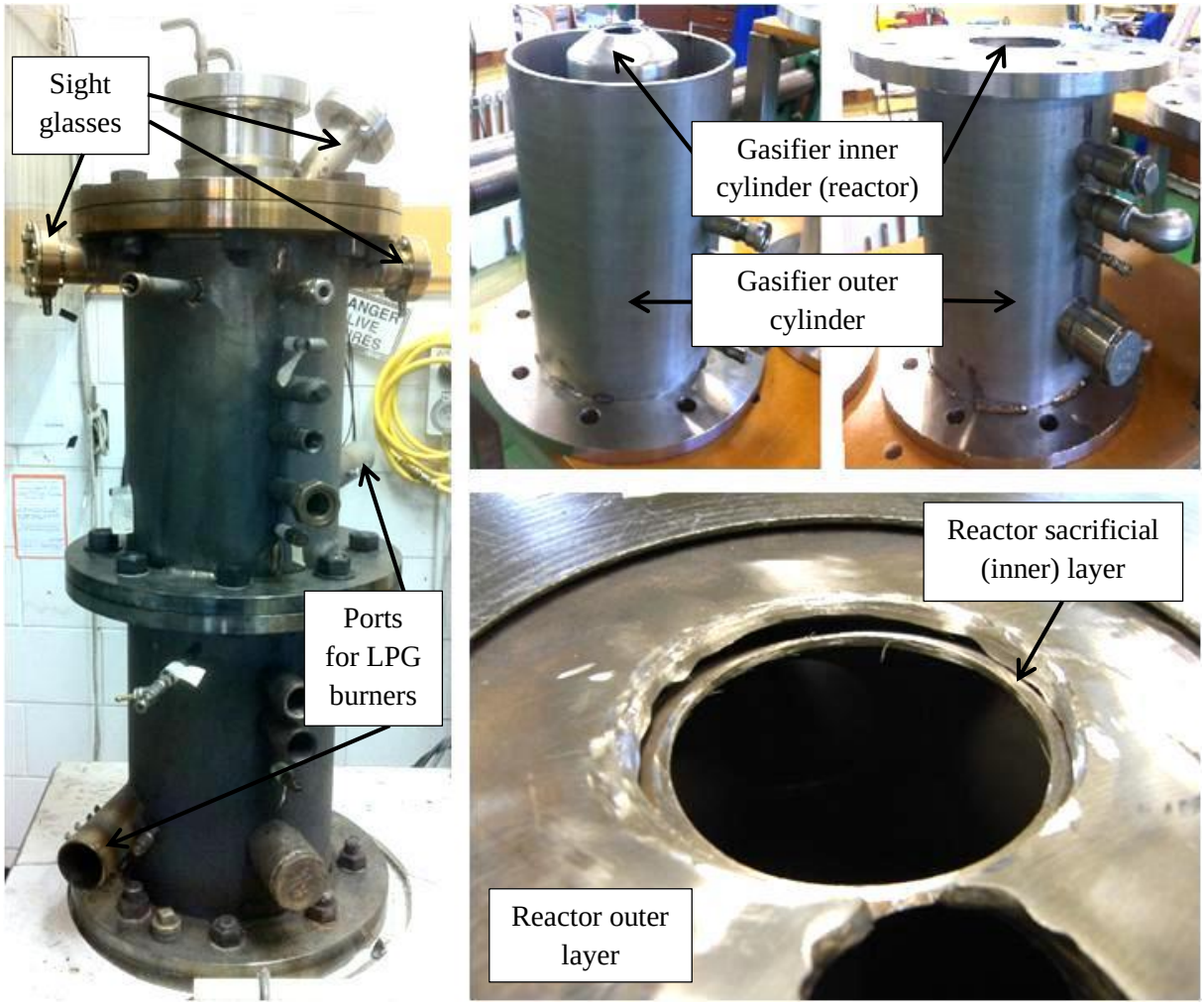

Figure 3–4: Selected photos of the assembled entrained flow gasifier body without insulation layer (Left), top and bottom sections of the gasifier body before assembly (Right top) and gasifier sacrificial layer (Right bottom)

For entrained flow gasification systems that use oxygen as the gasification agent such as that developed in this work, the gasifier reactor could be sub-divided into combustion and gasification zones. Combustion zone is a region near the inlets of pyrolysis oil and oxygen gas where partial combustion of pyrolysis oil takes place. Partial combustion is an important stage of gasification since it continuously supplies heat to the system and directly influences gasification temperature during an operation. The heat generated from pyrolysis oil combustion is also used to compensate significant heat loss from evaporation of water in pyrolysis oil, which otherwise causes rapid decline in the gasifier overall temperature.

Gasification zone, on the other hand is a region following combustion zone in which no oxygen remains; thus conversion of materials, both liquid and gas phases, in this region are dominated by non-oxidation reactions. Since oxygen supply into gasification system is well below stoichiometry, significant fraction of the pyrolysis oil is expected to enter this zone and react to yield high concentrations of gasification products such as H_2, CO and CH_4.

Figure 3–5 illustrates combustion and gasification zones for the entrained flow gasifier developed in this work during its operation. The figure also shows flame resulted from pyrolysis oil partial combustion at the top section of the gasifier (combustion zone) and unconverted pyrolysis oil spray droplets flowing into the gasification zone to involve in non-oxidative reactions and produce gasification products.

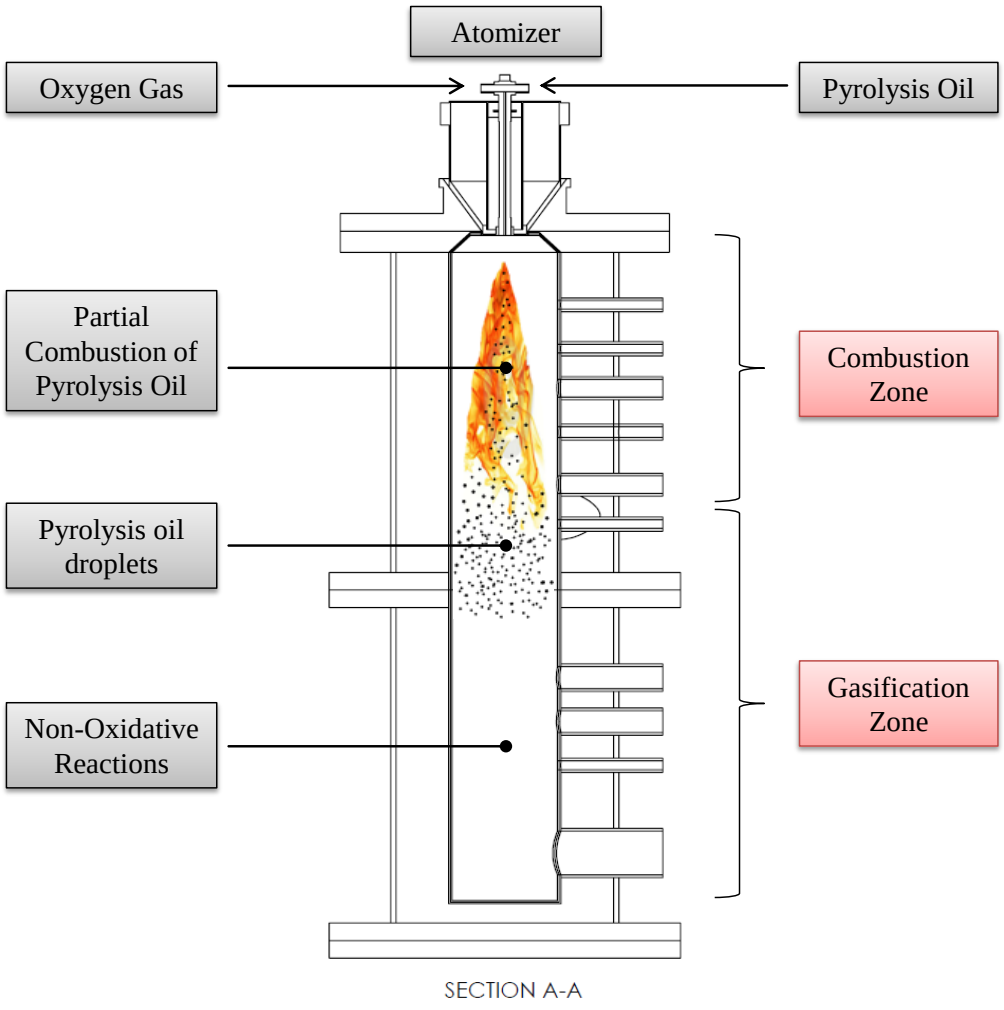

Figure 3–5: Schematic drawing of the entrained flow gasifier developed in this work and different regions involved during its operation.

3.3 Process Schematic Diagram

The overall process flow diagram and photograph of the entrained flow gasification system developed in this work is illustrated in Figure 3–6 and Figure 3–7 respectively.

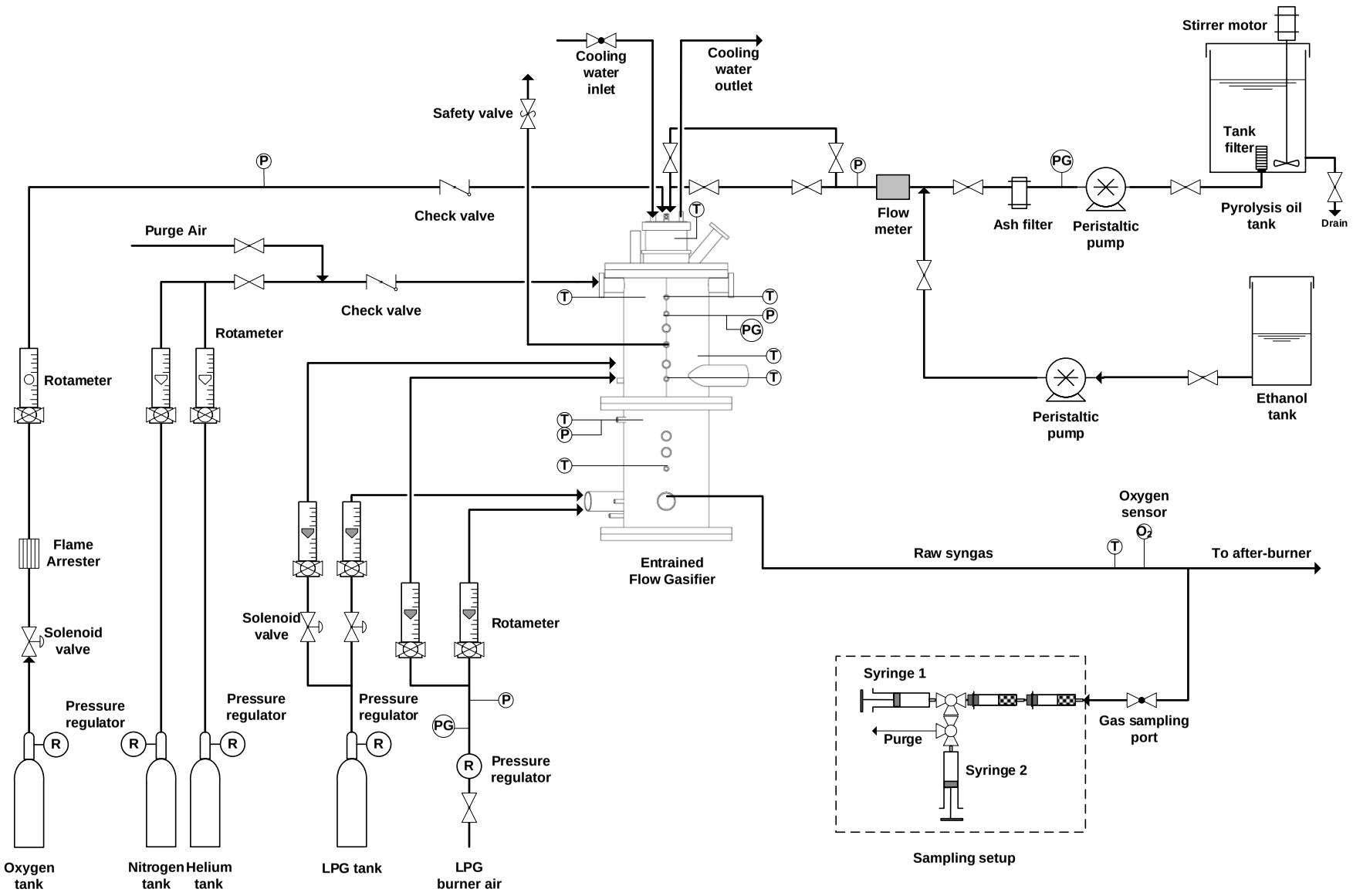

Figure 3–6: Process flow diagram of the entrained flow gasification system used in this work

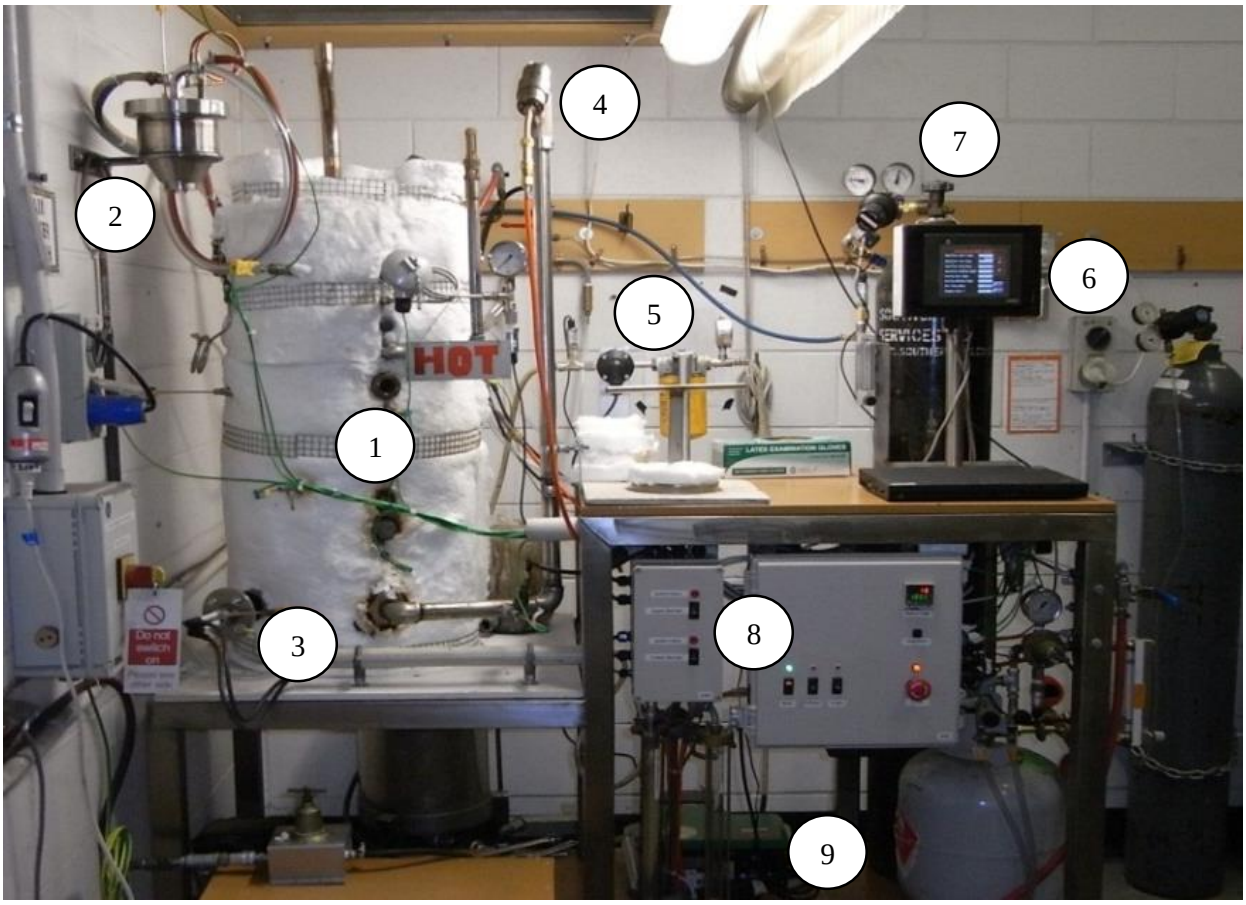

1. Entrained flow gasifier	4. Producer gas after-burner	7. Atomizing gas (oxygen)
2. Atomizer and cooling jacket	5. Oil filter and flow meter	8. PLC and control panel
3. Gas burner	6. Programmable Terminal	9. Peristaltic pump

Figure 3–7: Photograph of the entrained flow gasification system developed in this work

3.4 Gasifier Material Selection

As discussed in Chapter 2, one of the important considerations in design and construction of entrained flow gasification system is the selection of suitable materials for the gasifier. The materials should maintain the required mechanical properties and integrity under high temperatures and corrosive environment. Under such conditions, most materials are susceptible to severe material deterioration.

There are several important aspects of material performance that must be taken into consideration during the selection process, including material creep strength, thermal fatigue, mechanical fatigue, thermal shock, embrittlement and resistance towards corrosion attacks [1]. Amongst all these properties, corrosion

has been found to be the main cause of material failure in many high temperature applications [1], hence this property was taken as the main selection criterion for the entrained flow gasifier material.

In theory, corrosion attack on material occurs as a result of chemical reactions between the material and gases/liquids in its surrounding environment. There are four main corrosion modes that are most relevant to the entrained flow gasification application, which are oxidation, sulfidation, nitridation and carburization. For some materials, oxidation at high temperatures may be useful for formation of passive oxide layers on material surfaces that function as a protection barrier from other more severe and damaging corrosion attacks. The effectiveness of passive oxide layers protecting materials surfaces has given rise to many high temperature resistance alloys containing large percentages of dense oxidative compounds, such as chromium and aluminium, thus features excellent resistance towards corrosion attacks at high temperatures.

A thorough metallurgical study on more than 20 high temperature resistance alloys in typical coal gasification environments was conducted by Wire et al. [2] to investigate individual contributions of erosion and corrosion attacks on the materials deterioration. This work proved severe and potentially catastrophic material deterioration when corrosion and erosion attacks take place simultaneously in a system. This is because depletion of protective oxidation scale was found to be more severe in erosion-corrosion environment than that observed due to pure corrosion. The depth of corrosion penetration measured on materials surfaces were reported to increase dramatically from 5-10μm during pure corrosion environment to as high as 100μm when eroding particles was introduced.

Wire et al. [2] found that the material's corrosion, in terms of penetration depth of chemical attacks, is reduced with increase in chromium content in the alloys as shown in Figure 3–8. Similar findings were reported by Krishnan et al. [3] who studied effects of surface coatings on various materials for coal gasification, where high concentration of oxidizing agent such as chromium or aluminium was proven critical to provide sufficient protective oxide layers on material surfaces during gasification operations [3].

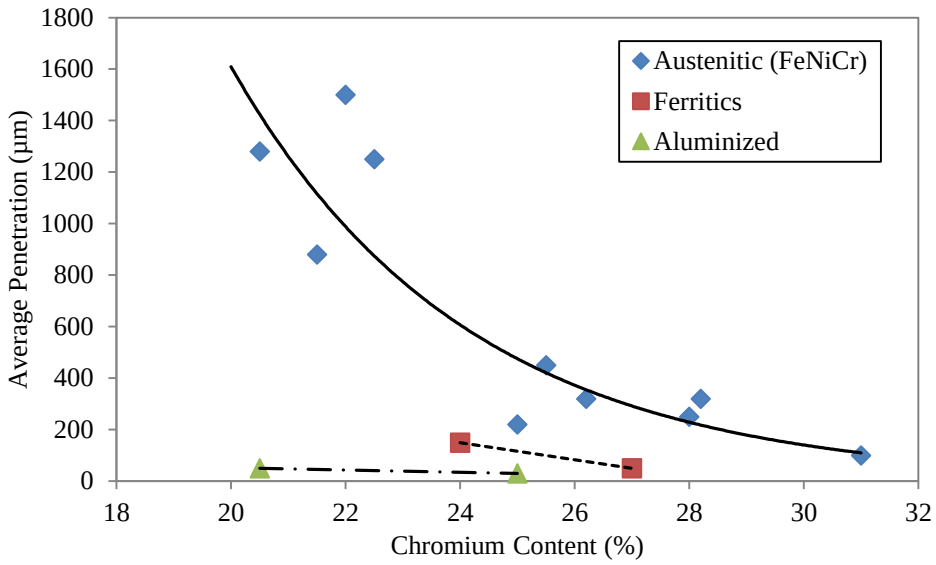

Figure 3–8: Effect of chromium content on corrosion and erosion actions in coal gasification environment at temperatures between 816°C and 982°C [adapted from [2]]

Formation of passive oxide layer is possible in environments with excess oxygen; however, this is not necessarily the case in low oxygen environments such as that expected during non-slagging entrained flow gasification. In relation to this, King et al. [4] showed that even without oxygen surrounding the austenitic alloy, layers of protective chromium oxide on material surface could still be formed at high temperatures with presence of water vapour. This finding was illustrated in Figure 3–9 (c) where oxygen enrichment on the material surface layer at a depth of 250 nm was very significant as soon as water vapour was introduced into the system. Typical chromium–nickel–oxygen composition profiles at the surface of a clean Alloy 690 used in this work were shown in Figure 3–9 (a) and (b) for comparison.

The substantial increase in oxygen content observed in Figure 3–9 (c) corresponds to an increasing amount of chromium oxide coating on the material surfaces, thus it proves oxide layer enrichment by water vapour is possible in non-oxidizing environment at high temperatures. King et al. [4] also found that at high temperatures, excessive water vapour in the system has insignificant impact on the result hence suggesting that sufficient surface oxidation occurs even at low water vapour concentrations.

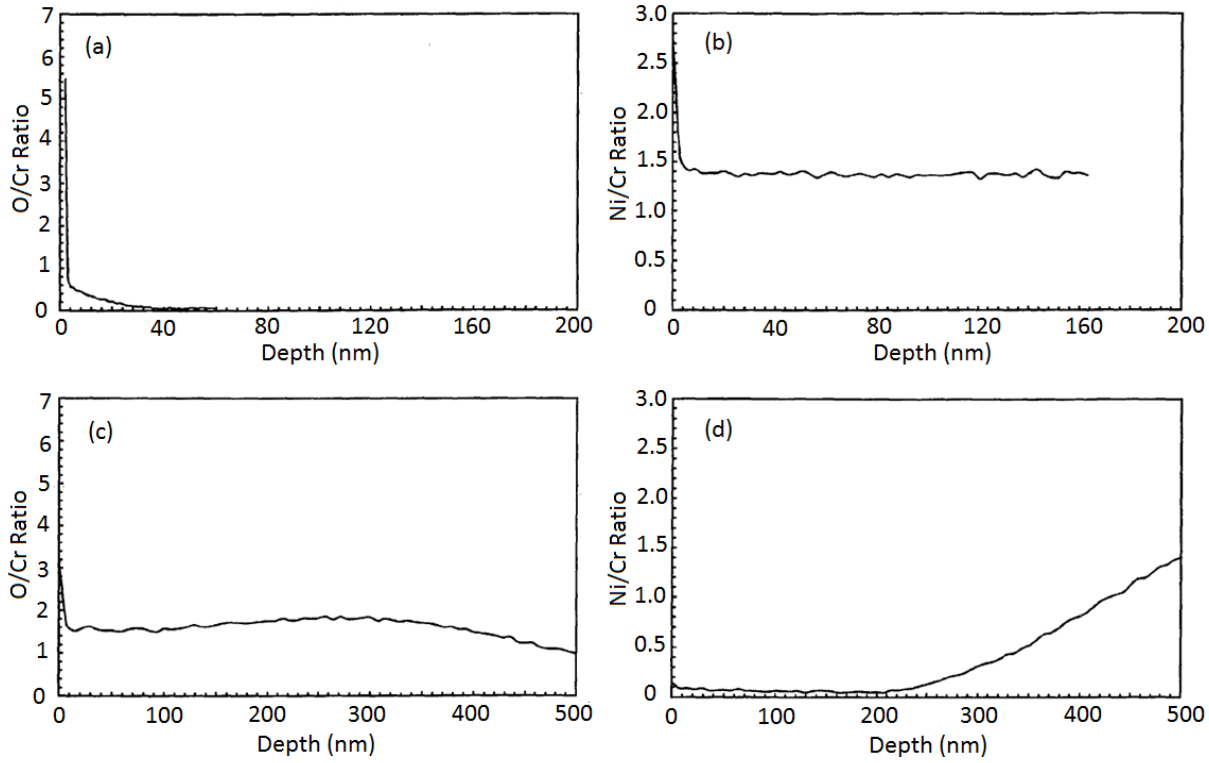

Figure 3–9: Surface composition profile in terms of ratios of O/Cr and Ni/Cr for Alloy 690 (a) and (b) before exposed to water vapour at high temperatures; (c) and (d) after exposure to water vapour at high temperatures. [adapted from [4]]

Besides enrichment in oxidizing agent on material surfaces, reduction of nickel and cobalt contents in high temperature resistance alloys also improves the materials' corrosion resistance by slowing down the formation of liquid sulphides that are harmful to the material. Liquid nickel and cobalt sulphides can be formed at temperatures as low as 635°C and 880°C, respectively [2].

Erosion is also an undesirable phenomenon deteriorating materials at high temperatures. Erosion refers to mechanical wear of a solid material due to physical friction by mixture of solids and liquid or mixture of solid and gas. In gasification, material damage due to erosion is likely considering presence of solid particles such as char, coke and ash in the gasification environment. Figure 3–10 illustrates effects of erosion on the material surface after exposure to high temperature coal gasification environment. It is worth noting the substantial contribution of erosion towards material deterioration caused by debris deposition on the material surface at high temperature.

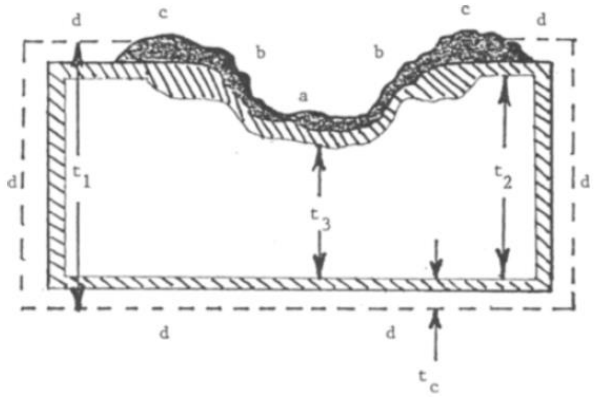

Definitions:

- t_1 = Initial material thickness
- t_2 = Average metal-to-metal thickness due to corrosion only
- t_3 = Thickness at the deepest point inside the crater excluding internal penetration
- a = Crater centre area
- b = Crater inner rim
- c = Crater outer rim
- d = Corrosion only area
- = Erosion-corrosion debris and scales
- = Internal penetration
- = Corrosion scales and internal penetration

Figure 3–10: Effects of corrosion and erosion attacks on material surface in a simulated coal gasification environment. The material surface was exposed to a mixture of alumina, chars and coke as the model erodent [adapted from [2]]

The harsh impact of erodent deposition on materials can be justified by considering harmful elements present in the erodent, such as carbon and sulphur that react to enhance corrosion due to carburization and sulfidation at the material-deposit interface. Further investigations into the material surface morphology also revealed the capability of eroding particles transforming protective oxidation layers from highly protective, dense and oxide–rich surfaces into needle-like, less protective configuration as illustrated in

Figure 3–11. Under these circumstances, the materials are susceptible to severe and potentially catastrophic material failure due to absence of reliable protective oxide layers on the material surfaces [1, 2].

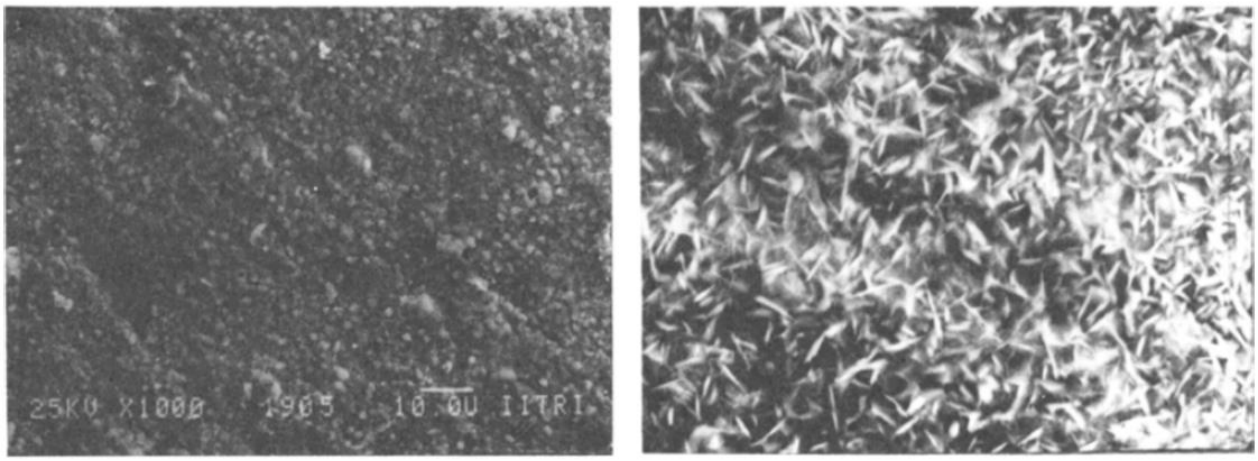

Figure 3–11: Surface morphology of protective oxide layer on 310 stainless steel alloy in pure corrosive gasification environment (a) and when embedded in coke erodent (b) [adapted from [2]]

The list of materials investigated by Wire et al., their compositions and depth of penetrations after erosion-corrosion attack are summarized in Table 3-1.

Table 3-1: List of alloys, their composition and penetration depths after exposure to coal gasification environment at temperature between 816 – 982°C [adapted from [2]]

Alloy	Penetration (μm)		Composition (wt %)				
	Average	Max	Ni	Fe	Co	Cr	W
IN-800	1270	5105	30.8	47.1	0.1	20.6	-
IN-601	1245	5893	59.5	15.9	0.03	22.5	-
HAYNES 150	584	3327	1.4	18	51.5	27.9	-
310	211	864	20	52	-	25	-
446	127	483	0.4	75	-	24	-
HL-40	107	660	19.4	47.1	-	30.9	-
IN-671	53	208	47.8	1.1	-	50.2	-
800 (Al)	51	137	-	-	-	-	-
310 (Al)	41	74	-	-	-	-	-
STELLITE 6B	28	99	2.8	1.9	57.1	28.1	4.8
Co-Cr-W No.1	18	28	-	-	53.5	30	12

Considering lack of information in literature on materials deterioration in biomass pyrolysis oil gasification environment, this study utilizes available facts from the well-studied coal gasification operations as reference. Gasification environment of pyrolysis oil is expected to be less severe compared to that of coal gasification because biomass is generally much cleaner due to its low ash, carbon and sulphur contents [5]. Moreover biomass contains higher oxygen, which helps promote formation of protective oxide layers on the material surfaces [6]. Table 3-2 shows some differences in element compositions between selected biomass species and coals.

Table 3-2: Ultimate analysis of different biomass and coal species [adapted from [6]]

Species	Typical Values					
	Carbon (%)	Hydrogen (%)	Nitrogen (%)	Sulphur (%)	Oxygen (%)	Ash (%)
Coal						
Bituminous coal	55.0	3.7	0.9	0.4	11.5	6.0
Lignite coal	58.8	4.2	0.9	0.5	13.6	22.0
Biomass						
Barley straw	46.9	5.3	0.7	0.1	41.0	5.9
Corn stover	43.7	6.1	0.5	0.1	44.6	5.1
Wheat straw	43.4	6	0.8	0.1	44.5	7.7
Wood bark	47.8	5.9	0.4	0.1	45.4	1.5
Willow	50.1	5.8	0.5	0.1	41.4	2.1
Hardwood	48.3	6.0	0.2	0.0	45.1	0.4

Based on the literature review, an austenitic chromium-nickel 253MA stainless steel alloy was chosen as the main material for the entrained flow gasifier construction in this study. 253MA is characterized by its high structure stability, corrosion resistivity and creep strength at high temperatures. This material contains high chromium content (21%) but low nickel content (11%) hence conforms with material specifications for applications in high temperature corrosive environment as suggested by Wire et al. [2] and Krishnan et al. [3]. Moreover unlike normal stainless steel alloy, 253MA performance has been enhanced through micro-alloying process where cerium and silicon are embedded into its matrix to further improve its resistances towards active oxidation, erosion, corrosion and oxide layer spallation during operation [7].

In comparison to the more readily available high temperature resistant 310 alloy, 253MA is found to be superior. 310 alloy is an austenitic stainless steel alloy that has high chromium and nickel contents thus features good resistance towards oxidation while still maintaining high mechanical strength, machinability and weldability. This alloy features good resistances towards erosion-corrosion attacks in coal gasification environment as presented earlier in Table 3-1. However, 310 alloy did not perform well in cyclic oxidation environment at high temperatures.

The superior performance of 253MA over 310 stainless steel alloy was based on comparative cyclic oxidation tests performed on these materials as well as on several other high temperature resistant materials [7, 8]. In the tests, all of the selected materials were exposed to a temperature of 1150ºC for 24 hours in air and then were cooled down to room temperature. The process of heating and cooling was repeated for a number of times, the mechanical properties and corrosion/erosion was examined. Results from the cyclic oxidation tests were presented in Figure 3–12 from which it is clear that the corrosion rate for 253MA was the least and consistently below 1 mm/year for temperatures of up to 1150ºC [8].

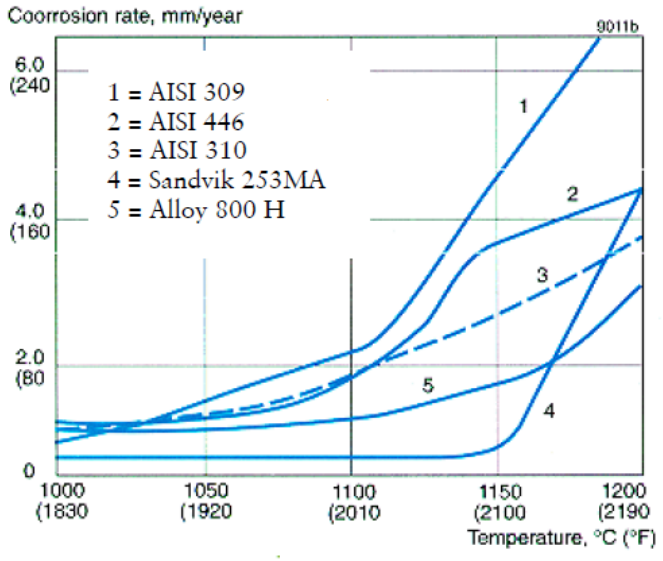

Figure 3–12: Corrosion rate of several high temperature resistant materials in air for cyclic oxidation tests [adapted from [8]]

In addition, 253MA also has superior resistance towards carburization attack. In comparing the resistances of 253 MA and 310 towards carburization, both materials were exposed to hot gas containing 10% methane, 0.5% oxygen and 90% argon for 500 hours at temperatures between 800ºC and 1000ºC. The performance of the materials is quantified by the carbon deposition on the surfaces and the results are

shown in Figure 3–12. Less carbon deposition was found on 253MA surface than that on 310 surface suggesting 253MA has higher resistance towards carburization at high temperatures [8].

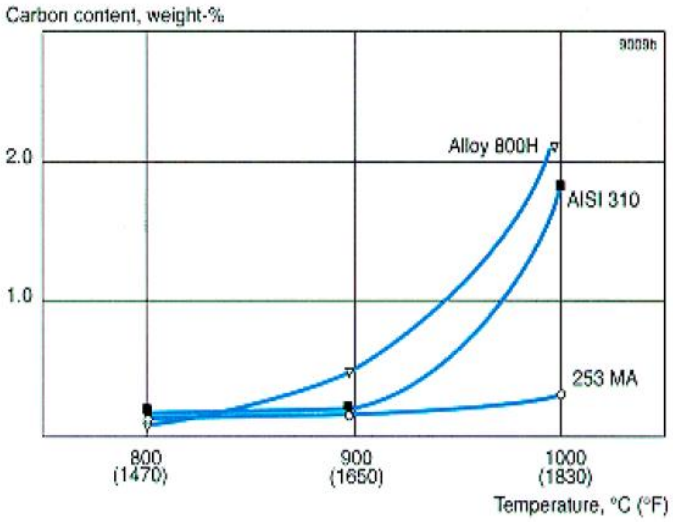

Figure 3–13: Carbon deposition due to carburization of material at different temperatures for 500 hours [adapted from [8]]

3.5 Gasifier Pre-Heating

The entrained flow gasifier must be pre-heated to a suitable start-up temperature prior to a gasification run. The minimum start-up temperature varies depending on auto-ignition temperature of the fuel used in the gasification, which in this work is biomass pyrolysis oil. Auto-ignition temperature is the minimum temperature required for a fuel to burn spontaneously without presence of external ignition source such as spark or pilot flame.

For entrained flow gasification of biomass pyrolysis oil, the start-up temperature is required to be well above its auto-ignition temperature so the pyrolysis oil could ignite and, subsequently, a series of gasification reactions take place. Pyrolysis oil generally contains significant quantity of water; therefore it is common to observe sudden drops of reactor temperature as a result of rapid liquid evaporation. Because of this reason, the amount of heat loss due to liquid evaporation must be taken into account in deciding the minimum start-up temperature, so the gasifier temperature remains sufficiently high to maintain continuous fuel ignition throughout the gasification operation.

In this study the gasifier start-up temperature was set at 750^{o}C, which is sufficiently high to account for variations in pyrolysis oil auto-ignition temperatures due to inconsistent pyrolysis oil properties and decline in gasifier temperature due to evaporation of water. The start-up temperature was chosen after proven suitable based on a number of gasification runs performed throughout this work.

In order to achieve the targeted start-up temperature, the gasifier is equipped with two independent LPG burners, where one burner is located at the top section and another burner in the bottom section of the gasifier. The burners are fixed at 45° from the gasifier tangential direction to induce swirling flames and so the hot gas from the burners can heat the hollow space between the inner and outer cylinders of the gasifier effectively. In addition, baffle plates are also used in the space to help increase the heat transfer from the flue gas to the reactor wall. The top and bottom cavity sections of the gasifier are interconnected by six symmetrical holes to facilitate flow of hot flue gas across the gasifier length. Thick insulation layers are wrapped around the gasifier body to minimize heat loss throughout the gasification operation. Illustration of the burner locations and pre-heating area of the gasifier has been given earlier in Figure 3–1.

After completion of the gasifier construction, commissioning was undertaken to check if the gasifier pre-heating system could perform as required. Figure 3–14 shows an example of gasifier temperature profiles in the gasifier pre-heating space and inside the reactor during start-up from one gasification experiment. The aimed start-up temperature of 750^{o}C was achieved within only an hour of pre-heating, while higher temperature could be achieved with longer pre-heating time. This example confirms that using LPG burners for pre-heating of the gasifier is satisfactory as it provides rapid temperature increase to fulfil the system's heating demand.

From Figure 3–14, it is also observed that the temperatures inside the gasifier reactor was very close to those in the pre-heating area, suggesting highly efficient heat transfer across the gasifier during the pre-heating stage.

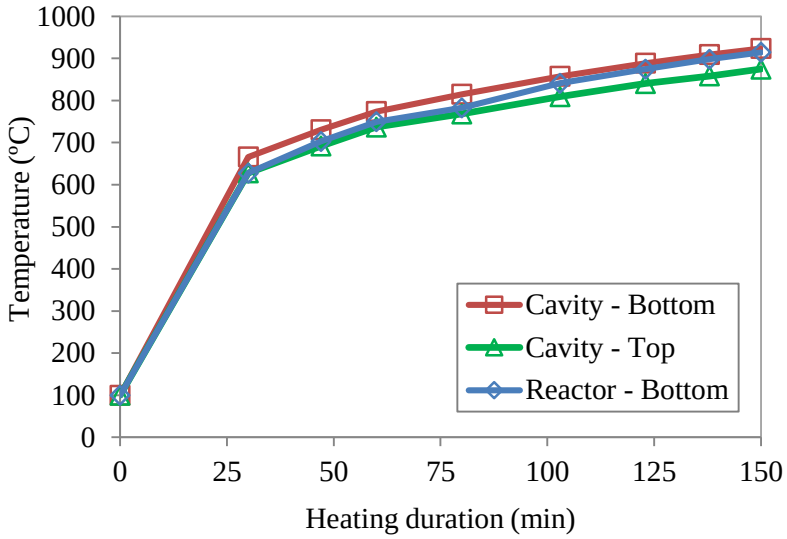

Figure 3–14: Start-up temperature profiles for entrained flow gasifier system developed in this work

3.6 Pyrolysis Oil and Oxygen Gas Feeding System

Pyrolysis oil and oxygen gas were fed into the system through an external mix twin-fluid atomizer. Pyrolysis oil feeding was done using a Watson Marlow peristaltic pump, which capable of delivering up to 2000 mL/min of liquid flow. Prior to gasification run, the required amount of pyrolysis oil was transferred into a stirred tank that can hold as much as 40L of oil at a time.

There are two particulate filters installed in the oil feeding system to eliminate solids from the oil. The first filter is installed at the outlet of the oil tank with capability of filtering solids above 100µm. The second filter, on the other hand, is installed on-line, after the peristaltic pump and capable of retaining much finer particles, as small as 10µm. In addition to these filters, the pyrolysis oil used in this work has also been pre-filtered at high temperature during its production thus has low solid content. A positive displacement flow meter is installed after the pump so that accurate flow rate measurements could be obtained at any point during experiment. The pump, filters, flow meter and atomizer are inter-connected by high resistance platinum-cured silicon tube of inner diameter 8.0mm and 2.4mm wall thickness for protection towards chemical degradation caused by pyrolysis oil.

In this work, pyrolysis oil feeding rate was not directly controlled, rather it depends on the peristaltic pump speed (measured in terms of revolution per minute, RPM), the oil viscosity, the atomizer liquid outlet diameter and pressure build-up across the on-line filter. Due to these interrelations, the pyrolysis oil

feeding rate could not be set constant hence vary significantly with operation time and between different gasification runs.

The oxygen feeding system, on the other hand, consists of an Industrial Grade oxygen cylinder (>99.5% purity), a flame arrester, a rotameter and a checked valve. The flow rate of oxygen gas feeding into the system was controlled by the rotameter which capable of supplying up to 4000 L/h of gas with accuracy of ±100 L/h. The oxygen flow rate measured by the rotameter were corrected based on the gas supply pressure and temperature.

3.7 Atomizer and Cooling Jacket

The atomizer used in this study is of model 1/4J SUE15B manufactured by Spraying Systems Co, which capable of producing fine liquid droplets with a flat spray pattern. The external mix configuration of the atomizer allows for adjustment of pyrolysis oil flow rate and oxygen flow rate independently for achieving desirable atomization. Flat spray pattern was chosen for the system as it is believed could improve mass and heat transfers between spray droplets and gasification environment.

Figure 3–15 shows close-up images of two main parts of the atomizer nozzle assembly to illustrate pyrolysis oil atomization mechanism and oil-oxygen mixing configurations. The ‘air cap’ and ‘liquid cap’ used in this study are of the model PA67228-45^{o} and PF1650, respectively. For this atomizer setup, liquid fuel exits the atomizer nozzle through the hole of 0.41 mm in diameter located at the tip of the atomizer liquid cap while atomizing gas exits the atomizer at high velocity through the three openings on the air cap. The impact between high velocity gas and the liquid breaks the liquid into fine spray droplets. Note that the middle hole on the air cap is where the liquid outlet tube of the liquid cap slots in, while leaving a narrow ring gap between the two parts for atomizing gas to flow and assist liquid atomization.

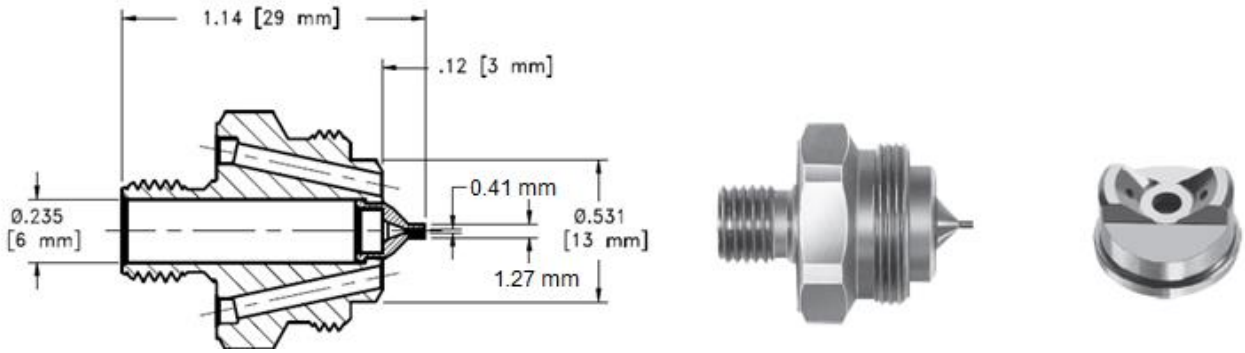

Figure 3–15: External mix 1/4J SUE15B atomizer for flat spray pattern. Left Image: Cross section view and dimensions of the atomizer liquid cap; Middle Image: Atomizer liquid cap; Right Image: Atomizer air cap

The atomizer's air cap and liquid cap are made of Hastelloy C-276 alloy to withstand high temperature and corrosive environment during gasification operation. This alloy contains 57% nickel, 16% chromium and 16% molybdenum and features good resistance to corrosion attacks in both oxidizing and reducing environments. The melting point of the material is 1350^{o}C. Other parts of the atomizer body, however, are made of 303 grade stainless steel alloy since they are not directly exposed to gasification harsh atmosphere.

The basic atomizer configuration supplied by the manufacturer was modified for exposure to high temperature conditions in the entrained flow gasification. In the modified system, the atomizer is surrounded by a specially designed water cooling jacket so it remains at low temperature throughout gasification operation thus avoiding undesirable pyrolysis oil polymerization within the atomizer. Polymerized pyrolysis oil could lead to severe blockage of the atomizer liquid passage and is difficult to be cleaned without disassembling of the whole atomizer and cooling jacket assembly. An extension tube is also added to the atomizer body to increases the total contact area between the atomizer and cooling water so that heat transfer rate is enhanced. Figure 3–16 shows cross section drawing of the cooling jacket and approximate location of the atomizer after assembly.

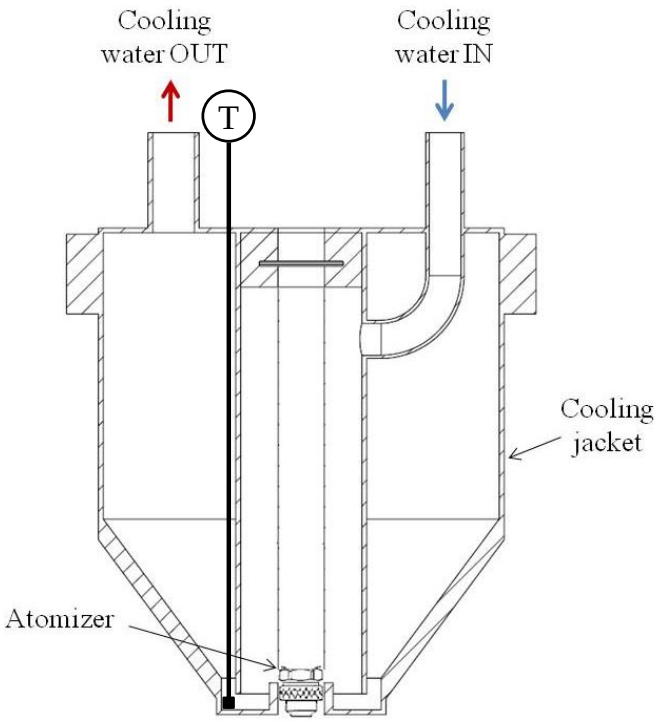

Figure 3–16: Cross section drawing of cooling jacket and atomizer assembly during gasification run

Figure 3–17, on the other hand, shows photos of the cooling jacket and atomizer assembly, as well as where it fits on the top of the entrained flow gasifier during operation. Note that the bottom section of the cooling jacket was purposely designed in conical shape for easy installation or removal from the gasifier body when required. The removal of the atomizer assembly is preferred during preheating period to avoid unnecessary heating of the atomizer when no pyrolysis oil or oxygen gas is fed to the gasifier. Once the preheating is completed, the atomizer and cooling jacket assembly are put back to place in the gasifier body; when the pyrolysis oil and oxygen gas are ready to be fed into the gasifier.

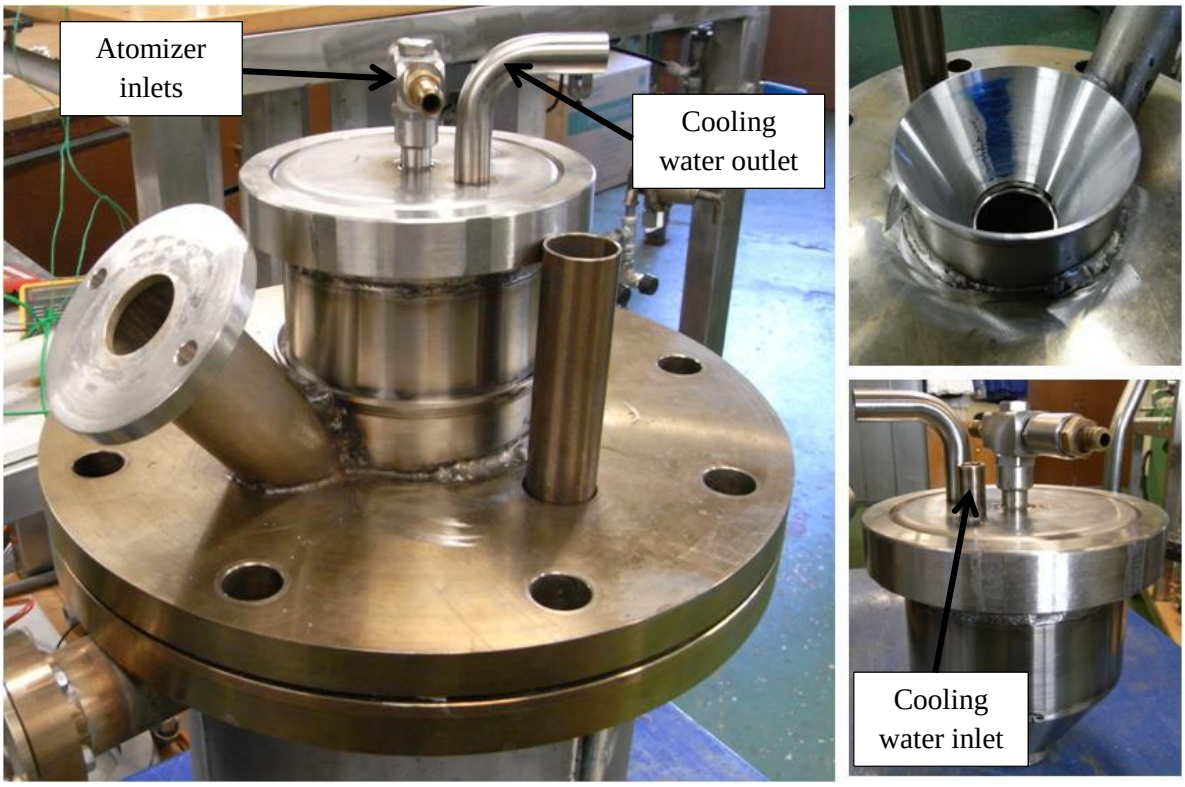

Figure 3–17: Photos of atomizer and cooling jacket location during gasification operation (Left), Cooling jacket slot on gasifier top (Right top), and Cooling jacket and atomizer assembly (Right bottom)

In addition, after the atomizer is placed in the gasifier, continuous flow of inert gas (nitrogen gas) is also bleeds through the atomizer to cool down the atomizer. When the temperature is stable, the nitrogen flow is stopped and feedings of oxygen and pyrolysis oil are initiated to start gasification. In order to further reduce the temperature of the atomizer during the gasification, effects of convective and radiative heat transfers from the hot gasification reactor to the atomizer are also minimized by reducing the atomizer total surface area exposed to the reactor.

The modified atomizer and cooling jacket assembly have satisfactorily reduced the atomizer temperature to a level so that there is no damage was observed on the atomizer after gasification operations. Cooling water temperature near the nozzle tip was found to be consistent between 25-30^{o}C throughout gasification operations.

3.8 Product Sampling

Products (mainly producer gas) from the gasification exit the gasifier through a port located at the bottom of the gasifier. The temperature of the product line usually remains between 450-600ºC depending on the operation temperature of gasification. For sampling purpose, a horizontal sampling port is created on the main product line so samples can be taken directly from the main product stream. To prevent condensation of tar compounds during sampling, the probe used for sampling is positioned at the centre of the stream so temperature difference between the probe and the producer gas are minimised. This is to make sure that any condensable products generated by the gasification process remain in vapour state and only condense after they are inside the sampling probe. Condensation of products outside the probe will lead to unaccounted loss of important compounds in the producer gas such as tars. In addition, the sampling probe length is kept as short as possible to maximize adsorption of the condensable products in solid phase extraction (SPE) columns.

The detailed arrangement of the product sampling assembly is illustrated in Figure 3–18. The sampling rod is 90mm long and inserts through the sampling valve. Two SPE columns with different packed materials are used to make sure that the final gas samples collected are free from condensable compounds such as water and tars, which are harmful to analytical instruments like Micro-GC. The other end of the SPE columns is connected to a 100mL syringe via a three way valve for manual gas extraction. One end of the valve is connected to another syringe (60mL) specially allocated for Micro-GC samples, so the main 100mL syringe does not need to be removed from the main sampling probe during gas analysis. During product sampling, 300-700 mL of producer gas is extracted from the system by the 100mL syringe, through many repetitions, aimed to trap as much condensable compounds in the SPE columns as possible for subsequent analyses.

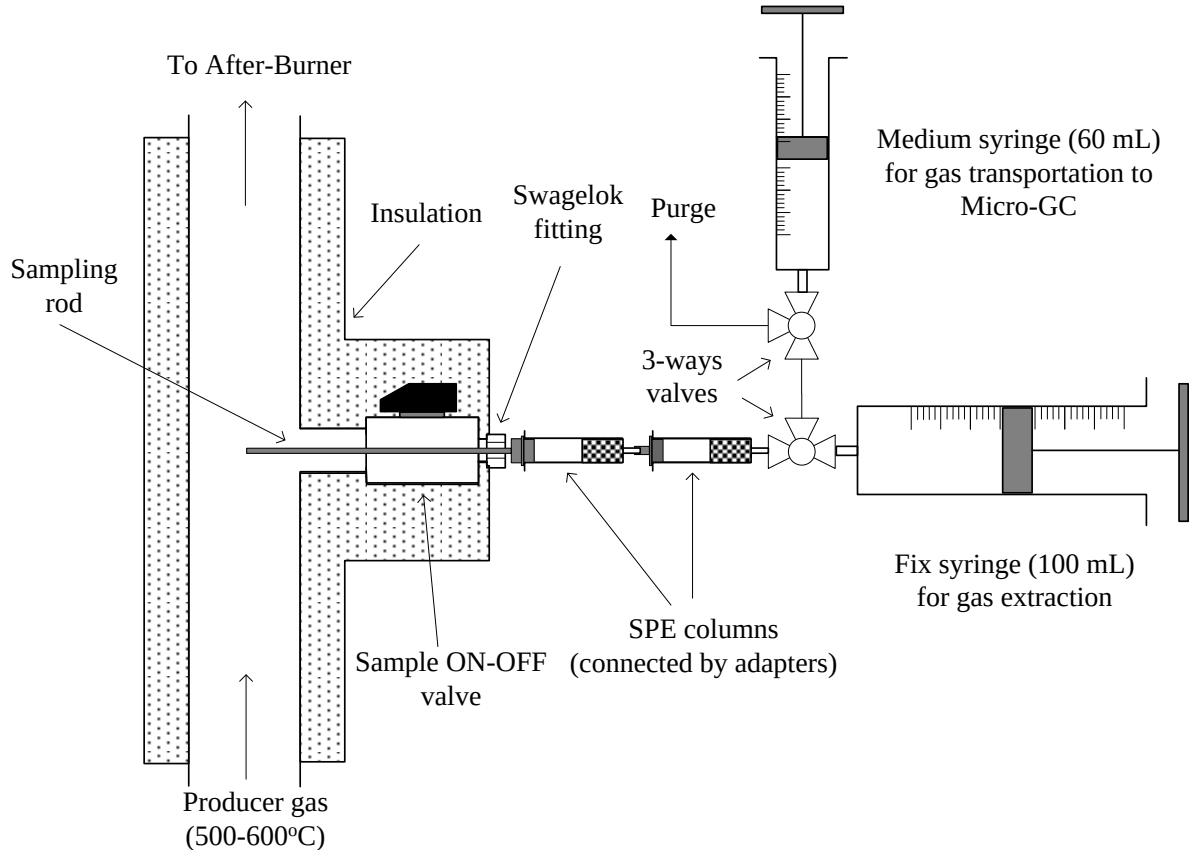

Figure 3–18: Illustration of sampling arrangement for entrained flow gasification system in this work

The first SPE column used to capture condensable products in this study is a model of Supelclean LC-Si column with packing of a silica gel based material with no bonded phase hence is extremely hydrophilic. The second SPE column is a model of Supelclean LC-NH_2 column with packing of a silica gel based material bonded with aminopropyl active group. This column was aimed for strong adsorption of polar, weak anion and organic acid compounds. Both SPE columns are supplied by Sigma-Aldrich.

As gas samples containing condensable products passes through the SPE columns, the condensable products are adsorbed on the packed material in the column and remain in the column until they are later flushed out with appropriate extracting solvents. After samples are taken, SPE columns containing condensed products are removed from the sampling assembly, labelled, sealed and stored at around 4ºC in a refrigerator until subsequent product extraction and analysis. Detailed descriptions of tar extraction and analysis method used in this work will be presented in Chapter 4.4 of this thesis.

With this sampling arrangement, product gas collected in the syringes is free of solids and condensable compounds. This is important because the Micro-GC used to analyse producer gas composition does not

tolerate condensable vapours, aerosols, liquid and solid particles. From the Micro-GC analysis, molar percentages of H_2, N_2, He, CH_4, CO, CO_2, C_2H_4 and C_2H_6 species at dry basis are determined. A more detailed description of the Micro-GC used in this work will be given in Chapter 4.2 for reference.

3.9 Automatic Safety Control and Responses

Entrained flow gasification is regarded as a high risk operation since it involves the use of combustible liquid, LPG gas and pure oxygen gas at elevated temperature. It was learnt that lack of careful plan, technical considerations and appropriate control measures for the gasification operation could lead to hazardous conditions, such as overheating, oxygen enrichment environment, CO poisoning and explosion.

Acknowledging the potential risks, a comprehensive Hazard and Operability (HAZOP) analysis was performed on the entrained flow gasification system developed in this work to account for possible hazards that could take place during its operation and methods to minimize the risks. A complete report of the HAZOP analysis is included in Chapter 10: Appendix A of this thesis for further reference. Technical drawings and the complete operating procedures for the entrained flow gasification system after HAZOP considerations are presented in Chapter 10: Appendix B and Appendix C respectively.

For added safety measures, the system is equipped with a Programmable Logic Control (PLC) to enable automatic safety responses in the event of unexpected deviations from the intended operating conditions. The list of responses programmed into the PLC is as follows:

1. Oxygen, LPG and pyrolysis oil supplies to the gasifier are automatically blocked if extraction fan is not switched ON. Extraction fan ensures good ventilation in the gasification site, thus helps to avoid accumulation of hazardous gas (mainly carbon monoxide) at any stage during the process.
2. Supply of LPG to gas burners is automatically cut when flame extinguishes. This avoids accumulation of LPG in the system which could lead to risk of serious explosion upon burner re-ignition at high temperature.
3. LPG gas burners switch to ‘Lock-Out’ mode after three fail ignition attempts to allow sufficient time for LPG gas purging out from the system. This measure prevents continuous attempts of re-igniting the burners which is the main source of significant LPG accumulation in the system.
4. Warning alarm is triggered when there is sudden decrease in burners air supply, indicating potential release of high carbon monoxide gas due to lack of air supply during combustion (rich combustion).

5. Oxygen and pyrolysis oil supplies to the gasifier are automatically stopped when temperature inside gasifier drop below the set minimum temperature (500^{o}C). This ensures continuous combustion of the pyrolysis oil during operation to avoid accumulation of unreacted oxygen gas in the system. This control also prevents pyrolysis oil from flooding the gasifier when the oil fails to ignite due to gasifier low temperature.
6. Oxygen, LPG and pyrolysis oil supplies to the gasifier are automatically stopped when temperature inside gasifier exceeds the set maximum temperature. This helps to avoid mechanical failure of the reactor construction material which could lead to other potential hazards.
7. Oxygen and pyrolysis oil supplies to the gasifier are automatically stopped when there is pressure build-up in oxygen gas supply stream. This condition indicates partial or total blockage of the oxygen feeding system.
8. Oxygen and pyrolysis oil supplies to the gasifier are automatically stopped when there is very low pressure in oxygen gas supply stream, suggesting serious leak or no oxygen supply into the system.
9. Oxygen and pyrolysis oil supplies to the gasifier are automatically stopped when there is pressure build up in the pyrolysis oil supply stream. This condition indicates partial or total blockage of the atomizer liquid outlet, or serious blinding of the on-line ash filter.
10. Oxygen and pyrolysis oil feed to gasifier are automatically stopped when oxygen sensor detects oxygen concentration above 5% in the producer gas. This is the primary measure of identifying presence of excessive amount of oxygen gas in the system during gasification.
11. Warning alarm is triggered when there is an increase of gasifier pressure due to partial or complete blockage of producer gas outlet.

All these safety actions trigger unique alarm sounds, indicating different warning levels and types of responses produced. These warning levels are described in more details in Table 3-3.

Table 3-3: Different alarm levels and automatic safety responses integrated in the entrained flow gasification system developed in this work to provide various warnings to operator

Warning Level	Alarm Type	Automatic Response
1	Single Long Beep	None
2	Repeated Short Beeps	None
3	Repeated Short Beeps	Cut LPG supply
4	Single Long Beep	Cut oxygen and oil supplies
5	Repeated Short Beeps	Cut oxygen and oil supplies
6	Continuous Beep	Cut oxygen, LPG and oil supplies

Each component of the automatic safety control system was individually checked and tested during the development stage by purposely inducing relevant operational deviations under controlled conditions. This was to check for their functions in respond to relevant deviations as programmed into the PLC. In addition during gasification runs throughout this study, various alarms and automatic responses were triggered thus verify the effectiveness of the automatic safety control minimizing potential risk during the gasification operation.

An EMERGENCY STOP button is also available near the system to force stop supplies of oxygen, LPG and pyrolysis oil into the gasifier in the event of emergency. When the emergency button is pressed, burner compressed air supply into the system remains enabled to help cooling the gasifier.

3.10 Feedstock

3.10.1 Pyrolysis oil properties

The pyrolysis oil used in this study was obtained from a local company, Alternative Energy Solutions (AES) Ltd, who has a demonstration scale fast pyrolysis plant to produce pyrolysis oil from radiata pine wood chips. The wood chips are fed into an auger-type pyrolysis reactor at temperature below 500^{o}C, while the residence time was kept below 4.5 seconds. During the period of this study, the fast pyrolysis plant was in its commissioning stage thus various improvements were made to the system and pyrolysis oil was typically delivered in small batches (20 litres).

Due to variations in the fast pyrolysis operation conditions during pyrolysis oil production, properties of the oil generated by the company usually also differ significantly from one supply to another. A single gasification run may consume up to 20 litres of oil hence repetition of runs using pyrolysis oil with similar properties was often not possible. In addition, due to modifications and technical challenges related to entrained flow gasification development and operations, the pyrolysis oil often needed to be stored for a period of time in lab until use. The prolonged storage may cause inconsistency and changes in properties of the pyrolysis oil between gasification runs.

Measurements of the oil properties were conducted for every new arrival of pyrolysis oil supplies; then followed by periodical measurements so changes of the oil properties due to ageing were recorded over time. Summary of pyrolysis oil properties used throughout this work are summarized in Table 3-4.

Table 3-4: Summary of relevant pyrolysis oil properties used in this work

Ultimate Analysis (wt%)			H_2O (wt%)	Density (kg/m^3)	Viscosity (cSt)	pH	Heating Value (MJ/kg)
C	H	O					
27.2 – 46.7	± 7.7	45.6 – 64.9	15 – 42	1160 – 1220	8 – 690	2.9 – 3.2	± 16

The elemental composition of carbon in pyrolysis oil (C wt%) was measured using a TOC analyser. In this study, the hydrogen content (H wt%) was found to vary insignificantly with an average value of 7.7 wt%. The consistency of hydrogen content between different production batches is believed to be related to consistent hydrogen content in the feedstock, radiata pine wood chips, for fast pyrolysis process. Oxygen content in pyrolysis oil (O wt%) was determined by difference between carbon and hydrogen contents in the oil based on the wood chip composition. Other trace species such as sulphur and nitrogen were also detected in the biomass pyrolysis oil; however, these are not reported due to their low contents.

3.10.2 Pyrolysis oil ageing

It is clear from Table 3-4 that pyrolysis oil properties vary significantly throughout the duration of this work. These variations result from differences in the operations of fast pyrolysis process during the oil production, as well as due to changes in the oil properties due to ageing. In order to understand effects of ageing on the oil properties, series of experiments were conducted to investigate changes of important

pyrolysis oil properties such as water content, viscosity, pH and density; upon storage at room temperature for an extended period of time.

For this purpose, properties of three pyrolysis oil samples were recorded over 80 days period starting from the day the oil was received from the supplier. Nonetheless the actual life of the oil prior to delivery was not specified by the supplier. All the oil samples were stored in closed, gas tight containers throughout this period. Results and analysis of the oil properties behaviour with storage time are presented in the following sections:

3.10.2.1 Water Content

The water content of the pyrolysis oil used in this study was measured using Karl Fischer titration method (ASTM E203). The titration reagent used during the measurements was supplied by Sigma Aldrich and of model HYDRANAL Composite 5, which contains mixture of all chemicals required for the titration including iodine, sulphur dioxide and an organic base. The complete procedure for pyrolysis oil water content measurement is given in Chapter 10: Appendix D for reference. Results from the water content measurement are presented in Figure 3–19.

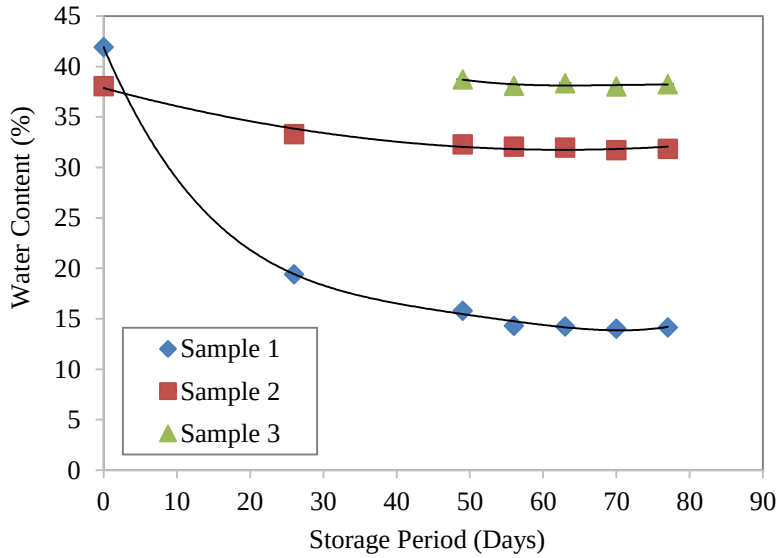

Figure 3–19: Pyrolysis oil water content when stored in gas tight containers for 80 days at room temperature

The figure shows rapid decline of water content in pyrolysis oil samples in the first 50 days of the oil storage. Water content of pyrolysis oil Sample 1 declined from 42% to 16%, indicating as much as 66% decline in the original water content. Smaller decline was observed in Sample 2, in which the water content dropped from 38% to 32%, accounting for 16% decline from the original value. In both cases, water contents become reasonably constant when stored for more than 50 days at room temperature. At this point, the water content of pyrolysis oil Sample 1 Sample 2 and Sample 3 stabilized at 14%, 31% and 38% respectively, regardless of the storage time.

It is interesting to highlight that the trend observed in these results are opposite to that normally reported in the literature. In general, water content of pyrolysis oil usually increase with storage time [9, 10]. To explain this unique trend, it is important to acknowledge the fact that during ageing, various types of reactions could take place in the pyrolysis oil that contributes to the overall change of the oil properties. Some of the reactions generate water such as that during etherification, esterification, condensation and acetalization; while other reactions consume water such as during hydration and homopolymerization. Because of this, the final water content in pyrolysis oil is determined by which of the two types of reactions is more dominant [10, 11].

Based on the trends observed in Figure 3–19, it is possible that water consuming reactions are more dominant during the ageing process thus reduces the final water content in the pyrolysis oil. Nevertheless, further investigations are required to fully explain the unique trend found for pyrolysis oil water content in this work.

3.10.2.2 Viscosity

In this work, viscosities of the pyrolysis oil were measured using glass capillary viscometer (ASTM D445 and ASTM D446). Several types of capillary viscometers were used for this analysis to cover pyrolysis oil large viscosity range, including the Cannon-Flask Routine #150, #200 and #300; BS/U-F and BS/IP/RF #5 viscometers. Viscosity range for each of these capillary viscometers is given in Table 3-5. The complete procedure for pyrolysis oil viscosity measurement is given in Chapter 10: Appendix D for reference.

Table 3-5: Types of capillary viscometer used in this work and their viscosity ranges

Viscometer Type	Cannon-Flask Routine			BS/IP/RF	BS/U
Viscometer Size	150	200	300	5	F
Viscosity Range (cSt or mm^2/s)	7-35	20-100	50-250	60-300	200-1000

Results from the pyrolysis oil viscosity measurement over a period of 80 days are presented in Figure 3–19. There was a rapid increase in pyrolysis oil viscosity for Sample 1 in the first 50 days of storage, in which the viscosity value increased from 25 cSt to approximately 470 cSt during this period. Then the oil viscosity stabilized at around this value regardless of the storage time. This trend is opposite to that observed for Sample 2 where the oil viscosity declined slightly from 36 cSt to 23 cSt over the 50 days period, and remained at this value with further increase in the storage time.

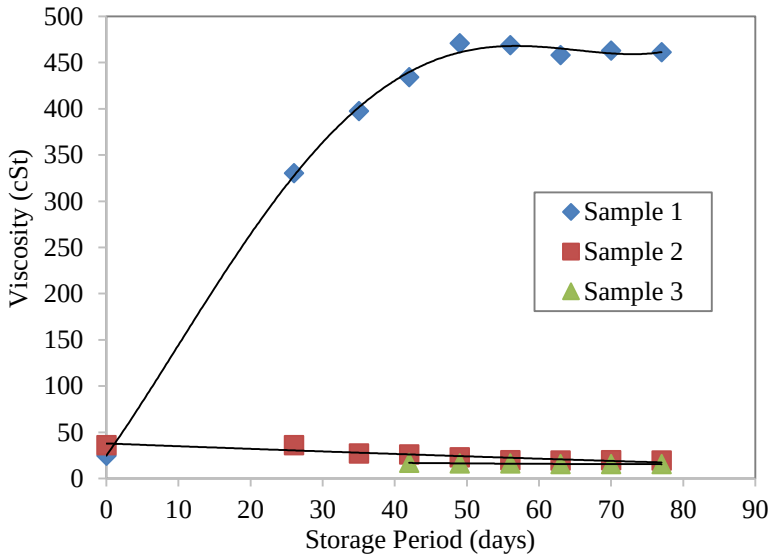

Figure 3–20: Changes in pyrolysis oil viscosity when stored at room temperature for 80 days

In general, increase in pyrolysis oil viscosity results from polymerization of various compounds in the oil. Increase of pyrolysis oil viscosity upon storage has been reported widely in the literature as discussed in detailed in [9, 11, 12]. The rapid increase in Sample 1 viscosity during the first 50 days of storage also associates with the significant decline in the oil water content as discussed in the previous section (Chapter 3.10.2.1).

On the other hand, the slight decline in Sample 2 viscosity may indicate insignificant polymerization reactions of the pyrolysis oil components during storage. Disagreement between Sample 1 and Sample 2 viscosity behaviour may result from variations in the pyrolysis oil initial physicochemical properties after fast pyrolysis process, which lead to different extent of ageing reactions even when both samples are stored in the same environment. Separate investigations are required in the future to explain the differences in pyrolysis oil viscosity trends such as that shown in Sample 1 and Sample 2 of this test.

3.10.2.3 Acidity

Pyrolysis oil acidity is measured in terms of pH and was determined using a pH meter. The complete procedure for pyrolysis oil pH measurement is given in Chapter 10: Appendix D for reference. In this test, pyrolysis oil pH was only measured from day 26th of storage. Results from pyrolysis oil pH measurements are summarized as in Figure 3–21.

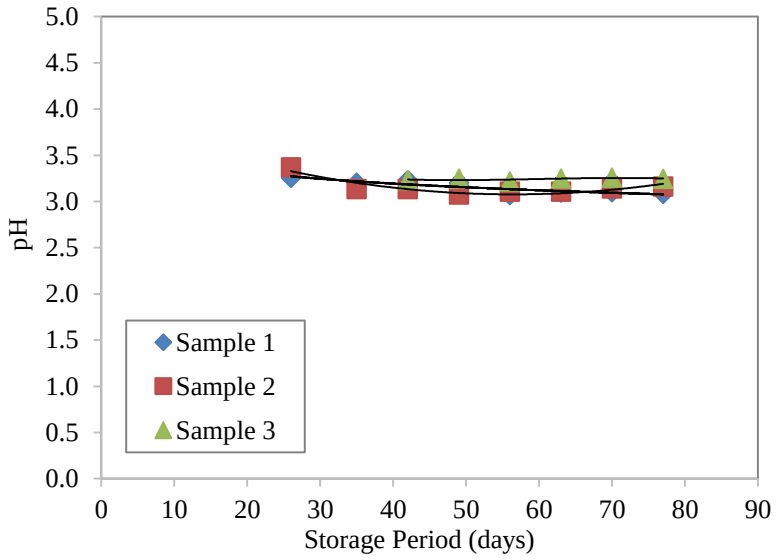

Figure 3–21: Pyrolysis oil pH values upon storage at room temperature

It could be seen from the figure that pyrolysis oil pH values vary insignificantly for all three samples throughout the test period. This trend is different from that usually reported in the literature where pyrolysis oil becomes more acidic with storage time as a result of oxidation reactions of alcohols and aldehydes components of pyrolysis oil [11]. With the pyrolysis oil used in this study, it is possible that oxidation reactions were not significant partly due to the oil storage in air tight containers, hence lead to stable pH values regardless of the storage time.

3.10.2.4 Density

Density of pyrolysis oil was measured using Anton Paar DMA60 digital density meter (ASTM D4052). Density of was determined based on oscillation frequency of constant volume U-tube located in the density meter, in which the oscillation frequency varies based on mass of pyrolysis oil hold by the U-tube during measurement. The complete procedure for pyrolysis oil density measurement is given in Chapter 10: Appendix D for reference.

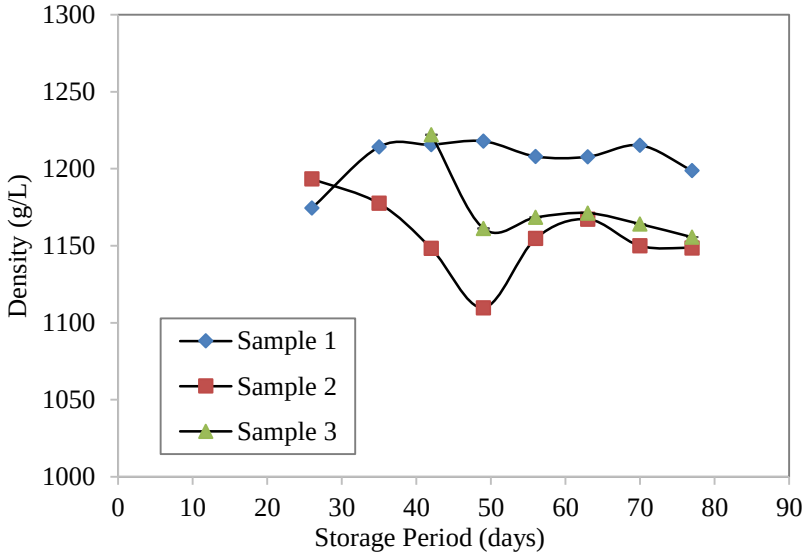

Figure 3–22: Pyrolysis oil density upon storage at room temperature

Results from pyrolysis oil density measurements show inconsistent trends between all the samples tested. The density of Sample 1 varies between 1170 g/L and 1220 g/L throughout the test duration. On the other hand, the density of Sample 2 varies from 1110 g/L to 1190 g/L during the test. There is no indication of any common trend between all three samples used for this test to justify pyrolysis oil density changes upon storage. Because of this reason, it is important that density of pyrolysis oil is measured prior to use in entrained flow gasification, to minimize errors associated with the operations.

In overall, results from pyrolysis oil ageing behaviour conducted in this study showed large variations in the oil properties upon storage at room temperature, particularly for the first 50 days period. After this period, the oil became more stable and less affected by further increase in storage time. An exception to this was with the oil density, in which the values did not show any clear trend during the storage period. Variations to the oil behaviour from one sample to another may be explained considering differences in

the oil initial physicochemical properties during its production via fast pyrolysis process. Further investigations are required to explore possible reaction mechanisms and other explanations to pyrolysis oil ageing behaviour found in this study; particularly in relation to the oil initial properties.

3.11 Interconnections between Process Variables and Gasification Products

The relationships between process variables on gasification behaviour and final products are complex. Process variables may include gasifier design, feed flow rates, temperature and pressure. Process variables could be manipulated and have direct or indirect impact on how the process behave and ultimately the final gasification products.

Figure 3–23 proposes a summary of potential relationships between different process variables involved during entrained flow gasification of pyrolysis oil on producer gas composition and tar formation. The flow chart highlights gasification conditions of most interest in this work, which are based on using oxygen as the gasification agent at relatively low gasification temperature (750-1000ºC) and atmospheric pressure. The relationships presented in the figure is expected to hold at varying gasification conditions, except when steam is used as the gasification agent since interactions associated with flow rates of pyrolysis oil and gas, equivalence ratio and their mixing behaviour are no more applicable.

During entrained flow gasification of pyrolysis oil, five process variables that are regarded to have the most important influences on gasification products are the gasifier design, atomizer selection, flow rates of pyrolysis oil and oxygen gas, pyrolysis oil properties and additive additions to the oil. These variables are numbered as (1) – (5) in Figure 3–23, while their influences on different aspects of gasification behaviour are presented. The blue boxes represent the main process variables that were of most interest in this work, while the orange boxes represent the final primary outcomes from these changes.

In this work, effects of two variables (atomizer design and flow rates of pyrolysis oil and oxygen) were investigated and their influences on gasification products were discussed based on experimental data from various gasification operations. Detailed elaborations on relationships between these variables and gasification products will be presented in Chapter 7 of this thesis.

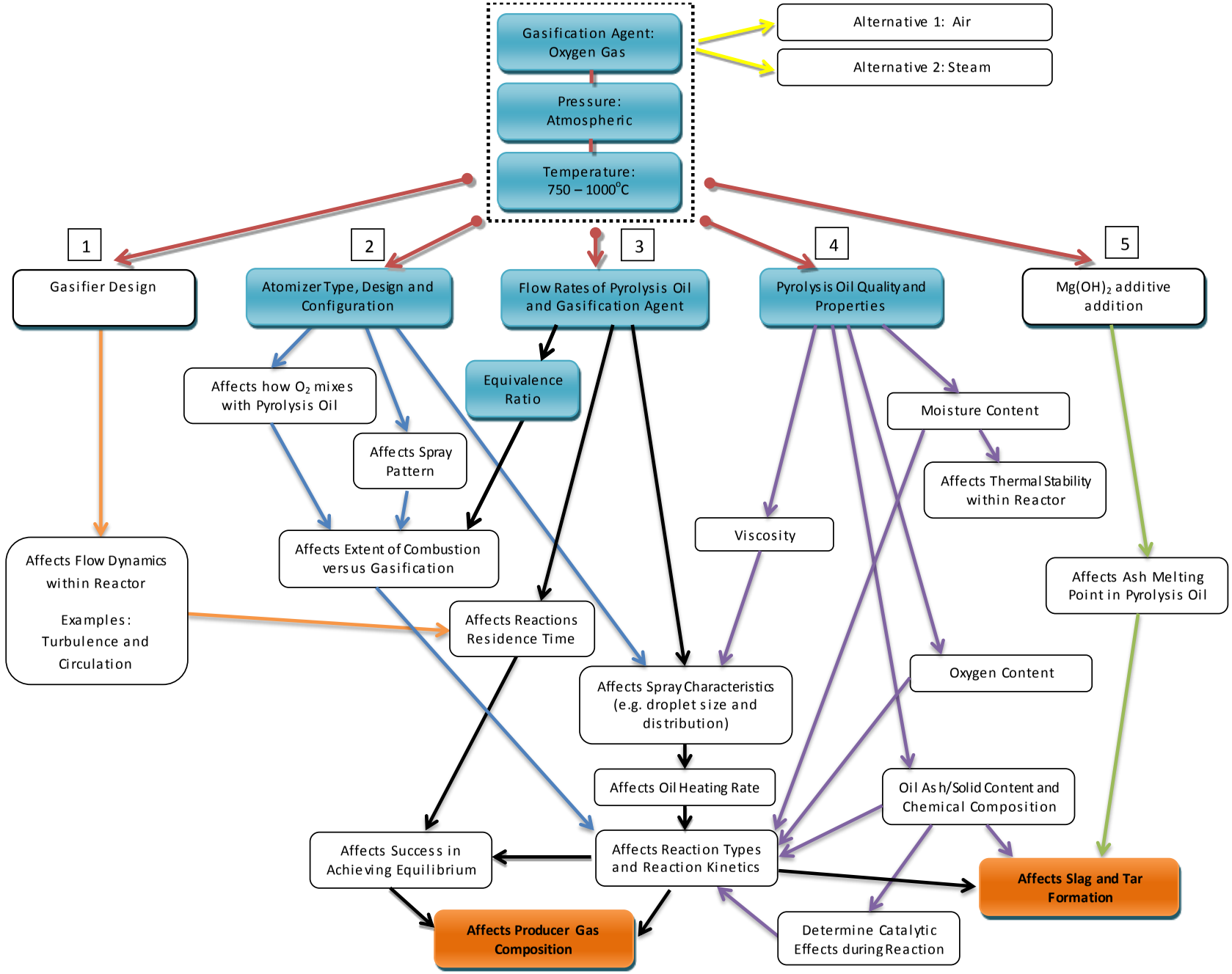

Figure 3–23: Flow chart showing gasification main operating parameters and how they affect gasification behavior and products

3.12 System Commissioning

The development of the entrained flow gasification system for biomass pyrolysis oil in this work has been challenging. There were many issues and problems encountered throughout the development process that have led to various operational difficulties at different stages of the entrained flow gasification operations. These issues often caused interruptions to the system's operation, affects the process stability, raised safety concerns as well as affecting accuracy and repeatability of results produced during the process.

This chapter aims to provide an overview of these challenges and how they were solved, so the information could be used to avoid similar problem from repeating in the future. Most of the issues were encountered during the commissioning stage; nevertheless, analysis, troubleshooting, modifications and solutions to the issues usually consumed significant amount of time thus were mostly extended throughout the entire period of this study.

3.12.1 Interruptions in LPG burners operation

3.12.1.1 Ignition difficulties

During gasifier pre-heating operations, each LPG burner was supplied with 4 L/min of LPG gas and 80 L/min of compressed air. At these feeding rates, however, chances of successful ignitions were slim. In order to increase the success rate, burner ignitions were performed at 2 L/min of LPG and 40 L/min of compressed air, before the flows were gradually increased to the desired inlet feeding rates.

The difficulties encountered during burner ignition may be explained by considering the confined space of which LPG combustion takes place inside the gasifier. Without open access to air, successful ignition depends strictly on how well LPG gas mixes with compressed air inside the burner nozzle, especially in region near the ignition probe. At high inlet feeding rates, mixing between LPG and air may be relatively poor due to high flow velocities across the burner nozzles. It is also possible that the use of custom built LPG burners in this work failed to promote sufficient mixing between LPG and air at high inlet flow rates, hence contributed to the ignition difficulties.

3.12.1.2 LPG regulator blockage

Another common cause of interruptions during burner operations is resulted from unexpectedly flame extinguishment in the middle of pre-heating stage. This situation was identified to have occurred due to

sudden stop of LPG supplies to the burners as indicated by dramatic decline in LPG bottle regulator pressure followed by LPG rotameter readings. Inspection on the LPG bottle indicated high LPG content in the bottle when this occurred hence ruled out low LPG supply as the root cause of the problem.

The interruptions were likely caused by formation of ice inside the LPG feeding system that blocked gas flow into the pressure regulator. This phenomenon is highly likely when the LPG bottle contains appreciable amount of moisture, which could have come from various sources during the gas production. Moisture could also become trapped in empty gas bottles during storage if their valves are not closed completely.

In order to explain how ice is formed and caused the regulator to block, it is important to understand that the amount of water that can co-exist with LPG varies depending on whether the LPG is present in liquid or vapour states. LPG in vapour state could hold water moisture 4-8 times more than that in liquid state, depending on its temperature. In gas bottles, LPG mainly present in liquid state due to high pressure thus excessive moisture in the bottle remains as 'free water', in which they exists separately at the bottom of the bottle [13].

During burner operations, liquid LPG turns into vapour while at the same time carries certain amount of moisture in its flow. As LPG vapour passes through a pressure regulator, it expands rapidly due to pressure difference between the inlet and outlet side of the regulator. Vapour expansion consumes energy from the surrounding thus caused significant decline in the regulator body temperature. This phenomenon is referred to as 'icing' and could be identified by formation of ice around the regulator body due to condensation of moisture in outside air upon contact with the regulator cold surfaces.

In practice, regulator icing is a common occurrence. This condition does not caused interruptions in LPG flow unless the regulator temperature drops below LPG boiling temperature. When this happen, LPG vapour condenses back into liquid state while at the same time loses its ability to hold moisture as much as when it was in vapour state. Because of this reason, moisture separates from the LPG and re-appears as 'free water' before quickly turns into ice, accumulates and eventually blocks the regulator [13]. Figure 3–24 illustrates an example of regulator internal conditions when such blockage occurs, while emphasizing on liquid LPG and ice formations near the inlet of the regulator.

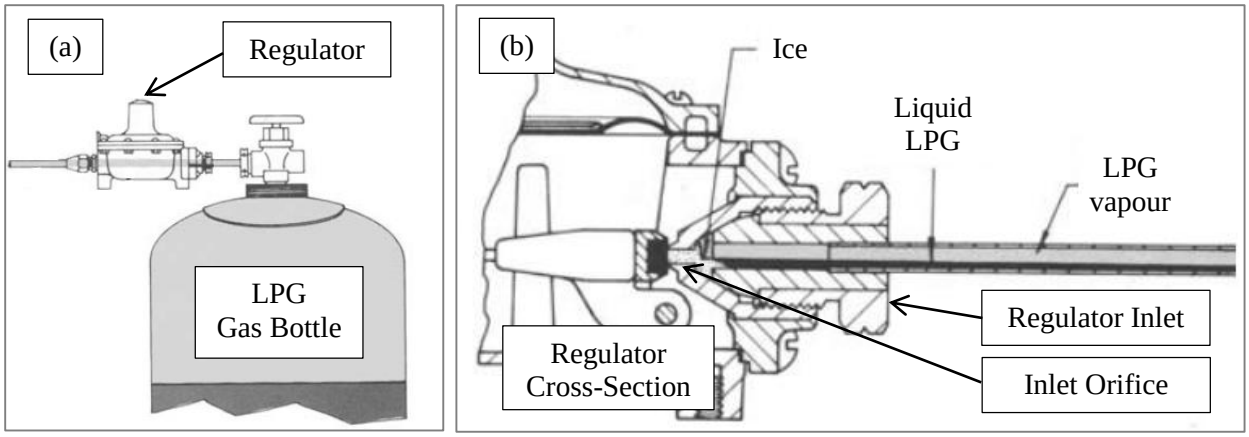

Figure 3–24: Images showing location of pressure regulator in the LPG feeding system (a) and internal condition of the regulator when blockage due to ice formation occur (b) [Image adapted from [13]]

When this problem occurred during entrained flow gasification operations, the regulator was removed from the LPG bottle to expose the internal parts of the regulator to ambient temperature so the ice could melt. Then the iced gas bottle was exchanged with a spare bottle to delay the same ice blockage problem from repeating. In this way, the problem was quickly solved and gasifier pre-heating could be resumed immediately.

To prevent this problem from occurring in the future, dry LPG gas should be used. While this is not always an option, the use of two stages pressure regulator should be considered so the outlet pressure reduction could be achieved in two small steps to prevent excessive temperature drop at a single point on the regulator. Besides that, the use of drying agents may also help to absorb moisture in the LPG gas from reaching the regulator.

3.12.1.3 Explosion

LPG gas is a highly flammable gas that readily burn in excess air when ignited. LPG also has high explosion risk particularly when used in a confined space and in environments with limited access to oxygen. LPG applications in environments above its auto-ignition temperature, such as in this work increase the risk of explosion exponentially in comparison to operations at room temperature. The auto-ignition temperatures of LPG made of pure propane or butane are 470ºC and 405ºC respectively [14].

Due to flame extinguishing problem in the middle of the gasifier pre-heating stage, the burners often need to be re-ignited when the gasifier temperature is already high. In most cases, re-ignition of the burners

have to be performed at temperatures higher than LPG auto-ignition temperature (around 500ºC), thus risk of explosion is significant. In this work, several minor explosions have occurred as a result of LPG supply into high temperature environments prior to successful ignitions.

Considering the serious risks associated with this operation, a set of important rules must be followed for re-attempting ignition at high temperature, as highlighted in Chapter 10: Appendix C of this thesis. This also provides an important justification of why small LPG flow rate must be used during ignition attempts; so accumulation of LPG gas inside the high temperature gasification system could be minimized.

3.12.2 Pyrolysis oil flow interruptions and inconsistencies

There were four main factors that contribute to pyrolysis oil flow inconsistencies during and between gasification operations which are the oil properties, blockage of the oil feeding system, interruptions to positive displacement flow meter operation as well as changes in peristaltic pump inlet suction requirements. Inconsistencies in pyrolysis oil flow could occur gradually, rapidly, temporarily or permanently depending on the nature of the interruptions. Inconsistencies in pyrolysis oil feeding are undesirable as it leads to poor control of the process variables during an operation. In addition, it also leads to significant variations between gasification operations, making comparisons between two or more operations often not possible.

3.12.2.1 Pyrolysis oil properties

Variation in pyrolysis oil viscosity is the most important factor that contributed to pyrolysis oil flow inconsistencies between gasification runs. Change in pyrolysis oil viscosity occurs with time as a result of ageing due to the oil unstable nature. Discussions on pyrolysis oil ageing have been presented earlier in Chapter 3.10.2.

In normal operations, the magnitude of disagreement between pyrolysis oil flows from one operation to another depends on the viscosity of the oil used. At a constant peristaltic pump speed, pyrolysis oil with higher viscosity produces smaller flow through the atomizer small orifice, as a result of greater flow resistance, than that produced by lower viscosity oil. Because of this reason, a new calibration graph that relates peristaltic pump speed with pyrolysis oil flow rate is consistently produced during each gasification operation.

Since pyrolysis oil flow rate has strong influence on gasification temperature and equivalence ratio, inconsistencies in the oil flow rate makes direct comparisons between different gasification operations and their products are always not practical.

3.12.2.2 Blockage of pyrolysis oil feeding system

Pyrolysis oil feeding blockage is one of the biggest challenges encountered during entrained flow gasification operations. Blockage of the feeding system can occurred either partially or completely depending on the severity of obstacles to the oil flow. In contrast to complete blockage where pyrolysis oil flow is completely stopped, partial blockage still allows pyrolysis oil to flow but at increased pressure and reduced flow rate. Partial blockage could be further divided into two categories which are permanent and temporary blockage. Temporary partial blockage takes place when obstruction to oil flow resolves quickly thus the pressure and flow rapidly return to their initial values. On the other hand, permanent partial blockage is more persistent causing the oil pressure and flow rate to shift to new values. In many cases, permanent partial blockage eventually leads to complete blockage if failed to be resolved quickly during the operations.

In this work, the most obvious cause of feeding system blockage is from rapid degradation of pyrolysis oil upon exposure to high gasification temperature. This situation was reasonably common particularly when the oil flow into the system is completely stopped. It was found that when the oil feeding rate was interrupted, even for a short period of time, the risk of blockage increase exponentially and almost certainly will lead to complete blockage of the feeding system. The main problem with complete blockage is that it is often not reversible and can only be resolved by complete disassembly of the atomizer for cleaning, which requires complete shutdown of the entrained flow gasification system.

Figure 3–25 shows example pyrolysis oil flow and pressure profiles when the feeding system progressively shifts from temporary partial blockage to permanent partial blockage, before eventually completely blocked during one gasification operation.

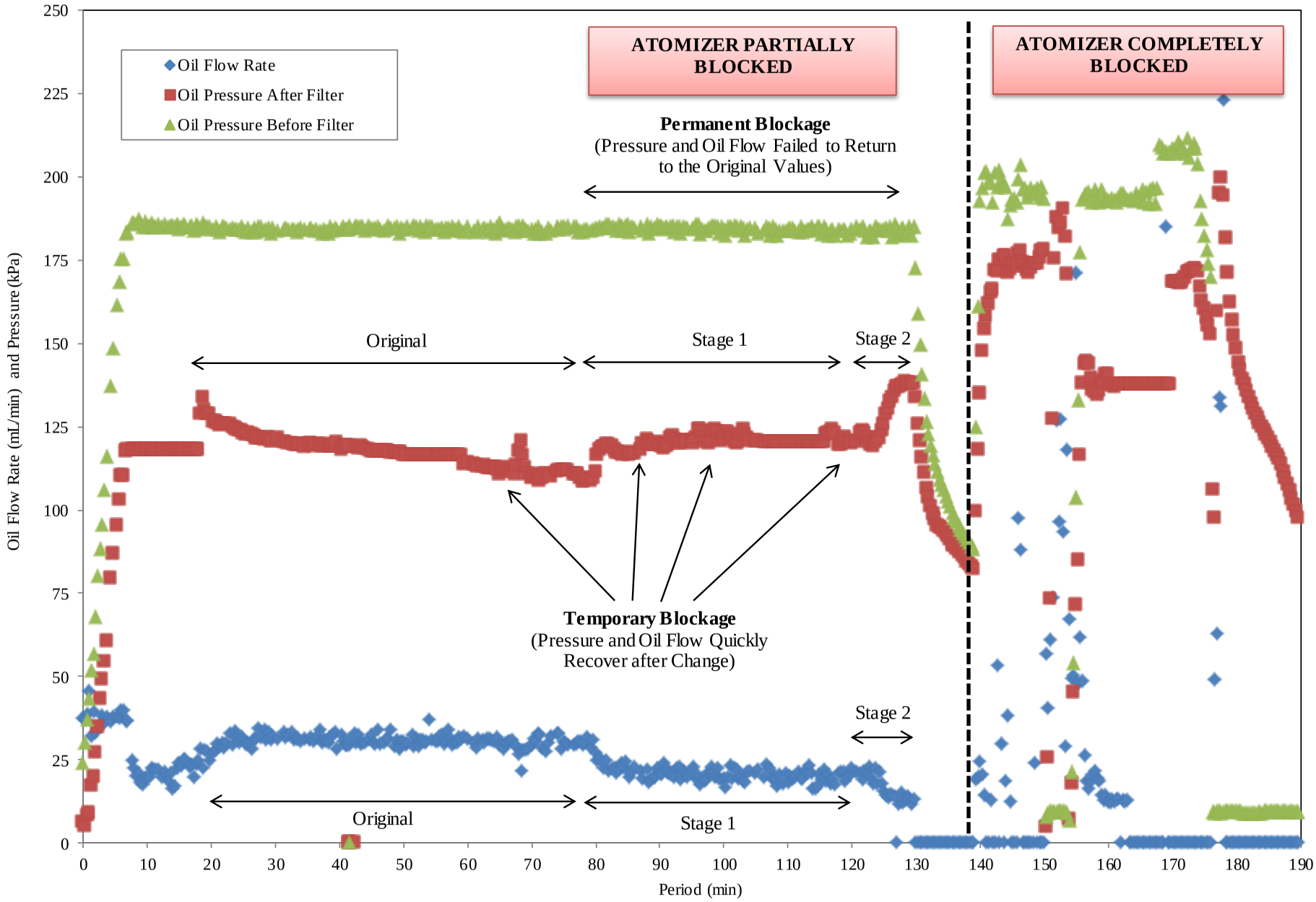

Figure 3–25: Pyrolysis oil flow rate and pressure profiles during partial and complete blockage of oil feeding system during gasification

It is also clear from Figure 3–25 that during normal operations, the pressure before the oil filter should remain at a constant value at a given pump speed. The pressure after the on-line filter, on the other hand usually decline gradually throughout a gasification operation as a result of increased pressure drops across the filter media/mesh when used continuously for a long period of time. Nevertheless, decline in the pressure after on-line filter should be much less significant if a new filter is used for the operation.

Decrease in pressure after online filter should not significantly affect pyrolysis oil flow rate because the pressure is generally much higher than the minimum pressure required for the specified flow, as a result of restriction on the atomizer liquid outlet. Therefore small changes to the oil pressure should not significantly affect its flow rate unless the pressure drops below the required minimum, in which case it is unable to overcome flow resistance caused by pyrolysis oil high viscosity.

On a separate note, sudden pressure builds up after the on-line filter indicates blockage to the feeding system hence should be attended appropriately.

The flow meter used in this work is capable of giving flow measurements as low as 10 mL/min. It was learnt that below this value, the flow meter will start to generate very large flow readings thus giving significant error to the oil flow measurements. Because of this reasons, it is important that pyrolysis oil flow rate is maintained above the minimum value at all time during gasification with the flow meter used in this work.

3.12.2.3 Interruptions to flow meter operation

Positive displacement flow meter is another source of pyrolysis oil flow inconsistencies during gasification operation. This type of flow meter consists of two oval gears that rotate to continuously displace constant volume of liquid in every revolution. The flow rate of liquid passing through the meter is determined based on rate of revolution of the gears, which are detected by a sensor before translated into flow rate measurements. Figure 3–26 shows internal section of the positive displacement flow meter used in this study and how it works.

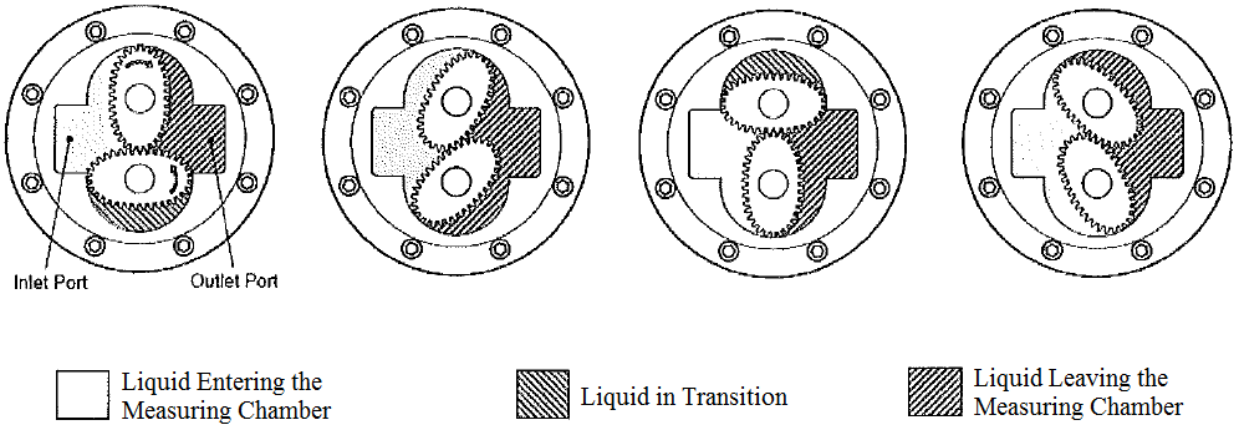

Figure 3–26: Diagram showing how positive displacement flow meter work [15]

Since this type of flow meter functions based on rotation of the gears, there were occasions where the gears were jammed and therefore lead to complete blockage of the oil feeding system. It is possible that this occurred due to solid or build-up of highly viscous components of pyrolysis oil throughout the operation.

In order to minimize risk of the flow meter failure, it is critical that the meter is cleaned periodically with ethanol so its internal parts are free from residues and viscous build-up. During maintenance process that requires the meter to be disassembled, it is also important that the internal parts are handled and re-assembled appropriately to prevent damage to the meter, as well as to make sure the meter works. Guidelines for cleaning and re-assembly the positive displacement flow meter used in this work has been given in Chapter 10: Appendix F for further reference. New calibration of the flow meter is required after maintenance to check for the meter's measurement accuracy after the re-assembly.

3.12.2.4 Increase in peristaltic pump inlet suction requirement

Peristaltic pump works based on series of alternating compression and relaxation actions on flexible tube carrying liquid to create flow. The tube is squeezed between rotating rollers and a track to create seal at the point of contacts, while transferring liquid of a specified volume as the roller revolves forward. As the tube is released to its original shape, partial vacuum (suction) is created hence drawing more liquid towards the pump inlet so the process cycle is continuous. Figure 3–27 shows peristaltic pump operation principles for reference.

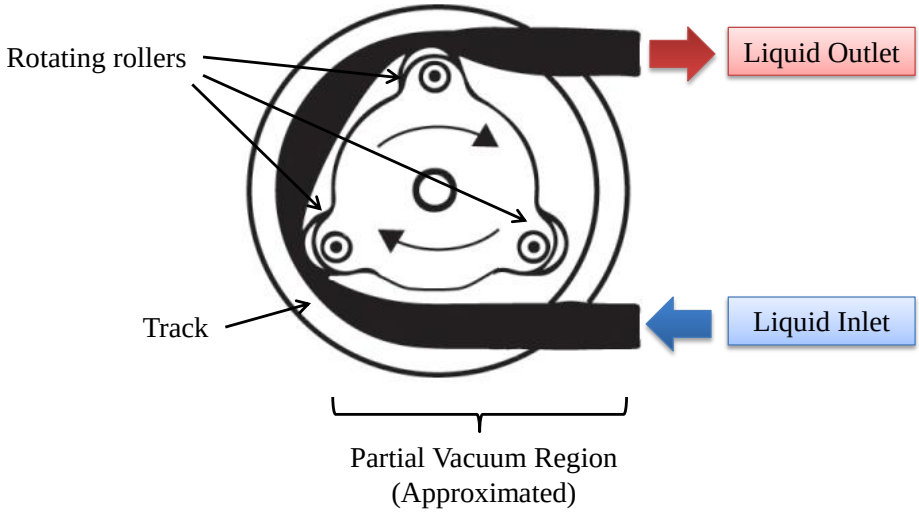

Figure 3–27: Peristaltic pump basic operation principles [Image adapted from [16]]

In cases where highly viscous liquid is used such as in this study, greater suction pressure is required to achieve successful pump operation compared to less viscous liquid, due to larger resistance of flow. In addition to that, the presence of 100µm mesh solid filter in the pyrolysis oil tank also adds resistance to pyrolysis oil flow thus increases the minimum suction required during an operation. During gasification commissioning runs, there were occasions where inlet suction of the pump was insufficient to draw pyrolysis oil from the tank thus causing decline in pyrolysis oil flow rate. When this occurs, pressure of pyrolysis oil after the pump was observed to decline too.

Increase in the pump suction requirement may result from increase in pyrolysis oil viscosity. During a constant viscosity operation, however, increase in the pump inlet suction requirement may occur as a result of filter blinding particularly after long gasification operations. To overcome this problem, the filter must be cleaned so pressure drop across the filter medium is restored to its minimum. Increasing pyrolysis oil level in the tank has also been proven helpful since this provides larger pressure head to the system thus promote pyrolysis oil flow towards the peristaltic pump inlet. On top of that, pyrolysis oil with low viscosity should always be preferred to minimize inlet suction requirement as well as to prevent various issues related to pyrolysis oil flow from taking place.

3.12.3 Impact of peristaltic pump pulsation on pyrolysis oil flow

The peristaltic pump head used in this work is designed with a twin offset tracks to reduce pulsation effect during its operation. In this configuration, inlet to peristaltic pump head is split into two flow channels which are pumped at conditions offsetting one another to neutralize pulses produced by each flow channel when the outlet flows are merged back together. In addition to the twin tracks, the pump head also has as many as six rollers to deliver liquid flow with minimal pulse in every revolution. Despite the pump's sophisticated design, small pressure pulsation is still expected to be observed in liquid flow during pump operation.

In this work, effect of pressure pulsation is more prominent due to pressure build-up in the oil feeding system as a result of flow resistance caused by the atomizer. Peristaltic pump operation at high speed also enhances pulsation in pyrolysis oil flow due to more rapid compression and relaxation actions at this condition. Pulsation is undesirable as it produces misleading pressure and flow changes on the positive displacement flow meter thus results significant fluctuations in pyrolysis oil flow rate readings.

In order to reduce pulsation hence stabilizes pyrolysis oil flow, a dampener must be installed. In this study, pulsation dampener was substituted with an on-line ash filter. The ability of the on-line filter to minimize pulses is due to the filter's reasonably large oil reservoir that absorbs sudden changes to the oil pressure and flow from the pump. Installation of the filter after peristaltic pump has significantly reduced pulse in the oil being pumped to the positive displacement flow meter, thus minimizes fluctuations in the oil flow reading by the meter. A photo showing the on-line oil filter setup in this work is shown in Figure 3–28.

Figure 3–29 on the other hand, shows major differences between pressure and flow rate profiles during operations with and without on-line filter installation for comparison. The results clearly show significant reduction in pyrolysis oil flow fluctuations when on-line filter is installed in the system.

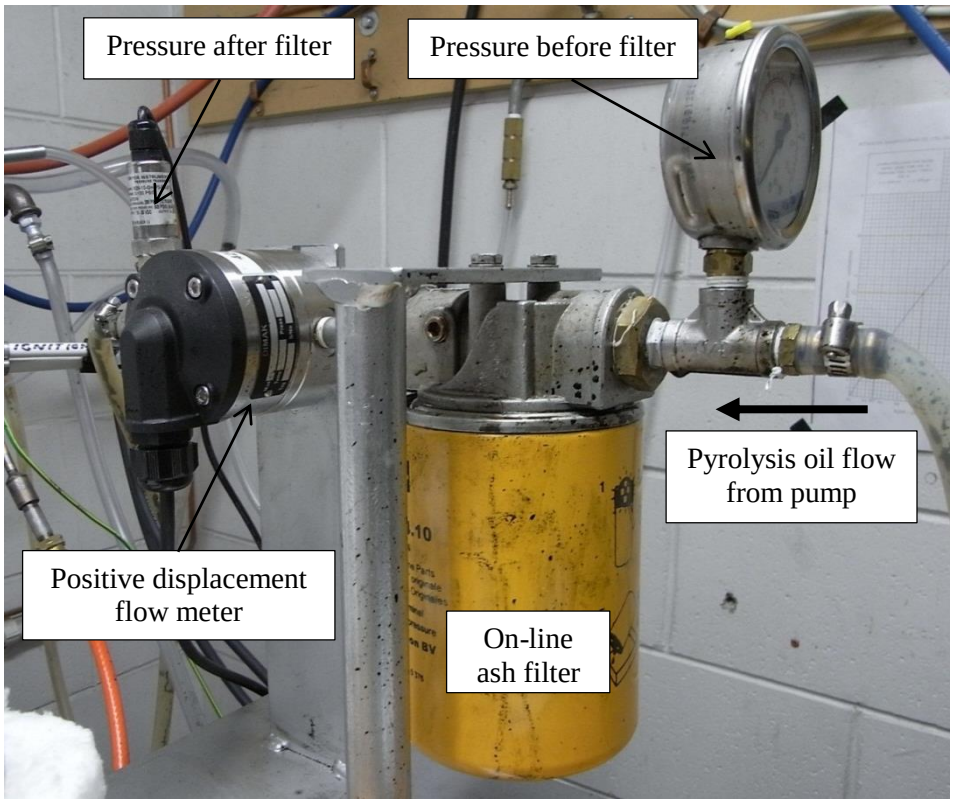

Figure 3–28: Photo showing location of on-line ash filter, positive displacement flow meter and pressure measurement devices (gauge and transducer) for pyrolysis oil feeding system

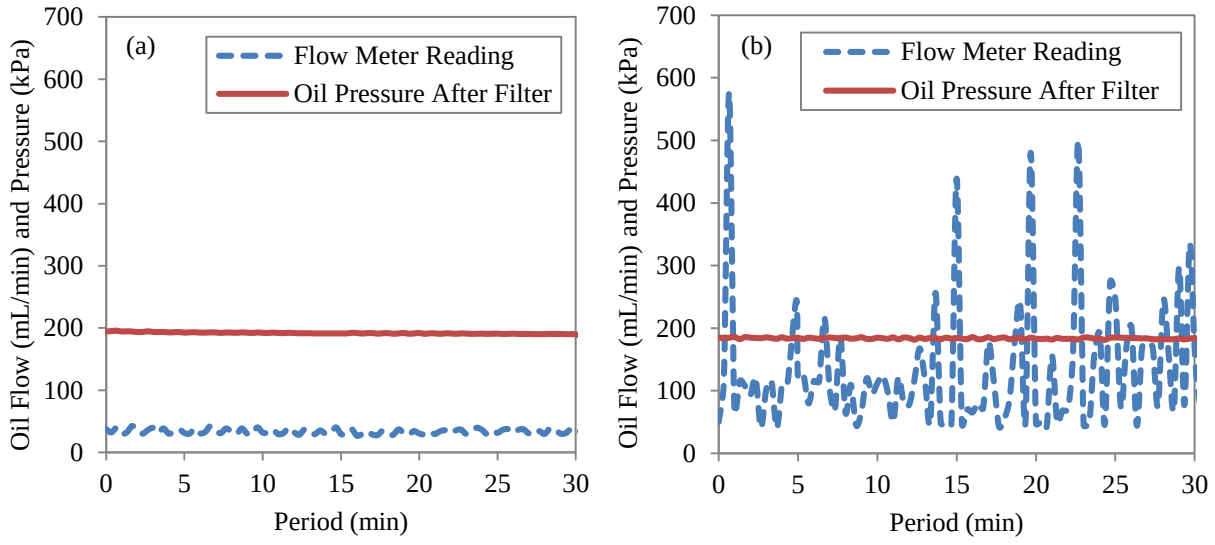

Figure 3–29: Comparison between positive displacement flow meter readings during peristaltic pump operation with (a) and without (b) on-line filter

Knowledge on effects of peristaltic pump pulsation on pyrolysis oil flow rate is important so any error resulted from the pump operation could be understood and taken into account. In this work, it was learnt that positive displacement flow meter may wrongly generate pyrolysis oil flow rate reading when the atomizer is completely blocked as a result of misleading pressure pulses generated by the peristaltic pump. An example to such condition is presented in Figure 3–30 where although no pyrolysis oil flow is produced by the pump (due to complete blockage), flow meter reading is still fluctuating between 0-90 mL/min during the operation as a result of pressure pulsation during the operation.

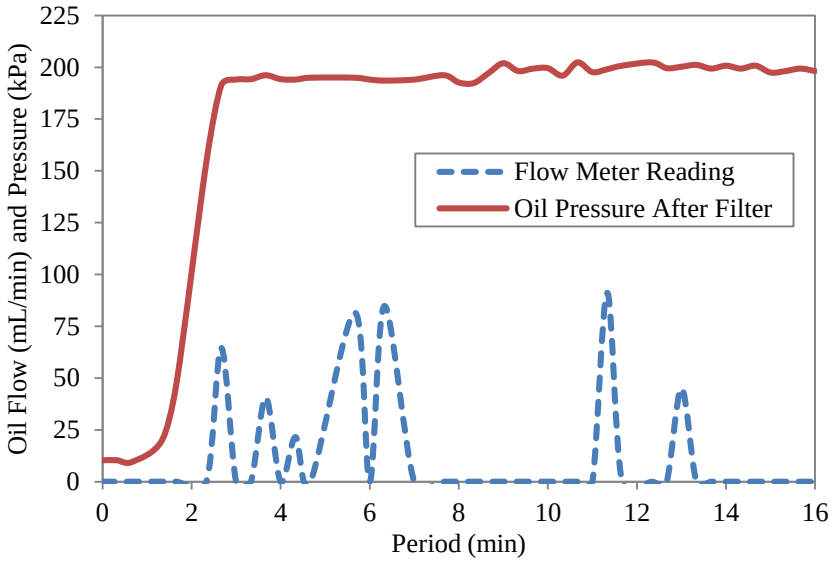

Figure 3–30: Misleading flow meter reading due to peristaltic pump pulsation during operation with complete atomizer blockage (Actual oil flow rate = 0 mL/min)

3.12.4 Oxygen analyser failure

Oxygen sensor is an important safety device installed in the entrained flow gasification system to monitor percentage of oxygen in the producer gas at all time throughout the operation. This is critical considering supply of pure oxygen gas into the system, which under certain circumstances, could lead to hazardous oxygen enrichment environment during the operation. Increase of oxygen concentration in the environment by several percentages can cause combustible materials to ignite more easily and rapidly due decline in their ignition and auto-ignition temperatures. In fact, oxygen rich environment could make most non-combustible materials burn thus health and safety consequences from this environment could be disastrous [17].

In normal gasification operations oxygen should be completely consumed by oxidation reactions with pyrolysis oil (partial combustion) as soon as both materials mix inside the gasifier; thus no oxygen is expected to present in the producer gas. Nevertheless in occasions where the system deviates from normal operations, increase in oxygen concentration in producer gas is likely thus can potentially lead to hazardous conditions. During entrained flow gasification operation, such condition has been observed as a result of various reasons such as due to poor mixing and poor reactions between pyrolysis oil and oxygen gas, extremely short reaction residence time and sudden interruptions to pyrolysis oil flow due to blockage in the oil feeding system.

In order to monitor oxygen concentration in the entrained flow gasification system, an oxygen analyser is used. In general, the use of oxygen sensor in gasification environment is reasonably challenging due to presence of tar, char and ash in the producer gas stream. Deposition of these materials on oxygen sensor is highly undesirable since this condition could cause the sensor to be completely covered and clogged with contaminants such as that illustrated in Figure 3–31.

Figure 3–31: Photo of oxygen sensor with solid deposition after entrained flow gasification operation

In addition to physical deposition by solid contaminants, prolonged oxygen sensor exposure in gasification environment was also discovered to cause irreversible deterioration of the sensor performance

that eventually leads to total failure of the device. This failure is likely caused by deactivation of the sensor catalyst (platinum) upon continuous exposure to harsh gasification environment. Figure 3–32 shows an image of a malfunction oxygen sensor with its protective cap removed to reveal its platinum embedded zirconium dioxide (ZrO_2) support.

Figure 3–32: Photo of the malfunction platinum embedded zirconium dioxide (ZrO_2) support after prolonged exposure to gasification environment

Comparison between the malfunction oxygen sensor and operational sensor revealed permanent discolouration of the ZrO_2 support (from white), upon exposure to gasification environment. From this observation, it is possible that the sensor was poisoned by condensation of tar on the catalyst active sites during the operations. In addition to that, it is possible that gasification extremely rich environment (ER < 0.75) may have also contributed to the sensor short lifespan due to more rapid deterioration of the catalyst, in comparison to that operating in lean (ER > 1) or free air environments [18].

Following these findings, it is therefore beneficial for the oxygen sensor to be installed in producer gas stream after removal of ash, char and tar contaminants so sensor deterioration during gasification operations can be overcome.

3.12.5 Char deposition on top temperature probe

The gasifier was initially installed with a thermocouple located at the top part of the reactor to measure temperature of pyrolysis oil flame during reactions with oxygen gas (partial combustion). The tip of the thermocouple is positioned at the centre of the gasifier aimed to measure temperature in the middle of the flame. Nevertheless this thermocouple was later removed due to severe deposition of char on the thermocouple probe, as illustrated in Figure 3–33.

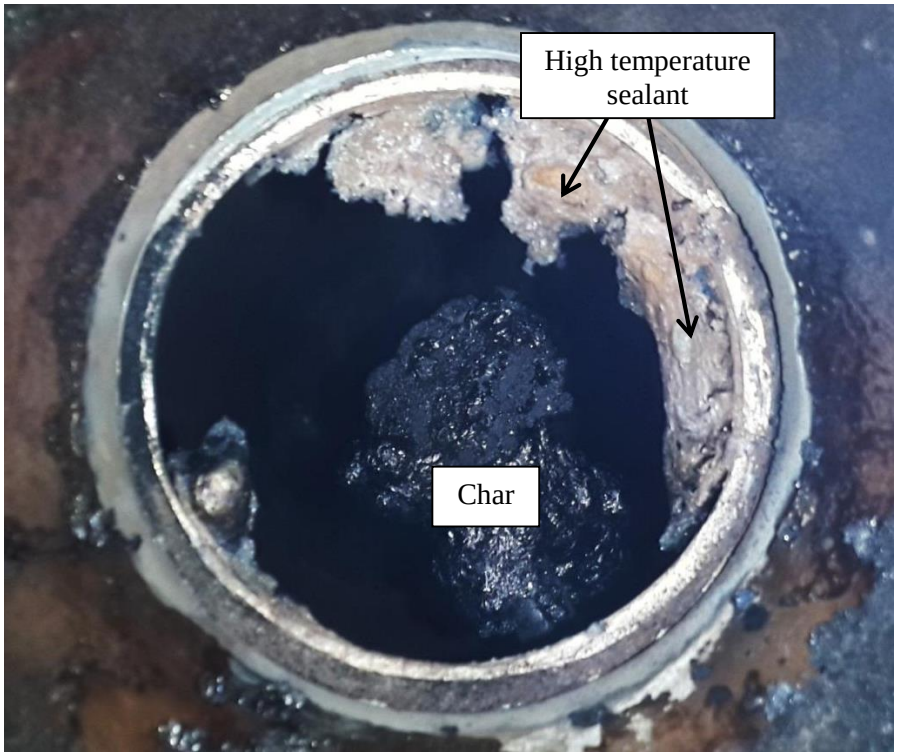

Figure 3–33: Photo of char deposition on the top thermocouple after gasification trial

The char deposition is believed to have resulted from direct impact of pyrolysis oil spray on the thermocouple probe before the spray droplets completely convert into vapour phase. This situation is highly likely considering the proximity of the thermocouple with atomizer nozzle, which is just around 60 mm apart. Because of this reason, it is possible that the thermocouple was positioned inside pyrolysis oil spray thus obstructing droplets pathways to flow down the gasifier. As oil droplets hit the probe they gradually solidify to form char deposit and continue to grow upon impact with more pyrolysis oil droplets.

The accumulation of char deposit on the top thermocouple probe progresses with gasification time thus if not stopped will lead to severe blockage of the reactor. Figure 3–34 shows photos of char accumulation during gasification operations viewed from the sight glasses, before the port is completely blocked.

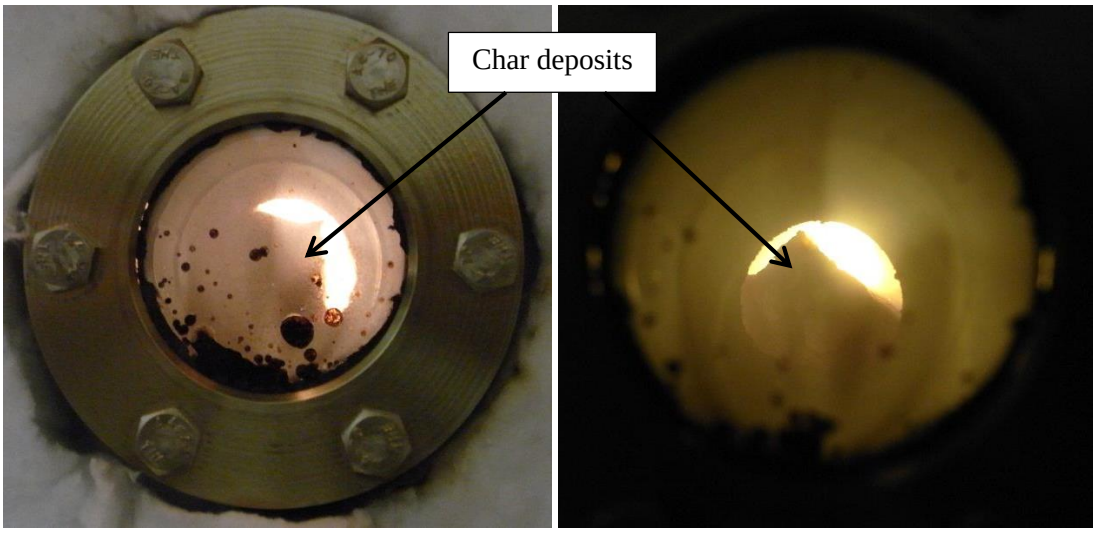

Figure 3–34: Photos showing char accumulation on top thermocouple probe during gasification, as viewed from the sight glasses, which were then blocked by the deposition

At constant pyrolysis oil flow rate, increase of oxygen feeding rate into the system was shown to remove some of the char deposits. Nevertheless this approach is not capable of removing the deposit completely. Once the char deposition is too significant, the best method to completely remove the char deposit is by purging the system with excess air so complete combustion of all the char throughout the entire gasifier reactor could take place.

Despite the severe char deposition problem, gasification at high oxygen feeding rate right from the beginning has been proven could minimize the amount of char formed during the gasification operation. This is relevant considering at high oxygen feeding rate, better atomization can be achieved thus produces pyrolysis oil spray with smaller droplets sizes. The small droplets sizes combust and devolatilize into vapour products more rapidly thus minimizes formation of char in the system as well as on the thermocouple probe.

Due to great tendency for severe char deposition, the top thermocouple was decided to be completely removed from the system, so obstruction to droplets flow as caused by the probe could be permanently eliminated. Removal of the thermocouple probe also improves the overall pyrolysis oil conversion during

gasification since spray droplets could flow more freely across the gasifier length without major obstruction.

3.12.6 Char deposition inside gasifier

Even after removal of the top thermocouple probe from the gasifier, char deposition may still occur during gasification operations. Although this is not normally the case, there were several instances where appreciable char depositions were observed in the gasifier during routine inspection after gasification runs. An example to this was observed during gasification using highly viscous pyrolysis oil (509 cSt), where a large char deposit was found on one side of the gasifier between the middle thermocouple and reactor wall, as shown in Figure 3–35. Besides the gasifier, char depositions was also observed on oxygen sensor and pipework leading to after-burner, as illustrated in Figure 3–36.

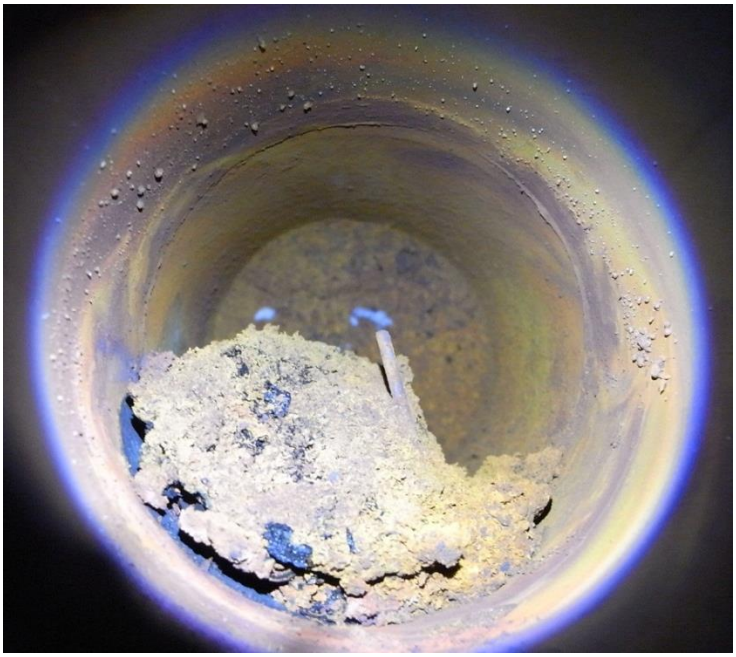

Figure 3–35: Char deposition inside gasifier upon inspection after gasification using high viscosity oil

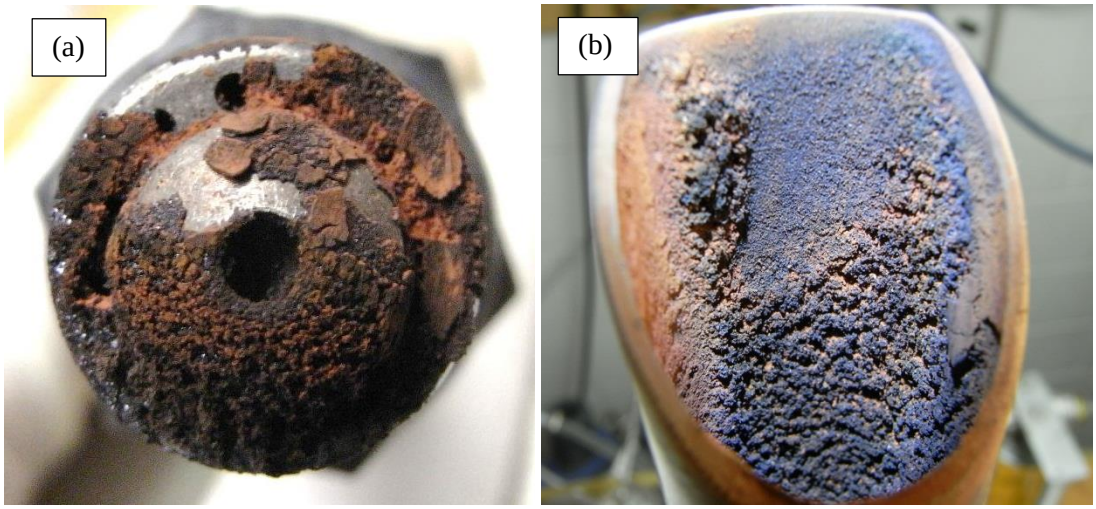

Figure 3–36: Photos showing severe deposit on oxygen sensor (a) and pipework near after-burner (b) from gasification operation using high viscosity oil

In this particular example, the significant char deposition could be related to the high viscosity of pyrolysis oil used during the operation. Liquid viscosity has strong influence on atomization performance, in which a highly viscous liquid is generally more difficult to be atomized than that using liquid with lower viscosity. At constant flow rates of pyrolysis oil and oxygen, highly viscous oil tends to yield less uniform spray, larger droplets sizes and poorer spray distributions in comparison to that produced using less viscous oil. Because of these reasons, it is highly likely that pyrolysis oil spray formed during this operation was poor thus lead to inefficient oil-gas conversion and consequently increased char formation and accumulation within the system.

This particular experience emphasizes critical influence of pyrolysis oil viscosity on gasification, as a result of variations in atomization performance. Following this, viscosities of pyrolysis oil in all subsequent gasification runs were closely monitored to make sure satisfactory atomization performance can be achieved during the operations. Other than pyrolysis oil viscosity, other causes of char deposition in entrained flow gasification system includes short residence time, low gasification temperature and interruptions to oxygen gas supply into the system.

3.12.7 Importance of gas purge after gasification

After every entrained flow gasification operation, it is important the gasifier is purged sufficiently with air so any char build-up inside the reactor could be burned as the first step of cleaning the system. Besides

eliminating char, purging the system with air is also critical to remove remaining vapour trapped in the system and to stop further reactions from taking place after the operation. Failure to follow this guideline could lead to maintenance difficulties due to condensation of tar and coke inside the system as the system cools down to room temperature.

In this study, severe deposition that completely filled the top half of the gasifier space was observed when the system was not purged after one gasification operation. Closer inspection of the deposit revealed transition of its physical characteristics from light and flaky carbonaceous matrix at the top of the gasifier into much denser deposition further down the gasifier length. Figure 3–37 shows images of deposit formed inside the gasifier, as well as differences in physical attributes of the deposits from the top to middle sections of the gasifier.

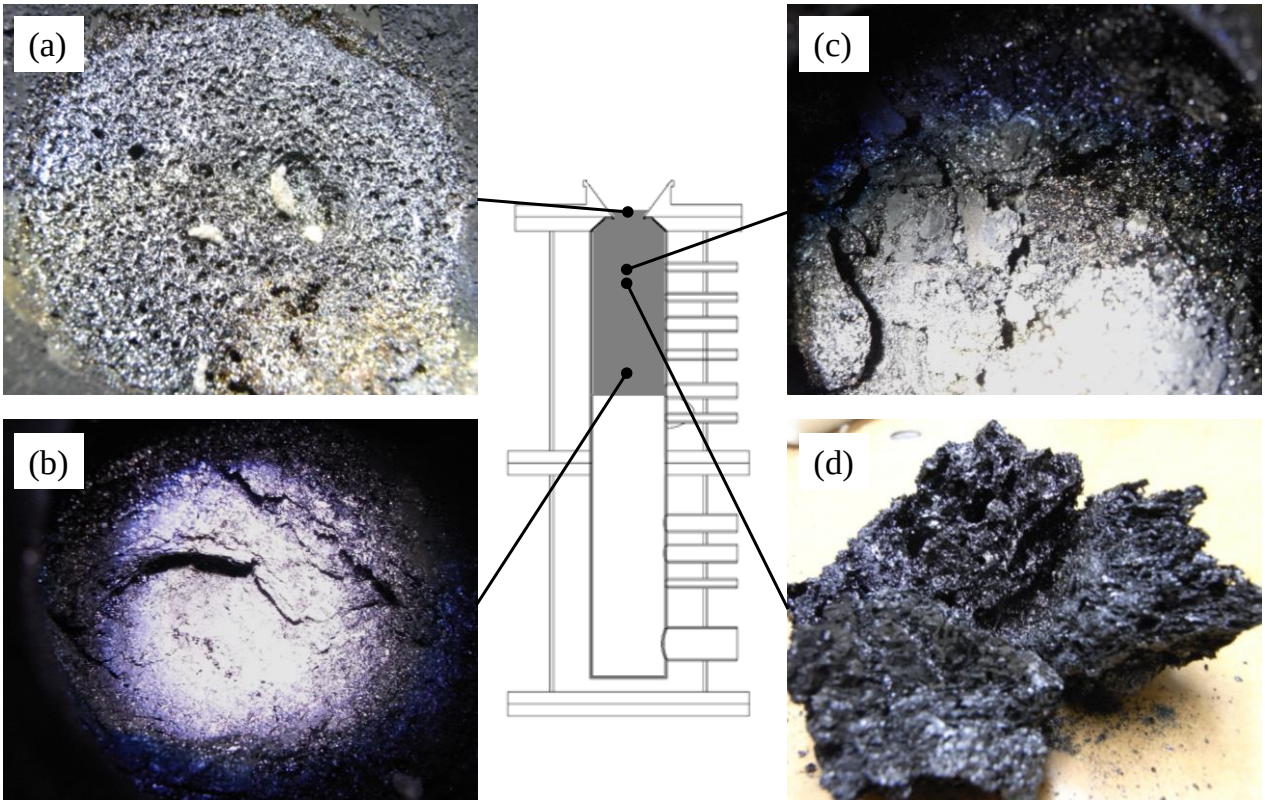

Figure 3–37: Images of deposit due to failure to purge system after gasification run; at top of the gasifier (a) middle of the gasifier (b) in transition area between the top and middle section of the gasifier (c) deposit sample as taken from transition area (d)

3.12.8 Modification of pyrolysis oil flushing system

Due to risk of blockage in the pyrolysis oil feeding system, supply of pyrolysis oil is intermittently switched to ethanol during gasification operations to make sure the system is maintained at its optimum condition. Pyrolysis oil dissolves in ethanol, thus flushing the system with this solvent prevents accumulation of undesirable compounds, such as highly viscous components of the oil that could eventually lead to interruptions of the oil flow. Discussions on all factors that contribute to pyrolysis oil flow interruptions have been presented earlier in Chapter 3.12.2.

In practice, the pyrolysis oil feeding system is cleaned with ethanol when partial blockage starts to take place frequently, which is an early symptom of deteriorating flow stability that could proceed to complete blockage of the oil feeding system if not appropriately resolved. Depending on the quality of pyrolysis oil used, frequency of ethanol flushing requirement varies significantly from one operation to another. In general, the risk of pyrolysis oil flow blockage rises dramatically when a system is operated without being flushed with ethanol for an extended period of time, especially when highly viscous oil is used.

The original ethanol flushing arrangement developed for the entrained flow gasification system in this work is presented in Figure 3–38. In this arrangement, ethanol is introduced into the main feeding stream before the positive displacement flow meter, while isolated with two ball valves. After the flow meter, pyrolysis oil and ethanol shares the same silicon tube connecting to the atomizer.

Major drawback to this setup is due to significant liquid hold-up in the silicon tube after the flow meter. During gasification, this section of tube is constantly filled with pyrolysis oil due to restriction of flow caused by the atomizer liquid outlet. The length of the tube is around 2.7 meters thus holds significant amount of oil (approximately 140 mL) in comparison to pyrolysis oil flow rate exiting the atomizer (average flow of 40 mL/min). In this case although feed into the atomizer is switched to ethanol, supply of ethanol into the atomizer does not occur quickly due to reasonably large pyrolysis oil volume held by the tube. In fact, this situation only dilutes the oil being fed into the atomizer thus is less effective to achieve ethanol flushing original purpose. Other than not fulfilling ethanol flushing main objective, mixing of pyrolysis oil and ethanol in the tube also change the original properties of the oil, thus lead to serious errors in gasification results produced during the operation.

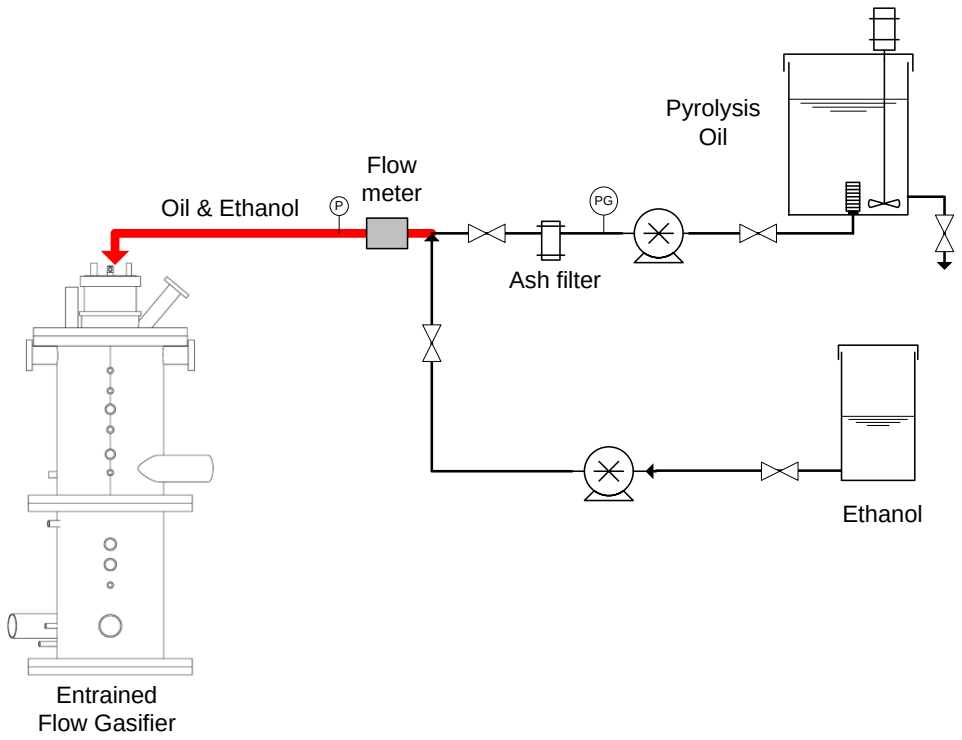

Figure 3–38: Flow diagram of ethanol and pyrolysis oil feeding system

Due to these limitations, the ethanol flushing arrangement was later modified to better achieve its purpose. The new ethanol flushing arrangement is illustrated in Figure 3–39. In the new ethanol flushing arrangement, separate silicon tubes are used for pyrolysis oil and ethanol after the flow meter to minimize cross contaminations between the two liquids during gasification. A total of four independent ball valves are installed on all ends of the silicon tube to isolate the undesirable mixing of ethanol with pyrolysis oil during the operation. Most importantly, the new setup also allows almost immediate supply of ethanol into the atomizer hence rapidly cleans the atomizer from accumulation with minimal time lag. This arrangement has been tested during gasification and was proven more efficient than the original flushing arrangement.

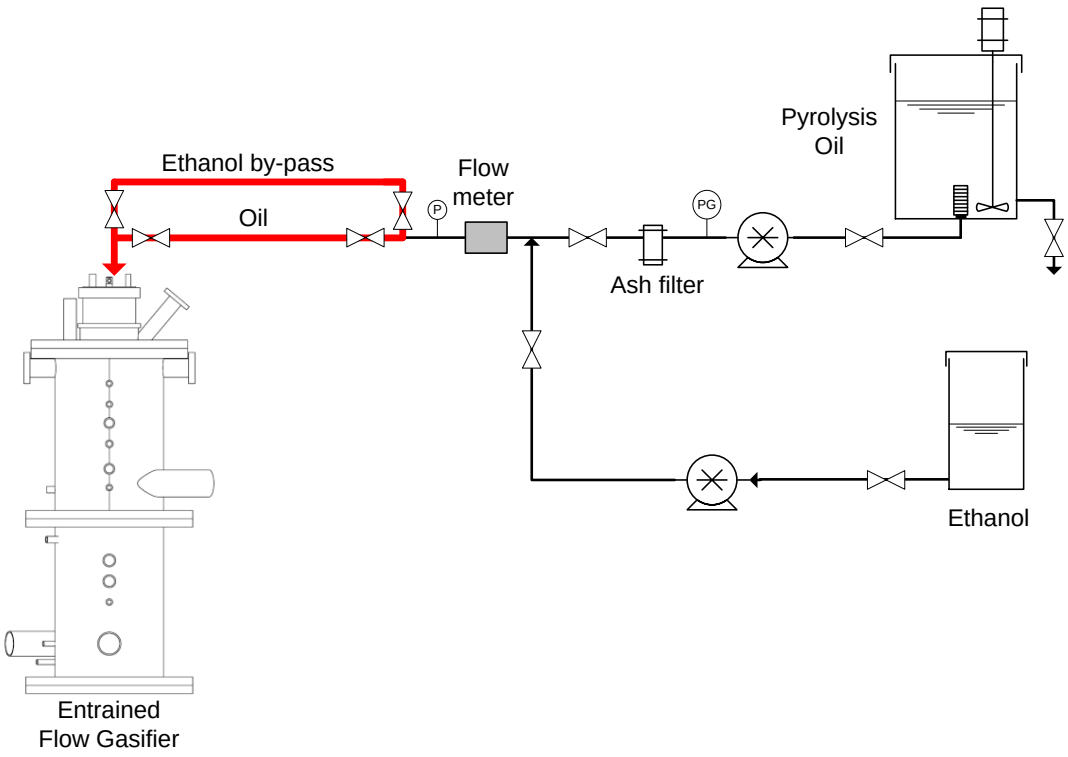

Figure 3–39: Flow diagram of ethanol and pyrolysis oil feeding system after modification

3.12.9 Soot and tar deposition on sight glasses

Formation of secondary gasification products such as soot and tars is a normal phenomenon during gasification operations. These products could deposit on different parts of the gasifier most obviously on parts that are exposed to low temperatures such as the sight glasses, sampling port, condensers, heat exchangers and pipework leading to the after-burner. Most parts of a gasifier body are generally well insulated to keep the system at high temperatures, thus deposition of tar and soot on these sections are less likely hence is not a concern.

In this work, the biggest concern related to soot and tar deposition is due to blockage of the sight glasses. Deposition of materials on sight glasses is a common occurrence during any gasification run and usually develops gradually with time. There are two sight glasses which are located at the top and middle section of the gasifier aimed to provide good observation of gasification progress at different gasifier height. These sight glasses are extruded out of the gasifier main geometry so they are not directly exposed to

flame or char deposition during operations. Example of deposition on each of these sight glasses after gasification operations are illustrated in Figure 3–40.

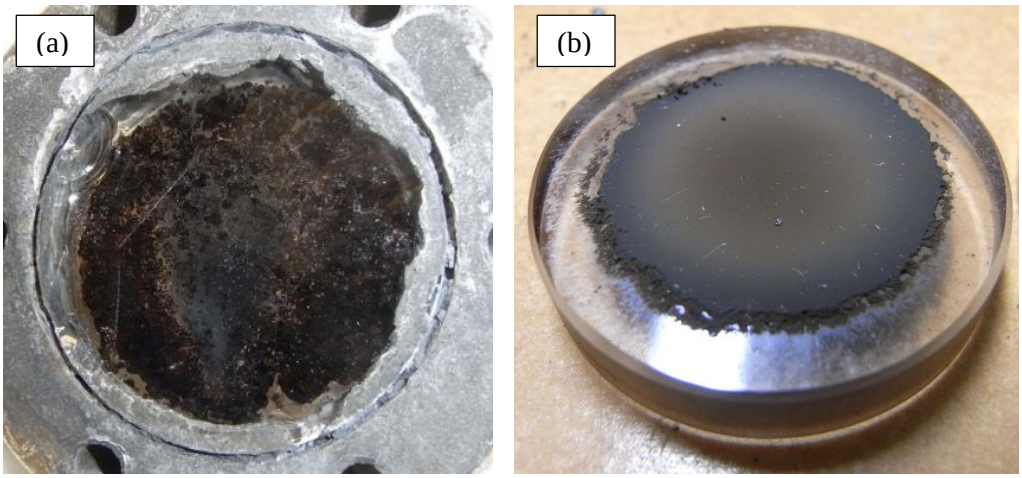

Figure 3–40: Images showing soot and tar deposition on top of gasifier sight glass (a) and middle of gasifier sight glass (b) during inspection after gasification operations

As shown in the figure, severe depositions were formed on both sight glasses after gasification operations. When comparisons were made between deposits from the two sight glasses, clear differences were observed particularly in terms of their physical appearance. Deposit collected on the top of gasifier sight glass as in Figure 3–40 (a) where shiny and adhere strongly to the glass while the opposite was observed on that at the middle of gasifier (Figure 3–40 b), in which the deposit were not shiny, dry and less sticky. From this observation, it is possible that the depositions were mainly from two different compounds in which the top sight glass was mainly covered by tar; while the sight glass located at the middle of the gasifier was covered by accumulation of soot during the operations.

In order to minimize deposition on the sight glasses, inert gas (nitrogen or helium) was continuously feed adjacent to the glass surfaces to promote better gas circulation in the affected area. This approach has been proven effective in reducing the amount of deposits on the top sight glass, as observed from all gasification operations performed after the introduction of inert gas into the system.

3.12.10 Char deposition on cooling jacket floor

Inspection of cooling jacket assembly after every gasification run revealed consistent paste-like deposition on the cooling jacket floor. The severity of the deposition varies from one operation to another. In cases where the deposit is more severe, crusty oil deposit was also formed near the nozzle outlet to an extent that almost obstructing pyrolysis oil atomization area. Figure 3–41 showed examples of photos captured after gasification operations showing deposition on the cooling jacket.

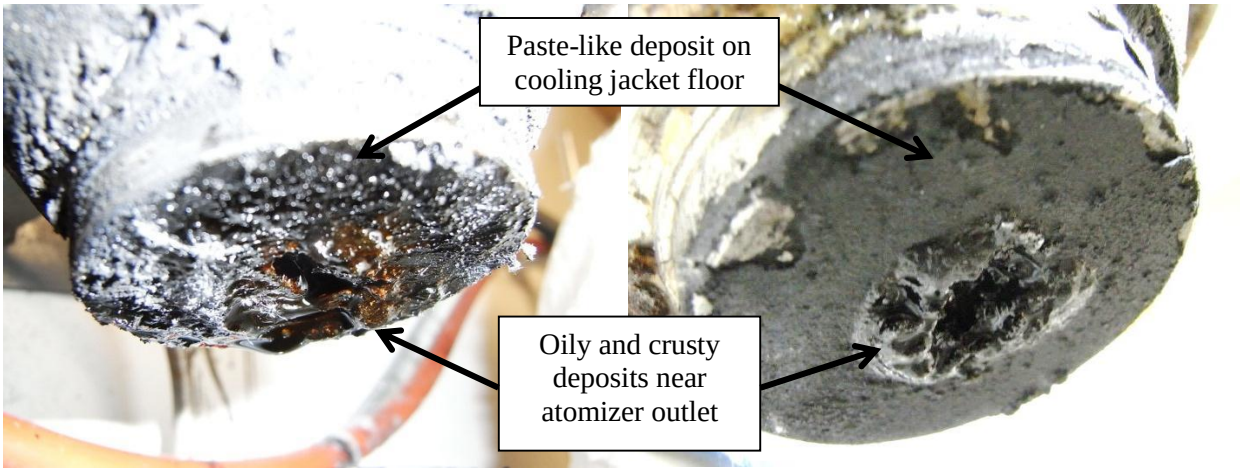

Figure 3–41: Picture showing cooling jacket floor condition after gasification

It is believed that the past-like deposit formed on cooling jacket surface may have resulted from pyrolysis oil mists that deposit on the cooling jacket floor during gasification operations. Entrained flow gasifier operates under turbulent flow regime with vigorous mixing and complicated flow patterns within the system. As soon as pyrolysis oil is injected and atomized in the system, small fractions of oil droplets and mists are expected to entrain in the turbulent flow and, in some circumstances, come into contact with reactor hot surfaces before turning into char from exposure to heat.

The crusty oil deposit, on the other hand, may have come from unsuccessful pyrolysis oil atomization that caused the oil to drip and gradually accumulated around the nozzle outlet. When exposed to gasification high temperature environment, the oil then swelled into crusty, swollen structure such as that is observed in Figure 3–41. The phenomenon of pyrolysis oil swelling at high temperature has been reported in the literature [19-21] and its effect is clearly shown in Figure 3–42. This provides a reasonable explanation to the unique deposition structure observed near the nozzle outlet area found in this study.

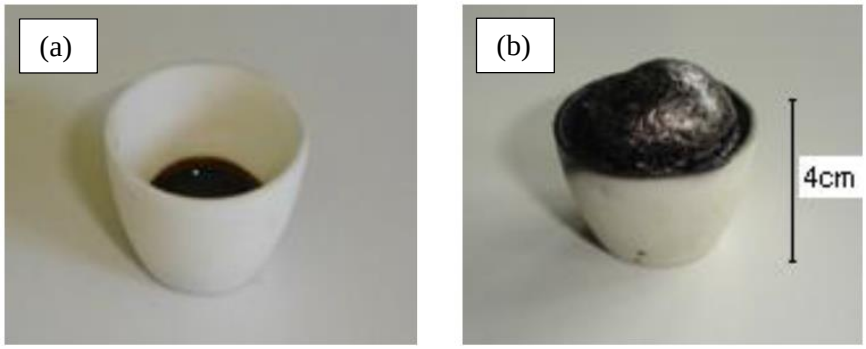

Figure 3–42: Effect of pyrolysis oil swelling after exposure to high temperature [adapted from [9]]

3.12.11 Atomizer and cooling jacket fouling during gasifier cooling down period

It is important that the atomizer and cooling jacket assembly are removed from the gasifier after every gasification operation to prevent excessive heating of the assembly when the system is not operating. Failure to remove the atomizer and cooling jacket assembly has been shown could lead to catastrophic fouling of the atomizer and its cooling system.

When gasification is stopped, supplies of oxygen gas and pyrolysis oil through the atomizer are also immediately cut. In this situation, certain amounts of oxygen and pyrolysis oil will still remain in the atomizer, corresponding to volumes of liquid and gas channels of the atomizer. Problem occurs when hot gasification environment in the gasifier continues to heat pyrolysis oil trapped in the atomizer and rapidly polymerization the oil to cause severe blockage to the atomizer liquid outlet. Severe polymerization and dehydration of pyrolysis oil upon exposure to heat for an extended period of time eventually forms thick solid layer of deposition on atomizer surfaces, thus making the condition even worse.

In addition to pyrolysis oil polymerization, release of condensable tar compounds from the oil at high temperature also lead to fouling due to tar condensing on the atomizer internal surfaces. Tar and polymerized oil are difficult to be removed, particularly on internal surfaces of the atomizer which are not easily accessible. Figure 3–43 provides selected photos showing severity of pyrolysis oil polymerization and tar decomposition on atomizer parts due to failure to remove the atomizer after gasification operation.

Figure 3–43: Images showing tar deposition and pyrolysis oil polymerization on atomizer parts when not removed from gasifier after gasification operation

In an event where the cooling jacket is left on the gasifier without continuous flow of cooling water, heat from the system rapidly boils remaining water in the cooling jacket into high temperature steam. This situation has been observed during commissioning run, in which the steam caused overheating of the silicon and rubber tubes, as well as PVC pipes used to supply water to the cooling jacket. Similar condition was observed for tubes and PVC pipes connecting the cooling jacket outlet and drain, but the effect was found to be more rapid and severe due to direct heating of air trapped in the system.

3.12.12 Pyrolysis oil phase separation

Since pyrolysis oil is a product of non-equilibrium process thus is relatively unstable, changes in its physicochemical properties with elapsed time are expected. Depending on the initial properties of the pyrolysis oil during fast pyrolysis process, changes to the oil properties may vary significantly from one production to another. In cases when pyrolysis oil is highly unstable, the oil usage for applications and for physicochemical measurements become more challenging; hence requires in-depth knowledge regarding pyrolysis oil ageing behaviour as well as careful planning of the operations.

In this work, the use of pyrolysis oil during measurements of its properties have been challenging due to its tendencies to phase separate. Pyrolysis oil phase separation can occur rapidly to an extent that replicates measurements of a sample produce significant variations and errors. This was observed during water content measurements using Karl Fischer titration method, in which consecutively injections of a same sample resulted decreasing trend as shown in Figure 3–44. In this experiment, pyrolysis oil was drawn into a 1 mL syringes before 0.1-0.2 mL samples were injected into the Karl Fischer successively for water content measurements. In between the replicate injections, the syringe was stored upright to prevent sample leak from the syringe. The test was also duplicated by taking new pyrolysis oil samples into syringe labelled ‘Duplicate 2’ and then ‘Duplicate 3’ to check for consistencies.

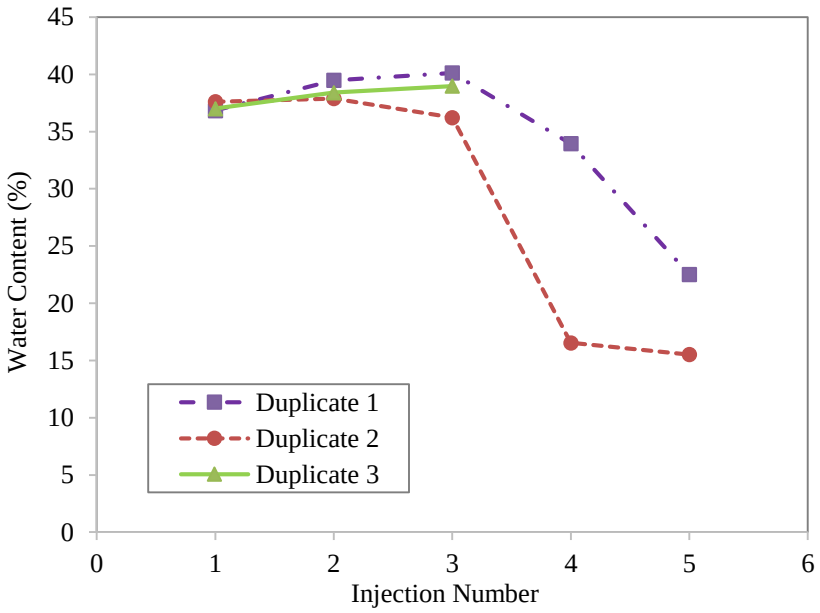

Figure 3–44: Pyrolysis oil water content measurements variations due to phase separation

The decreasing trends shown in Figure 3–44 could be explained by considering separation of light and heavy components of pyrolysis oil between replicate injections, where the heavier components settled at the bottom of the upright syringe hence injected later during the analysis. Heavy components of pyrolysis oil are generally non-polar and poorly coexist with water thus responsible for the low water content results in later injections as measured by the Karl Fischer titration. Similar trend was observed for the second duplicate in this study, thus verify phase separation problem of the sample used.

Phase separation also caused significant errors in pyrolysis oil viscosity measurements. Similar to water content results, rapid phase separation caused significant errors in replicate measurements. The use of capillary viscometer clearly showed pyrolysis oil separation into two distinct layers as shown in Figure 3–45.

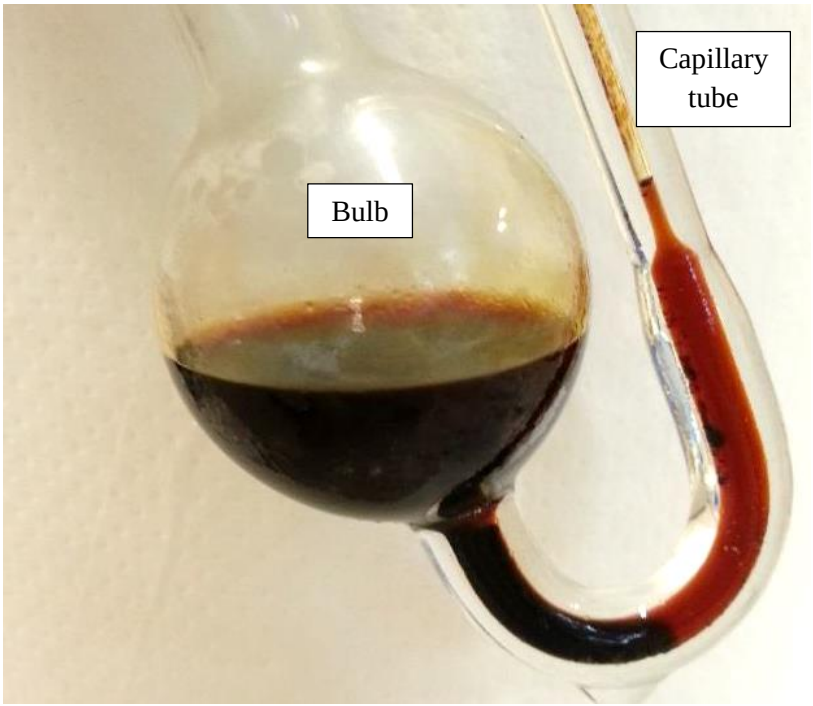

Figure 3–45: Image of pyrolysis oil in capillary viscometer showing distinctive phase separation between replicate measurements

Results for pyrolysis oil viscosity measurement are illustrated in Figure 3–46. Progressive phase separation of the pyrolysis oil caused the less viscous (lighter) components of the oil to fill the thin capillary section of the viscometer, which is the main section used for viscosity measurements. As more less viscous components of the oil accumulate in the capillary with time, continuous decline in the oil viscosity readings were observed. This error could be reduced by re-mixing the oil in the viscometer each

time prior to viscosity readings to make sure the oil is homogeneous during the measurements. Improvement on viscosity measurement after the mixing is also shown in Figure 3–46 for reference.

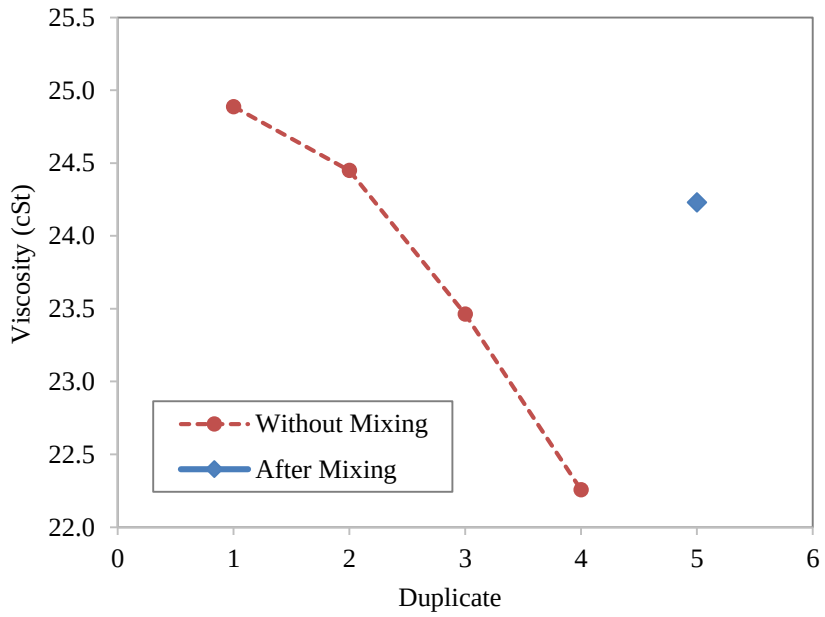

Figure 3–46: Pyrolysis oil viscosity measurement due to phase separation

Findings in this section highlight the importance of maintaining pyrolysis oil homogeneity at any time throughout properties measurement. Following that, all pyrolysis oil properties measurements should be conducted only after proper mixing of the samples, particularly between two or more replicate measurements. The findings also emphasize the importance of keeping pyrolysis oil properly mixed during gasification operations to minimized inconsistencies in the results. This was achieved by mixing pyrolysis oil continuously using an electric stirrer to prevent phase separation at any time during gasification operation.

3.12.13 Water and oxygen gas leak associated with cooling jacket

Cooling jacket leakage is highly undesirable as it often caused major interruptions to gasification operation, particularly when the problem is failed to be resolved quickly. Two modes of cooling jacket leakages that have been encountered in this work are:

i) Water leak from the cooling jacket into gasification system. Leakage of water into the gasifier alters gasification reactions and causes rapid decline in gasification temperature. In situations

where the problem is severe and failed to be overcome quickly, water will eventually flood the gasifier and consequently requires immediate shutdown of the entire process for maintenance works.

ii) Oxygen gas leak from the atomizer into cooling jacket. In this case, oxygen gas will mix with water and exit the cooling jacket towards the drain before escapes to the surrounding area. In an enclosed area such as inside a room or a building, this phenomenon could escalate to hazardous oxygen enrichment environment that could lead to various catastrophic accidents.

Figure 3–47 shows location of water leak from cooling jacket and two points on the atomizer-cooling jacket assembly that often responsible for leakage problems during gasification operations.

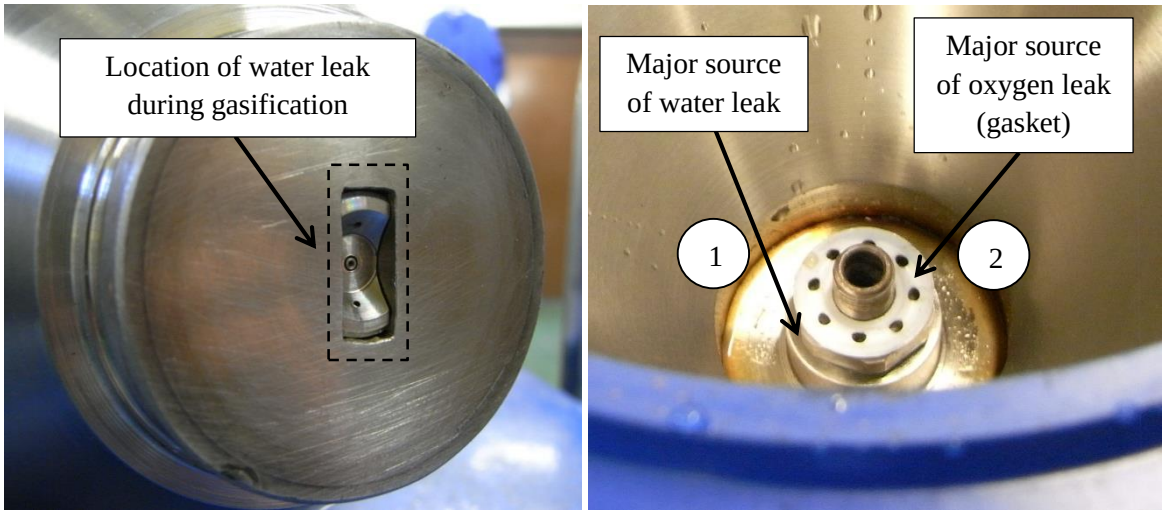

Figure 3–47: Images showing the location and major source of leaks on cooling jacket assembly

Outlet of water leak from the cooling jacket assembly is shown in Figure 3–47 (left) and could be solved by applying water repellent wax paste on the atomizer liquid cap threads during assembly, as shown in Figure 3–47 (1). This approach was taken so proper liquid seal could be achieved at the connection point. If leakage persists, complete disassemble of the atomizer-cooling jacket assembly is again required for this repair.

Solution to oxygen gas leak, however, is not straightforward. Gas seal between the liquid cap and atomizer body is achieved by Teflon gasket as shown in Figure 3–47 (2). Because of this reason, there should be a balance of how tight the liquid cap should be screwed to the atomizer body; while at the same time does not damage the atomizer liquid cap. Due to the atomizer size limitations, slight overpressure on the atomizer thread during its assembly is sufficient to cause damage to the atomizer thread.

During commissioning, two liquid caps were accidently broken while fixing the oxygen gas leakage problem, as shown in Figure 3–48. It is therefore important to maintain good balance on how tight the liquid cap has to be screwed to achieve gas tight connection between the two sections.

Figure 3–48: Pictures showing broken liquid cap (left) and normal liquid cap (right)

3.12.14 Producer gas leak between cooling jacket and gasifier top

As described in Chapter 3.7, the bottom section of the cooling jacket was designed in conical shape so it fits in the gasifier top flange perfectly when pyrolysis oil and oxygen gas are ready to be introduced into the system. Although the cooling jacket and its slot on the gasifier top flange are machined to fit perfectly together, the metal-metal connection is not gas tight thus minor gas leak from the system was still obtained during early gasification operations.

This leak released producer gas from inside the gasifier hence contains significant concentrations of hazardous and polluting gas components such as CO, CH_4, CO_2, soot and tar. Nevertheless the gas was rapidly removed from the area by an extraction fan thus did not pose direct threat to the operator. Producer gas leak from the cooling jacket was detected by presence of high CO concentration at the top section of the gasifier.

In order to solve this problem, a high temperature sealant was used in between the two metal surfaces to improve their connections. In this work, high temperature sealant of model DEACON 8875-Thin is used and has been proven capable of creating gas tight seal between the connections. DEACON 8875-Thin sealing performance has been consistent in all gasification runs. This sealant is selected due to its ability

to survive operation temperature as high as 980ºC thus is suitable for entrained flow gasification operations. Besides sealing the surfaces, the use of such sealant also acts as an anti-seize compound that prevents metal locking due to uneven expansions and cooling between the two metal surfaces.

3.13 References

1. Davis, J.R., ed. *ASM Speciality Handbook: Heat Resistant Materials*. 1997, ASM International.
2. Wire, G.L., E.J. Vesely, and S. Agarwal, *Erosion-corrosion of metals in coal gasification atmospheres.* Journal of Materials for Energy Systems, 1986. **8**(2): p. 150-167.
3. Krishnan, G.N., et al., *Diffusion Coatings for Corrosion-Resistant Components in Coal Gasification Systems*. 2005, Sri International.
4. King, P.J. and D.M. Doyle, *High temperature gaseous oxidation for passivation of austenitic alloys*. 2002, Google Patents.
5. Carlsson, P., et al., *Experimental investigation of an industrial scale black liquor gasifier. 1. The effect of reactor operation parameters on product gas composition.* Fuel, 2010. **89**(12): p. 4025-4034.
6. Clarke, S. and F. Preto. *Biomass Burn Characteristics: Fact Sheet*. 2011 [cited 2013 25 March]; Available from: http://www.omafra.gov.on.ca/english/engineer/facts/11-033.htm#5.
7. Outokumpu, *High Temperature Stainless Steels - Outokumpu MA Grades*. 2013, Outokumpu: Stainless Steel and High Performance Alloys.
8. Technology, S.M. *Sandvik 253 MA*. 2013; Available from: http://www.smt.sandvik.com/en/materials-center/material-datasheets/tube-and-pipe-seamless/sandvik-253-ma/.
9. Chhiti, Y., *Non catalytic steam gasification of wood bio-oil*. 2011.
10. Zhang, L., A. Chaparro Sosa, and K.B. Walters, *Impacts of Thermal Processing on the Physical and Chemical Properties of Pyrolysis Oil Produced by a Modified Fluid Catalytic Cracking Pyrolysis Process.* Energy & Fuels, 2016. **30**(9): p. 7367-7378.
11. Diebold, J.P., *A review of the chemical and physical mechanisms of the storage stability of fast pyrolysis bio-oils*. 2000: Citeseer.
12. Vispute, T., *Pyrolysis oils: Characterization, stability analysis and catalytic upgrading to fuels and chemicals*. 2011, University of Massachusetts: Amherst.
13. Emerson, *Plain Facts About Freezing Regulators*, in *Bulletin LP-24*. 2010, Emerson Process Management: Texas, USA.

14. Hahn, E. *The Properties and Composition of LPG*. [cited 2016 8th November 2016]; Available from: http://www.elgas.com.au/blog/453-the-science-a-properties-of-lpg.
15. Trimec, *Small Capacity Positive Displacement Pulse Flowmeter - Instruction Manual*. 2016, Trimec Industries Pty Ltd.
16. Lewin, C. *Precision Fluid Handling - Peristaltic Pump*. 2016; Available from: https://www.pmdcorp.com/resources/case_studies/4.
17. Neil McManus, C. and C. ROH, *Oxygen: Health Effects and Regulatory Limits Part I: Physiological and Toxicological Effects of Oxygen Deficiency and Enrichment.* 2009.
18. TechEdge, *Wideband Oxygen Sensor Installation Guide*. 2006, Tech Edge Pty Ltd.
19. Wornat, M.J., B.G. Porter, and N.Y.C. Yang, *Single Droplet Combustion of Biomass Pyrolysis Oils.* Energy & Fuels, 1994. **8**(5): p. 1131-1142.
20. Lehto, J., A. Oasmaa, and Y. Solantausta, *Fuel oil quality and combustion of fast pyrolysis bio-oils.*
21. Calabria, R., F. Chiariello, and P. Massoli, *Combustion fundamentals of pyrolysis oil based fuels.* Experimental Thermal and Fluid Science, 2007. **31**(5): p. 413-420.

4 CALCULATIONS AND METHOD DEVELOPMENT

This chapter presents various methods used for calculations and analyses of experimental data collected from the entrained flow gasification operations. It provides relevant formula and step-by-step guidelines on how raw data collected during experiments were analysed and interpreted to provide more useful information about the system's behaviour, producer gas yield and composition.

4.1 Block Diagram and Definition of Terms

Inlet and outlet materials for the entrained flow gasification of pyrolysis oil used in this study could be presented as a block diagram, as illustrated in Figure 4–1. The block diagram presents reactants and products species entering and exiting the system, as well as symbols used to represent their flow rates and compositions. These symbols will be used in the subsequent sections for calculating various parameters used to define gasification performance in this work.

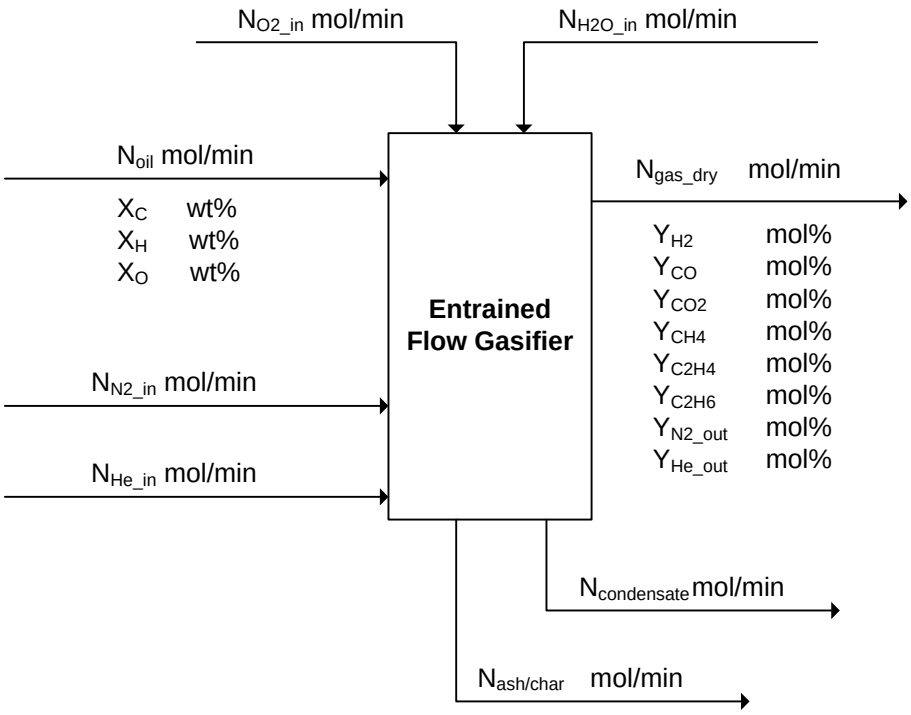

Figure 4–1: Block diagram for entrained flow gasification of pyrolysis oil used in this system

Inlet and Outlet Variables

N_{oil}	Molar flow rate of bio-oil feed into the gasifier (mol/min)
N_{O2_in}	Molar flow rate of oxygen gas feed into the gasifier (mol/min)
N_{N2_in}	Molar flow rate of nitrogen gas feed into the gasifier (mol/min)
N_{H2O_in}	Molar flow rate of water/steam addition into the gasifier (mol/min)
N_{He_in}	Molar flow rate of helium gas feed into the gasifier (mol/min)
N_{gas_dry}	Total molar flow rate of dry producer gas exiting gasifier (mol/min)
$N_{condensate}$	Total molar flow rate of condensate exiting gasifier (mol/min)
$N_{ash/char}$	Total molar flow rate of solid exiting gasifier (mol/min)
X_C	Carbon mass faction in bio-oil (wt%)
X_H	Hydrogen mass faction in bio-oil (wt%)
X_O	Oxygen mass faction in bio-oil (wt%)
Y_{H2}	Molar fraction of hydrogen gas in dry producer gas (mol/mol)
Y_{CO}	Molar fraction of carbon monoxide gas in dry producer gas (mol/mol)
Y_{CO2}	Molar fraction of carbon dioxide gas in dry producer gas (mol/mol)
Y_{CH4}	Molar fraction of methane gas in dry producer gas (mol/mol)
Y_{C2H4}	Molar fraction of ethylene gas in dry producer gas (mol/mol)
Y_{C2H6}	Molar fraction of ethane gas in dry producer gas (mol/mol)
Y_{N2_out}	Molar fraction of nitrogen gas in dry producer gas (mol/mol)
Y_{He_out}	Molar fraction of helium gas in dry producer gas (mol/mol)

$Q_{N\_gas\_dry}$ = Normal volumetric flow rate of dry producer gas (N L/min)

Q_{gas_dry} = Volumetric flow rate of dry producer gas (L/min)

$Q_{condensate}$ = Volumetric flow rate of condensate (L/min)

$Q_{N\_gas\_total}$ = Normal volumetric flow rate of total producer gas, including water (N L/min)

Q_{gas_total} = Volumetric flow rate of total producer gas, including water (L/min)

Q_{He_in} = Volumetric flow of Helium gas supplied into the system (L/min)

$M_{bio-oil}$ = Mass flow rate of pyrolysis oil feed into the system (g/min)

M_{gas_dry} = Mass flow rate of dry producer gas (g/min)

$M_{ash/char}$ = Mass flow rate of char, ash and other solids (g/min)

M_{gas_total} = Mass flow rate of total producer gas, including water (g/min)

ρ_i = Density of species (g/L)

MW_i = Molecular weight of species (g/mol)

$T_{gasification}$ = Gasification temperature (K)

$T_{ref\ (273K)}$ = Reference temperature (293K)

$P_{ref\ (1\ atm)}$ = Reference pressure (bar or atm)

$P_{gasification}$ = Gasification pressure (bar or atm)

$D_{reactor}$ = Diameter of EF gasifier reactor section (m)

$H_{reactor}$ = Height of EF gasifier reactor section (m)

v_{gas} = mean velocity of producer gas in reactor (m/s)

t_{gas} = producer gas residence time (s)

η_{cold_gas} = Cold gas efficiency

LHV_{gas} = Lower heating value of producer gas (MJ/Nm^3)

$LHV_{bio-oil}$ = Lower heating value of bio-oil (MJ/kg)

4.2 Determination of Gasification Dry Producer Gas Composition

Concentrations of components of the producer gas collected from gasification experiments were measured by using an Agilent 3000A Micro-GC with thermal conductivity detector (TCD). Micro-GC has low tolerance to water vapour in its operation, thus in this work producer gas composition is presented in water-free or dry basis.

Typical composition of producer gas from biomass gasification has been reported to consist of hydrogen (H_2), carbon monoxide (CO), carbon dioxide (CO_2), methane (CH_4), ethylene (C_2H_4) and ethane (C_2H_6). To quantify all of the producer gas components, two analytical columns were used in the Micro-GC. The first column was a MolSieve 5A Plot 10m x 0.32mm column, operating at 110^{o}C, which was used to determine H_2, N_2, CH_4 and CO species. The second column was a Plot Q 8m x 0.32mm column, operating at 60^{o}C, which was used to determine CO_2, C_2H_4 and C_2H_6 gas species.

The carrier gases for MolSieve 5A Plot and Plot Q columns were Argon and Helium, respectively. In the experiments, Micro-GC was also used to determine the concentration of tracer gas, helium, which information was then used to calculate the producer gas flow rate and product yield as described in the following section. Helium was detected in the MolSeive 5A Plot column.

The analysis method used to quantify producer gas composition in this work is similar to that used by Saw et al. [1-3].

4.3 Determination of Dry Producer Gas Flow Rates and Yields

In this work, helium gas was used as the tracer gas due to its inert nature. The flow rate of the helium gas entering the gasifier system was between 2.5 and 5 L/min and was controlled using a calibrated rotameter with an accuracy of ± 0.15 L/min. Molar flow rate of helium gas (mol/min) entering the system was derived from the gas volumetric flow rate as measured by gas rotameter (L/min) using conversion equation as follows:

$$N_{He\_in} = \frac{Q_{He\_in} \times \rho_{He}}{MW_{He}} \qquad \text{Equation 1}$$

Considering the inert nature of the helium gas, the molar flow rate or the mass flow rate into the gasifier is equal to that out of the gasifier:

$$N_{He\_in} = N_{He\_out} \qquad \text{Equation 2}$$

Once the helium outlet flowrate is known and the helium concentration in the producer gas is determined, the producer gas flow rate is calculated by:

$$N_{He\_out} = N_{gas\_dry} \times Y_{He\_out} = N_{He\_in} \qquad \text{Equation 3}$$

The flow rate of producer gas calculated with this method is based on water dry basis since the concentrations of helium tracer gas, as measured by Micro-GC, was based on water free concentration. A separate term was used to quantify water content and other condensates ($N_{condensate}$). Rearrangement of the equation gives the total moles of dry producer gas exiting the system:

$$N_{gas\_dry} = \frac{N_{He\_in}}{Y_{He\_out}} \qquad \text{Equation 4}$$

From the total dry producer gas molar flow rate, the producer gas volumetric flow rate at normal condition (25°C and 1atm) could be calculated:

$$Q_{N\_gas\_dry} = N_{gas\_dry} \times 24 \ (\frac{L}{mol}) \qquad \text{Equation 5}$$

The normal volumetric flow rate value obtained from this calculation can then be used to estimate the actual producer gas volumetric flow rate at gasification temperature according to Ideal Gas law principle as follows:

$$Q_{gas\_dry} = Q_{N\_gas\_dry} \times \frac{T_{gasification}}{T_{ref\,(273K)}} \times \frac{P_{ref\,(1\,atm)}}{P_{gasification}} \quad \text{Equation 6}$$

In this calculation, several important assumptions were made as listed below:

i. $T_{gasification}$is the average gasification temperature as calculated from the middle and bottom sections of the gasifier
ii. Any change of producer gas volumetric flow rate due to reactions after exiting the gasifier is considered negligible

The mass flow rate of dry producer gas was calculated by summing mass flow rates of each gas components present in the producer gas as illustrated in the following equation:

$$M_{gas\_dry} = \sum Y_i \times N_{gas\_dry} \times MW_i \quad \text{Equation 7}$$

4.4 Determination of Tar Species in Producer Gas

The methods used to determine species and concentrations of tar present in the producer gas during gasification were adapted from [2-4]. Species of tar present in the producer gas are determined using a gas chromatography (GC). The GC used in this study is Varian CP-3800 model with a flame ionization detector (FID) for tar components detection. The GC column used for this analysis is a 50% phenyl and 50% dimethyl-polysiloxane fused silica capillary with dimensions of 30m x 0.25 µm x 0.25µm. Tar analysis was performed at temperature of 300^{o}C using Helium as the carrier gas (1 mL/min).

In order to extract the tar molecules trapped in the SPE columns, solvents with suitable properties were used. In this work, two extraction solvents of Dichloromethane (DCM) and Isopropanol (IPA) were used to extract most tar compounds adsorbed to the SPE column matrix. DCM is a non-polar solvent and was used to flush off less-polar compounds such as naphthalene, acenaphthalene, fluoranthene, pyrene and chrysene from the SPE column. On the other hand, polar IPA solvent was used to extract polar compounds such as phenol, toluene, xylene, cresol and styrene from the column.

During tar extraction, weak polarity compounds like most polycyclic aromatic hydrocarbons (PAH) were extracted by flushing the columns with 0.9 mL of the DCM solvent into a 2 mL vial. Meanwhile, more polar tar compounds were extracted by flushing the same SPE columns with 0.9 mL of the IPA solvent. In both approaches, 0.1 mL of 400 ppm of n-dodacane was added into the vials to act as an internal standard (IS) during tar analysis in the GC.

The solvents containing tar compounds extracted from SPE columns were labelled accordingly before being stored in a refrigeration unit at temperature below 4ºC until analysis using GC. The complete operating procedures for extraction solvent preparations, tar extraction and tar calibration in the GC are presented in Chapter 10: Appendix E for reference.

4.5 Determination of Gas Residence Time

In this context, gas residence time is defined as the time of producer gas travelling across the entrained flow gasifier height. The residence time was calculated as the reactor height (m) divided by the gas mean velocity (m/s) as the following equation:

$$t_{gas} = \frac{H_{reactor}}{v_{gas}} \qquad \text{Equation 8}$$

In order to obtain the mean velocity of producer gas in the gasifier, the total volumetric flow rate of the producer gas (m^3/min) was divided by the cross section area of the gasifier reactor (m^2).

$$v_{gas} = \frac{Q_{gas\_total}}{1000 \times 60} \times \frac{4}{\pi {D_{reactor}}^2} \qquad \text{Equation 9}$$

Q_{gas_total} is the sum of Q_{gas_dry} and $Q_{condensate}$. $Q_{condensate}$ is calculated from mass flow rate of condensate (g/min) from the gasification operation divided by density of water (g/L).

4.6 Determination of Carbon Conversion Efficiency

The percentage of carbon converting to producer gas from pyrolysis oil during gasification can be calculated by dividing the total mass of carbon measured in the producer gas by the total carbon in the pyrolysis oil feed into the system. This is represented by the following equation:

$$\eta_c = \frac{M_{carbon\_gas}}{M_{carbon\_feed}} \times 100\% \qquad \text{Equation 10}$$

While the total carbon in pyrolysis oil was obtained directly from the oil elemental analysis, the amount of carbon exiting the system is calculated based on molar flow rates of producer gas components containing carbon, in this case, CO, CO_2, CH_4, C_2H_4 and C_2H_6. The equation used for this calculation is as follows:

$$\eta_c = \frac{[N_{CO} + N_{CO2} + N_{CH4} + (2 \times N_{C2H4}) + (2 \times N_{C2H6})] \times MW_C}{X_C \times M_{bio-oil}} \times 100\% \qquad \text{Equation 11}$$

4.7 Determination of Producer Gas Lower Heating Value (LHV)

The heating value of producer gas varies largely depending on the amount of combustible gas species it contains. The common combustible gas species in producer gas include H_2, CO, CH_4, C_2H_4 and C_2H_6. In general, producer gas with high heating values indicate better gas quality as it contains more useful gases for downstream applications such as direct combustion, methanation and bio-diesel production. In this work, heating values of producer gas was determined in terms of its lower heating values (LHV), which is estimated by taking the sum of each producer gas constituent heating values (LHV_i) multiplied by their corresponding molar or volumetric percentages (Y_i).

$$LHV_{gas} = \sum(Y_i \times LHV_i) \qquad \text{Equation 12}$$

The heating values of combustible gas species in producer gas are listed as follows [5]:

H_2 = 10.79 MJ/Nm^3

CO = 12.63 MJ/Nm^3

CH_4 = 35.80 MJ/Nm^3

C_2H_4 = 59.46 MJ/Nm^3

C_2H_6 = 64.35 MJ/Nm^3

4.8 Determination of Thermal Efficiency

Thermal efficiency of a system is defined as the ratio of the total chemical energy contained in the products to the energy of the original feedstock supplied into the system. Thermal efficiency can be presented by either cold gas efficiency, hot gas efficiency or net gasification efficiency. This study used

cold gas efficiency as a representation of the system's thermal efficiency and is calculated using the total energy output from producer gas divided by the total energy input from pyrolysis oil feedstock.

$$\eta_{cold\_gas} = \frac{Q_{N\_gas\_dry} \times LHV_{gas}}{M_{bio-oil} \times LHV_{bio-oil}} \quad \text{Equation 13}$$

4.9 Determination of Gas Yield

Gas yield of individual components of producer gas generated during gasification is determined by the ratio of mass flow rate of each gas species (M_i) to the total mass flow of pyrolysis oil fed into the system ($M_{bio-oil}$).

$$GY_i = \frac{M_i}{M_{bio-oil}} \quad \text{Equation 14}$$

The total producer gas yield, on the other hand, is calculated by dividing the total dry mass flow rate of producer gas (M_{gas_dry}) with the total mass flow of pyrolysis oil entering the system ($M_{bio-oil}$). This calculation is represented by the following equation:

$$GY_{total} = \frac{M_{gas\_dry}}{M_{bio-oil}} \quad \text{Equation 15}$$

Using this calculation method, the results are presented in weight basis, often in g_{gas}/g_{oil} unit. Gas yield could also be presented in volume/mass basis in which the unit is Nm^3/kg, and could be calculated using the following equation:

$$GY_{total} = \frac{Q_{N\_gas\_dry}}{M_{bio-oil}} \quad \text{Equation 16}$$

4.10 References

1. Saw, W., et al., *Production of hydrogen-rich syngas from steam gasification of blend of biosolids and wood using a dual fluidised bed gasifier.* Fuel, 2012. **93**(0): p. 473-478.
2. Saw, W.L. and S. Pang, *The influence of calcite loading on producer gas composition and tar concentration of radiata pine pellets in a dual fluidised bed steam gasifier.* Fuel, 2012. **102**(0): p. 445-452.

3. Saw, W.L. and S. Pang, *Co-gasification of blended lignite and wood pellets in a 100kW dual fluidised bed steam gasifier: The influence of lignite ratio on producer gas composition and tar content.* Fuel, 2013. **112**(0): p. 117-124.
4. Brage, C., et al., *Use of amino phase adsorbent for biomass tar sampling and separation.* Fuel, 1997. **76**(2): p. 137-142.
5. Waldheim, L. and T. Nilsson, *Heating value of gases from biomass gasification.* Report prepared for: IEA bioenergy agreement, Task, 2001. **20**.

5 INVESTIGATION ON ATOMIZATION OF PYROLYSIS OIL AND SPRAY CHARACTERISTICS IN A COLD MODEL

5.1 Introduction

Combustion of liquid in spray form is an important principle that by itself is a comprehensive field of study. Knowledge in spray combustion behaviour in particularly is extremely valuable as it leads towards high efficiency combustions for wide-range applications such as in piston engines, industrial furnaces and gas turbines. Spray combustion behaviour is rather complicated as it varies significantly from one application to another based on physicochemical properties of the liquid as well as chemical reactions involved between the spray droplets and their surroundings [1].

Recently, advances in computational modelling have made it possible for sophisticated mathematical models to be solved to predict spray combustion behaviour at various operation conditions. In general, mathematical modelling provides more universal outcome in comparison to experimental data. While mathematical models have successfully predicted combustion behaviour in many aspects, applications of the model results in practical spray combustion are still limited because of wide variability of systems and operation conditions. In a more complex two phases reacting system where the spray exists in both liquid and vapour forms during combustion, comprehensive knowledge on thermodynamics, fluid dynamics, physical interactions, chemical reaction and kinetics are also required during model development in order for the mathematical models to be more accurate to reality [1].

There are several important factors that determine combustion behaviour of a spray, one of which is the spray characteristics which include spray pattern, spray dimensions, spray angle, droplets size, droplets spatial distribution, spray propagation and droplet velocities [2]. The relationship between spray characteristics and combustion behaviour has been discussed earlier in Chapter 2.5. Some physical attributes of a spray, like droplets spatial distribution and spray propagation, can also provide information on interactions between individual droplets within the spray; hence this information can be used to better understand spray combustion behaviour at high temperatures.

In this work, experiments were conducted at room temperature to investigate the relationship between atomization inlet conditions (pyrolysis oil and oxygen flow rates) and spray characteristics. Results from this study will be used in Chapter 7 to help understand influences of pyrolysis oil spray characteristics on gasification products in entrained flow gasification of biomass pyrolysis oil.

5.2 Materials and Method

5.2.1 Experimental Setup

In order to simulate pyrolysis oil spraying characteristics within the entrained flow gasifier, a cold model of pyrolysis oil atomization was designed and built. The setup consists of an enclosed spray chamber, with the front and back walls made of clear Perspex material to provide good light penetration for observation and sample collection. The chamber is integrated with a custom built air curtain located at the front wall to prevent pyrolysis oil mist from staining the wall, so it remains clear throughout the experiment. There is also a constant flow of fresh air across the spray chamber initiated by an extraction fan to avoid accumulation of spray mist within the chamber.

During operation, pyrolysis oil and atomizing gas are fed from the top of chamber. For safety reasons, compressed air was used as the atomization gas in this study as a replacement to oxygen gas. This is because oxygen gas is a highly reactive reactant that could easily oxidize pyrolysis oil under normal ambient conditions. This substitution would not affect the results for this part of study as the goal was to investigate spray formation and its characteristics under various pyrolysis oil and gas flow rates.

For the experiments, oxygen and pyrolysis oil are fed into the system through a twin-fluid atomizer. Pyrolysis oil is supplied into the spray chamber using a peristaltic pump to generate flow rate up to 2000 mL/min. Two particulate filters are located on the pyrolysis oil supply line to remove solids contaminants as small as 10μm from the oil. A positive displacement flow meter is installed after the pump so that accurate flow rate measurements could be obtained at any point during experiment. The pump, filters, flow meter and atomizer are inter-connected by high resistance platinum-cured silicon tube of inner diameter 8.0mm and 2.4mm wall thickness for protection towards chemical degradation caused by pyrolysis oil.

5.2.2 Process Schematic Diagram

Figure 5–1 shows process flow diagram of the cold model atomization experimental setup developed in this work.

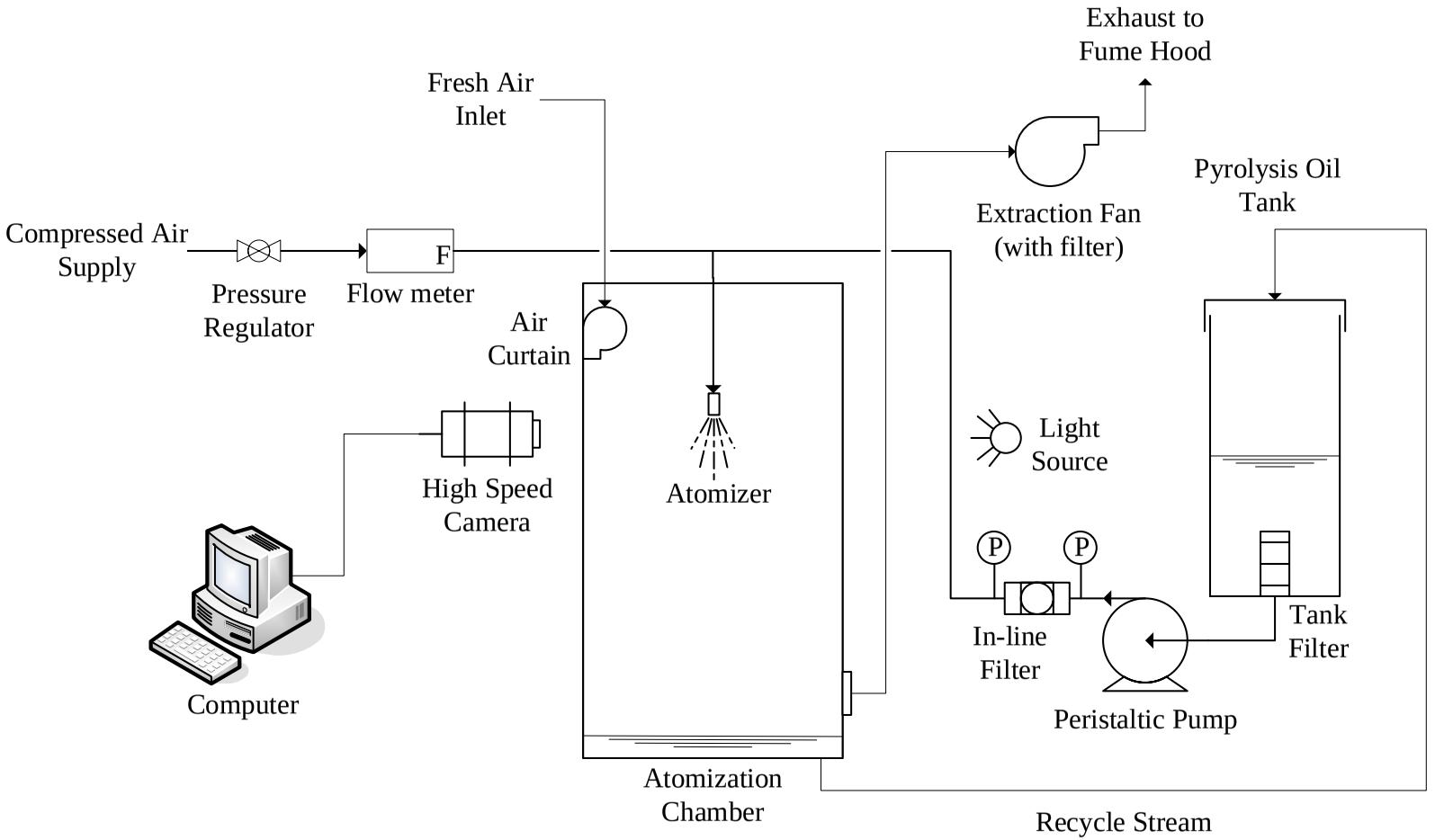

Figure 5–1: Process flow diagram for pyrolysis oil spray characteristics experimental setup

5.2.3 Experiments

Information regarding the atomizer used in this work has been given in Chapter 3.7. The atomizer consists of two main components which are 'liquid cap' and 'air cap'. For this investigation, three different atomizer liquid caps were tested in this work to select the cap which can achieve the required spray characteristics. The only difference between these caps was the diameter of orifice where liquid exits the nozzle. Images of the atomizer liquid cap are shown in Figure 5–2 while the diameters of liquid outlet for the three caps tested were specified as in Table 5-1.

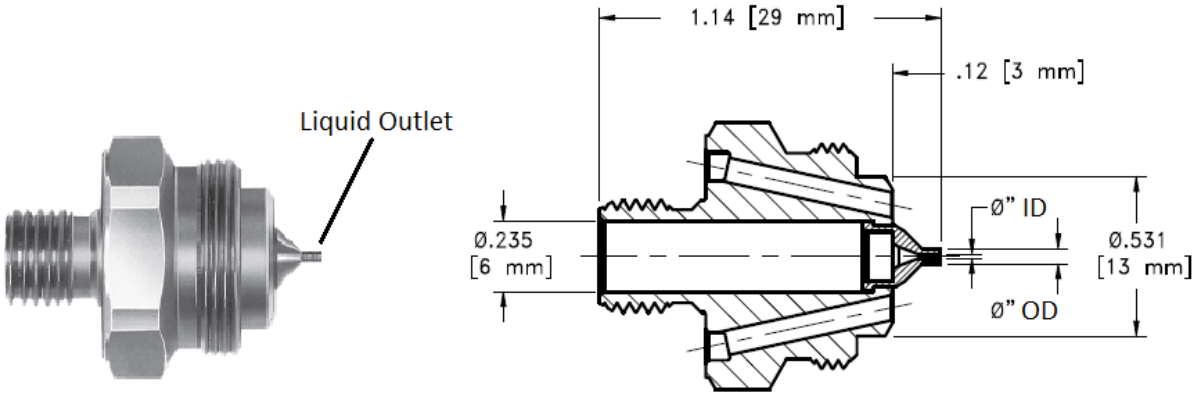

Figure 5–2: Images of atomizer liquid cap showing its liquid outlet and dimensions

Table 5-1: Liquid outlet sizes of three different liquid caps tested in this study

Number	Liquid Cap Model	Liquid Outlet Diameter (mm)	
		Inner (ID)	Outer (OD)
1	1650	0.41	1.27
2	2050	0.51	1.27
3	2850	0.71	1.27

In theory, liquid cap with the smallest liquid outlet diameter (model 1650) creates the finest liquid jet upon exiting the nozzle hence breaks the liquid into fine liquid droplets more easily when impacted by the atomizing gas. On the other hand, small liquid outlet means greater restrictions to pyrolysis oil flow thus significantly reduces the total throughput for the entrained flow gasification system. Small liquid outlet diameter also escalates risks of atomizer blockage by ash and other solids contaminants in the pyrolysis oil. The opposites are true for liquid cap with the largest outlet diameter (model 2850).

The atomizer air cap used in this work was designed to have two dissimilar sides in order to enable formation of flat spray pattern during its operation. To differentiate between these two sides, one side is named as ‘edge side’ and the other as ‘front side’, respectively. Figure 5–3 illustrates the shape of the air cap used in this study and different images produced from both sides for comparison. In the results and discussion sections of this chapter, if it is not mentioned, the results are for the sprays from edge view.

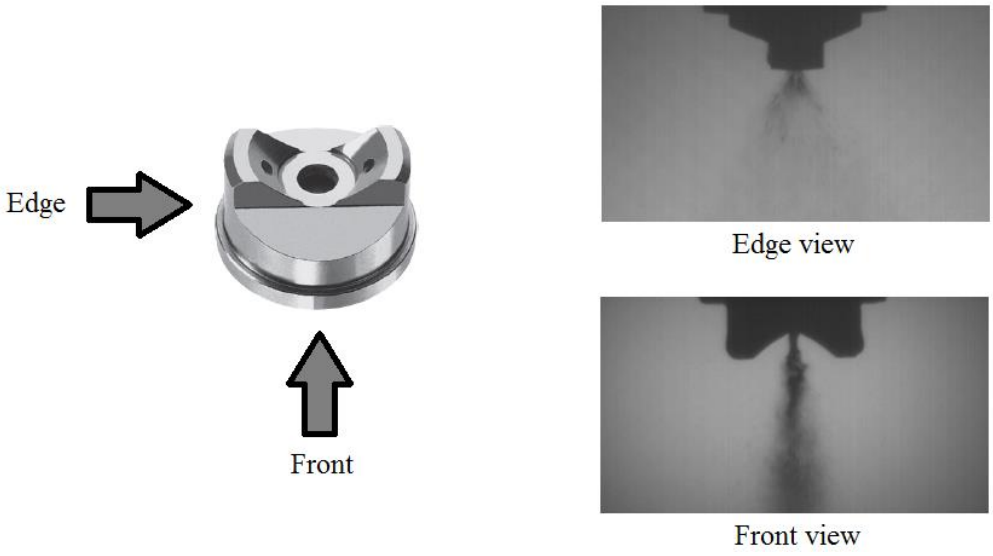

Figure 5–3: Different sides of atomizer air cap and examples of their corresponding spray views

5.2.4 Sampling and Analysis Method

For quantifying the spray characteristics, this study utilized ‘direct photography’ approach where a camera was used to capture spray images at various operating conditions. These images were then analysed by an image processing software. Direct photography is a convenient method for this study because no probe or obstruction was required to be inserted into the spray chamber during data collection. However, measurements from this sampling method are limited to the outer region of a spray [2].

The spray characteristics analysis using direct photography method has been improved by using high speed cameras. This device is capable of capturing multiple images within extremely short time intervals (≤ 0.0009 seconds) hence freezes any objects in motion for highly accurate analysis. Application of high speed camera in direct photography method has been used in many atomization studies such as that reported by Kolb et al. [3] who measured spray droplets sizes and velocities using high definition charged-coupled device (CCD) camera with NdYang laser flash as the source of light. Similar method has been used in studies on black liquor spray characteristics as described in [4-7].

In this work, spray images were captured using Mega Speed MS50K high speed camera which capable of capturing at least 1068 frames per second. A halogen light was placed behind the spray to supply maximum brightness during shortest shutter exposure times to add clarity on every image captured. The images were then analysed using Image-J software to determine the resulted spray characteristics. During the analysis, attention was given only on spray characteristics near atomizer nozzle since spray development downstream of this region is significantly influenced by the initial spray behaviour upon leaving the atomizer [8].

5.3 Results and Discussions

5.3.1 Calibration of Peristaltic Pump

In this investigation, the peristaltic pump used to feed the biomass pyrolysis oil into the entrained flow gasifier was first calibrated. In the calibration, the pump rotation speed, measured in revolution per minute (RPM) was gradually increased from 5 to 90 and the pyrolysis oil flow rates (mL/min) were measured for a specific liquid cap. This was repeated for all of the three caps. Pyrolysis oil flow rate was measured using a positive displacement flow meter. This particular type of flow meter was chosen due to its ability to generate accurate flow readings regardless of liquid pressure and physical properties. This feature is critical considering pyrolysis oil unstable nature where important properties such as viscosity, density and surface tension could change noticeably due to ageing effects. Change in liquid viscosity, in particular, is known to have significant impact on flow rate of liquid exiting an orifice where viscous liquid is generally more difficult to flow due to greater resistance, thus making instantaneous pyrolysis oil flow rate measurements independent of liquid properties crucial for this operation.

Figure 5–4 shows the calibration results from which it is found that the relationships between the pyrolysis oil flow rate and the pump rotation speed were different for different liquid caps. As expected, at the same pump rotation speed, the oil flow rate using cap 1650 was the lowest and that using cap 2850 was the highest. The variations of flow supply from different liquid caps relates to flow restriction caused by the liquid outlet orifice where depending on the diameter of the orifice, the resulted flow rate of pyrolysis oil can change from one operation to another although the pump speed was kept constant.

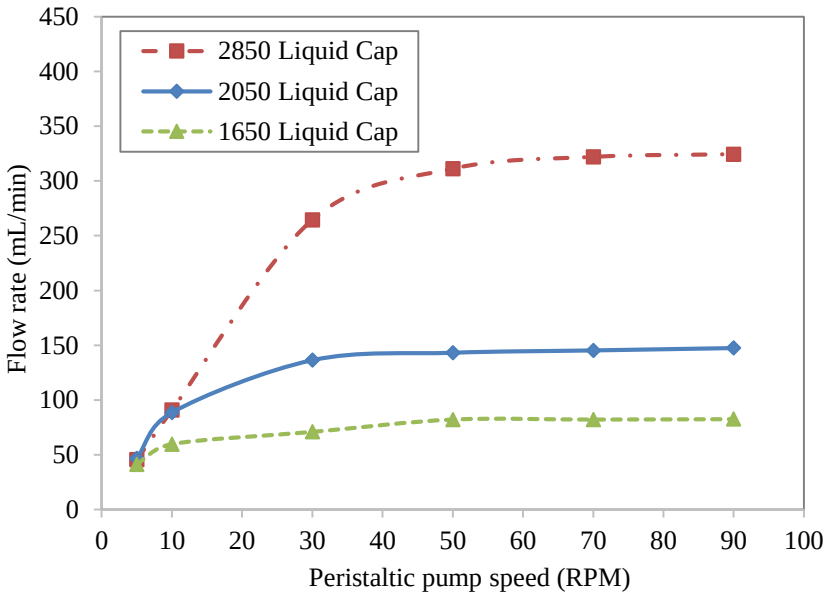

Figure 5–4**:** Relationship between peristaltic pump speed and pyrolysis oil flow rate

For a given liquid cap, the oil flow rate was only in linear relationship with the pump rotation speed at low values. With further increase in the pump speed, the relationship became non-linear where further increase of pump speed eventually caused little changes to the oil flow rate. The critical pump speed in which the pump function started to become non-linear vary depending on the liquid cap and were shown to increase sequentially from as early as 10 rpm for both 1650 and 2050 caps to around 30 rpm for 2850 liquid cap. The trends observed in Figure 5–4 can be used as operation guide for the peristaltic pump to achieve target pyrolysis oil flow rate.

To further investigate the pump performance and for safety reasons, oil pressure at the pump outlet was also measured where the pressure was the highest in the system. The pump head was designed to supply liquid with pressure up to approximately 200kPa. Build-up of liquid pressure occurs due to restriction of liquid flow by the atomizer liquid cap and is proportional to pump speed. Therefore, the pump head pressure limit functions as a safety requirement to prevent over-pressuring or bursting the silicon tube.

In practice when liquid pressure exceeds the operation limit, the pump's rotor rollers are unable to perform peristaltic action (alternating compressions and relaxations) efficiently and consequently fail to pump more oil into the tube. Figure 5–5 shows the oil pressure at the pump outlet as a function of pump rotation speed. The limit to the pump operating pressure also justifies the non-linearity of pyrolysis oil flow when the critical pump speed is reached during the operation.

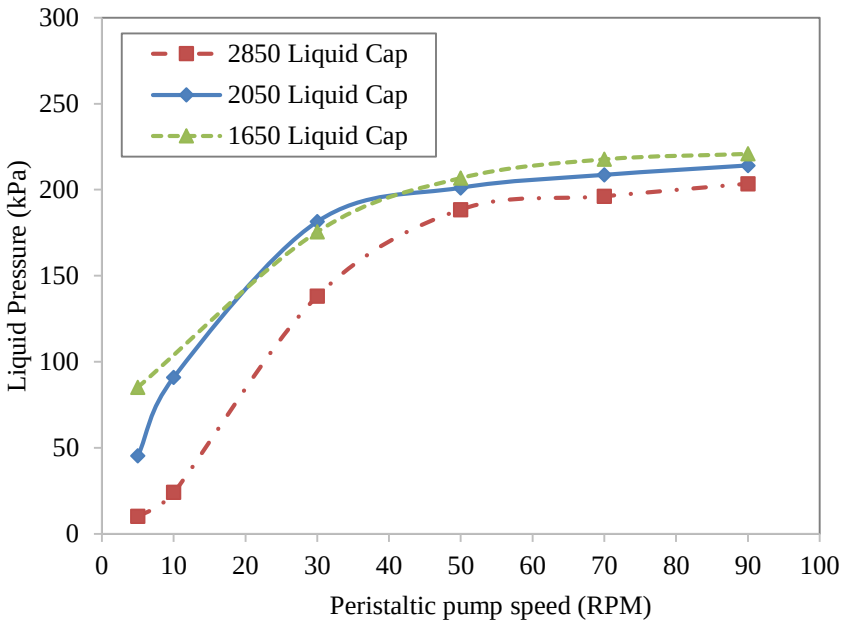

Figure 5–5: Relationship between liquid pressure at pump outlet and the pump rotation speed.

Information on liquid pressure during peristaltic pump operation can also be used to determine if the pyrolysis oil feeding system is partially or completely blocked so appropriate actions could be taken. Blockage of pyrolysis oil flow is a serious issue during entrained flow gasifier operation with pyrolysis oil that could cause severe interruptions during gasification operations if not managed accordingly. In addition, if blockage of pyrolysis oil flow is fail to be identified and oxygen feed continues, the gasifier will contain excessive amount of oxygen that will lead to complete combustion and potentially caused the gasifier to be over-heated. Most importantly this condition could also escalate to hazardous conditions if the condition is not attended appropriately. Therefore, detection of pyrolysis oil feed blockage is undoubtedly important.

As previously discussed in Chapter 3.12.2.2, blockage in the pyrolysis oil feeding system can be identified by monitoring the pressure profiles before and after the on-line filter. During normal operations, liquid pressure after the filter should be much less than that before the filter as a result of pressure drop across filter media at the constant oil flow rate through the atomizer. However, when blockage occurs, flow of pyrolysis oil exiting the system is interrupted or completely stopped thus causing pressure build-up throughout the entire feeding system. In this case only small pressure differences are expected before and after the filter, due to pressure drop across the filter media. Figure 5–6 shows differences in pyrolysis oil pressure during normal operation compared to that when the oil feeding system is completely clogged.

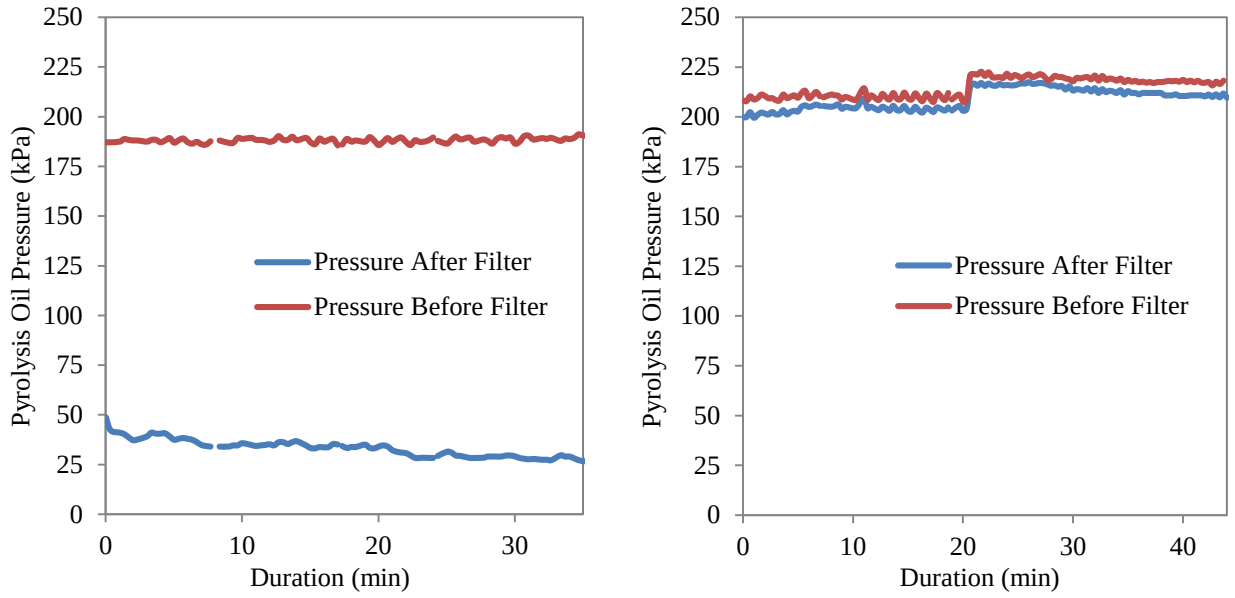

Figure 5–6: Pyrolysis oil pressure profiles during (a) normal operation without blockage (b) operation with total blockage on liquid cap

In most cases, blockage of pyrolysis oil feeding system occurred due to interruptions of the oil flow through the atomizer. Causes of atomizer blockage during entrained flow gasification of biomass pyrolysis oil could be categorized into external and internal factors which are briefly discussed in the following sections:

1) External blockage from char deposition

Pyrolysis oil is introduced into the entrained flow gasifier in a form of fine spray droplets upon impact with high velocity oxygen gas during atomization. As soon as pyrolysis oil is atomized in the system, small fractions of oil droplets and mists are expected to entrain in the system's turbulent flow and, in some circumstances, come into contact with reactor hot surfaces before turning into char. Severe char deposition on cooling jacket floor surrounding the atomizer's nozzle has been observed in this study and was found could potentially lead to blockage of pyrolysis oil feeding into the gasifier. Detailed discussion on char deposition problem on cooling jacket floor has been discussed earlier in Chapter 3.12.10 of this thesis.

Figure 5–7 shows examples of char depositions on cooling jacket external floor around the atomizer's nozzle outlet after gasifier operations. In these examples, both liquid and gas outlets of the atomizer nozzle were free from obstructions by char depositions.

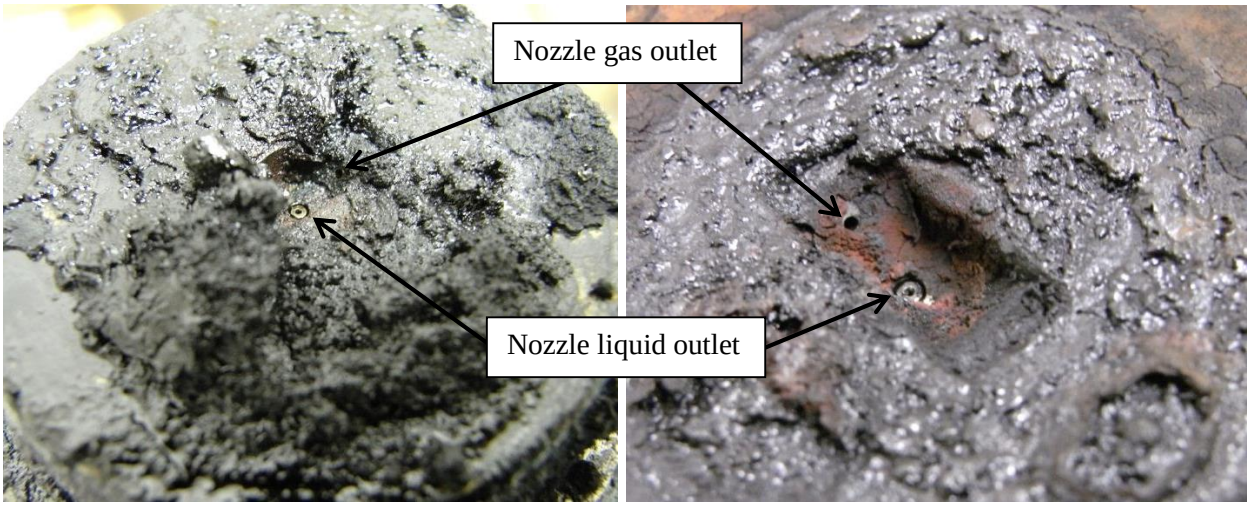

Figure 5–7: Pictures of cooling jacket floor with char deposition of different severity after entrained flow gasification with pyrolysis oil at high temperature

2) Internal blockage from pyrolysis oil

Plugging of pyrolysis oil passage in an atomizer (internal blockage) is more likely to occur in pyrolysis oil atomization applications due to complex physicochemical properties of the oil. Internal blockage of atomizer by pyrolysis oil could occur in three different ways which are:

(a) Blockage due to solid obstruction inside spray nozzle

Atomizer liquid outlet blockage due to solid obstruction is likely when pyrolysis oil with high solid content is used in the operation. This problem could be minimized by using filters with sufficiently small mesh size to make sure that the pyrolysis oil is free from large particles that can clog the atomizer outlet.

(b) Blockage due to excessive heating of pyrolysis oil inside spray nozzle

Pyrolysis oil exposure to heat is known to cause polymerization of chemical compounds in the oil that increases its viscosity and eventually could lead to blockage of atomizer nozzle outlet. If the cooling system in ineffective, this phenomenon is expected to occur progressively throughout the operation period and, consequently, the pyrolysis oil flow rate is expected to decline gradually. Besides that, polymerization of oil is also likely when feeding of oil into the system is stopped in the middle of a gasification operation, thus subjecting stagnant oil remaining in the nozzle to convective and radiative heat transfers from the hot gasification environment; and eventually plugs the atomizer liquid outlet.

(c) Blockage due to accumulation of waxy materials, heavy tars and fine char inside nozzle

Blockage to the atomizer could also occur as a result from pyrolysis oil complex multiphase structure where presence of waxy materials, fine char and heavy components of the oil (heavy tars) can form viscous clot that clog the atomizer liquid outlet orifice under certain circumstances.

Waxy compounds such as fatty acids, sterols, aliphatic hydrocarbons and fatty alcohols; pyrolytic lignin and solids in pyrolysis oil tend to form viscous three-dimensional networks at low temperatures [9]. Besides affecting the oil viscosity, the waxy compounds is also responsible for promoting crystallization of various compounds in the oil [10]. Heavy components of the pyrolysis oil also present in a relatively viscous form. Although these compounds are not solid, they may still be filtered by the 10μm filter due to their viscous nature. Over a time period, there is a potential that these materials accumulated on filter mesh and permeated through filter mesh, particularly in cases when there is a sudden surge in pressure upstream of the filter.

In cases where the accumulation is significant, sudden interruptions to the oil flow during atomization could occur. However, if the clot eventually makes its way out of the nozzle tip, the interruptions will be temporary and therefore flow of oil and upstream pressure will quickly recover. On the opposite, if the clot fails to pass through the nozzle tip, the obstruction will be persistent and the atomizer liquid cap will be either partially or completely clogged.

In contrast to other causes of atomizer blockage, pyrolysis oil flow interruptions due to accumulation of viscous compounds is difficult to be proven experimentally since whenever this occurs, rapid polymerization of the oil trapped inside the atomizer nozzle will follow and consequently eliminate evidences to prove atomizer blockage due to viscous oil accumulation. Because of this reason, further investigations are required so relationship between pyrolysis oil multiphase structure and its contribution to atomizer blockage problem can be proven, studied and therefore eliminated.

5.3.2 Effect of Pyrolysis Oil and Atomizing Gas Flow Rates on Spray Characteristics

5.3.2.1 Effects on spray angle

In order to examine the effect of atomizing gas flow rates on spray characteristics, atomization tests were conducted at three gas flow rates (800L/h, 1200L/h and 1600L/h), with peristaltic pump speed kept at a constant value of 10 RPM. The tests were then repeated using different liquid caps to investigate influence of different liquid outlet diameters on the resulted spray characteristics.

In this section, spray characteristics were measured in terms of the spray angle, determined from analysis of spray images captured during the experiments. The spray angle was derived from the angle of which the spray dispersed upon atomization near the atomizer nozzle. The angles of sprays as measured from atomization at various gas flow rates using the 1650, 2050 and 2850 liquid caps were summarized in Table 5-2.

From the results it is evident that spray angle was strongly influenced by atomizing gas flow rate and liquid cap outlet diameter. The spray angle increased with gas flow rate (from 800L/h to 1600L/h) and the cap's outlet diameter. With increase in the gas flow rate, more atomizing gas tried to flow through the nozzle at higher pressure. Once the gas and the oil mix outside the nozzle outlet, the mixture spreads widely while resulting a larger spray angle. This trend was true for all of the three caps although the 2850 liquid cap showed insignificant increase in the spray angle (67 to 68°) when the gas flow was increased from 1200L/h to 1600L/h. It is likely that this represents the maximum spray angle achievable with the particular nozzle configurations used in this study.

Table 5-2: Spray angle at various atomizing gas flow rates while pyrolysis oil flow rate was fixed at peristaltic pump speed of 10 RPM

Liquid Cap Model	Atomizing Gas Flow Rate (L/h)		
	800	1200	1600
	Spray Angle (°)		
1650 (Oil Flow Rate: 68 mL/min)	36	46	54
2050 (Oil Flow Rate: 67 mL/min)	42	55	63
2850 (Oil Flow Rate: 115 mL/min)	59	67	68

At a constant atomizing gas flow rate, the spray angle increased with the cap's outlet diameter and this trend is consistent for all atomizing gas flow rates tested in this work. This is understandable as the pyrolysis oil velocity and pressure in the atomizer were lower for large diameter nozzle thus the gas is more dominant for the spray formation once the gas and oil mix, spreading widely in the chamber. Based on the above tests, at a given oil flow rate, target oil spray can be achieved by adjusting the gas flow rate and choosing the right cap.

It is believed that the velocity of pyrolysis oil exiting the atomizer plays a significant role affecting dispersion of the oil during spray formation. The oil flow rate can be converted to oil velocity for a given cap. As shown in Figure 5–8, velocities of pyrolysis oil exiting 1650 liquid cap were consistently higher than those exiting 2050 and 2850 caps thus giving the resulted spray droplets greater velocities in vertical direction after atomization. In contrast, the relatively low pyrolysis oil velocity exiting 2850 liquid cap results spray with lower velocity in vertical direction causing droplets to disperse better in both vertical and horizontal directions upon impact with gas during atomization.

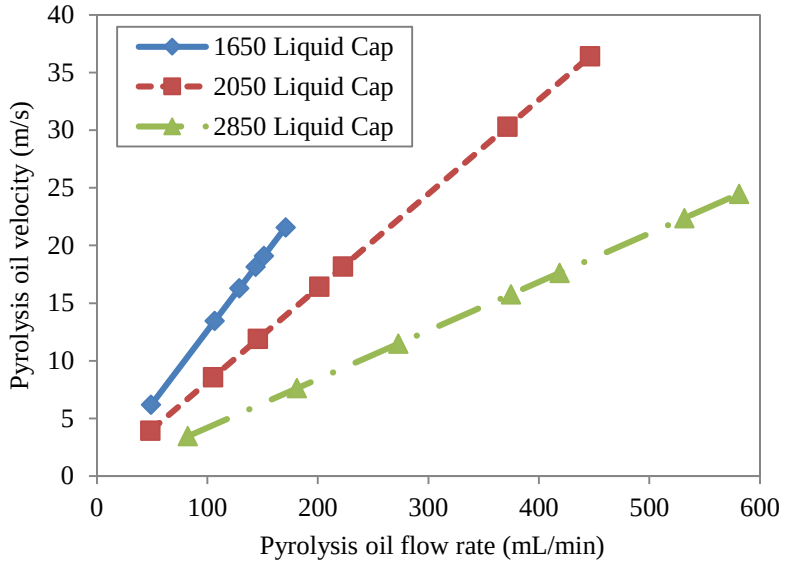

Figure 5–8: Relationship between pyrolysis oil flow rate and velocity from different atomizer liquid caps

Figure 5–9 demonstrates effects of vertical velocity component of liquid on the resulted spray angle during atomization at constant atomizing gas flow rate.

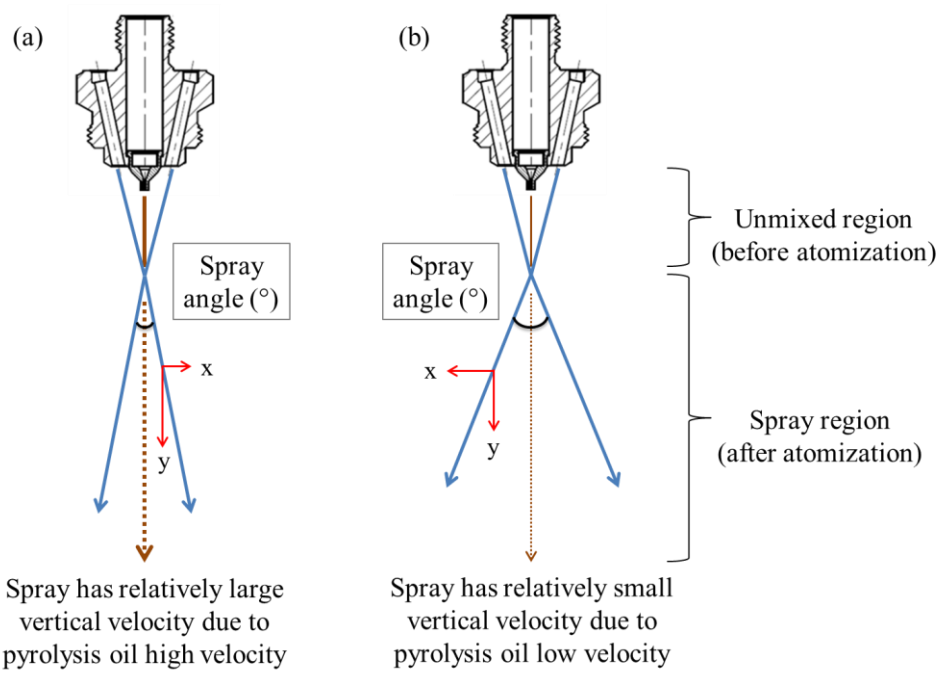

Figure 5–9: Illustrations showing pyrolysis oil velocity influence on spray angle at (a) higher velocity pyrolysis oil (b) lower velocity pyrolysis oil

The relationship between the oil velocity and cap outlet diameter has confirmed the results obtained from this study. As shown in Table 5-2, when the oil flow rates were identical at around 67.5 mL/min (10rpm) for both 2050 cap and 1650 cap, the 2050 liquid cap consistently yielded spray with larger angles than that produced by the 1650 liquid cap at a given atomizing gas flow rate.

Since all results presented so far in this section were obtained from the edge side of the atomizer, this paragraph aimed to determine whether or not the relationships found from the images of edge view apply to the sprays from the front view. For this purpose, the atomizer cap was rotated 90^{o} from its original position and tested at atomizing gas flow rate from 800L/h to 1600L/h. The results showed pyrolysis oil spray angle remained constant at around 27° regardless of the atomizing gas flow rate changes, thus it is concluded that the effects of atomizing gas flow rates is only applied to the sprays from the edge view. Figure 5–10 illustrates the direction of spray growth with increase in atomizing gas flow rate, as found in this study.

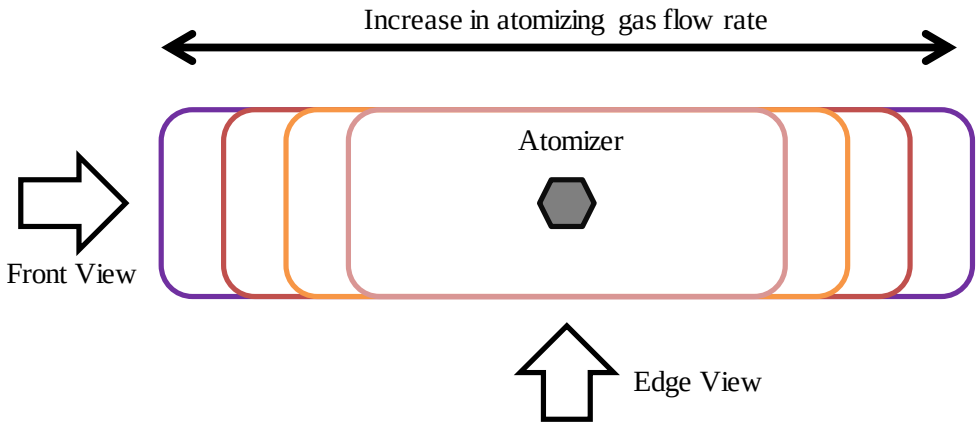

Figure 5–10: Illustration of change in flat spray pattern in relation to atomizing gas flow rates for atomizer configuration used in this study. This image represents spray patterns as observed from top view

Furthermore, tests were also conducted to investigate effects of increasing peristaltic pump speed on spray angle at constant atomizing gas flow rate. In these tests, atomizing gas flow rate was fixed at 1600L/h while peristaltic pump speed was varied from 10 to 20 RPM for all of the three liquid caps. Adjustments of peristaltic pump speed were made to represent changes to pyrolysis oil flow rate into the atomizer. Table 5-3 summarizes the average pyrolysis oil feeding rate into the atomizer during operation at various peristaltic pump speed and liquid caps conducted in these tests. Results from these tests are summarized in Table 5-4.

Table 5-3: Average pyrolysis oil flow rate during operation at different peristaltic pump speeds and liquid caps

Liquid Cap	Peristaltic Pump Speed (RPM)		
	10	15	20
	Pyrolysis Oil Flow Rate (mL/min)		
1650	68	87	107
2050	67	86	106
2850	115	148	181

Table 5-4: Spray angle at various peristaltic pump speed while atomizing gas flow rate was fixed at 1600L/h

Liquid Cap	Peristaltic Pump Speed (RPM)		
	10	15	20
	Spray Angle (°)		
1650	54	54	54
2050	63	63	64
2850	68	69	68

From Table 5-4, it is found that at a constant atomizing gas flow rate of 1600L/h, the spray angle maintained almost constant for a given cap when the pump speed was increased from 10-20 RPM. The spray angles were about 54˚, 63˚ and 68˚ for liquid caps 1650, 2050 and 2850 respectively.

Increase in pyrolysis oil flow rate also leads to higher velocity flow thus should lead to decline in spray angle. This effect, however, was not visible at high gas flow rate, such as that obtained Table 5-4 due to dominant effect of gas flow rate during atomization. At lower atomizing gas flow rate this relationship becomes more prominent where decline in spray angle can be clearly observed at increased pyrolysis oil feeding rate. To show this, similar tests were conducted but at lower atomization gas flow rate (800L/h) and the results are summarized in Table 5-5.

Table 5-5: Pyrolysis oil spray angles at various pump speed and liquid caps during atomization at 800L/h gas flow rate

Liquid Cap	Peristaltic Pump Speed (RPM)	
	5	10
	Spray Angle (°)	
1650	63	40
2050	68	41
2850	66	62

In overall, findings in this section proved influences of atomizing gas flow rate, pyrolysis oil flow rate and liquid outlet diameter on spray angle during atomization. At high atomizing gas flow rate, however, effect of pyrolysis oil flow rate on spray angle becomes less important due to more dominant effect of atomizing gas flow at this condition.

5.3.2.2 Effects on spray formation and droplet size

From images of the pyrolysis oil spray captured during the cold model spray tests, pyrolysis oil spray formation and droplets sizes were examined and examples of these sprays for different flow rates of atomizing gas and pyrolysis oil are shown in Figure 5–11. It is found that increasing atomizing gas flow rate significantly enhanced fragmentation of pyrolysis oil jet into fine spray droplets upon exiting the atomizer nozzle. At low atomizing gas flow rates, disintegration of oil stream into spray were relatively poor thus yielded large spray droplets and oil filaments that reduced effective surface area of the spray for reactions during gasification.

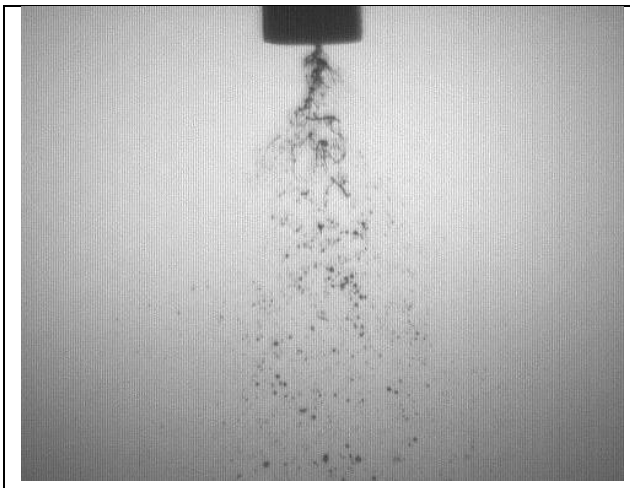

Pyrolysis oil flow rate: 76 mL/min
Atomizing gas flow rate: 800L/h
Liquid cap: 1650

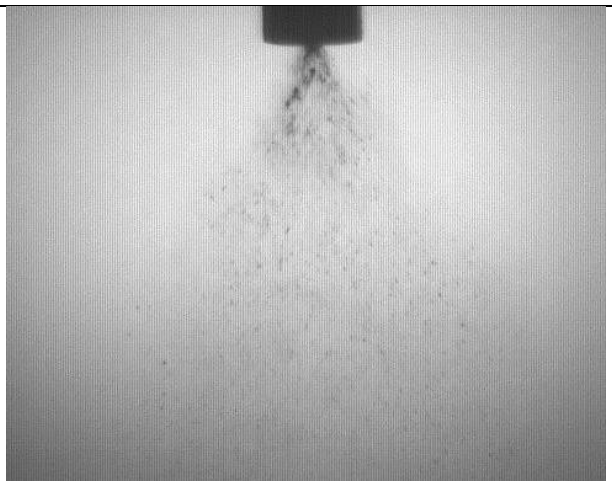

Pyrolysis oil flow rate: 76 mL/min
Atomizing gas flow rate: 1200L/h
Liquid cap: 1650

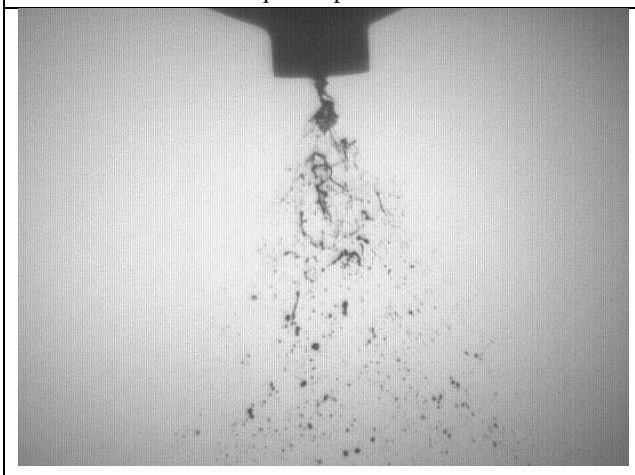

Pyrolysis oil flow rate: 93 mL/min
Atomizing gas flow rate: 800L/h
Liquid cap: 2050

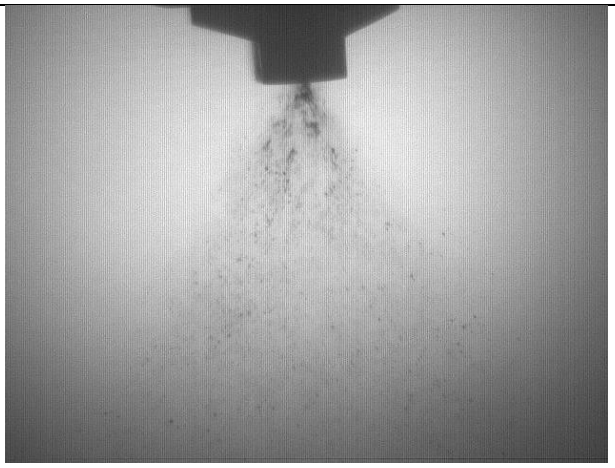

Pyrolysis oil flow rate: 93 mL/min
Atomizing gas flow rate: 1200L/h
Liquid cap: 2050

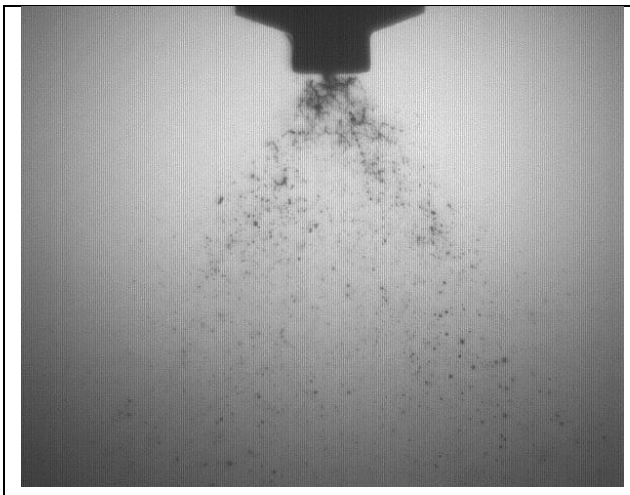

Pyrolysis oil flow rate: 93 mL/min
Atomizing gas flow rate: 800L/h
Liquid cap: 2850

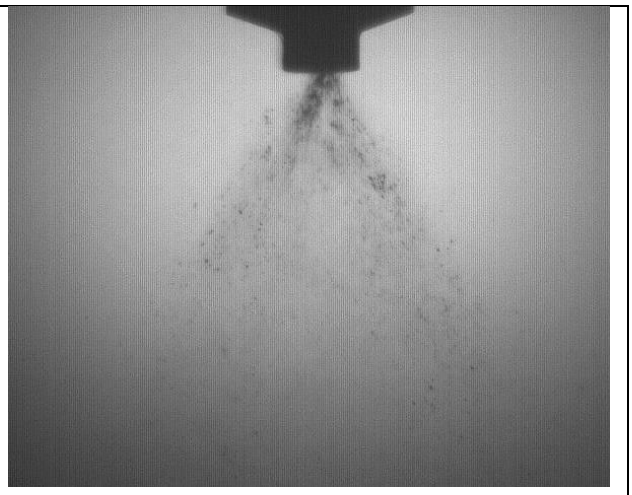

Pyrolysis oil flow rate: 93 mL/min
Atomizing gas flow rate: 1200L/h
Liquid cap: 2850

Figure 5–11: Images of pyrolysis oil spray showing the effect of atomizing gas flow rate

The images in Figure 5–11 also clearly show that atomizing gas flow rates has significant impact on spray shape and droplets distribution, where higher gas flow rate leads to formation of more uniform spray with better droplets distributions. In this study, diameters of individual spray droplets were not analysed quantitatively due to limitations of the sampling method used during the tests. In addition, the spray chamber was also occasionally blurred with fine spray mist during the atomization at high atomizing gas flow rates, which resulted in low quality spray images. Acknowledging the importance of droplet size for spray characterization, comprehensive investigation into this particular aspect of pyrolysis oil atomization is recommended to be conducted in the future.

5.3.3 Effect of Gas-to-Fuel Ratio (GFR) and Equivalence Ratio (ER) on Spray Characteristics

In the previous section, effects of individual flows of pyrolysis oil and atomizing gas were examined. However, the ratio between these two parameters may also affect the spray characteristics. This ratio is a controlled operation parameter in entrained flow gasification thus the results will be useful in practical gasification operation. It has been known that for the external mix twin-fluid atomizer as used in this study, formation of spray and spray distribution are directly related to collision impacts between the atomizing gas and the pyrolysis oil streams. Poor spray characteristics, as an example, generally results from less efficient gas-liquid impact during the atomization.

The ratio of gas to liquid feeding rates into a combustion system can be represented by the term ‘gas-to-fuel ratio’ (GFR). In this section, potential relationship between GFR and spray characteristics was

investigated to test whether this parameter has any influence on spray characteristics. For this purpose, pyrolysis oil was atomized at different flow rates of pyrolysis oil and atomizing gas to represent spray at various GFR values. Figure 5–12 shows examples of spray images captured in this test along with their corresponding atomization conditions.

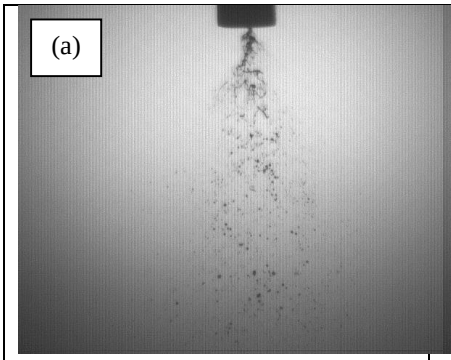 (a)	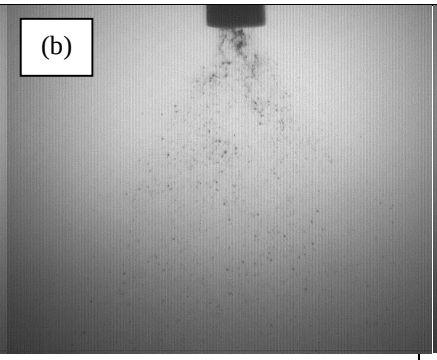 (b)	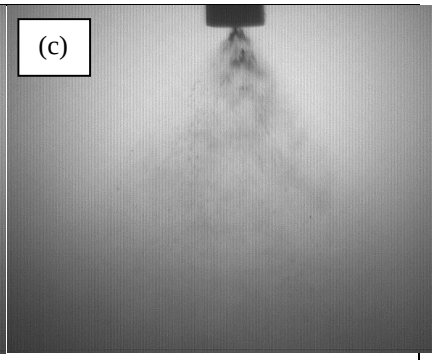 (c)
Gas-fuel ratio [GFR]: 169 (v/v) Pyrolysis oil flow rate: 75 mL/min Atomizing gas flow rate: 800L/h Equivalence ratio: 0.27 Liquid cap: 1650	Gas-fuel ratio [GFR]: 276 (v/v) Pyrolysis oil flow rate: 48 mL/min Atomizing gas flow rate: 800L/h Equivalence ratio: 0.44 Liquid cap: 1650	Gas-fuel ratio [GFR]: 238 (v/v) Pyrolysis oil flow rate: 119 mL/min Atomizing gas flow rate: 1600L/h Equivalence ratio: 0.36 Liquid cap: 1650
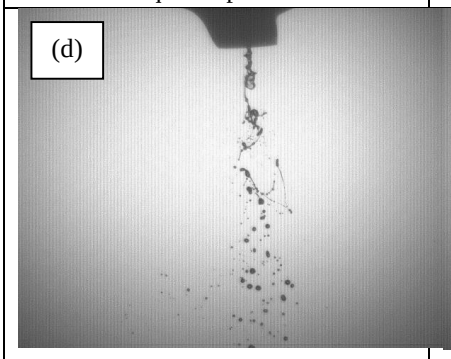 (d)	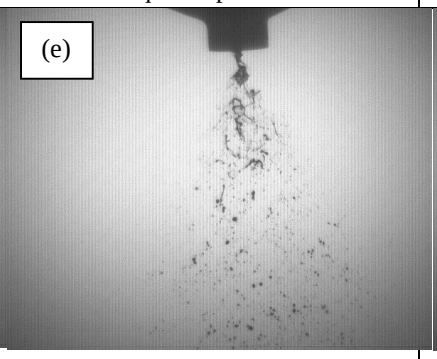 (e)	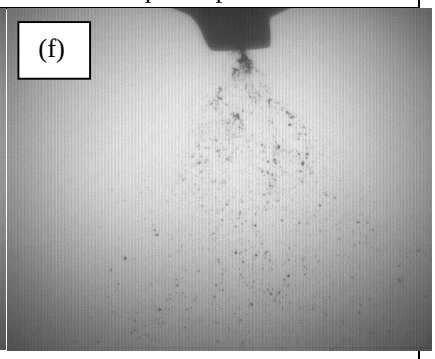 (f)
Gas-fuel ratio [GFR]: 144 (v/v) Pyrolysis oil flow rate: 46 mL/min Atomizing gas flow rate: 400L/h Equivalence ratio: 0.23 Liquid cap: 2050	Gas-fuel ratio [GFR]: 148 (v/v) Pyrolysis oil flow rate: 93 mL/min Atomizing gas flow rate: 800L/h Equivalence ratio: 0.24 Liquid cap: 2050	Gas-fuel ratio [GFR]: 290 (v/v) Pyrolysis oil flow rate: 46 mL/min Atomizing gas flow rate: 800L/h Equivalence ratio: 0.46 Liquid cap: 2050

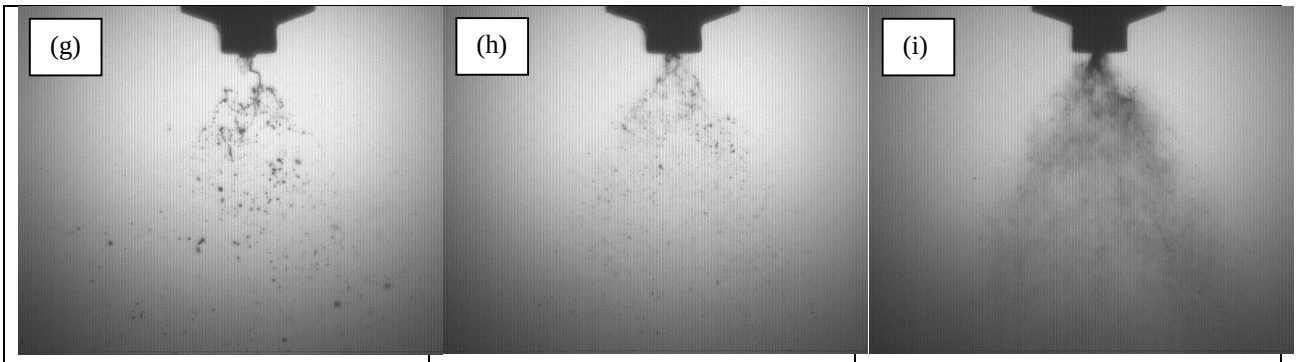

Gas-fuel ratio [GFR]: 142 (v/v) Pyrolysis oil flow rate: 47 mL/min Atomizing gas flow rate: 400L/h Equivalence ratio: 0.23 Liquid cap: 2850	Gas-fuel ratio [GFR]: 288 (v/v) Pyrolysis oil flow rate: 47 mL/min Atomizing gas flow rate: 800L/h Equivalence ratio: 0.46 Liquid cap: 2850	Gas-fuel ratio [GFR]: 142 (v/v) Pyrolysis oil flow rate: 186 mL/min Atomizing gas flow rate: 1600L/h Equivalence ratio: 0.23 Liquid cap: 2850

Figure 5–12: Examples of spray images during pyrolysis oil atomization at different combinations of oil and gas flow rates, corresponding to various GFR.

At a constant atomizing gas flow rate (for example 800 L/h), increase in GFR values (from decreasing pyrolysis oil flow rate) clearly shows improvements in spray characteristics where droplets formed were much finer than that formed at lower GFR, as observed in Figure 5–12 (a) for GFR of 169 and Figure 5–12 (b) for GFR of 276 using atomizer cap 1650. Similar behaviour can also be observed for atomizer cap 2050 as shown in Figure 5–12 (e) for GFR of 148 and Figure 5–12 (f) for GFR of 290. Mechanism of improvements in spray characteristics at higher GFR is in a similar manner as the improvements with higher gas flow rates at a given pyrolysis oil flow rate, which has been discussed in the previous section.

However, at a given GFR, the spay characteristics are also affected by the actual atomizing gas flow rate. This phenomenon for atomizer cap 1650 is illustrated in in Figure 5–12 (b) for gas flow rate of 800 L/h and in Figure 5–12 (c) for gas flow rate of 1600 L/h. Similarly the results for atomizer cap 2050 are shown in Figure 5–12 (d) for gas flow rate 400 L/h and in Figure 5–12 (e) for gas flow rate of 800 L/h. Atomizer cap 2850 also shows a clear improvements with increase in gas flow rate from 400–1600 L/h as illustrated in Figure 5–12 (g), (h) and (i). These comparisons confirm that the atomizing gas flow rate has dominant influence on the spray characteristics, and thus should be carefully controlled in practical operation of entrained flow gasification.

In summary, the cold model tests on pyrolysis oil atomization show that the atomizing gas plays a dominant role affecting spray characteristics. At constant atomizing gas flow rate, GFR also affects spray characteristics where increase of the GFR improves the spray characteristics. The above findings apply to all of the three liquid caps.

Equivalence ratio is defined as the ratio of oxygen to pyrolysis oil flow rates supplied into the system (GFR) to that required for stoichiometric combustion ($GFR_{stoichiometric}$) [11]. In operation of entrained flow gasification, equivalence ratio is often used as a control parameter. However, it is unknown how equivalence ratio affects the spray characteristics in the pyrolysis oil atomisation. Based on conditions in the cold model spray atomization tests, equivalence ratio values were calculated for each run and are also included in Figure 5–12.

From the results, it is found that ER is not an independent parameter affecting the spray characteristics as it is linearly related to GFR. Because of this reason, atomizing gas still plays a dominant role in determining spray characteristics as concluded in the previous section. As observed in Figure 5–12 (d), (e), (g) and (i), atomization at a constant equivalence ratio value may result in both, good or poor spray characteristics depending on the atomizing gas flow rate.

This finding leads to a conclusion that low equivalence ratio values, which are typically desired during gasification, do not necessarily results in poor spray characteristics as long as the oxygen flow rate is set sufficiently high to generate good spray. On the opposite, gasification at high equivalence ratio values do not necessarily guarantee good spray characteristics if the oxygen flow rate is set at low values or when the pyrolysis oil flow rate is too high (low GFR). In this regard, it is therefore advantageous to operate the entrained flow gasifier at high gas flow rates, while in operations when the gas flow rate is fixed, higher GFR value or lower pyrolysis oil flow rate is preferred to give better spray characteristics.

While equivalence ratio has no direct impact on spray characteristics, this parameter still remains as a key parameter during gasification operations due to major influences it has on gasification reactions, conversion performance and its final products. Following this, it is important that equivalence ratio, GFR and atomizing gas flow rate are monitored and optimized simultaneously during gasification operations, so good spray characteristic could be guaranteed without sacrificing the gasification performance.

It is important to highlight that pyrolysis oil spray characteristics resulted from varying flow rates of pyrolysis oil and atomizing gas, as shown in this chapter, are also greatly influenced by the viscosity of oil used during the operation. This is because at given flow rates of pyrolysis oil and atomizing gas, liquid with high viscosity is more difficult to be atomized compared to that using less viscous liquid [12] thus generally results spray with relatively poorer characteristics. As discussed earlier in Chapter 2.1 of this thesis, pyrolysis oil is a chemically and thermally unstable material in which increase in storage time and oil temperature have been shown to alter its viscosity considerably. Changes in pyrolysis oil temperature in particular, decrease the oil viscosity almost instantly hence is expected to significantly influence the oil spray characteristics upon atomization.

Acknowledging influence of pyrolysis oil temperature on the resulted spray characteristics, the oil temperature must be maintained at a constant value during an operation so undesirable variations in the oil spray characteristics could be eliminated.

5.4 Conclusions

Influences of pyrolysis oil flow rate and atomizing gas flow rates for three atomizer liquid caps have been successfully investigated in this study. In overall, findings in this chapter showed dominant influence of atomizing gas in determining pyrolysis oil spray characteristics during atomization.

Increase in atomizing gas flow rate has been shown to cause increase in the angle of spray formed during atomization. In addition to that, high gas flow rate is also responsible for enhanced fragmentation of pyrolysis oil into finer droplets and more uniform spray. These improvements result from significant impact of atomizing gas on pyrolysis oil stream at higher gas flow rates, which disperses liquid stream more efficiently into sprays with better characteristics. Increase in pyrolysis oil flow rate, on the other hand negatively influence spray characteristics as it leads to larger droplet sizes, reduced spray angle and less uniform spray upon atomization.

It is useful to learn that changes to spray angle occurred only on one side of the atomizer at all conditions due to the nature of atomizer configuration used in this study. Spray angle as measured from the atomizer 'front side' showed no effects towards changes in the atomizing gas flow rates and remained consistent at 27° throughout this investigation.

At constant peristaltic pump speed, increase in liquid outlet diameter caused consistent increase in spray angle as observed from 1650, 2050 and 2850 liquid caps respectively. This trend could be justified by considering variations in pyrolysis oil flow rates and therefore the oil velocities upon exiting atomizer with different liquid outlet diameters. Smaller oil velocity from liquid cap with larger outlet diameters was shown to result spray with greater dispersions thus larger spray angle due to more efficient impact with high velocity gas during atomization.

During atomization at constant gas flow rate, increase in GFR values due to decrease of oil flow rate, showed improvements in spray characteristics where droplets formed were finer and more uniform than that produced at lower GFR. Nevertheless at varying atomizing gas flow rate, influence of gas flow rate on spray characteristics was more significant thus was concluded as the most dominant factor determining spray performance. This study also proved equivalence ratio was not an independent parameter affecting

spray characteristics, rather depends on flow rates of pyrolysis oil and atomizing gas used during atomization.

Findings in this work ultimately showed advantages of conducting atomization at high gas flow rates in order to maximize atomization performance. In operations when the gas flow rate is fixed, higher GFR value or lower pyrolysis oil flow rate should be used. This information applies to entrained flow gasification and will be used to provide better understanding of gasification operation with pyrolysis oil in the coming chapters in this thesis.

5.5 References

1. Rajakaruna, H.T.B., *A mathematical model for liquid fuel spray combustion. (BL: DXN049816)*. 1997, De Montfort University (United Kingdom): England.
2. Williams, A., *Combustion of Liquid Fuel Sprays*. 1990, London: Butterworth & Co (Publishers) Ltd.
3. Kolb, T., T. Jakobs, and N. Zarzalis, *Syngas from biomass-based slurry entrained flow gasification*, in *10th Conference on Energy for a clean Environment*. 2009.
4. Empie, H.J., et al., *Spraying characteristics of commercial black liquor nozzles.* Tappi Journal, 1995. **78**(1): p. 121-128.
5. Miikkulainen, P. and A. Kankkunen, *The characteristics of black liquor sprays*, in *Colloquium on Black Liquor Combustion and Gasification*. 2003: Utah, USA.
6. Mackrory, A.J., D.R. Tree, and L.L. Baxter, *Characteristics of black liquor sprays from gas-assisted atomizers in high-temperature environments.* Tappi Journal, 2008. **7**(1): p. 19-24.
7. Risberg, M., *Spray visualisation of gas-assisted atomisation of black liquor*, in *Department of Applied Physics and Mechanical Engineering*. 2008, Lulea University of Technology.
8. Yao, S., J. Zhang, and T. Fang, *Effect of viscosities on structure and instability of sprays from a swirl atomizer*. Experimental Thermal and Fluid Science, 2012. **39**(0): p. 158-166.
9. Ba, T., et al., *Colloidal Properties of Bio-Oils Obtained by Vacuum Pyrolysis of Softwood Bark. Storage Stability*. Energy & Fuels, 2004. **18**(1): p. 188-201.
10. Garcia-Perez, M., et al., *Multiphase structure of bio-oils.* Energy & Fuels, 2006. **20**(1): p. 364-375.
11. Abdoulmoumine, N., A. Kulkarni, and S. Adhikari, *Effects of Temperature and Equivalence Ratio on Pine Syngas Primary Gases and Contaminants in a Bench-Scale Fluidized Bed Gasifier.* Industrial & Engineering Chemistry Research, 2014. **53**(14): p. 5767-5777.

12. Schick, R.J., *Spray Technology Reference Guide: Understanding Drop Size*. 2008, Spray Analysis and Research Services - Spraying Systems Co.: Illinois, USA.

6 CHEMICAL EQUILIBRIUM MODEL FOR ENTRAINED FLOW GASIFIER

6.1 Introduction

Chemical equilibrium model is an important tool to help better understand processes involving a series of reactions such as those found in gasification. Chemical equilibrium is a thermodynamically stable state where rates of forward and reverse reactions are equal; therefore, there are no further changes in product concentrations at this condition. In a system involving a series of reaction chains, similar principle applies to each individual reaction in the system thus predictions of the final product concentrations at the equilibrium are not straightforward.

With the help of computational techniques, chemical equilibrium could be mathematically modelled and has been shown to be capable of predicting equilibrium behaviour at varying operating conditions [1-3]. In many applications, equilibrium model is used for comparison between the equilibrium state and the actual state of a reaction or a series of reactions, and to check how close the experimental results are to those expected at equilibrium state. Chemical equilibrium modelling has been used in various applications as it requires limited input information such as molar flow rates of species entering a system, dominating reactions and process operation conditions to predict the final product compositions at equilibrium. In this way, the model is capable of generating output composition of products without demanding comprehensive information such as reactor type, reactor design and thermodynamic behaviour of all chemical reactions involved; thus the equilibrium model approach is highly convenient [1].

There are two equilibrium model approaches that are available, namely stoichiometric and non-stoichiometric models. Both approaches are based on similar assumptions of equilibrium state of reactions, and the models are solved using similar technique of minimizing Gibbs free energy of a system. Due to these reasons, both approaches should produce identical results. Stoichiometric model is developed based on selection of main gas species expected in the product at equilibrium. In most cases, there is also a need to specify several dominant reactions involved in the system to fully define the model. On the other hand, the non-stoichiometric model is a relatively simpler approach where it does not require specification of any reactions taking place during a process but predicts product composition only by minimizing Gibbs free energy of the system based on molar flow rates of elements entering the system and its operation conditions [2].

Application of chemical equilibrium model for gasification is not new. For entrained flow gasification of biomass, chemical equilibrium modelling has been reported and shown to be able to predict results with reasonable agreement with commercial scale gasifiers operating at temperatures between 800^{o}C to 1800^{o}C [3].

A chemical equilibrium model was developed in this work to predict equilibrium products for entrained flow gasification of biomass pyrolysis oil at various operation conditions. This chapter will provide description, derivations of equations used for the model development and validation of the model to prove its ability to predict gasification products accurately. In the last section of this chapter, the validated model will be used to predict general trends of producer gas compositions expected during entrained flow gasification of pyrolysis oil at varying temperature and equivalence ratio.

6.2 Model Description and Calculations

In this study, equilibrium model for entrained flow gasification of biomass pyrolysis oil was developed based on stoichiometric approach where the main gas species expected in product at equilibrium are H_2, CO, CO_2, CH_4, N_2 and H_2O. Since reactions in entrained flow gasifier takes place very rapidly due to high reaction temperature, no solid was expected to remain at equilibrium hence the system was assumed to be homogeneous. In this work, Gibbs free energy information from two dominant gasification reactions were used to define the model at equilibrium, which are the Water-Gas Shift reaction and the Steam Reforming reaction [1, 2].

Water-Gas Shift reaction:

$CO + H_2O \leftrightarrow CO_2 + H_2$ ΔH_r = -41 kJ/mol Reaction 1

Steam/Methane Reforming reaction:

$CH_4 + H_2O \leftrightarrow CO + 3H_2$ ΔH_r = +206 kJ/mol Reaction 2

The equilibrium model was developed in Microsoft Excel spreadsheet by using a built-in Solver Add-Ins that enables efficient iterative calculations to be made. Main assumptions made in the equilibrium model development are summarized as follows:

i. Perfect mixing between all compounds present in the system;
ii. The products have reached equilibrium in the reactor;
iii. No tar is present in the producer gas after gasification;

iv. CH_4 is the only hydrocarbon compound present in the producer gas;

v. No char or other solids remain in the producer gas;

vi. No temperature gradient across the gasifier (uniform gasification temperature)

In comparison to the commercial equilibrium software such as that used in [4-6], the equilibrium model developed in this work was specifically developed for entrained flow gasification for pyrolysis oil, hence was fully customized according to entrained flow gasification process and product analysis requirements. In addition to producer gas composition, other useful information related to gasification products at equilibrium are also generated by this model including producer gas individual components molar flow rates, mass flow rates, gas yield (g_{gas}/g_{oil}) as well as results in nitrogen-free and water-free basis.

Figure 6–1illustrates the inlet and outlet flows of species involved during entrained flow gasification of biomass pyrolysis oil for development of the equilibrium model.

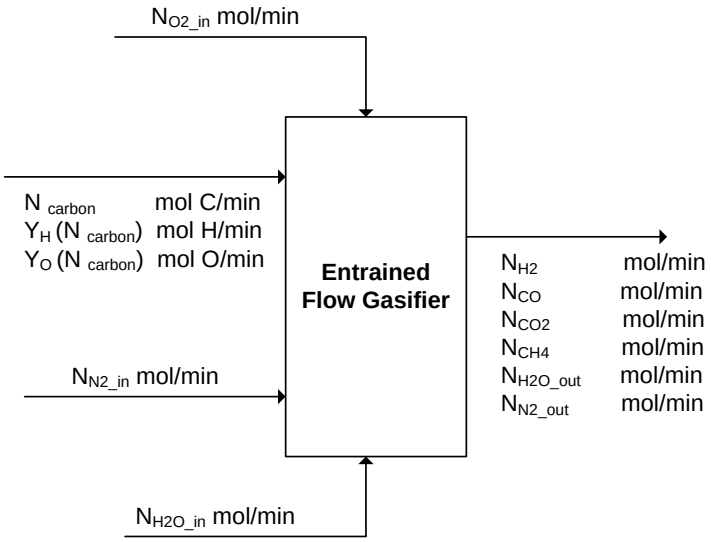

Figure 6–1: Illustration of an equilibrium model for entrained flow gasification system

In Figure 6–1, N_{carbon} is the molar flow rate of carbon (mol C/min) supplied into the gasifier in the form of pyrolysis oil. Y_H is the hydrogen-to-carbon (H:C) molar ratio in pyrolysis oil while Y_O is the oxygen-to-carbon (O:C) molar ratio in pyrolysis oil. Following that, $Y_H(N_{carbon})$ and $Y_O(N_{carbon})$ are the molar flow rates of hydrogen and oxygen in the pyrolysis oil (mol H/min and mol O/min), respectively, into the system. On the other hand, molar flow rates of other species, *i* entering and exiting the gasifier are represented by N_i (mol/min).

In solving the equilibrium model, six unknowns are required to be determined, which are molar flow rates of H_2, CO, CO_2, CH_4, N_2 and H_2O in producer gas exiting the system. Molar flow rates of four of these species are defined from material balances of C, H, O and N elements involved in the system; while the remaining two unknowns are derived from total Gibbs free energies of the two dominant gasification reactions specified earlier. Step-by-step derivations for all equations used to define this model are given in the coming paragraphs.

Material balances of the four elements involved in this system (C, H, O and N) can be written in the following forms:

Carbon balance:

$$N_{carbon} = N_{CO} + N_{CO2} + N_{CH4}$$

Hydrogen balance:

$$Y_H(N_{carbon}) + 2N_{H2O\_in} = 2N_{H2} + 2N_{H2O\_out} + 4N_{CH4}$$

Oxygen balance:

$$2N_{O2\_in} + Y_O(N_{carbon}) + N_{H2O\_in} = N_{CO} + 2N_{CO2} + N_{H2O\_out}$$

Nitrogen balance:

$$2N_{N2\_in} = 2N_{N2\_out}$$

These equations are transformed into augmented matrix form so they can be manipulated to give four sets of equations, which are used to define molar flow rates of CO_2, CO, H_2 and N_2 exiting the system. The four equations produced after the augmented matrix operations are presented in Equations (1) – (4).

$$N_{CO2} = N_{carbon}(Y_O - 1) + 2N_{O2\_in} + N_{CH4} - N_{H2O\_out} + N_{H2O\_in} \quad \text{Equation 1}$$

$$N_{CO} = N_{carbon}\,(2 - Y_O) - 2N_{CH4} + N_{H2O\_out} - 2N_{O2\_in} - N_{H2O\_in} \quad \text{Equation 2}$$

$$N_{H2} = N_{carbon}\left(\frac{Y_H}{2}\right) - 2N_{CH4} - N_{H2O\_out} + N_{H2O\_in} \quad \text{Equation 3}$$

$$N_{N2\_in} = N_{N2\_out} \quad \text{Equation 4}$$

In these equations, the terms N_{carbon}, N_{O2_in}, N_{N2_in} and N_{H2O_in} are molar flow rates of materials fed into the entrained flow gasification system, hence are known variables. On the other hand, Y_H and Y_O

values can be determined from elemental analysis of pyrolysis oil used during the operation. To fully define Equations (1) – (4) the remaining two unknowns (N_{H2O_out} and N_{CH4}) have to be calculated. Derivations of equations used to calculate N_{H2O_out} and N_{CH4} values are presented in the remainder of this section.

At equilibrium state, the relationship between each individual species in producer gas is given by equilibrium constant, *K*. Equilibrium constant calculates molar fractions of reactants and products involved during a reaction, in which, during operations at atmospheric pressure is given by Equation (5):

$$aR_1 + bR_2 \rightarrow cP_1 + dP_2$$

$$K = \sum Y_i^{v_i} = \frac{({P_1}^c)({P_2}^d)}{({R_1}^a)({R_2}^b)} \qquad \text{Equation 5}$$

P_1 and P_2 are mole fractions of products of the reaction while R_1 and R_2 are mole fractions of reactants involved in the reaction. On the other hand *a* and *b* are the stoichiometric number of moles of reactants while *c* and *d* are the stoichiometric number of moles of products in the reaction respectively.

Applying Equation (5) to Water Gas Shift and Steam Reforming reactions, separately, the equations were then re-arranged so mole fractions of H_2O and CH_4 in the producer gas could be defined. At this condition, the re-arranged equilibrium constant equations for Water Gas Shift (WGS) and Steam Reforming (SR) reactions can be written as Equation (6) and Equation (7) respectively.

$$Y_{H2O\_out} = \frac{Y_{CO2}\, Y_{H2}}{Y_{CO}\, K_{WGS}} \qquad \text{Equation 6}$$

$$Y_{CH4} = \frac{Y_{CO}\, {Y_{H2}}^3}{Y_{H2O}\, K_{SR}} \qquad \text{Equation 7}$$

To solve for Y_{H2O} and Y_{CH4}, the equilibrium constant values, *K*, have to be calculated from the total Gibbs free energy of the Water Gas Shift and Steam Reforming reactions. Total Gibbs free energy of reactions at a given operating condition ($\Delta G_{reaction}$) is given by Equation (8).

$$\Delta G_{reaction} = \Delta {G^o}_{reaction} + RT \ln K \qquad \text{Equation 8}$$

This equation consists of two parts: (i) Gibbs energy at standard condition (273K and 1 atm); and (ii) additional term to account for deviation of reaction conditions (T and P) from the standard condition. At equilibrium state, however, the Gibbs energy of a reaction ($\Delta G_{reaction}$) is zero thus Equation (8) can be simplified to Equation (9).

$$\ln K = -\frac{\Delta G^o{}_{reaction}}{RT}$$ Equation 9

According to Equation (9), the Gibbs free energy at standard condition ($\Delta G^o{}_{reaction}$) can be used directly to calculate equilibrium constant, *K*. Equation to calculate $\Delta G^o{}_{reaction}$ is given in Equation (10).

$$\Delta G^o{}_{reaction} = \sum v_i G^o{}_{i,products} - \sum v_i G^o{}_{i,reactants}$$ Equation 10

In order to solve for $\Delta G^o{}_{reaction}$, stoichiometric number of moles of all components of a reaction (v_i) must be identified. $G^o{}_i$ on the other hand represents the standard Gibbs energy of all components of the reaction and are determined based on tabulated values from the literature [7].

Once $\Delta G^o{}_{reaction}$ is calculated, Equation (9) can be solved for Water-Gas Shift and Steam Reforming reactions equilibrium constants, *K* values respectively. Then the *K* values can be used in Equations (6) and (7) to solve for Y_{H2O} and Y_{CH4} values in the producer gas. Using the calculated Y_{H2O} and Y_{CH4} values, the molar flow rates of these two species can be calculated by multiplying species molar fraction values with the total producer gas molar flow rate, $N_{producer\_gas}$.

$$N_{CH4} = Y_{CH4} \times N_{producer\_gas}$$ Equation 11

$$N_{H2O\_out} = Y_{H2O} \times N_{producer\_gas}$$ Equation 12

In order to solve all six unknowns (N_{H2} , N_{CO} , N_{CO2} , N_{CH4} , N_{H2O_out} , N_{N2_out}) in the equilibrium model, Equations (1), (2), (3), (4), (6) and (7) are solved simultaneously in Microsoft Excel. This is performed by setting initial guesses for Y_{H2O} and Y_{CH4} values, in which these values are then used to solve for N_{H2} , N_{CO} , N_{CO2} and N_{N2_out} in Equations (1)–(4). Molar flow rates of these components are then re-used to calculate Y_{H2O} and Y_{CH4} values from Equations (6) and (7), but this time using Gibbs free energy information from the system. This calculation cycle occurred repeatedly, up to 10,000 iterations, during which Y_{H2O} and Y_{CH4}values are manipulated until molar flow rates of all six components in the producer gas are in agreement with one other, following relationships given in Equations (1), (2), (3), (4), (6) and (7).

These operations are performed with the aid of Microsoft Excel Solver Add-In for effective iterative calculations. The guessed values of Y_{H2O_out} and Y_{CH4} are repeatedly altered until the error between these values and that calculated using Gibbs free energy are minimized, indicating agreement between all values in the specified equations. The completed model developed in this study is presented in Chapter 10: Appendix G for further reference.

6.3 Model Validation

Validation is important for checking reliability of the developed equilibrium model. It provides an indication whether or not the model is capable of generating accurate results without errors and bugs in the calculations. Once the model is proven reliable, it can then be used to examine how close the practical operation is to equilibrium state. In this work, validations of the model developed were performed by comparing the equilibrium results with that generated by another equilibrium model used in the literature as well as with a commercial thermodynamic software.

For comparison with literature, a thermochemical software model (FactSage) used by Chhiti et al. [4] was selected since the model was also used for predicting equilibrium for entrained flow gasification of pyrolysis oil. In addition, similar thermochemical software was also used by Coda et al. [5, 6] for entrained flow gasification of solid biomass. Details for the FactSage software can be found in [8, 9].

During validation, the same gasification conditions used by Chhiti et al. [4] were used for the model developed in this study. Important gasification conditions used in both equilibrium model calculations were summarized in Table 6-1. Note that in this case, steam was used as the gasification agent while the temperature range was fixed between 1000-1400°C. Results from this comparison are illustrated in Figure 6–2.

Table 6-1: Entrained flow gasification conditions used by Chhiti et al. [4] and this equilibrium model

Properties/Conditions	Values
Pyrolysis Oil Flow Rate	100 mL/min
Steam-Carbon (S:C) Ratio	8.3%
Equivalence Ratio (ER)	0
Gasification Temperature	1000 – 1400°C
Gasification Pressure	1 atm
Pyrolysis Oil Elemental Composition	C = 42.9 % H = 7.1 % O = 50.0 %

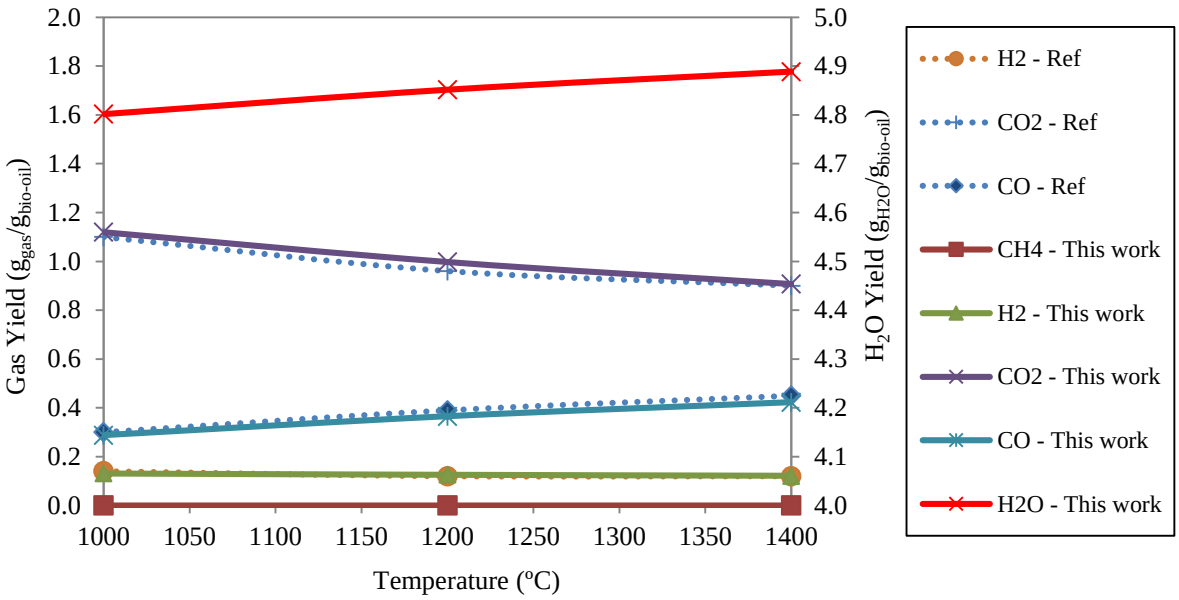

Figure 6–2: Producer gas yield predicted by equilibrium model developed in this study compared with those of Chhiti et al. [4] as labelled by 'Ref' at similar gasification conditions.

From Figure 6–2, it is clear that the results of producer gas composition from the equilibrium model developed in this work are in close agreement with those reported by Chhiti et al. [4]. Errors between these two models were calculated and represented in the form of Root-Mean-Square (RMS) value, which is defined as [2]:

$$RMS = \sqrt{\frac{\sum (V_{literature} - V_{this\ work})^2}{N}} \qquad \text{Equation 13}$$

where $V_{literature}$ is the values obtained from equilibrium model of Chhiti et al. [4], $V_{this\ work}$ is the results calculated from the model developed in this work, and N is the number of data used for the comparison. RMS errors are found to be 0.014, 0.026 and 0.016, respectively, for reaction temperatures of 1000˚C, 1200˚C and 1400˚C.

Similar validation of the developed equilibrium model was also undertaken by comparison with producer gas results predicted using another commercial software Honeywell UniSim Design Suite. In contrast with the comparison made with [4] presented earlier, this time, gasification conditions used for comparison with Honeywell UniSim Design Suite software were based on inputs defined by users, thus more comprehensive comparisons between the two equilibrium models could be made. The operation conditions used in this comparison are given in Table 6-2.

Table 6-2: Entrained flow gasification conditions used in the equilibrium models calculations

Properties/Conditions	Values
Pyrolysis Oil Flow Rate	100 mL/min
Oxygen Flow Rate	2000 L/h
Equivalence Ratio (ER)	0.3
Gasification Temperature	600 – 1600°C
Gasification Pressure	1 atm
Pyrolysis Oil Elemental Composition	C = 42.9 % H = 7.1 % O = 50.0 %

In this part, validation was made based on operating conditions most relevant to entrained flow gasification of pyrolysis oil intended in this work. Therefore, oxygen gas was chosen as the gasification agent with the equivalence ratio fixed at 0.3. The gasification temperature was varied between 600°C and 1600°C to cover both low and high gasification temperatures. The composition of pyrolysis oil, however, was taken from that used by Chhiti et al. [4] as a reference point.

Producer gas compositions generated by both equilibrium models are given in Figure 6–3. Close agreement have been found between these two tools with RMS errors remained remarkably small and consistent in all conditions tested. RMS errors declined from 0.006 to 0.001 as gasification temperature increased from 600°C to 1200°C indicating improvements in the results as temperature increase. Above this point, RMS errors remained at 0.001 regardless of the gasification temperature.

In overall, this section has proven the ability of the equilibrium model developed in this study to predict entrained flow gasification at equilibrium state.

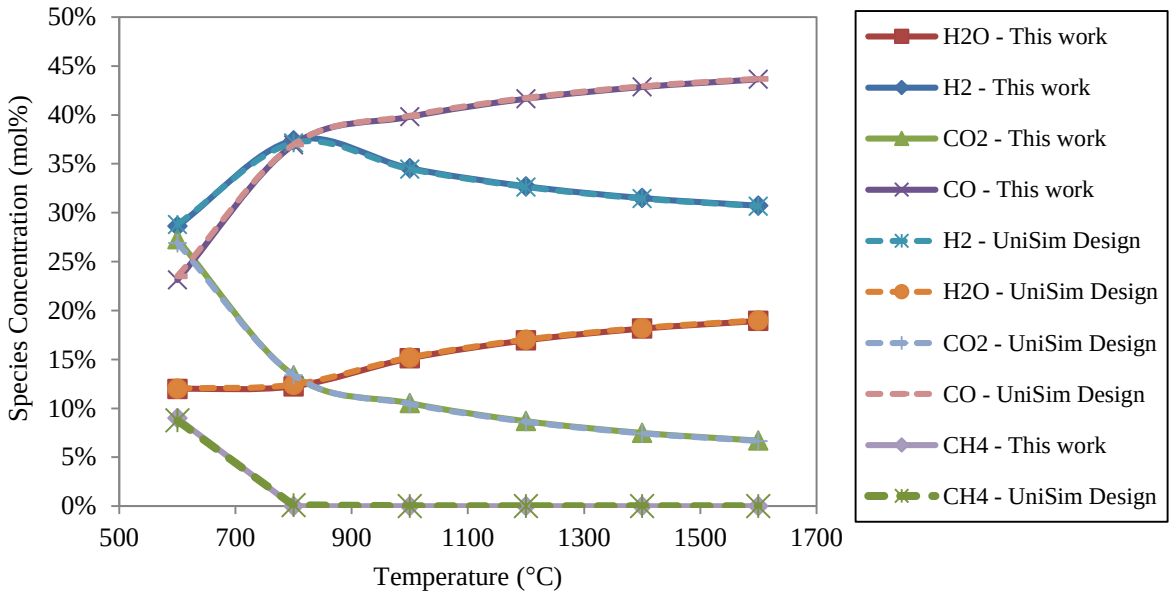

Figure 6–3: Equilibrium producer gas compositions calculated by equilibrium model developed in this work in comparison to that simulated by Honeywell UniSim Design software

6.4 Equilibrium Producer Gas Compositions for Entrained Flow Gasification of Radiata Pine Pyrolysis Oil at Various Operation Conditions

The validated equilibrium model developed in this study has been used to predict general trends of producer gas compositions generated during entrained flow gasification of pyrolysis oil. In this section, influences of gasification temperature and equivalence ratio on producer gas compositions at equilibrium are presented.

The operating conditions used in this simulation are summarized as in Table 6-3. These conditions were chosen to imitate the entrained flow gasification operating conditions planned in this work, so behaviours of producer gas compositions at equilibrium with changing gasification temperature and equivalence ratio could be observed and understood prior to the actual gasification runs. The pyrolysis oil composition specified in Table 6-3 was taken from elemental analysis results of one pyrolysis oil sample used in this study, as a reference.

Table 6-3: Gasification operating conditions and properties of pyrolysis oil used by the equilibrium model

Properties/Conditions	Values
Pyrolysis Oil Flow Rate	60 mL/min
Equivalence Ratio (ER)	0 – 0.6
Gasification Temperature	600 – 1400°C
Gasification Pressure	1 atm
Pyrolysis Oil Elemental Composition	C = 27.2 % H = 7.7 % O = 64.9 % N = 0.12 % S = 0.03 %

Effects of temperature on producer gas composition at equilibrium are presented in Figure 6–4 from which it can be found that as gasification temperature increases, the concentrations of H_2, CO_2 and CH_4 in the producer gas decrease. However, the concentrations of CO and H_2O increase with gasification temperature.

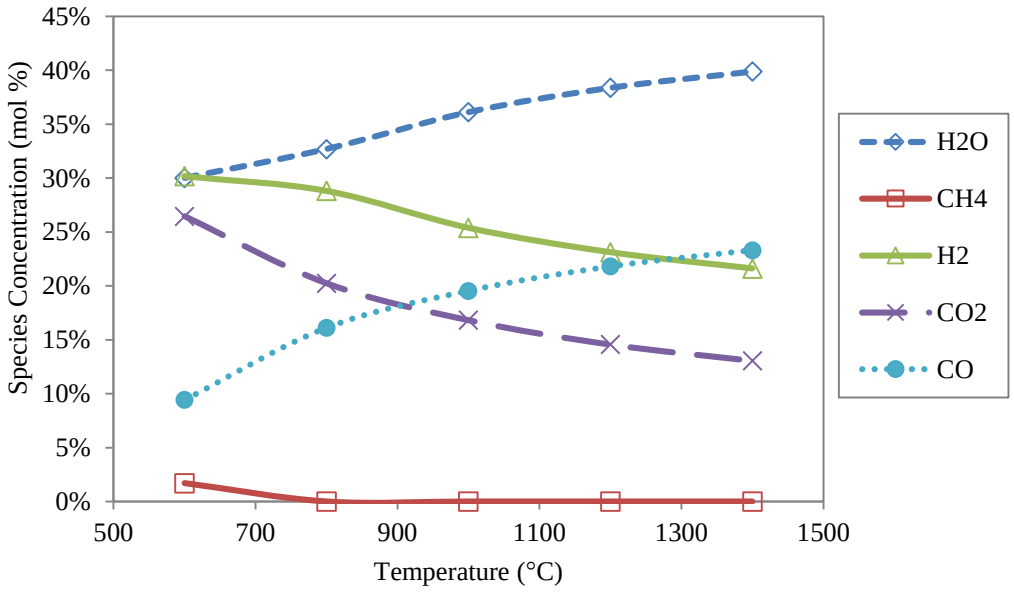

Figure 6–4: Effect of temperature on producer gas composition at equilibrium in entrained flow gasification of pyrolysis oil at ER: 0.35

Producer gas composition trends observed in Figure 6–4 could be explained by considering domination of Water-Gas Shift reaction (Reaction (1)) during gasification operation at varying temperature. Water-Gas Shift reaction is a reversible exothermic reaction that is thermodynamically favoured at low temperature. When gasification temperature increases to a sufficiently high value, this reaction reverses to favour production of CO and H_2O while consuming H_2 and CO_2 from the system. It is possible that supply of H_2 for the reverse Water-Gas Shift reaction is linked to endothermic Steam Reforming reaction (Reaction (2)), in which increase in temperature favours production of H_2 and CO in the product by reactions between CH_4 and CO_2. From the trend shown in Figure 6–4, reverse Water Gas Shift and Steam Reforming reactions are shown to dominate the system concurrently thus leading to higher concentrations of CO and H_2O in the producer gas as the gasification temperature increases.

In practical gasification operation, however, producer gas compositions could deviate significantly from these trends when the system is unable to reach equilibrium state. In this regard, Chhiti et al. [4] and Sakaguchi et al. [10] reported that failure to reach equilibrium state mostly occurred during gasification at low operating temperatures. This situation is predictable because at low gasification temperature, chemical reactions are more likely constrained by poor kinetics thus prevents the system from reaching equilibrium within the required process residence times. As the gasification temperature increases, kinetics of reaction are expected to improve significantly thus driving the system closer to equilibrium. In entrained flow gasification of pyrolysis oil, equilibrium state was reported could only be achieved when gasification temperature was as high as 1400°C [4].

Effects of equivalence ratio on producer gas composition as predicted by the equilibrium model are presented in Figure 6–5. In these tests, gasification temperature was fixed at 1000°C while the equivalence ratio was varied between 0–0.6 to simulate equivalence ratio range most favourable during a gasification operation.

Results from Figure 6–5 clearly show that at increasing equivalence ratio, concentrations of H_2O and CO_2 increased while the opposite was observed for H_2 and CO. These changes could be explained by considering addition of more oxygen into the system at higher equivalence ratio, which gradually takes over non-oxidation reactions domination of the system. This is because during gasification at low equivalence ratio, gasification is mainly dominated by non-oxidation reactions such as Water-Gas Shift, Steam Reforming, Hydrogasification and Boudouard reactions; thus favour production of H_2, CO and CH_4 in the producer gas. However, as more oxygen is added into the system with increased equivalence ratio, oxidation reactions gradually become more dominant thus rapidly oxidize gasification products such as H_2, CO and CH_4 into higher concentrations of H_2O and CO_2 in the product.

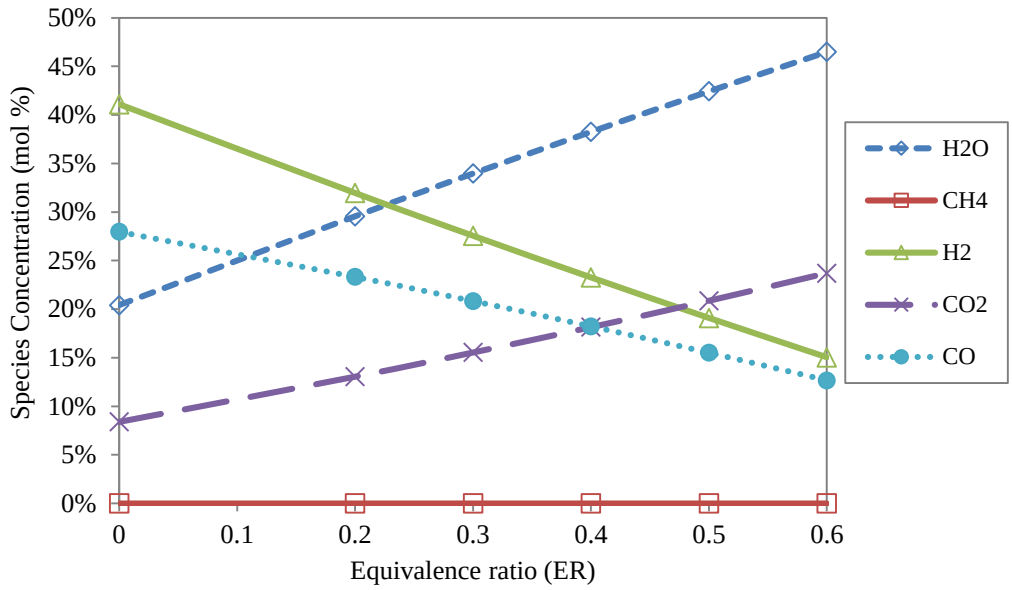

Figure 6–5: Effect of equivalence ratio on producer gas composition at equilibrium in entrained flow gasification of pyrolysis oil at 1000°C

Nonetheless, these trends also apply only when a system is at equilibrium state. Results from practical entrained flow gasification as reported in the literature showed increase in CO concentration when equivalence ratio was increased during the operation [11-13]. Studies in literature reported conflicting trends for concentrations of H_2, CO_2 and CH_4 in producer gas at varying equivalence ratio [11-13], thus proving most gasification systems are not operating at equilibrium state at normal gasification conditions.

The common deviations of gasification products from equilibrium as discussed in this section proved the importance of using equilibrium model for evaluating a system's behaviour and performance. It is worthwhile emphasizing that in practical large scale entrained flow gasification system such as that developed in this study; effects of adjusting equivalence ratio and gasification temperature are not as straightforward as in theory. This is because during real gasification operations, temperature is dependent on heat released during exothermic reactions of pyrolysis oil with oxygen (partial combustion), thus may increase or decrease parallel with adjustments of equivalence ratio values. Due to this reason, effects of equivalence ratio and gasification temperature on producer gas composition are strongly interrelated, thus need to be accounted simultaneously.

The interconnection between equivalence ratio and temperature in such system leads to complex gasification performance and products behaviour; hence use of reliable equilibrium model which capable of predicting gasification at various conditions, such that developed in this study, becomes even more important.

The practical relationship between feed flow rates (pyrolysis oil and oxygen gas), equivalence ratio, temperature and producer gas composition from entrained flow gasification of pyrolysis oil will be discussed in great detailed in Chapter 7. Experimental results from the entrained flow gasification operations will be compared with equilibrium products as predicted by the equilibrium model developed in this study, for in-depth analysis and evaluation of the gasification operations performances.

6.5 References

1. Rutherford, J., *Heat and power applicationof advance biomass gasifier in New Zealand's wood industry*, in *Chemical and Process Engineering*. 2006, University of Canterbury: Christchurch.
2. Karamarkovic, R. and V. Karamarkovic, *Energy and exergy analysis of biomass gasification at different temperatures.* Energy, 2010. **35**(2): p. 537-549.
3. Higman, C. and M. van der Burgt, *Chapter 2 - The Thermodynamics of Gasification*, in *Gasification (Second Edition)*, C. Higman and M.v.d. Burgt, Editors. 2008, Gulf Professional Publishing: Burlington. p. 11-31.
4. Chhiti, Y., et al., *Wood Bio-Oil Noncatalytic Gasification: Influence of Temperature, Dilution by an Alcohol and Ash Content.* Energy & Fuels, 2010. **25**(1): p. 345-351.
5. Coda, B., M.K. Cieplik, and J.H.A. Kiel. *Slagging behaviour of wood ash upon entrained-flow gasification conditions: Preliminary studies*. 2004.
6. Coda, B., et al., *Slagging Behavior of Wood Ash under Entrained-Flow Gasification Conditions.* Energy & Fuels, 2007. **21**(6): p. 3644-3652.
7. Lide, D.R., *CRC Handbook of Chemistry and Physics 84th Edition*. 2004: CRC Press LLC.
8. Bale, C.W., et al., *FactSage thermochemical software and databases — recent developments.* Calphad, 2009. **33**(2): p. 295-311.
9. GTT-Technologies, T. *FactSage 6.4*. 2014 [cited 2014 6/3/2014]; Available from: http://www.factsage.com/.
10. Sakaguchi, M., A.P. Watkinson, and N. Ellis, *Steam Gasification of Bio-Oil and Bio-Oil/Char Slurry in a Fluidized Bed Reactor*. Energy & Fuels, 2010. **24**(9): p. 5181-5189.
11. Chhiti, Y., M. Peyrot, and S. Salvador, *Soot formation and oxidation during bio-oil gasification: experiments and modeling*. Journal of Energy Chemistry, 2013. **22**(5): p. 701-709.
12. Marda, J.R., et al., *Non-catalytic partial oxidation of bio-oil to synthesis gas for distributed hydrogen production.* International Journal of Hydrogen Energy, 2009. **34**(20): p. 8519-8534.
13. Qin, K., et al., *Biomass Gasification Behavior in an Entrained Flow Reactor: Gas Product Distribution and Soot Formation.* Energy & Fuels, 2012. **26**(9): p. 5992-6002.

7 ENTRAINED FLOW GASIFICATION EXPERIMENTS, RESULTS AND DISCUSSIONS

7.1 Experiments and Plans

In this part of study, experiments on entrained flow gasification of pyrolysis oil were designed to investigate the influence of operation conditions on the gasification performance and to determine the operability of the entrained flow gasification system developed in this work. In total, 12 experimental runs on entrained flow gasification were conducted, in which 8 runs were successful while the remaining runs were not able to produce useful results due to unforeseen interruptions and technical difficulties during the operations. Typical gasification duration during successful runs were between 4-5 hours, excluding pre-heating stage and downtime.

The single most common issue encountered during these operations were related to interruptions in pyrolysis oil feeding into the system. Factors that contribute to this problem have been discussed in detailed in Chapter 3.12.2 of this thesis. The most frequent source of interruption to the oil feeding system occurred due to unexpected atomizer blockage in the middle of gasification operations. Although the pyrolysis oil had already been pre-filtered at three different stages to remove solids up to 10μm prior to atomization, plugging of the atomizer still occurred, thus suggesting inherent issues associated with pyrolysis oil flow through the atomizer's tiny liquid outlet orifice.

In many cases, atomizer blockage occurred due to pyrolysis oil polymerization upon exposure to gasification high temperature environment. There were also gasification runs where atomizer blockage was proven not caused by pyrolysis oil polymerization, rather due to accumulation of viscous components of the oil (waxy materials, small char and heavy tar compounds) during the operations. Detailed elaborations of these problems as well as other possible causes of atomizer blockage during gasification operations have been discussed earlier in Chapter 5.3.1 of this thesis.

As for the successful gasification runs, various operation conditions were tested to observe their effects on gasification products and performance. In these runs, no interruptions to the pyrolysis oil feeding was encountered thus atomizer blockage due to oil polymerization was successfully avoided. In addition to that, the pyrolysis oil used in these runs also did not form significant accumulation of viscous compounds in the oil feeding system to block the atomizer. The summary of gasification conditions tested in these runs are summarized as in Table 7-1.

Table 7-1: Summary of operation conditions tested during successful gasification runs in this work

Run #	Pyrolysis Oil Flow Rate (mL/min)	Oxygen Gas Flow Rate (L/h)	Equivalence Ratio, ER
1	35 – 67	500 – 3200	0.10 – 0.81
2	52 – 59	1000 – 2400	0.21 – 0.54
3	50 – 58	1400 – 1600	0.30 – 0.39
4	32 – 37	1400 – 3200	0.48 – 1.19
5	22 – 56	900 – 3000	0.23 – 0.86
6	31 – 61	900	0.16 – 0.32
7	20 – 32	900	0.23 – 0.37
8	13 – 29	600 – 1500	0.38 – 0.83

The operation conditions of which the gasification were operated were not fully controlled due to significant variations in the properties of pyrolysis oil used between the runs. The flow rate of pyrolysis oil strongly depends on the oil viscosity which has been proven to change as a result of ageing. In addition to that, the oil flow rate is also influenced by the peristaltic pump speed and build-up of pressure drop across the on-line filter, thus contributes to the inconsistencies in the conditions tested during the runs. Oxygen gas feed flow rates were closely controlled during gasification runs, however this parameter alone was not sufficient to maintain consistencies in the operation conditions between different runs.

Technical information and findings from these gasification runs will be discussed in great details in Sections 7.2 – 7.5 which were constructed as a collection of four research articles that will be submitted to relevant journals. Each section is the copy of one paper which has a specific focus on investigation and analysis. It must be pointed out here that the materials in 'Introduction' and 'Experimental' of the following sections may be repetitive to some extent.

In particular, Section 7.2 will discuss the influences of pyrolysis oil and oxygen gas flow rates on gasification temperature, producer gas flow rate (g/min) and gas yield (g_{gas}/g_{oil}). Section 7.3 on the other hand, will investigate influences of equivalence ratio on producer gas compositions during gasification at constant oxygen feeding rates. The producer gas compositions from the experiments will be compared with those predicted by the equilibrium model developed in Chapter 6. Section 7.4 will investigate the effects of varying oxygen gas feeding rate on producer gas composition during gasification at constant

equivalence ratio. Similar to Section 7.3, the experimental results presented in this section will be compared with those predicted by the equilibrium model. In the last section (Section 7.5), influences of equivalence ratio on tar species distribution and tar concentrations during the entrained flow gasification will be discussed.

7.2 Non-Slagging Entrained Flow Gasification of Biomass Pyrolysis Oil: Gasifier Development and Performance Investigation

This section will be submitted as a research paper in the international journal Biomass and Bioenergy

Abstract:

In this work, a pilot scale entrained flow gasification system was developed to gasify biomass pyrolysis oil with oxygen as the gasification agent at atmospheric pressure and maximum temperature of 1100^{o}C. The system is equipped with an external mix twin-fluid atomizer capable of generating fine pyrolysis oil droplets after impact with the oxygen gas. The pyrolysis oil used in this study was derived from New Zealand radiata pine wood chips through a fast pyrolysis process. This article presents important design characteristics of the entrained flow gasification system and effects of oxygen and pyrolysis oil feed flow rates on gasification performance. The results showed superior effect of oxygen gas flow rate on gasification temperature over that showed by pyrolysis oil flow rate. The opposite was found for producer gas flow rates (g/min) where pyrolysis oil flow rate has more significant influence on the product flow. Investigation on dry producer gas yield (g_{gas}/g_{oil}) at different equivalence ratio values showed a unique trend where the gas yield increased dramatically to a critical equivalence ratio of 0.3 before decreased gradually as the equivalence ratio continued to increase. . The critical ER value represents the optimum combination of residence time and reaction kinetics that promotes good pyrolysis oil conversion as well as balance between oxidation and non-oxidation reactions during the gasification operation.

Keywords: Entrained flow gasification, oxygen, biomass pyrolysis oil, external mix atomizer

7.2.1 Introduction

In past two decades, extensive research has been conducted to explore alternative energies that could reduce the current world dependency on fossil fuels [1]. This situation has consequently driven rapid developments of technologies for using renewable energy resources such as wind, solar and biomass. Biomass resource is abundant in the world and thus has a promising potential as a reliable source of renewable energy in the future. Presently biomass energy contributes to approximately 14% of the total energy consumption in the world [2]. The biomass-derived energy is considered as carbon neutral because with strategic re-plantation of forest or other energy crops, there will be no net addition of CO_2 to the atmosphere as CO_2 released during energy production or consumption is recycled during plant growth via photosynthesis [1, 3-6].

In conversion of biomass to energy, gasification is one of the most efficient processes [2] while at the same time it provides flexible applications of the gas product. Entrained flow gasification could be considered as one of the earliest and most popular gasification technologies available where it has been extensively used for gasification of coal, black liquor and refinery residues from petrochemical industries [3, 7-13]. This type of gasifier is characterized by its high operating temperature and ability to achieve near 100% carbon conversion at significantly short residence times [1, 2, 4]. With high gasification temperature in the entrained flow gasifier, the formation of condensable hydrocarbon compounds (tar), which are the common challenges in every biomass gasification process, are also significantly reduced [4].

Despite the high conversion efficiency and low tar content in entrained flow gasification processes, there are also many challenges associated with its operation that require careful considerations before it could be successfully commercialized for biomass feedstock. One of the biggest challenges is the strict feedstock size requirement [14-17], where the process generally demands feed particles size of less than 0.1 mm [18] so maximum reaction kinetics could be achieved within the system's short residence time. While this requirement may not be an issue for coal, solid biomass is difficult to be pulverized into small and consistent particle size due to its fibrous nature [16]. In addition, entrained flow gasification also shares similar challenges with any solid biomass-to-energy conversion processes due to biomass high moisture content, and low mass and energy densities; which consequently lead to undesirable high costs for handling, transportation and storage [2, 5, 16, 19, 20].

To reduce the operation costs and solve the strict feedstock requirements, solid biomass could be first densified through fast pyrolysis process, in which the biomass is rapidly heated at 500^{o}C in the absence of oxygen to produce up to 75 wt% liquid [21, 22]. This liquid product is commonly referred to as 'pyrolysis

oil' or 'bio-oil' and contains up to 70% of the total energy from the solid biomass input while having much higher mass and energy densities. In some applications, the oil is mixed with char to make 'pyrolysis slurry' so its energy content could be further increased to as high as 90% of the energy in the original biomass feedstock [23].

Other than solving gasification feed requirements and solid biomass high handling costs [5, 15, 23], feeding liquid or slurry is also more convenient for high pressure gasification system [15]. In terms of reaction kinetics point of view, feeding of liquid feedstock into the gasification system is advantageous as it can be atomized into fine spray droplets as small as 10μm, thus significantly enhances reaction kinetics, feed conversions and the overall efficiency of the system. Other than that, gasification of pyrolysis oil was also reported could reduce CO_2concentration in the producer gas [21] and therefore is more environmental friendly compared to when using solid biomass feedstock.

The pyrolysis oil and pyrolysis oil and char slurry derived from the biomass fast pyrolysis is suitable for entrained flow gasification application. As a result, research has been conducted to investigate performance of entrained flow gasification using these fuels for producer gas production. In studies on entrained flow gasification of biomass pyrolysis slurry, effects of various gasification parameters on the products and carbon conversion were examined experimentally. Examples of gasification parameters explored are the slurry char content, char particle size, gasification temperature, equivalence ratio and feed flow rates [5, 6, 23-28]. Some studies also reported influence of slurry atomization characteristics on entrained flow gasification performances [24-26]. Economic analyses of pyrolysis slurry entrained flow gasification were also conducted in several studies to predict the feasibility of this process [5, 23, 29].

While research on entrained flow gasification of pyrolysis slurry is abundant, the amount of information found in the literature on entrained flow gasification application for pyrolysis oil is limited. Gasification of pyrolysis oil will have great potential when solid char can be used for other applications such as activated carbon and gas cleaning sorbent. Currently, studies on pyrolysis oil entrained flow gasification are mostly restricted to relatively small scale operations [22, 30-34]. Chhiti et al. [22] have explored steam gasification of pyrolysis oil in an entrained flow gasifier with pyrolysis oil feeding rate of 0.3 g/min. In this study, effects of gasification temperatures (550-1000^{o}C), heating rates and pyrolysis oil ash contents on producer gas composition and gas yield were investigated. Gasification of pyrolysis oil at higher temperature (1000-1400^{o}C) was also tested by Chhiti et al. in separate studies [30, 35] where carbon conversion and hydrogen gas yield were reported to increase significantly with increase in gasification temperature.

In other studies, Creager et al. [32] investigated entrained flow gasification of pyrolysis oil with oxygen gas as the gasification agent. In this study, the gasification temperature was fixed at 850^{o}C and the operation pressures were at 1 bar and 6.8 bar, respectively. The pyrolysis oil and oxygen gas were introduced into the gasifier through a twin-fluid atomizer. The pyrolysis oil feeding rate was 10 mL/min while the equivalence ratio was fixed at 0.25. The term equivalence ratio (ER) refers to the ratio of oxygen supplied into the system during gasification to that theoretically required for stoichiometric pyrolysis oil combustion [36]. Results in this study showed important influence of atomization performance and gasification pressure affecting producer gas composition during gasification operations. Nevertheless, detailed analyses of the results were not reported.

Marda et al. [33] also investigated entrained flow gasification of pyrolysis oil with oxygen gas but at temperatures between 625-850^{o}C and equivalence ratio between 0 to 0.35. This study used an automatic syringe pump to feed the pyrolysis oil into an ultrasonic nozzle at flow rates up to 10 mL/min. The findings showed significant influences of equivalence ratio and temperature influencing composition of producer gas generated during the gasification operations. The results also highlighted more dominant effect of equivalence ratio improving carbon conversion during gasification in comparison with that caused by temperature and other parameters.

The limited information in the literature on entrained flow gasification of pyrolysis oil with oxygen as the gasification agent has caused uncertainty on the optimum design of the equipment and operation of the process. The objectives of this study were to develop a new entrained flow gasification system at pilot scale for gasifying biomass pyrolysis oil, and to investigate effects of operation conditions on the gasification performance. This article will present the development of this new system and examine influences of pyrolysis oil and oxygen gas flow rates on gasification temperature, producer gas flow rate (g/min) and gas yield (g_{gas}/g_{oil}). Further studies and detailed results from the entrained flow gasification operations will be discussed in the subsequent papers in Section 7.3 – 7.5. This research will contribute to fundamental understanding of the entrained flow gasification operation and the results can be used for identifying and resolving technical challenges in practical applications.

7.2.2 Materials and Methods

7.2.2.1 Feedstock

The pyrolysis oil used in this study was obtained from a local company, Alternative Energy Solutions (AES) Ltd, who has a demonstration scale pyrolysis reactor to produce pyrolysis oil from radiata pine

wood chips. Due to scale limitation, the pyrolysis oil was collected from the company over a short period of time and then stored in lab until use. This situation may cause inconsistency and changes in properties of the pyrolysis oil between gasification runs.

Measurements of the oil properties were conducted periodically so changes of the oil properties due to ageing were recorded over time. Results from the measurements of bio-oil used in this work over 7 weeks period are summarized in Table 7-2. In order to reduce the variation in the pyrolysis oil properties, gasification experiments were conducted as early as practical after a batch of oil was received.

Table 7-2: Summary of relevant pyrolysis oil properties used for gasification in this work as measured in 7 week durations

Ultimate Analysis (wt%)			H_2O	Density	Viscosity	pH	LHV
C	H	O	(wt%)	(kg/m^3)	(cSt)		(MJ/kg)
36.7 – 46.7	± 7.7	45.6 – 55.6	19 – 39	1160 – 1222	15 – 330	3.2	± 16

The elemental composition of carbon in pyrolysis oil was measured using a TOC analyser. In this study, the hydrogen content was found to vary insignificantly with an average value of 7.7 wt%. The consistency of hydrogen content between different production batches is believed to be related to consistent hydrogen content in the feedstock radiata pine wood chips for fast pyrolysis process. Oxygen content was determined by difference between carbon and hydrogen contents in the oil based on the wood chip composition. Other trace species such as sulphur and nitrogen were also detected in the biomass pyrolysis oil; however, these are not reported due to their small values. Moisture contents, density, viscosities and pH of the pyrolysis oil were measured using Karl Fischer titration (ASTM E203), digital density meter (ASTM D4052), glass capillary viscometer (ASTM D445 and ASTM D446) and pH meter respectively.

7.2.2.2 Entrained flow gasification system

The entrained flow gasifier developed in this study is capable for gasification or combustion of liquid fuel at atmospheric pressure and maximum operating temperature of 1100^{o}C. The gasifier mainly consists of two stainless steel concentric cylinders with diameters of 120 mm and 248 mm, respectively. The inner cylinder is the gasification reactor with its wall being made of two layers of 2 mm high temperature and corrosion resistance 253MA (micro-alloyed) stainless steel. The outer cylinder, on the other hand, was made of 316 grade stainless steel due to less extreme reaction environment requirements. The hollow

space between the two concentric cylinders is used for preheating of the system at the start-up stage and for heat insulation during normal gasification operation. The total height of the reactor is 850 mm.

Schematic drawing of the gasifier with emphasis on main sections and important components of the gasifier construction is illustrated in Figure 7–1.

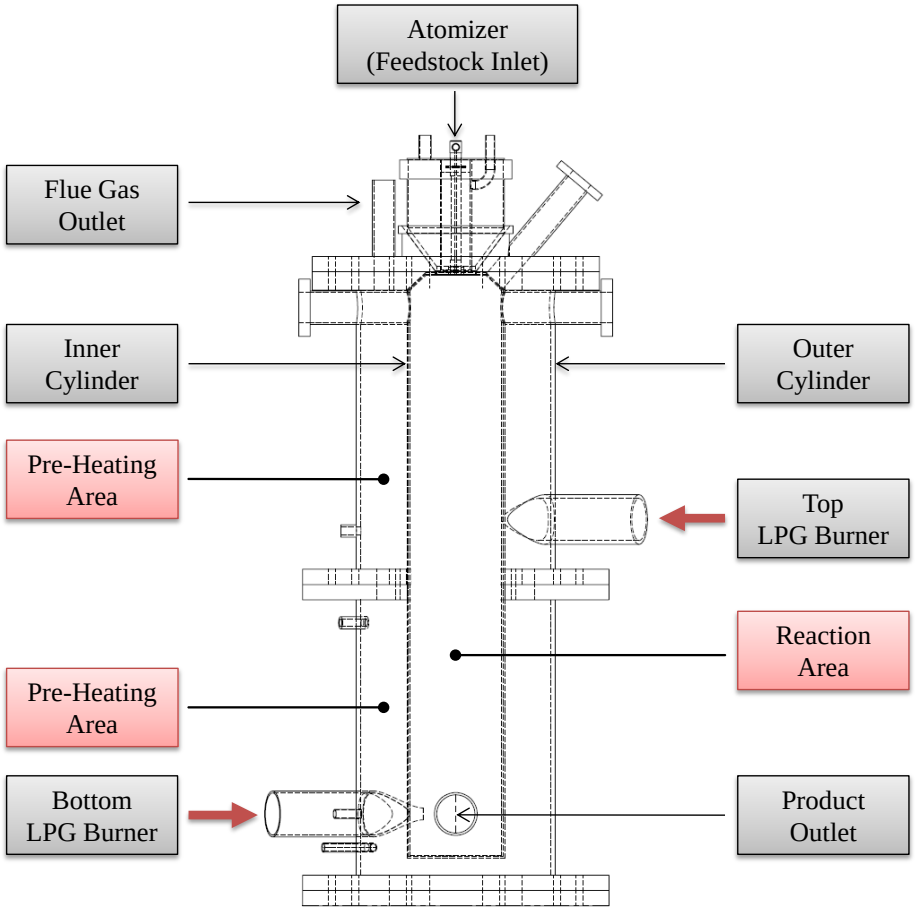

Figure 7–1: Schematic drawing of the entrained flow gasifier developed in this work and some of its major components

Within the hollow space, one LPG burner is located at the top section and another burner at the bottom section of the gasifier. The burners are mounted to fire the cavity at an angle approximately 45° from the tangential direction of the gasifier wall to induce spiral motion of hot air within the space to improve heat flow and distribution. Several baffle plates are also mounted within the space aiming to increase hot gas residence time and turbulence, thus improving heat transfers rates during the pre-heating stage.

To measure temperature profile along the gasifier reactor, two thermocouple probes are installed at different heights of the gasifier. The temperature at the top of the reactor is not measured since it is too

close to the pyrolysis oil spray and was found to interfere with spray formation and combustion during operation. To resolve this issue, a specially designed surface thermocouple was installed to measure the gasifier inner cylinder temperature for safety monitoring purpose. In addition, a pair of thermocouple was installed at the top and the bottom cavity spaces, respectively, to measure temperature changes during the pre-heating stage. Two pressure probes were also installed to monitor pressure profile in both the cavity and the reactor during operation. Producer gas outlet port is located close to the gasifier bottom and connected to a pipe leading to an after-burner. A sampling port is connected to this pipe before the after-burner for collection of producer gas and tar samples. Two more ports are also made on the reactor for safety valve and viewing glass.

Pyrolysis oil and oxygen gas are introduced into the system through an atomizer. The atomizer is twin-fluid atomizer of model 1/4J SUE15B, manufactured by Spraying Systems Co. as shown in Figure 7–2. The atomizer is an 'external mix' atomizer, therefore, the liquid pyrolysis oil and oxygen gas streams flow separately and only come into contact when both streams exit the nozzle. The use of external mix atomizer is advantageous as it allows independent adjustments of pyrolysis oil and oxygen flow rates during atomization, thus enables control of the desired spray characteristics by adjustment of only one parameter at a time. This particular atomizer model is capable of producing fine liquid droplets in a flat spray pattern.

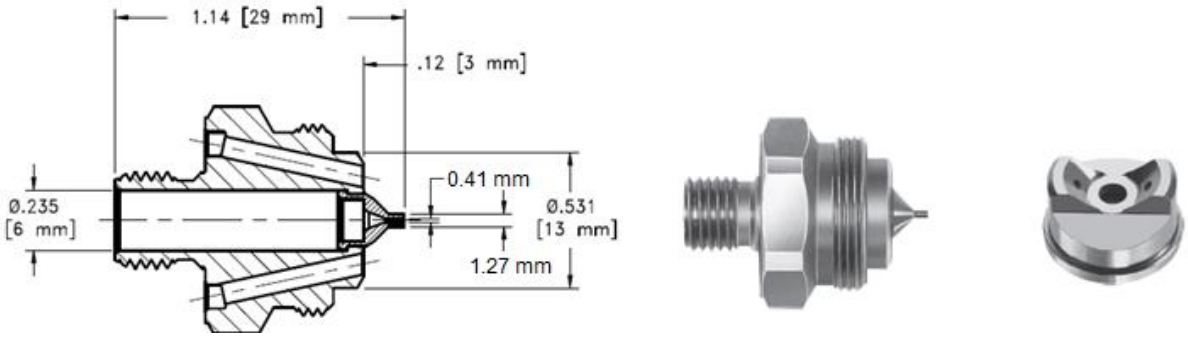

Figure 7–2: Images of external mix 1/4J SUE15B atomizer. Left Image: Cross section view and dimensions of the liquid cap; Middle Image: Atomizer liquid cap (#1650); Right Image: Atomizer air cap

In comparison to the more commonly used internal mixing atomizer, the external mixing atomization provides a much safer combustion environment for pyrolysis oil and oxygen gas by minimizing risk of undesirable internal combustion within the atomizer or flame flashback during gasification at high temperature [37].

The atomizer is surrounded by a specially designed water cooling jacket so it remains at low temperature to prevent undesirable pyrolysis oil polymerization and blockage to the atomizer outlet during operation. To minimize unnecessary heating of the atomizer during gasification pre-heating period, the atomizer and cooling jacket assembly is only fitted on the gasifier body once the targeted start-up temperature is achieved and the system is ready for pyrolysis oil injection. A high temperature sealant is used to create gas-tight seal between the cooling jacket and the gasifier metal-metal connections to prevent gas leak.

7.2.2.3 Experimental procedures

The start-up temperature for the gasifier reactor prior to any gasification run was set at 750^{o}C and was accomplished using the two LPG burners. When the system stabilized at this temperature, both LPG burners were switched off and the assembly of atomizer and cooling jacket was then fixed on the gasifier. Following this pyrolysis oil supply into the system was made using a Watson Marlow peristaltic pump at flow rates between 10 – 70 mL/min. The flow rate of pyrolysis oil was measured using a positive displacement flow meter installed after the pump. When supply of pyrolysis oil was successful, oxygen gas was injected at flow rates in the range between 600-3000 L/h depending on the objective of an individual gasification run. The oxygen flow rate was controlled using a rotameter corrected to the gas temperature and pressure. Once the system stabilized, samples of producer gas and tar were taken from the sampling line for analysis. In the experiments, only a small fraction of producer gas was sampled while the main stream of producer gas was burnt in an after-burner.

During gasification, the gasifier temperature was dependent on the heat generated from partial combustion of pyrolysis oil with oxygen gas upon leaving the atomizer. Equivalence ratio values were determined based on flow rates of pyrolysis oil and oxygen gas entering the system. During any set of gasification run, the oxygen gas flow rate was set to a constant value while the pyrolysis oil flow rate was periodically changed to alter the equivalence ratio. In all runs, the system was allowed to stabilize for at least 20-30 minutes before the first sample was taken for analysis. The interval between two consecutive samplings was maintained between 10-15 minutes to minimize inconsistencies. It is expected that the gasification process is rapid with residence time in the range between 1-5 seconds; therefore, production of producer gas at a new gasification condition should stabilize reasonably quickly.

7.2.2.4 Sampling method

The temperature of the producer gas exiting the gasifier was maintained at high temperature (450-600^{o}C) to prevent condensation of tar compounds during the sampling. The probe used for sampling was placed at the centre of producer gas flow so that the temperature difference between the probe and gas was insignificant. Besides that, the sampling probe length was kept as short as possible to maximize adsorption of condensable products onto solid phase extraction (SPE) column packed bed.

The arrangement of the product sampling assembly is illustrated in Figure 7–*3*. The sampling rod is 90 mm long and can be inserted through the sampling valve into the producer gas main stream. Two SPE columns of different packed materials were used in every sample to make sure gas collected in the syringe for Micro-GC analysis was free from condensable compounds such as water and tars. The other end of the SPE column was connected to a 100 mL fixed syringe via a three way valve for manual gas extraction. This syringe was used for collection of tars while the remaining end of the valve was connected to a medium sized syringe (60 mL), which was removable thus was specially dedicated for Micro-GC analysis.

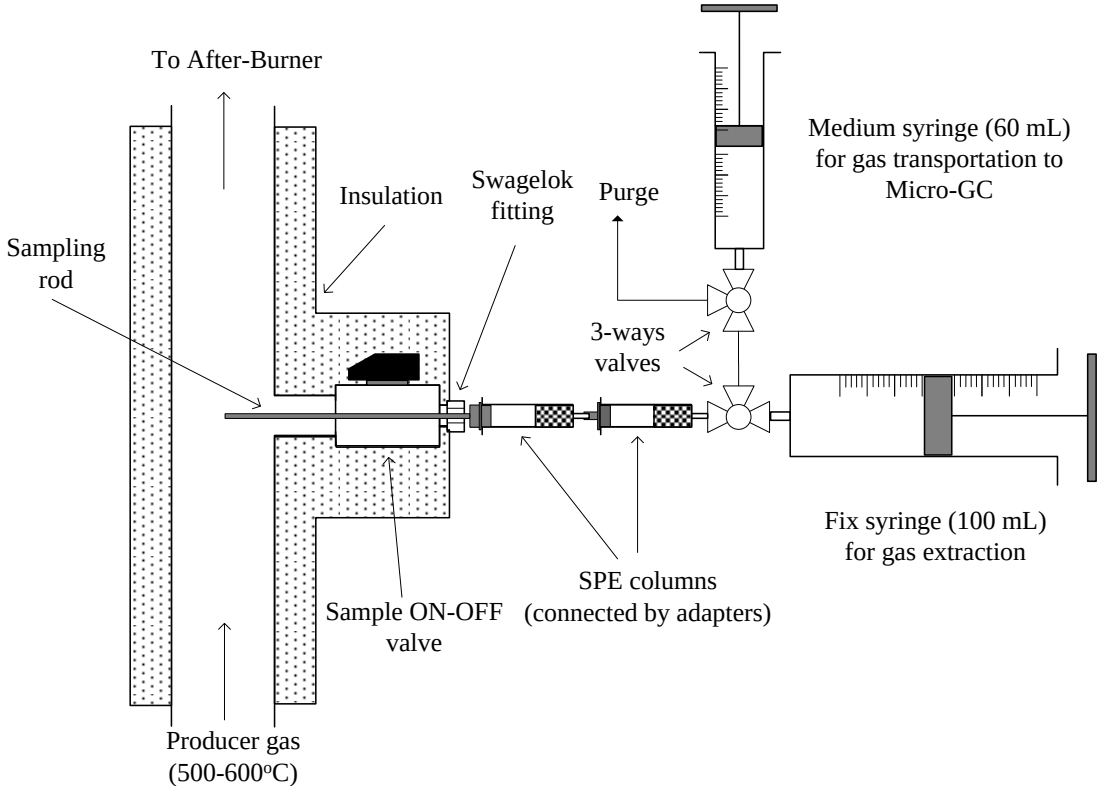

Figure 7–3: Illustration of sampling arrangement for entrained flow gasification system in this work

During each product sampling, a total of 200-300 mL of producer gas from the gasification system was passed through the SPE columns, aimed to trap as much tar compounds as possible. From this amount only a small fraction of the gas was used for Micro-GC analysis. After sampling was completed, the sampling probe and the SPE columns containing tar were removed from the sampling assembly, sealed and stored in a refrigerator ready for tar extraction and analysis using GC.

7.2.2.5 Producer gas analysis

Producer gas samples collected from the 60 mL syringes were analysed using a Micro-GC (Agilent 3000A) with thermal conductivity detector (TCD) to determine concentrations of producer gas components. Producer gas from biomass gasification have been reported to mainly consist of hydrogen (H_2), carbon monoxide (CO), carbon dioxide (CO_2), methane (CH_4), ethylene (C_2H_4) and ethane (C_2H_6) gas species. To separate and quantify all the producer gas components, two analytical columns were used in the Micro-GC. The first column was a MolSieve 5A Plot 10m x 0.32mm column, operating at 110^{o}C, which was used to separate H_2, N_2, CH_4 and CO species. The second column was a Plot Q 8m x 0.32mm column, operating at 60^{o}C, which was used to separate CO_2, C_2H_4 and C_2H_6 gas species. The carrier gases for MolSieve 5A Plot and Plot Q columns were Argon and Helium respectively. Besides analyzing composition of producer gas, Micro-GC was also used to determine the concentration of tracer gas, helium, which was used to calculate the producer gas flow rate and product yield as described in the following section. Helium was separated and detected in MolSeive 5A Plot column.

7.2.2.6 Producer gas flow rate (g/min) and dry yield (g_{gas}/g_{oil})

In this work, helium gas was used as the tracer gas due to its inert nature. The flow rate of the helium gas entering the gasifier system was between 2.5 and 5 L/min and was controlled using a calibrated rotameter with accuracy of ± 0.15 L/min.

Based on conservation of mass balance across the system for helium gas, the following equation was derived to calculate the total flow rate of dry producer gas (N_{gas_dry}) exiting the system:

$$N_{gas\_dry} = \frac{N_{He\_in}}{y_{He\_out}}$$

In which N_{He_in} is the molar flow rate of the helium tracer gas injected to the gasifier (mol/min) and y_{He_out} is the helium concentration in the producer gas (mol/mol).

The flow rate of producer gas calculated with this method is based on water-free or dry basis since the concentrations of helium tracer gas, as measured by Micro-GC, was based on water free concentration.

The producer gas yield, on the other hand, presents the results in terms of the ratio between the producer gas flow rate (g/min) and the pyrolysis oil feeding rate (mL/min) to account for changes in the pyrolysis oil feeding rate during gasification operation. The gas yield was calculated in weight basis, considering phase difference between pyrolysis oil and producer gas (liquid versus gas phase). The mass flow rate of producer gas used in this calculation is a sum of mass flow rates of all producer gas components, based on the following equation:

$$M_{gas\_dry} = \sum Y_i \times N_{gas\_dry} \times MW_i$$

7.2.3 Results and Discussions

7.2.3.1 Effects of pyrolysis oil and oxygen flow rates on gasification temperature

The ratio between pyrolysis oil and oxygen gas feeding rates in gasification applications is best presented in terms of the equivalence ratio. In practice, equivalence ratio of 1 represents sufficient oxygen supply for stoichiometric combustion of pyrolysis oil while equivalence ratio of 0 represents no supply of oxygen into the system. Gasification is usually operated at equivalence ratio as low as possible, where oxygen supply only aims to partially combust the pyrolysis oil to generate sufficient heat to drive subsequent endothermic gasification reactions downstream of the reactor.

Based on this definition, equivalence ratio also reflects the amount of heat released from partial combustion of pyrolysis oil during the process, thus the gasification temperature. In this work since no external heat was supplied to the system during the gasification process, effect of equivalence ratio on the temperature could be effectively investigated. The relationship between equivalence ratio and gasification average temperature is shown in Figure 7–4. As illustrated in the figure, three oxygen gas feeding rates were used in these tests while the equivalence ratio values were adjusted by varying the pyrolysis oil feeding rate. The average gasification temperature was calculated from temperatures measured at mid and bottom part of the gasifier during the experiments.

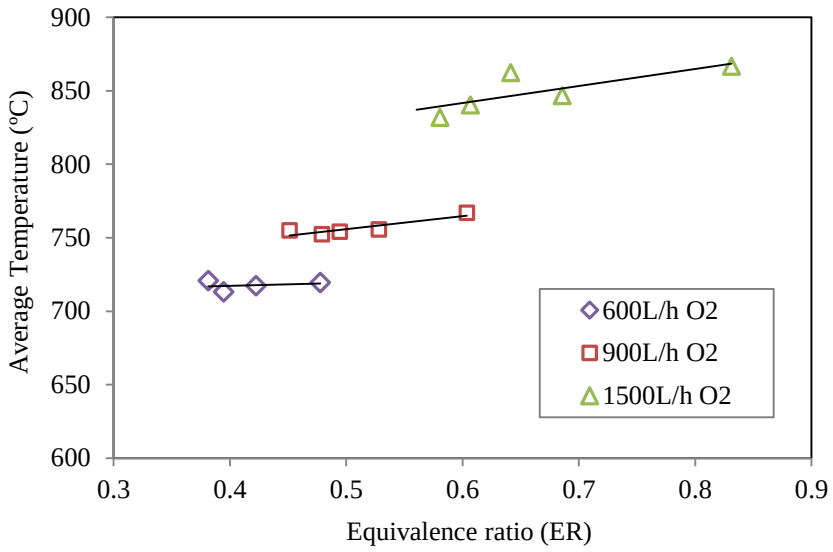

Figure 7–4: Gasification average temperatures at different oxygen flow rates and equivalence ratio

It is clear from Figure 7–4 that gasification temperature increased slightly but steadily with the equivalence ratio. The increase in gasification temperature at higher equivalence ratio is expected considering the system's shifts closer to the stoichiometric combustion ratio that enhances exothermic oxidation reactions of the pyrolysis oil thus releasing more heat to the system. It is interesting to note that at constant equivalence ratio, the average temperature measured during gasification increased rapidly when the oxygen gas flow rate was increased from 600 L/h to 1500 L/h; indicating changes on the overall feeding flow rates (both oxygen and pyrolysis oil) also have significant impact on gasification temperature.

Based on the above observations, further analysis was performed to separately examine effect of pyrolysis oil and oxygen gas feeding rates on the gasification temperature. The results from this analysis are shown in Figure 7–5.

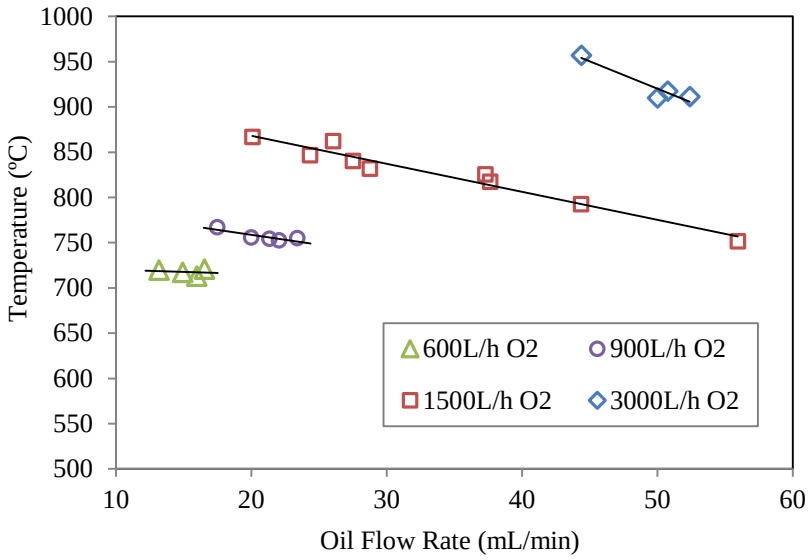

Figure 7–5: Effects of pyrolysis oil flow rate and oxygen flow rate on gasification temperature

In these experimental runs, pyrolysis oil flow rates were changed between 10 mL/min and 60 mL/min, and oxygen feed flow rates were varied between 600 L/h and 3000 L/h. As observed in Figure 7–5, increase in pyrolysis oil flow rate decreased the average gasification temperature, which could be explained considering more heat is consumed during evaporation of moisture in the oil (endothermic) at higher oil flow rate. It is also noticed that at low oxygen feeding rates (600 L/h and 900 L/h), the average gasification temperature decreased slightly with increase in the pyrolysis oil feeding rate; but at higher oxygen feeding rates (1500 L/h and 3000 L/h), the gasification temperature deceased more noticeably with pyrolysis oil feeding rate.

However at a constant pyrolysis oil flow rate, it is clear that the gasification temperature increased dramatically with the oxygen feeding rate, therefore, confirms the more dominant effect of oxygen flow rate on gasification temperature in comparison with the effect of pyrolysis oil flow rate.

7.2.3.2 Effects of pyrolysis oil and oxygen flow rates on producer gas flow rate

In gasification, the amount of producer gas generated is an important parameter to quantify the gasification performance. In this study, information on producer gas flow rate was presented in dry basis or water vapour free gas flow. Figure 7–*6* shows effects of both pyrolysis oil and oxygen feeding rates on the producer gas flow rate from gasification experiments at oxygen flow rates of 600L/h, 900 L/h and 1500L/h.

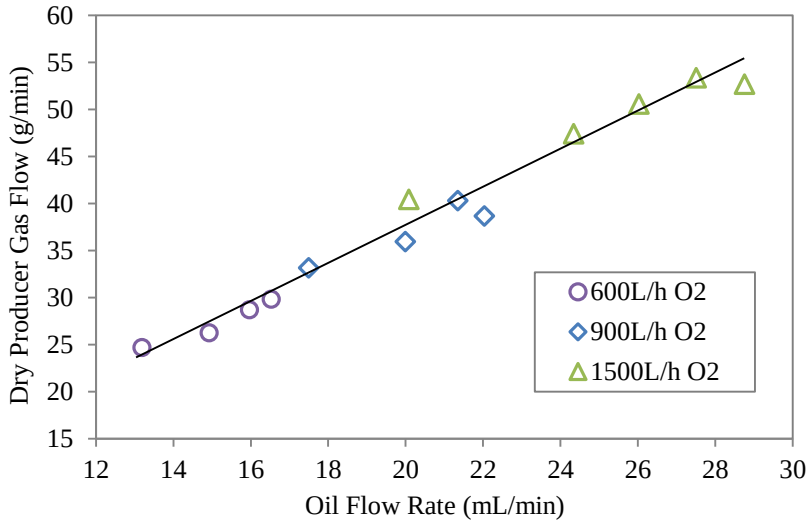

Figure 7–6: Effects of oxygen flow rate and pyrolysis feed flow rate on producer gas flow

From the figure, it is clear that the producer gas flow increased linearly with the oil flow rate; which is believed to be due to more oil available for conversion into producer gas during the gasification. Effects of oxygen flow rate on the producer gas, on the other hand, were found to be less important considering minor changes on the product flow as the oxygen flow rate was increased from 600 L/h to 900 L/h and 1500 L/h. The more dominant effect of pyrolysis oil on producer gas flow rate, compared to oxygen, is relevant considering the oxygen gas supplied into the system was consumed completely for partial oxidation reactions, making decomposition and devolatilization of pyrolysis oil as the primary source of producer gas in gasification.

7.2.3.3 Effects of equivalence ratio on dry producer gas flow rate

Figure 7–7 shows effects of equivalence ratio on dry producer gas flow rate during gasification at various oxygen feeding rates (600, 900, 1500 L/h). At a given equivalence ratio, producer gas flow rate increased with oxygen flow rates, while during constant oxygen feeding rate producer gas yield decreased with the equivalence ratio. It is interesting to find that at the same equivalence ratio, the producer gas flow rates from gasification at 1500L/h oxygen flow rate were almost doubled in comparison with that obtained during 900L/h gasification. Similar finding was observed between gasification at 900L/h and 600L/h oxygen flow rates at a comparable equivalence ratio.

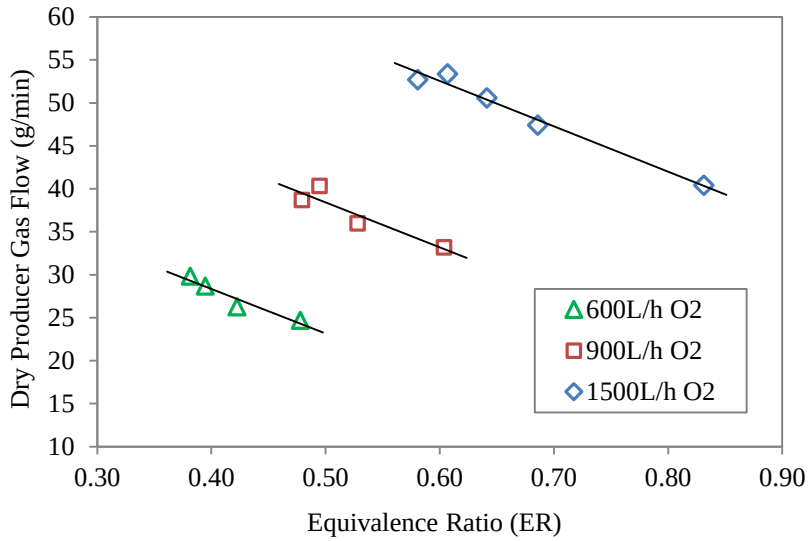

Figure 7–7: Total dry producer gas flow rate from gasification at different oxygen flow rates

Although the graph literally shows significant rises of dry producer gas yield when the oxygen gas flow rate was increased from 600L/h to 1500L/h, however, the change was primarily resulted from increase of pyrolysis oil feeding rate at higher oxygen flow rates in order to keep the equivalence ratio value constant during gasification. The corresponding changes of pyrolysis flow rates at different equivalence ratios and oxygen flow rates are shown in Figure 7–8 to highlight this relationship.

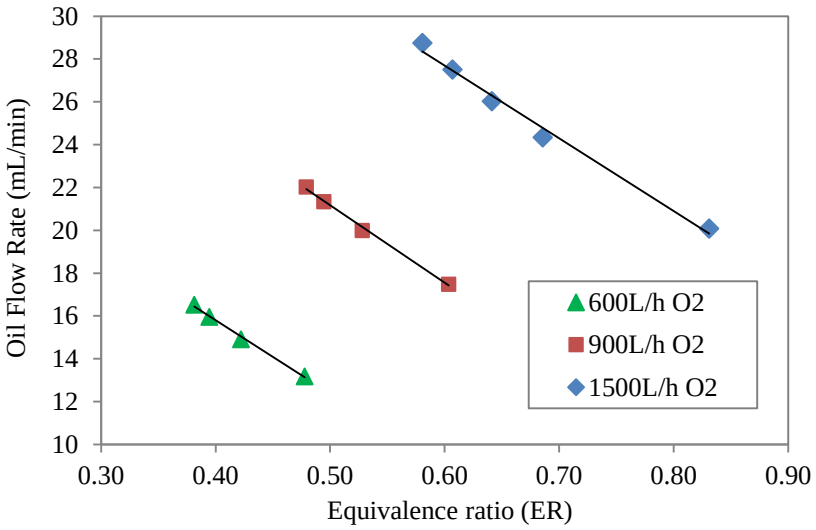

Figure 7–8: Relationship between equivalence ratio and oil flow rates during gasification at 600L/h, 900L/h and 1500L/h oxygen flow rates

While this result re-emphasizes the strong influence of pyrolysis oil flow rate on dry producer gas flow rate as previously discussed in Section 7.2.3.2, it also proves the advantage of conducting gasification at high oxygen flow rates since higher producer gas flow rates are generated compared to that at lower oxygen flow rate, when a constant equivalence ratio is considered. This is particularly useful when gasification is aimed to be operated at a specific equivalence ratio value, for example when the optimum equivalence ratio is known so the total amount of producer gas flow rate produced at this point could be maximized.

7.2.3.4 Effects of equivalence ratio on dry producer gas yield at constant oxygen flow rate

In order to obtain fair comparisons between gasification at different pyrolysis oil flow rates, producer gas yield is presented as ratio between the flow of dry producer gas and the flow of pyrolysis oil (g_{gas}/g_{oil}). The effect of equivalence ratio on the dry producer gas yield was examined and results obtained during gasification at oxygen flow rate of 900 L/h are presented in Figure 7–9. It is clearly observed from the figure that dry producer gas yield increased initially with the equivalence ratio up to the critical value of 0.3. However with further increase of the equivalence ratio after this critical value, the producer gas yield appears to decrease gradually.

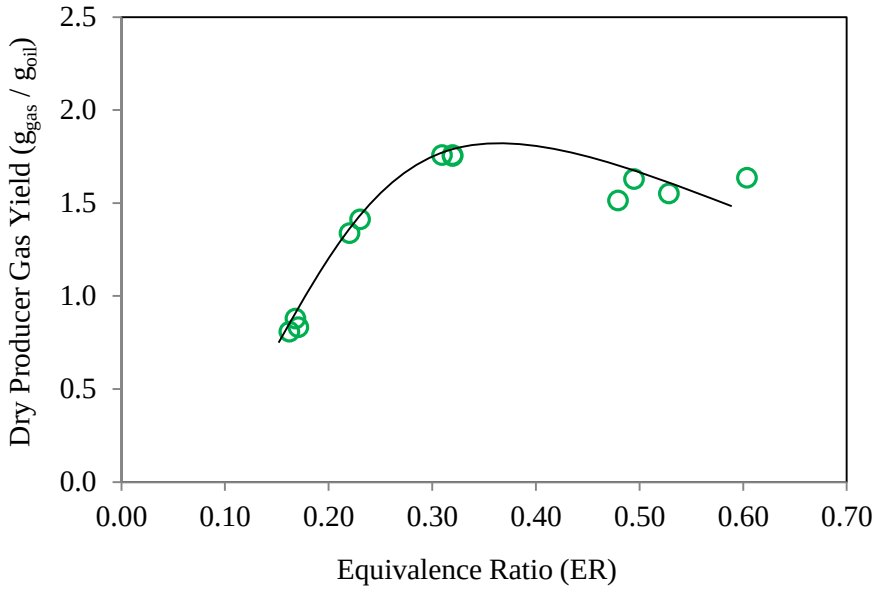

Figure 7–9: Effect of equivalence ratio on the total dry producer gas yield at 900L/h of oxygen flow rate

The increasing dry producer gas yield at equivalence ratio before the critical ER could be explained by considering improvements in pyrolysis oil conversion into producer gas as a result of better spray

characteristics at higher equivalence ratio. At constant oxygen flow rate of 900 L/h, increase of equivalence ratio from 0.1 to 0.6 in Figure 7–9 was obtained by decreasing pyrolysis oil feeding rate into the system.

For characterizing the pyrolysis oil spray, the gas-to-fuel ratio (GFR) is the most influencing factor which in this case defines the ratio of oxygen gas to pyrolysis oil entering the system. GFR is a standard term commonly used in combustion application to describe the ratio between air and liquid fuel in a system. It is usually used to determine whether a combustion mixture is 'rich' or 'lean' by comparison with the stoichiometric (GFR_{stoich}). In applications where twin-fluid external mix atomizer are used, gas-to-fuel ratio may also be used for a different emphasis where it also represents relative severity of collisions impacts between atomizing gas (oxygen) and liquid (pyrolysis oil), therefore are closely related to atomization performance. GFR is directly proportional to equivalence ratio values in which their relationship can be written in the following form:

$$\underset{Ratio}{Equivalence}\ (ER) = \frac{GFR_{actual}}{GFR_{stioch}}$$

In order to understand pyrolysis oil atomization performance at different GFR (hence equivalence ratio) in the entrained flow gasifier, separate experiments were conducted using the same atomizer to spray the pyrolysis oil at room temperature. The setup consists of an enclosed spray chamber, with the front and back walls made of clear Perspex material to provide good light penetration for observation and sample collection. In these experiments, air was used to represent the oxygen gas during atomization considering oxygen gas is a highly reactive reactant.

Pyrolysis oil was atomized at various pyrolysis oil and atomizing gas flow combinations to generate spray at various GFR values. Spray images were captured using Mega Speed MS50K high speed camera which capable of capturing at least 1068 frames per second, thus freezes any objects in motion for highly accurate analysis. The images were then analysed using Image-J software to determine the resulted spray characteristics. Examples of pyrolysis oil spray images as captured from the cold spray chamber for GFR values of 169 and 276 are shown in Figure 7–10.

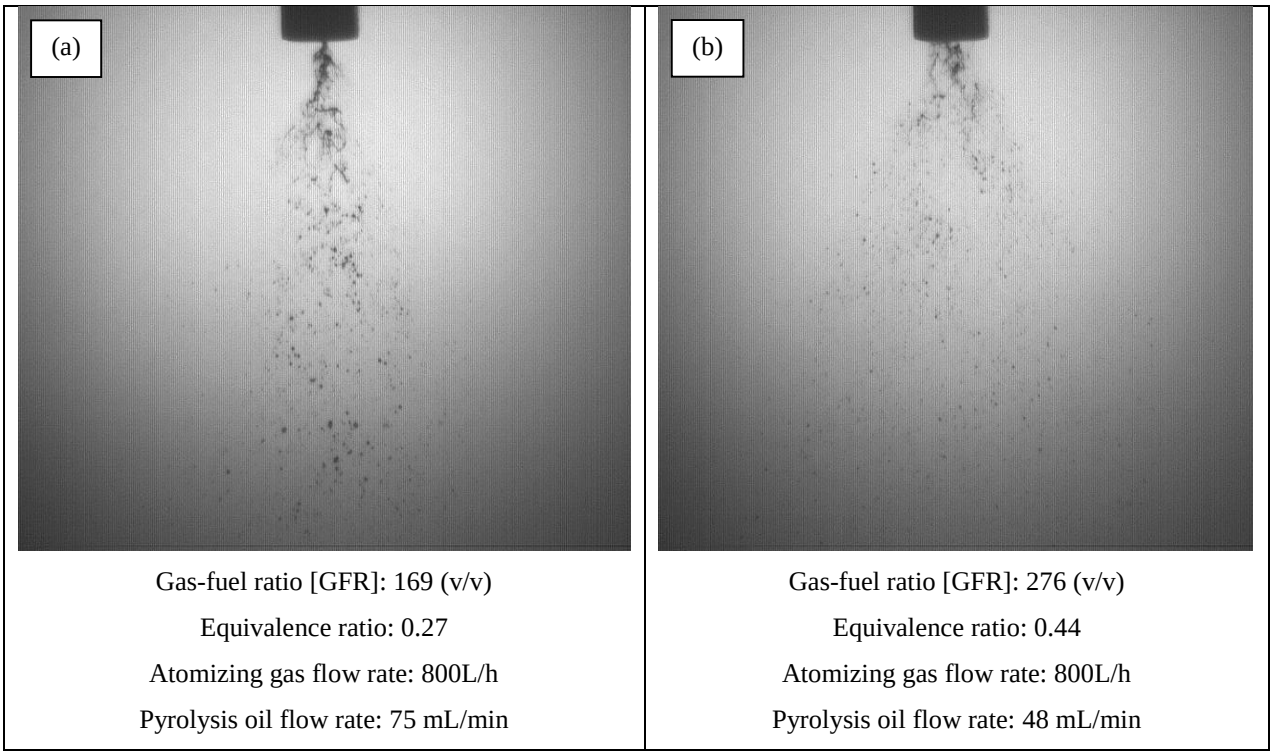

Figure 7–10: Improvements of pyrolysis oil spray characteristics at constant atomizing gas flow rate but decreasing oil flow rate (increasing GFR values)

From Figure 7–10 it is clear that at higher GFR value, the spray droplets are more uniform, finer and better distributed in comparison to that produced at lower GFR. This confirms that in the entrained flow gasifier, higher GFR hence equivalence ratio improves the oil spray characteristics thus enhances mass and heat transfers between oxygen and oil droplets. Therefore, reaction kinetics increased and more gas product is generated up to a certain value of equivalence ratio. In addition, decline of pyrolysis oil flow rate at higher equivalence ratio also lead to production of smaller producer gas flow rate hence giving the process a longer residence time. Improvements of reaction kinetics and residence time combined, enhanced conversions of the spray droplets into producer gas hence increasing the gas yield as observed when the equivalence ratio increased from 0.1 to 0.3.

The types of chemical reactions involved during gasification also contribute to the gas yield trend shown in Figure 7–9. Pyrolysis oil conversion into producer gas takes place following a complex series of chemical reactions, while kinetics of each reaction may be affected in different ways with the changes of the operation conditions. At equivalence ratio below 0.3 in particular, considering the small amount of oxygen present in the system, non-oxidation reactions are expected to be highly dominant. In fact amongst all the possible non-oxidation reactions, Water Gas Shift and Steam Reforming reactions are expected to dominate during gasification at low equivalence ratio. This means that as non-oxidation

reactions advance at higher equivalence ratio due to improved oil-gas conversion, steam is rapidly consumed to generate various gas products hence increasing the total dry gas yield produced by the system [38-42].

Water-gas shift:

$CO + H_2O \leftrightarrow CO_2 + H_2$ Reaction 1

Steam/methane reforming

$CH_4 + H_2O \leftrightarrow CO + 3H_2$ Reaction 2

$CH_4 + CO_2 \leftrightarrow 2CO + 2H_2$ Reaction 3

Char-steam reforming:

$C + H_2O \leftrightarrow CO + H_2$ Reaction 4

$C + 2H_2O \leftrightarrow CO_2 + 2H_2$ Reaction 5

The dry producer gas yield increased with the equivalence ratio until it reached the critical ER value at 0.3, after which effects of oxidation reactions become more dominant and the gas yield decreased with further increase in the equivalence ratio. With equivalence ratio increasing above 0.3, the rates of H_2O and CO_2 production from oxidation reactions were higher than those of their consumptions by non-oxidation reactions. As a consequence, H_2O production increased while the total dry producer gas yield decreased consistently with equivalence ratio. In this work, the increase of H_2O in the product was clearly observed from formation of more condensate drops in the sampling probe as the equivalence ratio increased closer to equivalence ratio of 1 (stoichiometric combustion). In addition to that, decline of pyrolysis oil feeding rate at higher equivalence ratio also reduced the amount of reactant in the system hence limiting the amount of gas yield that could be generated during gasification operation.

From the above discussion, it is clear that gas yield is strongly affected by the pyrolysis spray characteristics, the residence time and the types of reactions involved during gasification. This finding can be used to help derive the optimum condition for an entrained flow gasification operation. In the case of gasification at 900 L/h oxygen flow rate, as presented in this section, the critical ER value occurred at 0.3. The critical ER value represents the best combination of residence time and reaction kinetics that promotes balance between oxidation and non-oxidation reactions during gasification operation to produce the highest gas yield.

7.2.3.5 Comparison between experimentally measured and model predicted dry producer gas yield

Using the equilibrium model developed in this study, theoretical dry gas yields when gasification was assumed at equilibrium state were also predicted. Results from the model prediction were used to illustrate the trend that should be expected if the system was at equilibrium, in comparison to that measured from gasification experiments.

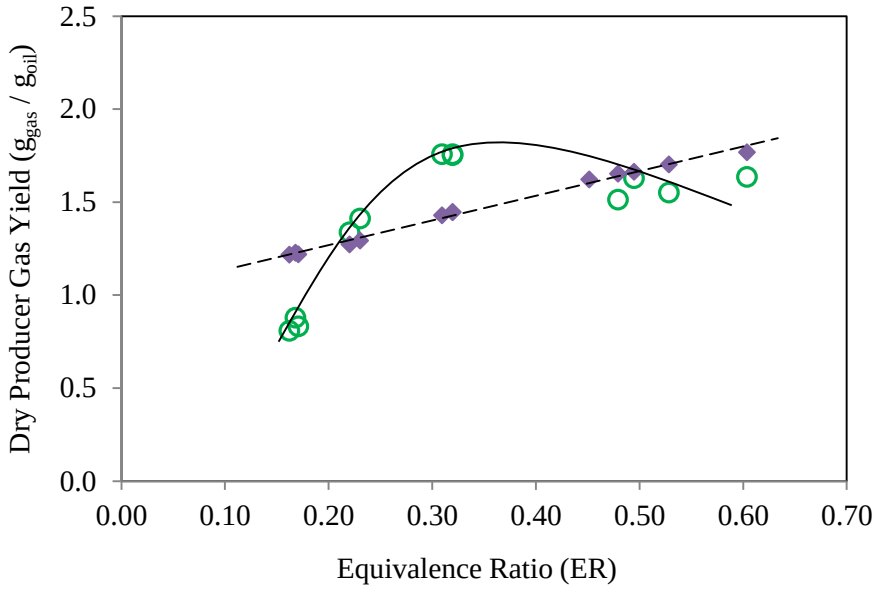

Figure 7–11: Effect of equivalence ratio on the total dry producer gas yield at 900 L/h of oxygen flow rate as measured experimentally (○) and predicted at equilibrium (◆)

As shown in Figure 7–11, producer gas yield at equilibrium is expected to increase linearly with equivalence ratio as a result of increase in gasification temperature at higher equivalence ratio. When comparison was made between the experimental gas yield and that predicted at equilibrium at low equivalence ratio, the experimental gas yield values were found to be smaller than that at equilibrium. Nonetheless, the experimental values increases more rapidly with further increase in equivalence ratio and eventually exceeds the equilibrium. This condition could be explained by taking into account production of more gas species and less water in the product during the gasification experiment, in comparison to that produced when the system is at equilibrium state.

Results from this comparison highlights the advantages of conducting gasification at the critical ER so maximum gas yield could be obtained during the gasification run.

7.2.4 Conclusion

In this work, a pilot scale entrained flow gasification system has been developed and tested for biomass pyrolysis oil. Then influences of pyrolysis oil and oxygen gas feeding rates on gasification temperature, producer gas flow rates and gas yield were investigated. Key findings from this work could be summarized as follows:

i. Gasification temperature is greatly influenced by flow rates of pyrolysis oil and oxygen gas feed into the system during operation. During gasification at constant oxygen feeding rate, increase of pyrolysis oil flow rate decreases gasification temperature due to more heat is consumed during evaporation of moisture in the oil. On the other hand, addition of oxygen into the system enhances exothermic oxidative reactions of pyrolysis oil that releases more heat into the system thus increases the gasification temperature.

ii. Changes in pyrolysis oil flow rate has more dominant influence on dry producer gas flow rate (g/min) in comparison to that caused by oxygen gas. In this work, increase in pyrolysis oil flow rate was shown to cause consistent increase of dry producer gas flow rate as a result of more pyrolysis oil converting into gas products during gasification.

iii. During gasification at constant equivalence ratio, higher oxygen gas feeding rate is desirable since this condition rapidly increases the gasification temperature while also generates larger producer gas flow rate in comparison to that at lower oxygen gas flow. The increase of producer gas flow rates during gasification at higher oxygen flow rate mainly results from increased pyrolysis oil feeding into the system in order to keep the equivalence ratio constant.

iv. During gasification at constant oxygen flow rate, there is a critical equivalence ratio value that gives the highest producer gas yield (g_{gas}/g_{oil}). This condition represents the best combination of residence time and reaction kinetics that promote good pyrolysis oil conversion as well as balance between oxidation and non-oxidation reactions during the gasification operation.

7.2.5 Acknowledgements

This work was funded by the Ministry of Business, Innovation and Employment New Zealand and Ministry of Higher Education Malaysia. The authors would like to thank the sponsors, Alternative Energy Solutions (AES) Ltd. for the pyrolysis oil supplies and technical staffs in the University of Canterbury, New Zealand for their support.

7.2.6 References

1. Qin, K., et al., *High-temperature entrained flow gasification of biomass.* Fuel, 2012. **93**(0): p. 589-600.
2. Xiao, R., et al., *Pyrolysis pretreatment of biomass for entrained-flow gasification.* Applied Energy, 2010. **87**(1): p. 149-155.
3. Carlsson, P., et al., *Experimental investigation of an industrial scale black liquor gasifier. 1. The effect of reactor operation parameters on product gas composition.* Fuel, 2010. **89**(12): p. 4025-4034.
4. Zhou, J., et al., *Biomass–oxygen gasification in a high-temperature entrained-flow gasifier.* Biotechnology Advances, 2009. **27**(5): p. 606-611.
5. Henrich, E., N. Dahmen, and E. Dinjus, *Cost estimate for biosynfuel production via biosyncrude gasification.* Biofuels, Bioproducts and Biorefining, 2009. **3**(1): p. 28-41.
6. Raffelt, K., et al., *The BTL2 process of biomass utilization entrained-flow gasification of pyrolyzed biomass slurries.* Applied Biochemistry and Biotechnology, 2006. **129**(1-3): p. 153-64.
7. Whitty, K., *Investigation of Pressurized Entrained-Flow Kraft Black Liquor Gasification in an Industrially Relevant Environment - Annual Topical Report - Year 1*. 2006, University of Utah.
8. Whitty, K., R. Backman, and M. Hupa, *Influence of pressure on pyrolysis of black liquor: 1. Swelling.* Bioresource Technology, 2008. **99**(3): p. 663-670.
9. Kankkunen, A., et al., *Spraying characteristics of mixed black liquor - Two different spraying cases.* The Swedish and Finnish National Committees of the International Flame Research Foundation.
10. Whitty, K., et al., *Influence of pressure on pyrolysis of black liquor: 2. Char yields and component release.* Bioresource Technology, 2008. **99**(3): p. 671-679.
11. Higman, C. and M. van der Burgt, *Chapter 5 - Gasification Processes*, in *Gasification (Second Edition)*. 2008, Gulf Professional Publishing: Burlington. p. 91-191.
12. Lee, S.H., et al., *Gasification characteristics of coke and mixture with coal in an entrained-flow gasifier.* Energy, 2010. **35**(8): p. 3239-3244.
13. Murthy, B.N., et al., *Petroleum coke gasification: A review.* Canadian Journal of Chemical Engineering, 2013.
14. Kirkels, A.F. and G.P.J. Verbong, *Biomass gasification: Still promising? A 30-year global overview.* Renewable and Sustainable Energy Reviews, 2011. **15**(1): p. 471-481.
15. Van der Drift, A., et al. (2004) *Entrained flow gasification of biomass*.

16. Abdullah, H., et al., *Bioslurry as a Fuel. 3. Fuel and Rheological Properties of Bioslurry Prepared from the Bio-oil and Biochar of Mallee Biomass Fast Pyrolysis.* Energy & Fuels, 2010. **24**(10): p. 5669-5676.
17. Svoboda, K., et al., *Pretreatment and feeding of biomass for pressurized entrained flow gasification.* Fuel Processing Technology, 2009. **90**(5): p. 629-635.
18. Samiran, N.A., et al., *Progress in biomass gasification technique – With focus on Malaysian palm biomass for syngas production.* Renewable and Sustainable Energy Reviews, 2016. **62**: p. 1047-1062.
19. Abdullah, H. and H. Wu, *Bioslurry as a Fuel. 4. Preparation of Bioslurry Fuels from Biochar and the Bio-oil-Rich Fractions after Bio-oil/Biodiesel Extraction.* Energy & Fuels, 2011. **25**(4): p. 1759-1771.
20. Manzer, L. *Recent developments in the conversion of biomass to renewable fuels and chemicals*. 2009.
21. Johansson, D., P.T. Franck, and T. Berntsson, *Hydrogen production from biomass gasification in the oil refining industry - A system analysis.* Energy, 2012. **38**(1): p. 212-227.
22. Chhiti, Y., *Non catalytic steam gasification of wood bio-oil*. 2011.
23. Dahmen, N., et al., *The bioliq® bioslurry gasification process for the production of biosynfuels, organic chemicals, and energy*. Energy, Sustainability and Society, 2012. **2**(1): p. 1-44.
24. Santo, U., et al., *Conversion of Biomass Based Slurry in an Entrained Flow Gasifier.* Chemical Engineering & Technology, 2007. **30**(7): p. 967-969.
25. Kolb, T., T. Jakobs, and N. Zarzalis, *Syngas from biomass-based slurry entrained flow gasification*, in *10th Conference on Energy for a clean Environment*. 2009.
26. Kolb, T., et al., *Production of Syngas from Biomass-Based Slurry in an Entrained-Flow Gasifier.* 2009.
27. Henrich, E. and F. Weirich, *Pressurized Entrained Flow Gasifiers for Biomass.* Environmental Engineering Science, 2004. **21**(1): p. 53-64.
28. Raffelt, K., E. Henrich, and J. Steinhardt. *Production and properties of slurries from biomass for biomass gasification*. in *Herstellung und eigenschaften von slurries aus biomasse für die biomassevergasung*. 2004.
29. Trippe, F., et al., *Techno-economic assessment of gasification as a process step within biomass-to-liquid (BtL) fuel and chemicals production.* Fuel Processing Technology, 2011. **92**(11): p. 2169-2184.
30. Chhiti, Y., et al., *Wood Bio-Oil Noncatalytic Gasification: Influence of Temperature, Dilution by an Alcohol and Ash Content.* Energy & Fuels, 2010. **25**(1): p. 345-351.

31. Chhiti, Y., et al., *Thermal decomposition of bio-oil: Focus on the products yields under different pyrolysis conditions.* Fuel, 2012. **102**(0): p. 274-281.
32. Creager, N. and R.C. Brown. *High pressure, oxygen blown entrained-flow gasification of bio-oil*. 2012.
33. Marda, J.R., et al., *Non-catalytic partial oxidation of bio-oil to synthesis gas for distributed hydrogen production.* International Journal of Hydrogen Energy, 2009. **34**(20): p. 8519-8534.
34. Chhiti, Y., M. Peyrot, and S. Salvador, *Soot formation and oxidation during bio-oil gasification: experiments and modeling*. Journal of Energy Chemistry, 2013. **22**(5): p. 701-709.
35. Chhiti, Y. and S. Salvador, *Gasification of Wood Bio-Oil*. Gasification for Practical Applications. 2012.
36. Abdoulmoumine, N., A. Kulkarni, and S. Adhikari, *Effects of Temperature and Equivalence Ratio on Pine Syngas Primary Gases and Contaminants in a Bench-Scale Fluidized Bed Gasifier.* Industrial & Engineering Chemistry Research, 2014. **53**(14): p. 5767-5777.
37. Williams, A., *Combustion of Liquid Fuel Sprays*. 1990, London: Butterworth & Co (Publishers) Ltd.
38. Ricketts, B., et al. *Technology status review of waste/biomass co-gasification with coal*. in *IChemE Fifth European Gasification Conference*. 2002.
39. Higman, C. and M. van der Burgt, *Chapter 2 - The Thermodynamics of Gasification*, in *Gasification (Second Edition)*, C. Higman and M.v.d. Burgt, Editors. 2008, Gulf Professional Publishing: Burlington. p. 11-31.
40. Kunze, C. and H. Spliethoff, *Modelling, comparison and operation experiences of entrained flow gasifier.* Energy Conversion and Management, 2011. **52**(5): p. 2135-2141.
41. Hernández, J.J., et al., *Effect of steam content in the air–steam flow on biomass entrained flow gasification.* Fuel Processing Technology, 2012. **99**(0): p. 43-55.
42. Basu, P., *Chapter 1 - Introduction*, in *Biomass Gasification and Pyrolysis*, P. Basu, Editor. 2010, Academic Press: Boston. p. 1-25.

7.3 Non-Slagging Entrained Flow Gasification of Biomass Pyrolysis Oil: Influence of Equivalence Ratio on Producer Gas Composition and Gasification Thermal Efficiency during Gasification at Constant Oxygen Feeding Rate

This section will be submitted as a research paper in the international journal Biomass and Bioenergy

Abstract:

An entrained flow gasification system was developed in this work to gasify biomass pyrolysis oil at atmospheric pressure and gasification temperature of up to 1100^{o}C. The pyrolysis oil was derived from New Zealand radiata pine wood chips via fast pyrolysis process. The oil was feed into the system through an external mix twin-fluid atomizer which capable of producing fine spray droplets after impact with oxygen gas (gasification agent). This article mainly investigates effects of equivalence ratio on producer gas composition during gasification at constant oxygen flow rate. The results showed unique relationship between equivalence ratio and producer gas composition where instead of giving linear relationships as usually reported in the literature, H_2, CO and CO_2 concentrations showed parabolic trends with presence of maximum and minimum points as the equivalence ratio continued to increase. Comparisons between experimental producer gas compositions and that expected at equilibrium state were also performed. Experimental deviations from equilibrium were found to be noticeably large when comparisons were made at low equivalence ratio; however the deviation declined dramatically as the equivalence ratio progressed towards the critical ER value. After this point, experimental data showed consistent trends compared to that predicted by the equilibrium model. Investigation on the process thermal efficiency at different equivalence ratio revealed a parabolic relationship, with the maximum thermal efficiency occurred at the critical ER. This article ultimately demonstrated advantages of conducting gasification at the critical ER value in order to maximize the process efficiency as well as to obtain the highest quality producer gas during constant oxygen flow rate operations.

Keywords: Entrained flow gasification, oxygen, biomass pyrolysis oil, equivalence ratio, equilibrium

7.3.1 Introduction

Entrained flow gasification has a great potential in the future as one of the efficient technologies to convert renewable biomass into gaseous fuel. This technology has been used extensively in coal and black liquor gasification processes as well as in petrochemical refineries [1-8]; hence knowledge and experience are available in its design and operation. Entrained flow gasifier is capable of delivering near 100% carbon conversion at short residence times [9-11]. In addition, the producer gas from the entrained flow gasification has low tar contents [11] mainly as a result of its high operation temperatures in comparison with other gasification technologies.

However, when processing biomass as the feedstock, the use of entrained flow gasification is challenging due to its strict feedstock size requirement. In order to obtain high conversion at short residence time, the feedstock needs to be pulverized into fine particles of size below 0.1 mm [12] so that high reaction rate could be achieved. While this requirement is not an issue for coal, solid biomass grinding into particles with uniform size is difficult due to its fibrous structure [13]. In addition, energy demand for grinding solid biomass into fine particles is also high [14], making the use of solid biomass in entrained flow gasification system less practical and economically less viable.

To solve the strict feedstock requirement for solid biomass, biomass can be first transformed into liquid through fast pyrolysis process. Fast pyrolysis is a thermal decomposition process where solid feedstock is decomposed into lighter compounds in the form of liquid, char and non-condensable gaseous products. The liquid is the major product from fast pyrolysis (up to 75 wt% yield) and is known as ‘pyrolysis oil’ or ‘bio-oil’.

The pyrolysis oil can then be fed to an entrained flow gasifier to produce hydrogen-rich gas product, called producer gas. Feeding pyrolysis oil into the entrained flow gasification system is advantageous because the strict size requirement could easily be fulfilled with liquid atomization [15, 16], in which droplets size as small as 10μm could be obtained. In addition, liquid feeding is also more convenient for pressurized gasification system. More importantly, costs for transportation and storage of the pyrolysis oil can be significantly reduced because of its increased density and liquid form [14, 16].

Studies have been reported on entrained flow gasification of biomass pyrolysis oil with focus on exploring the operating conditions and examining feasibility of this technology [17-22]. In some studies steam was added into the system as gasification agent to enhance H_2 yield [17, 20, 22]. In these studies, effects of gasification temperature, droplet heating rates, oil ash content and oil dilution with ethanol on gasification performance have been investigated. The gasification performance includes carbon conversion, products distributions, producer gas compositions, gas yield and soot formation.

Limited information has been found in the literature on entrained flow gasification of biomass pyrolysis oil with oxygen gas as gasification agent. Creager et al. [21] conducted experiments on entrained flow gasification of pyrolysis oil at 850^{o}C and operating pressures of 1.01 bar and 6.9 bar, while the equivalence ratio was fixed at 0.25. Equivalence ratio (ER) is the ratio of oxygen supplied to the system during gasification over that required for theoretical stoichiometric combustion [23], therefore ER: 1 represents sufficient oxygen for stoichiometric combustion while ER: 0 represents no supply of oxygen into the system. The pyrolysis oil was fed into the system through a twin-fluid atomizer. In this study effects of pressure and pyrolysis oil atomization on gasification products were investigated. The results showed that the atomization performance had substantial influence on the producer gas compositions. In addition, the H_2 content was increased with operation pressure, however, concentrations of other gas components (CO, CO_2, CH_4, C_2H_4 and C_2H_6) decreased with increase in the operation pressure.

Marda et al. [19] also investigated pyrolysis oil gasification with oxygen as gasification agent but at operation temperature varied between 625 to 850^{o}C. In this work, the oil was fed into the system with an ultrasonic nozzle. Effects of temperatures on carbon conversion and product gas components yields at equivalence ratio up to 0.35 were investigated. The results showed high carbon conversion could be achieved at temperature as low as 700^{o}C as a result of enhanced steam reforming and carbon gasification reactions due to high steam concentrations in the system. The findings also showed more dominant influence of equivalence ratio on carbon conversion in comparison with the influence of gasification temperature.

Chhiti et al. [20], on the other hand, conducted experiments on oxidative entrained flow gasification of pyrolysis oil at higher temperature (1000-1400^{o}C). In their study, pyrolysis oil was introduced into the system using a pressure jet atomizer with equivalence ratio of up to 0.5. The results showed effects of temperature and equivalence ratio on producer gas composition, which have similar trends as reported by Marda et al [19]. In addition, Chhiti et al. [20] also showed that the soot content in the producer gas was decreased as the equivalence ratio increased.

The limited information on oxidative entrained flow gasification of biomass pyrolysis oil cannot confirm if this gasification technology is practically feasible. In addition, the technical issues and advantages of this technology have not been fully explored. The aim of this study was to develop a new entrained flow gasification system for gasifying biomass pyrolysis oil at low temperatures (less than 1000°C) and effects of operation conditions on gasification performance were to be investigated. In this article, influences of equivalence ratio on the resulted producer gas compositions were experimentally investigated. The

producer gas compositions were then compared with those predicted at thermodynamically equilibrium state so experimental deviations from theoretical equilibrium state could be determined.

7.3.2 Materials and Methods

7.3.2.1 Feedstock

The pyrolysis oil used in the experiments was produced from radiata pine wood chips through a fast pyrolysis reactor by a local company, Alternative Energy Solutions (AES) Ltd. Measurements of the oil properties were conducted periodically so changes of the oil properties due to ageing were recorded over time. Results from pyrolysis oil properties measurements over a period of 7 weeks have been summarized in the previous paper (Section 7.2) in Table 7-2.

7.3.2.2 Entrained flow gasification system

The entrained flow gasifier developed in this study is capable for gasification or combustion of liquid fuel at atmospheric pressure and maximum operating temperature of 1100^{o}C. Two independent LPG burners are located at the top and bottom sections of the gasifier to pre-heat the system to the desired start-up temperature, prior to any gasification run. Pyrolysis oil and oxygen gas feeding into the system are made through a twin-fluid atomizer which capable of producing fine spray droplets in a flat spray pattern. The atomizer uses an 'external mix' atomization approach where the liquid and gas streams flow separately and only come into contact when both streams exit the nozzle.

In comparison to the more commonly used internal mixing atomizer, the external mixing atomization offers a much safer operation for pyrolysis oil and oxygen gas by lowering risk of flame flashback or internal combustion within the atomizer at high temperature [24]. In addition, the use of external mix atomizer also allows for independent adjustments of pyrolysis oil and oxygen flow rates during atomization, thus enables better control of the pyrolysis oil spray characteristics by alteration of only one parameter at a time. The atomizer is integrated with a specially designed cooling jacket so it remains at low temperature to prevent pyrolysis oil polymerization that could cause plugging of the oil feeding system.

Descriptions of the entrained flow gasification system and the gasifier design could be found in more detailed in the previous paper (Section 7.2).

7.3.2.3 Experimental procedures

The start-up temperature of the gasifier reactor prior to any gasification run was set at 750^{o}C. When the system stabilized at this temperature, pyrolysis oil was fed into the system at flow rates up to 70 mL/min, followed by oxygen gas. In this investigation, the flow rates of oxygen gas feed into system was fixed at either 900L/h or 1500 L/h. Equivalence ratio values were calculated based on the flow rates of pyrolysis oil and oxygen gas entering the system.

Once the system stabilized, samples of producer gas and tar were taken from the sampling line for analysis. In all runs, the system was allowed to stabilize for at least 20-30 minutes before the first sample was taken for analysis. The interval between two consecutive samplings was 10-15 minutes to minimize inconsistencies. A more comprehensive description of the experimental procedures for this investigation has been given in the previous paper in Section 7.2.2.3.

7.3.2.4 Sampling method and producer gas analysis

Products of gasification exit the system through a port located at the bottom of the gasifier. To avoid condensation of tar, the product line temperature is maintained between 450-600^{o}C throughout the operation. In addition, the length of probe used for product sampling was also designed as short as possible to minimize temperature difference between the system and the sampling setup to minimize error due to tar condensation. In this work, the concentrations of producer gas components produced during gasification was analysed using a Micro-GC. Detailed descriptions of the sampling method adopted in this work as well as information about the producer gas analysis have been given in the previous paper from Section 7.2.2.4 to Section 7.2.2.6.

7.3.2.5 Equilibrium model

In order to have depth understanding of the entrained flow gasification process and to predict the gasification performance, an equilibrium model was developed and solved. The model was developed based on *stoichiometric* approach, where producer gas composition at equilibrium was obtained by minimizing the system's Gibbs free energy based on the main gas species expected in the product, which in this case H_2, CO, CO_2, CH_4, N_2 and H_2O. In this work, Gibbs free energy information from gasification two dominant reactions were used to define the model at equilibrium; which are the Water-Gas Shift reaction and the Steam Reforming reaction [25]. Other information required to define the model are derived from C, H, O and N material balances across the system.

Water gas shift reaction:

$CO + H_2O \leftrightarrow CO_2 + H_2$ ΔH_r = -41 kJ/mol Reaction 1

Steam/methane reforming reaction:

$CH_4 + H_2O \leftrightarrow CO + 3H_2$ ΔH_r = +206 kJ/mol Reaction 2

The equilibrium model was developed in Microsoft Excel spreadsheet by using a built-in Solver Add-Ins that enables efficient iterative calculations to be made. Main assumptions made in the equilibrium model development are summarized as follows:

i. Perfect mixing between all compounds present in the system;
ii. The products have reached equilibrium in the reactor;
iii. No tar is present in the producer gas after gasification;
iv. CH_4 is the only hydrocarbon compound present in the producer gas;
v. No char or other solids remain in the producer gas;
vi. No temperature gradient across the gasifier (uniform gasification temperature)

Figure 7–12 illustrates the inlet and outlet flows of species involved during entrained flow gasification of biomass pyrolysis oil for development of the equilibrium model.

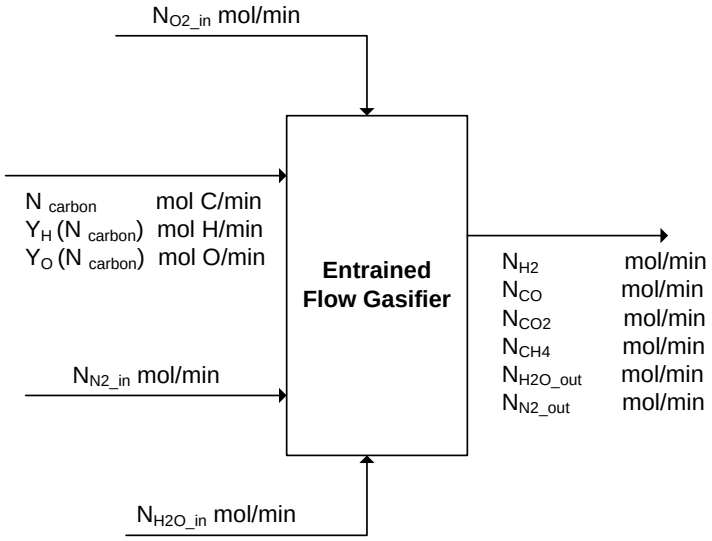

Figure 7–12: Illustration of an equilibrium model for entrained flow gasification system

In Figure 7–12, N_{carbon} is the molar flow rate of carbon (mol C/min) supplied into the gasifier in the form of pyrolysis oil. Y_H is the hydrogen-to-carbon (H:C) molar ratio in pyrolysis oil while Y_O is the oxygen-to-

carbon (O:C) molar ratio in pyrolysis oil. Following that, $Y_H(N_{carbon})$ and $Y_O(N_{carbon})$ are the molar flow rates of hydrogen and oxygen in the pyrolysis oil (mol H/min and mol O/min), respectively, into the system. On the other hand, molar flow rates of other species, *i* entering and exiting the gasifier are represented by N_i (mol/min).

In solving the equilibrium model, six unknowns are required to be determined, which are molar flow rates of H_2, CO, CO_2, CH_4, N_2 and H_2O in producer gas exiting the system. Molar flow rates of four of these species are defined from material balances of C, H, O and N elements involved in the system; while the remaining two unknowns are derived from total Gibbs free energies of the two dominant gasification reactions specified earlier. Step-by-step derivations for all equations used to define this model are given in the coming paragraphs.

Material balances of the four elements involved in this system (C, H, O and N) can be written in the following forms:

Carbon balance:

$$N_{carbon} = N_{CO} + N_{CO2} + N_{CH4}$$

Hydrogen balance:

$$Y_H(N_{carbon}) + 2N_{H2O\_in} = 2N_{H2} + 2N_{H2O\_out} + 4N_{CH4}$$

Oxygen balance:

$$2N_{O2\_in} + Y_O(N_{carbon}) + N_{H2O\_in} = N_{CO} + 2N_{CO2} + N_{H2O\_out}$$

Nitrogen balance:

$$2N_{N2\_in} = 2N_{N2\_out}$$

These equations are transformed into augmented matrix form so they can be manipulated to give four sets of equations, which are used to define molar flow rates of CO_2, CO, H_2 and N_2 exiting the system. The four equations produced after the augmented matrix operations are presented in Equations (1) – (4).

$$N_{CO2} = N_{carbon}(Y_O - 1) + 2N_{O2\_in} + N_{CH4} - N_{H2O\_out} + N_{H2O\_in} \quad \text{Equation 1}$$

$$N_{CO} = N_{carbon}\,(2 - Y_O) - 2N_{CH4} + N_{H2O\_out} - 2N_{O2\_in} - N_{H2O\_in} \quad \text{Equation 2}$$

$$N_{H2} = N_{carbon}\left(\frac{Y_H}{2}\right) - 2N_{CH4} - N_{H2O\_out} + N_{H2O\_in} \quad \text{Equation 3}$$

$$N_{N2\_in} = N_{N2\_out}$$ Equation 4

In these equations, the terms N_{carbon}, N_{O2_in}, N_{N2_in} and N_{H2O_in} are molar flow rates of materials fed into the entrained flow gasification system, hence are known variables. On the other hand, Y_H and Y_O values can be determined from elemental analysis of pyrolysis oil used during the operation. To fully define Equations (1) – (4) the remaining two unknowns (N_{H2O_out} and N_{CH4}) have to be calculated. Derivations of equations used to calculate N_{H2O_out} and N_{CH4} values are presented in the remainder of this section.

At equilibrium state, the relationship between each individual species in producer gas is given by equilibrium constant, *K*. Equilibrium constant calculates molar fractions of reactants and products involved during a reaction, in which, during operations at atmospheric pressure is given by Equation (5):

$$aR_1 + bR_2 \rightarrow cP_1 + dP_2$$

$$K = \sum Y_i^{v_i} = \frac{({P_1}^c)({P_2}^d)}{({R_1}^a)({R_2}^b)}$$ Equation 5

P_1 and P_2 are mole fractions of products of the reaction while R_1 and R_2 are mole fractions of reactants involved in the reaction. On the other hand *a* and *b* are the stoichiometric number of moles of reactants while *c* and *d* are the stoichiometric number of moles of products in the reaction respectively.

Applying Equation (5) to Water Gas Shift and Steam Reforming reactions, separately, the equations were then re-arranged so mole fractions of H_2O and CH_4 in the producer gas could be defined. At this condition, the re-arranged equilibrium constant equations for Water Gas Shift (WGS) and Steam Reforming (SR) reactions can be written as Equation (6) and Equation (7) respectively.

$$Y_{H2O\_out} = \frac{Y_{CO2}\, Y_{H2}}{Y_{CO}\, K_{WGS}}$$ Equation 6

$$Y_{CH4} = \frac{Y_{CO}\, {Y_{H2}}^3}{Y_{H2O}\, K_{SR}}$$ Equation 7

To solve for Y_{H2O} and Y_{CH4}, the equilibrium constant values, *K*, have to be calculated from the total Gibbs free energy of the Water Gas Shift and Steam Reforming reactions. Total Gibbs free energy of reactions at a given operating condition ($\Delta G_{reaction}$) is given by Equation (8).

$$\Delta G_{reaction} = \Delta {G^o}_{reaction} + RT \ln K$$ Equation 8

This equation consists of two parts: (i) Gibbs energy at standard condition (273K and 1 atm); and (ii) additional term to account for deviation of reaction conditions (T and P) from the standard condition. At equilibrium state, however, the Gibbs energy of a reaction ($\Delta G_{reaction}$) is zero thus Equation (8) can be simplified to Equation (9).

$$\ln K = -\frac{\Delta G^{o}_{reaction}}{RT} \qquad \text{Equation 9}$$

According to Equation (9), the Gibbs free energy at standard condition ($\Delta G^{o}_{reaction}$) can be used directly to calculate equilibrium constant, *K*. Equation to calculate $\Delta G^{o}_{reaction}$ is given in Equation (10).

$$\Delta G^{o}_{reaction} = \sum v_i G^{o}_{i,products} - \sum v_i G^{o}_{i,reactants} \qquad \text{Equation 10}$$

In order to solve for $\Delta G^{o}_{reaction}$, stoichiometric number of moles of all components of a reaction (v_i) must be identified. G^{o}_{i} on the other hand represents the standard Gibbs energy of all components of the reaction and are determined based on tabulated values from the literature [26].

Once $\Delta G^{o}_{reaction}$ is calculated, Equation (9) can be solved for Water-Gas Shift and Steam Reforming reactions equilibrium constants, *K* values respectively. Then the *K* values can be used in Equations (6) and (7) to solve for Y_{H2O} and Y_{CH4} values in the producer gas. Using the calculated Y_{H2O} and Y_{CH4} values, the molar flow rates of these two species can be calculated by multiplying species molar fraction values with the total producer gas molar flow rate, $N_{producer\_gas}$.

$$N_{CH4} = Y_{CH4} \times N_{producer\_gas} \qquad \text{Equation 11}$$

$$N_{H2O\_out} = Y_{H2O} \times N_{producer\_gas} \qquad \text{Equation 12}$$

In order to solve all six unknowns (N_{H2} , N_{CO} , N_{CO2} , N_{CH4} , N_{H2O_out} , N_{N2_out}) in the equilibrium model, Equations (1), (2), (3), (4), (6) and (7) are solved simultaneously in Microsoft Excel. This is performed by setting initial guesses for Y_{H2O} and Y_{CH4} values, in which these values are then used to solve for N_{H2} , N_{CO} , N_{CO2} and N_{N2_out} in Equations (1)–(4). Molar flow rates of these components are then re-used to calculate Y_{H2O} and Y_{CH4} values from Equations (6) and (7), but this time using Gibbs free energy information from the system. This calculation cycle occurred repeatedly, up to 10,000 iterations, during which Y_{H2O} and Y_{CH4}values are manipulated until molar flow rates of all six components in the producer gas are in agreement with one other, following relationships given in Equations (1), (2), (3), (4), (6) and (7).

These operations are performed with the aid of Microsoft Excel Solver Add-In for effective iterative calculations. The guessed values of Y_{H2O_out} and Y_{CH4} are repeatedly altered until the error between these values and that calculated using Gibbs free energy are minimized, indicating agreement between all values in the specified equations.

7.3.3 Results and Discussions

7.3.3.1 Effect of equivalence ratio on producer gas composition at constant oxygen flow rate

Figure 7–13 shows producer gas composition as a function of equivalence ratio from gasification at constant oxygen flow rate of 1500 L/h. The gas composition presented in the figure is free of H_2O, He and N_2. Ethylene (C_2H_4) and ethane (C_2H_6) are not included in these figures due to their very low concentrations.

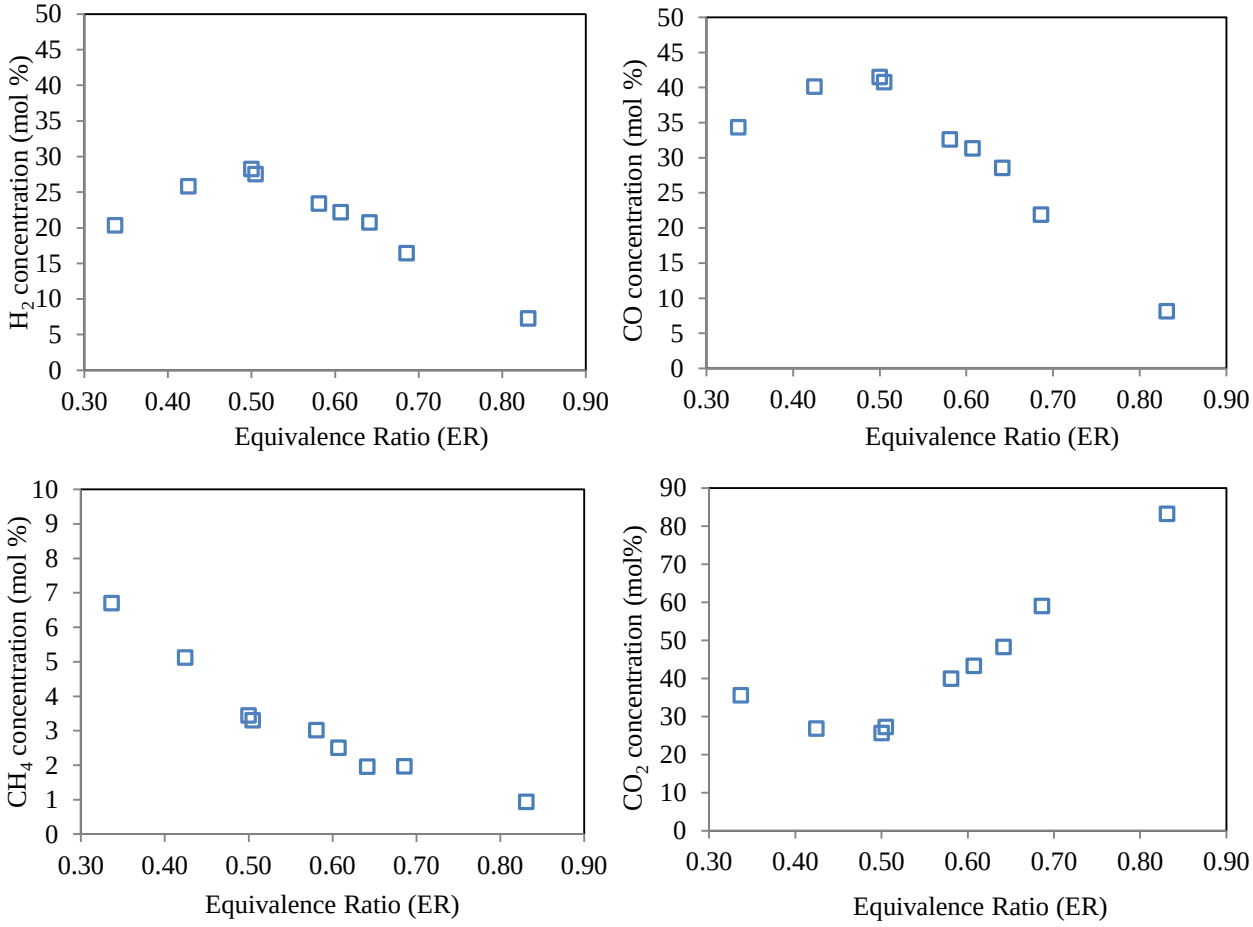

Figure 7–13: Producer gas composition from gasification at 1500 L/h oxygen flow rate

It is interesting to note that the trends of the gaseous species in the producer gas are not in linear relationships with the equivalence ratio as reported in the literature [19, 20]. The concentrations of H_2 and CO increased with the equivalence ratio to a maxima at a critical ER of 0.5 (28% for H_2 and 41% for CO) and then decreased with further increase in the equivalence ratio. However, the opposite trend was observed for CO_2 gas where a minimum value of 26% was found at the critical ER value. With increase in the equivalence ratio from 0.3 to 0.9, the concentration of CH_4 consistently declined from 7% to 1%.

Similar non-linear trends were also found during gasification at oxygen flow rate of 900 L/h, however, the critical ER occurred at equivalence ratio of 0.3. The differences in the equivalence ratios of which the critical ER occurred between gasification at 900 L/h and 1500 L/h oxygen flow rates will be discussed in detailed in the next paper (Section 7.4).

The trends of gas concentration changes with the equivalence ratio in Figure 7–13 can be explained by considering the types of chemical reactions involved in the entrained flow gasification process and the availability of reactants (C, H and O) at different equivalence ratios. Gasification products are strongly influenced by the amount of oxygen gas feed into the system, considering the high selectivity of oxidation reactions of pyrolysis oil and most gasification products such as H_2, CO, CH_4, C_2H_4 and C_2H_6 due to their combustible nature.

To clearly demonstrate the relationship between the types of reactions and producer gas composition, the equivalence ratio range tested in Figure 7–13 was divided into two parts; which are before and after the critical equivalence ratio.

i. Equivalence ratio below the critical ER

During gasification at constant oxygen feeding rate (in this case at 1500 L/h), low equivalence ratio is obtained when the pyrolysis oil feeding rate into the system is high. In this condition insufficient amount oxygen was available in the system to react with the large amount of pyrolysis oil at stoichiometric. This condition resulted in the oxygen gas reacting with only a small fraction of the pyrolysis oil soon after both streams exited the atomizer. Since only a small fraction of pyrolysis oil was involved in oxidation reactions, most of the oil droplets devolatilized and thermally decomposed into gasification products such as H_2, CO, CO_2, H_2O, CH_4 and other light hydrocarbons. Thermal decomposition of pyrolysis oil into lighter compounds could be presented by Reaction (3) [27].

Pyrolysis oil thermal decomposition:

$$C_xH_yO_z \rightarrow C_mH_nO_k + gases\left(H_2, CO, CO_2, CH_4, H_2O, C_xH_y\ etc\right) + C_{residues}$$ Reaction 3

In the gasification process, oil droplets also reacted with steam generated during pyrolysis oil combustion and moisture evaporation. The pyrolysis oil and steam reaction produced CO and H_2 as the product and can be described by the following Reaction (4) [27].

Pyrolysis oil steam gasification:

$$C_xH_yO_z + (x-z)H_2O \rightarrow x\ CO + \left(x - z + {}^{y}/_{2}\right) H_2$$ Reaction 4

Steam gasification and thermal decomposition reactions are classified as non-oxidation reactions since oxygen gas is not a reactant in the reactions. Other non-oxidation reactions that could take place during gasification are Water-Gas Shift reaction (Reaction 1), Steam Reforming reaction (Reaction 2), as well as those presented in Reactions (5) – (9) [28-32].

Boudouard reaction:

$$C + CO_2 \leftrightarrow 2CO$$ Reaction 5

Hydrogasification:

$$C + 2H_2 \leftrightarrow CH_4$$ Reaction 6

Char-steam reforming:

$$C + H_2O \leftrightarrow CO + H_2$$ Reaction 7

$$C + 2H_2O \leftrightarrow CO_2 + 2H_2$$ Reaction 8

Steam/methane reforming

$$CH_4 + CO_2 \leftrightarrow 2CO + 2H_2$$ Reaction 9

It has been discussed in the previous paper (Section 7.2) that as the equivalence ratio continued to increase with constant oxygen feeding rate, less producer gas is generated during gasification thus residence time is increased and pyrolysis oil spray is more uniform. The improvements of spray characteristics and increase in residence time at increasing equivalence ratio also enhanced non-oxidation reactions described in Reactions (1) – (9), thus giving higher concentrations of useful gas species such H_2 and CO in the product. In this condition, non-oxidation reactions involving H_2O released during pyrolysis

oil evaporation and combustion, such as Water Gas Shift, Steam Reforming and steam gasification are also significantly promoted, thus contributing to increase in H_2 and CO concentrations in the producer gas observed in Figure 7–13. The above phenomena maintain until the equivalence ratio reaches the critical ER value of 0.5 for gasification at 1500 L/h oxygen flow rate.

ii. Equivalence ratio higher than the critical ER

As the equivalence ratio exceeded the critical ER value, more oxygen was available for pyrolysis oil oxidation hence suppresses the non-oxidation reactions in Reactions (1) – (9) for competitive consumption of pyrolysis oil. Reactions between oxygen gas and pyrolysis oil could be presented as in Reactions (10) and (11).

Pyrolysis oil complete combustion:

$$C_xH_yO_z + \left[{}^1/_2\left(\frac{y}{2} - z\right) + x\right]O_2 \rightarrow x\,CO_2 + {}^y/_2\,H_2O \qquad \text{Reaction 10}$$

Pyrolysis oil partial combustion:

$$C_xH_yO_z + \left[{}^1/_2\,(x - z)\right]O_2 \rightarrow x\,CO + {}^y/_2\,H_2 \qquad \text{Reaction 11}$$

It is possible that the oxygen gas also reacted with combustible gasification products such as H_2, CO, CH_4, C_2H_4, C_2H_6 when the available oxygen became more abundant. This situation explains the declining concentrations of H_2, CO and CH_4 in the producer gas with increase in the equivalence ratio, as observed in Figure 7–13. Oxidation reactions of the gasification products could take place following Reactions (12) – (14) [28-32]:

Gas combustion/oxidation

$$CO + {}^1/_2\,O_2 \rightarrow CO_2 \qquad \text{Reaction 12}$$

$$H_2 + {}^1/_2\,O_2 \rightarrow H_2O \qquad \text{Reaction 13}$$

$$CH_4 + {}^1/_2\,O_2 \rightarrow CO + 2H_2 \qquad \text{Reaction 14}$$

Oxygen gas may also react with solid residues and cenospheres from incomplete pyrolysis oil conversion following Reactions (15) and (16) which further contributed to increase in the CO_2 concentration in the product [31].

Solid carbon combustion/oxidation

$C + O_2 \rightarrow CO_2$ Reaction 15

$C + {}^{1}/_{2}\, O_2 \rightarrow CO$ Reaction 16

In the entrained flow gasifier developed in this study, the oxygen and pyrolysis oil were mixed outside the external mix atomizer, therefore, it is more likely that oxygen gas was available for oxidative reactions described in Reactions (12) – (16) to take place at high equivalence ratio in comparison with an internal mix atomizer. From the above analysis, it is therefore important that the entrained flow gasifier is aimed to be operated at the critical ER so the maximum concentrations of useful gas species such as H_2 and CO could be obtained in the producer gas.

7.3.3.2 Correlation between equivalence ratio and gasification temperature at constant oxygen flow rate

Figure 7–14 shows gasification temperature profile with equivalence ratio during the entrained flow gasification at a constant oxygen feeding rate of 1500L/h in this study. The figure agrees the trend presented in the previous paper (Section 7.2). The increasing trend of temperature is expected due to continuous decline in pyrolysis oil feeding rate when the equivalence ratio was increased from 0.3 to 0.9 thus enhancing exothermic oxidative reactions that release more heat to the system.

High gasification temperature enhances the overall gasification reactions and thus the carbon conversion, which can also be used to explain improvements in both oxidation and non-oxidation reactions and their products at higher equivalence ratio as discussed earlier. However, the overall energy efficiency is reduced, and the reactor design and operation are more complicated.

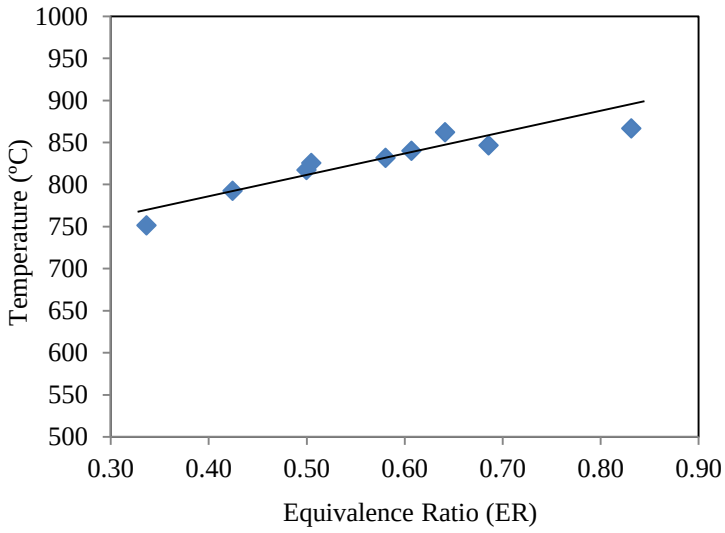

Figure 7–14: Gasification temperature profile as a function of equivalence ratio at constant oxygen feeding rate of 1500 L/h.

7.3.3.3 Comparison between experimentally measured and model predicted producer gas compositions

Using the equilibrium model developed in this study, producer gas compositions were predicted assuming the system was at equilibrium. Results from the model prediction can be used to analyse how far the gasification process deviates from the equilibrium state and what operation conditions contribute to this deviation. In this work, producer gas compositions at equilibrium were calculated from the model presented in this paper based on the same gasification conditions as in the experiments, which were recorded when gas samples were taken. Comparison between the experimentally measured and model predicted producer gas compositions are shown in Figure 7–15 for different equivalence ratio at a constant oxygen feeding rate of 1500 L/h.

From Figure 7–15, it is found that the producer gas compositions as predicted by the equilibrium model are in reasonably good agreement with the measured data when the equivalence ratio is above the critical value of 0.5. However, with the equivalence ratio below this critical value, significant variations have been observed between the experimental and the equilibrium results. Below the critical value, the deviations increased as the equivalence ratio continued to decline with the maximum deviations found at the lowest equivalence ratio.

These trends are true for all of the gaseous species at high equivalence ratio (higher than the critical ER) which confirms that the entrained flow gasification process is close to the equilibrium state thus the operation is expected to be more stable within this range. However, the operation is unstable when the equivalence ratio is less than the critical value as the process deviates from the equilibrium state and the situation worsens when the equivalence ratio is close to 0.3.

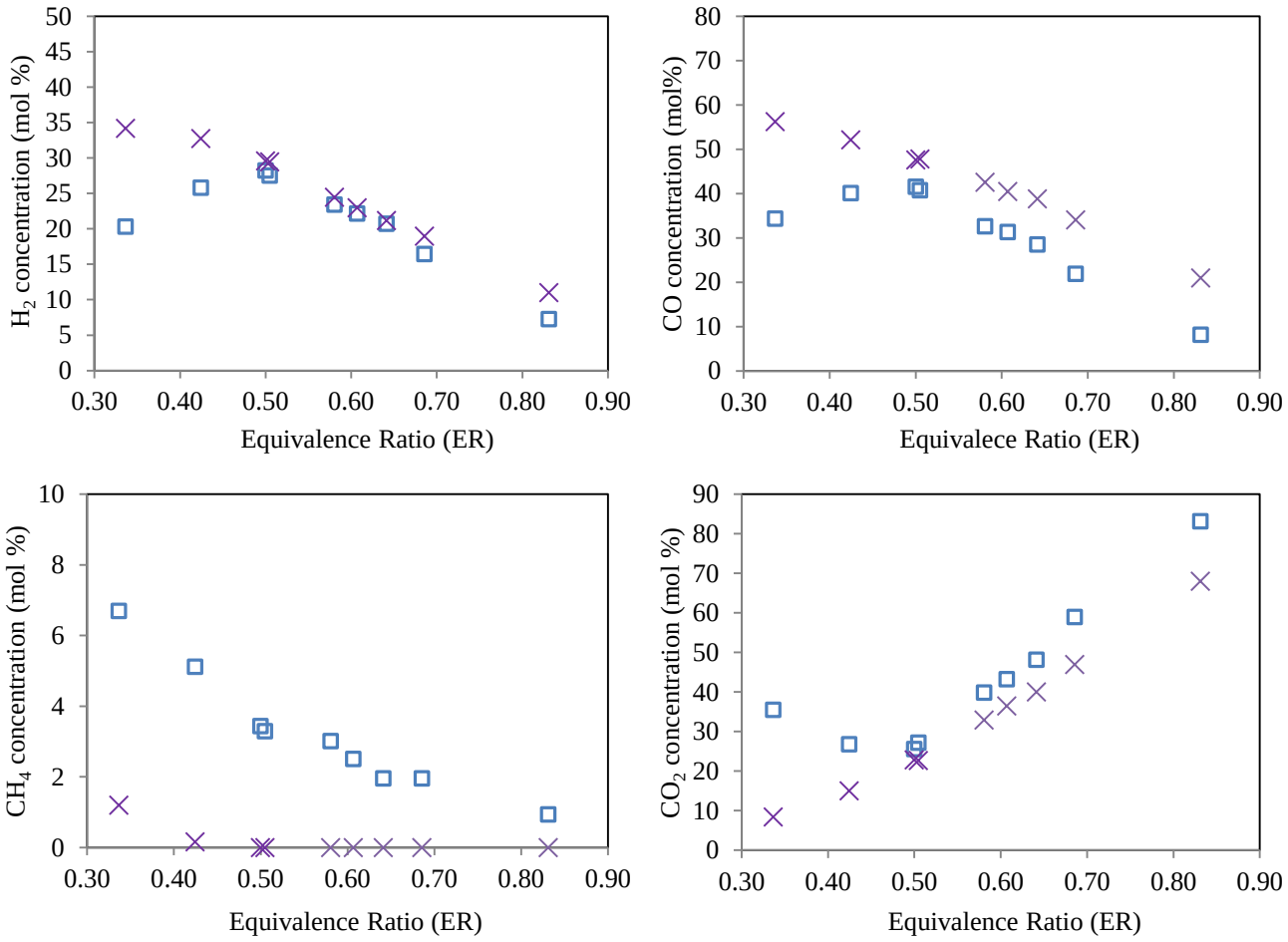

Figure 7–15: Comparison between experimentally measured (□) and model predicted (×) producer gas concentrations at constant oxygen feeding rate of 1500L/h.

The trends obtained in Figure 7–15 can be explained by considering increase in the gasification residence time and overall reaction kinetics as the equivalence ratio was increased during the operation. Effects of equivalence ratio on reaction kinetics and residence time during entrained flow gasification have been discussed in detailed in the previous paper (Section 7.2) and were concluded to be the main reason for improved pyrolysis oil-to-gas conversion at higher equivalence ratio. Using the same principles,

elaborations on how reaction kinetics and residence time influence agreements between the experimental and equilibrium results could be explained as follows:

i. At low equivalence ratio (below the critical ER):

At constant oxygen flow rate, gasification at low equivalence ratio is achieved with high pyrolysis oil feeding rate into the system. This situation results pyrolysis oil spray with low gas-to-fuel ratio (GFR), which is an indication of a poor spray characteristics and therefore slow reaction kinetics. At the same time, the high pyrolysis oil flow rate also generates large producer gas yield which shorten the residence time of the system. The combination of poor spray kinetics and short residence time at low equivalence ratio restrict progresses of important reactions during gasification hence prevent the system from reaching equilibrium.

As the equivalence ratio increases, the pyrolysis oil feeding rate into the system declines continuously resulting better spray characteristics as well as longer residence time for gasification reactions to take place. This condition enhances pyrolysis oil conversion into gaseous products, while at the same time drive the system closer to the equilibrium state. These improvements occur consistently with increasing equivalence ratio until the experimental producer gas composition reaches the critical ER value, which during gasification at 1500 L/h oxygen flow rate occurred at equivalence ratio of 0.5.

ii. At high equivalence ratio (above the critical ER):

The critical equivalence ratio implies the minimum combination of reaction kinetics and residence times required by the system before thermodynamic influences of gasification reactions become more prominent. Once the critical equivalence ratio is achieved, most materials in the system are expected to present in gas or vapour form and the system's ability to reach equilibrium depends on the kinetics and thermodynamics of relevant homogeneous reactions during the operations. Homogeneous reactions domination on the producer gas composition from the experimental results are clearly visible in Figure 7–15 where further increase in equivalence ratio values above the critical ER value lead to consistent producer gas compositions trends with that predicted at equilibrium.

It is worthwhile noting that small discrepancies between the experimental and equilibrium model producer gas compositions are expected even when the system is at equilibrium, considering the gasification non-ideal operations relative to that predicted by the equilibrium model. The equilibrium model was developed based on a list of ideal-case assumptions that are often difficult to be fulfilled during practical gasification operations. For the entrained flow gasification system developed in this work in particular, temperature gradient across the gasifier length was consistently observed during all

gasification runs as a result of exothermic oxidation reactions of pyrolysis oil at the top and endothermic gasification reactions dominating the bottom section of the gasifier; thus may have contributed to some errors in the predicted results generated by the equilibrium model.

Results in Figure 7–15 ultimately show advantages of conducting gasification at equilibrium in order to generate producer gas with the highest H_2 and CO concentrations. During gasification at constant oxygen feeding rate, the system is closer to the equilibrium state at higher equivalence ratio as a result of improved spray characteristics and longer residence time. Nevertheless, too high equivalence ratio is not beneficial as this situation leads to continuous decline in the H_2 and CO concentrations in the producer gas as a result of oxidation reactions domination. It is therefore important that gasification is operated at the critical ER value so the system is close to equilibrium and the highest concentrations of H_2 and CO could be obtained in the producer gas during the operation.

7.3.3.4 Effects of equivalence ratio on gasification thermal efficiency

Following the unique trends observed during gasification as discussed in the previous sections, it is therefore useful to investigate the relationship between equivalence ratio and the process thermal efficiency. Thermal efficiency for gasification application is calculated from the ratio of the total chemical energy contained in producer gas to the energy in pyrolysis oil feed supplied into the system. In this work, thermal efficiency of the gasification process is presented in terms of cold gas efficiency, as presented in Equation 13.

$$\eta_{cold\_gas} = \frac{Q_{N\_gas\_dry} \times LHV_{gas}}{M_{bio-oil} \times LHV_{bio-oil}} \qquad \text{Equation 13}$$

In the equation, $Q_{N\_gas\_dry}$ and $M_{bio-oil}$ represent flow rates of dry producer gas (N L/min) and pyrolysis oil (g/min) respectively. On the other hand, the term LHV_{gas} and $LHV_{bio-oil}$ refer to heating values of the producer gas and the oil.

Heating values of producer gas generated during gasification at oxygen feeding rate of 900 L/h for different equivalence ratio values are shown in Figure 7–16.

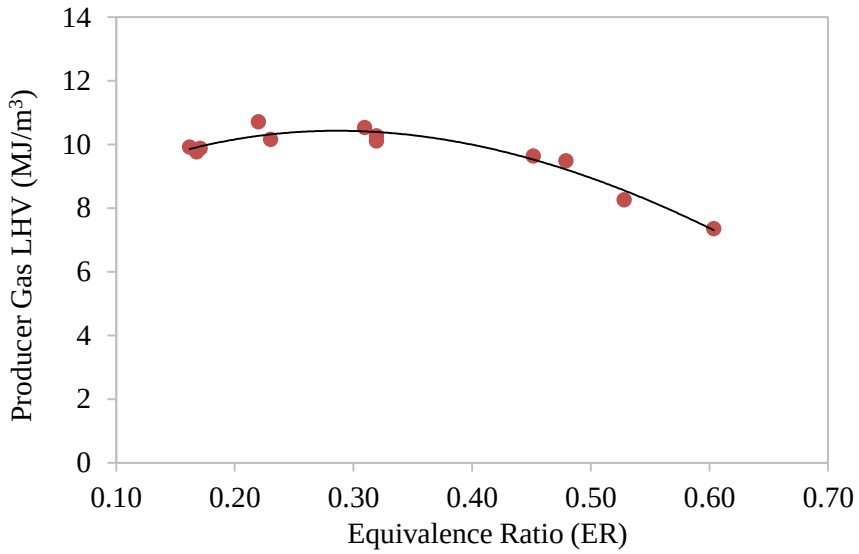

Figure 7–16: Heating values of producer gas during gasification at different equivalence ratio

At low equivalence ratio, the producer gas yield appears to be reasonably stable at around 10 MJ/m^3. This condition is likely a result of simultaneous change in the concentrations of H_2, CO, CH_4, C_2H_4, C_2H_6 and other combustible gases in the producer gas when gasification is operated at different equivalence ratio. This is because each gas species holds different heating values thus fluctuations in the gas species compositions may responsible for the insignificant change to the producer gas heating values.

Using the gas heating values calculated in Figure 7–16, thermal efficiency of the gasification process could be calculated. The relationship between thermal efficiency and equivalence ratio for gasification at oxygen feeding rate of 900 L/h is as plotted in Figure 7–17.

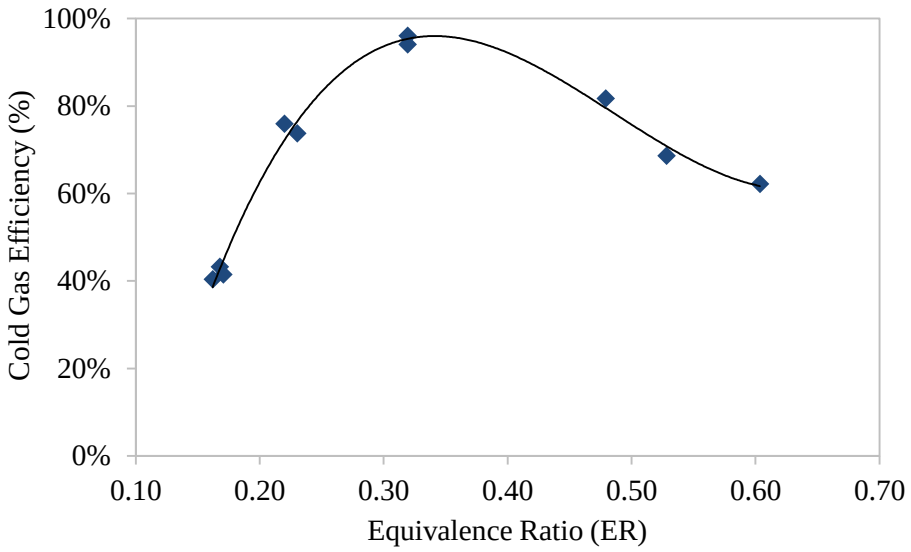

Figure 7–17: Cold gas efficiency of the gasification operation at different equivalence ratio

Results in Figure 7–17 clearly show parabolic relationship between cold gas efficiency and equivalence ratio, with the maximum thermal efficiency reached as high as 96% when gasification operates at the critical ER of 0.3. Below the critical ER, increase in equivalence ratio increases the process thermal efficiency since conversion of pyrolysis oil into producer gas is rapidly enhanced within this range, generating larger producer gas yield thus responsible for the increase in total energy exiting the system.

In contrary, increase in the equivalence ratio above the critical ER causes consistent drop in the process thermal efficiency as a result of consistent decline in all combustible gas species in the producer gas (H_2, CO, CH_4, C_2H_4 and C_2H_6) with addition of more oxygen into the system. The lowest thermal efficiency occurred when gasification is operated at the lowest equivalence ratio, which in this case at 0.15. It is interesting to highlight that at this operation condition, although the producer gas has a high heating value (10 MJ/m^3), the thermal efficiency of the process was significantly low due to poor oil-gas conversion.

These findings further supports the importance of conducting gasification at the critical ER to maximize the thermal efficiency of the process while at the same time producing producer gas with the highest heating value.

7.3.4 Conclusion

In this work, effect of equivalence ratio on producer gas composition during gasification at constant oxygen flow rate (1500 L/h) has been investigated. The findings show unique relationship between the

equivalence ratio and producer gas composition, where instead of giving linear relationships as usually reported in the literature; the results show parabolic trends where H_2 and CO concentrations increase to a maximum at critical equivalence ratio of 0.5 before decrease consistently with further increase in the equivalence ratio. The opposite trend is observed for CO_2 gas.

The producer gas composition unique trends can be explained by considering the reaction kinetics, residence times and types of chemical reactions involved during gasification and the availability of reactants (C, H and O) at different equivalence ratio. During gasification at low equivalence ratio, non-oxidation reactions are highly dominant thus favour production of H_2, CO and CH_4 in the producer gas. As the equivalence ratio continues to increase towards the critical ER value, pyrolysis oil conversion into producer gas improves gradually as a result of longer residence times and improved spray characteristics thus giving consistent increase in H_2 and CO concentrations in the product. However as soon as the equivalence ratio exceeds the critical ER, effects of oxidation reactions become more dominant thus causing increase in CO_2 concentrations while reducing H_2 and CO concentrations in the producer gas.

At low equivalence ratio, the experimental producer gas compositions obtained in this work deviate significantly from that predicted at equilibrium. As the equivalence ratio increases, the differences decline rapidly until the equivalence ratio reaches the critical ER value, after which the experimental producer gas compositions are consistently close to that predicted by at equilibrium. These trends indicate the system's tendency to reach equilibrium when the equivalence ratio is high as a result of improved reaction kinetics and longer residence time.

Investigation on the process thermal efficiency at different equivalence ratio shows parabolic trend with the maximum efficiency occurs at the critical ER. Findings from this investigation ultimately indicate the advantage of gasification at the critical ER value so the process thermal efficiency could be maximized, while at the same time, producer gas with the highest H_2 and CO concentrations could be generated from the operation.

7.3.5 Acknowledgements

This work was funded by the Ministry of Business, Innovation and Employment New Zealand and Ministry of Higher Education Malaysia. The authors would like to thank the sponsors, Alternative Energy Solutions (AES) Ltd. for the pyrolysis oil supplies and technical staffs in the University of Canterbury, New Zealand for their support.

7.3.6 References

1. Whitty, K., *Investigation of Pressurized Entrained-Flow Kraft Black Liquor Gasification in an Industrially Relevant Environment - Annual Topical Report - Year 1*. 2006, University of Utah.
2. Whitty, K., R. Backman, and M. Hupa, *Influence of pressure on pyrolysis of black liquor: 1. Swelling.* Bioresource Technology, 2008. **99**(3): p. 663-670.
3. Kankkunen, A., et al., *Spraying characteristics of mixed black liquor - Two different spraying cases.* The Swedish and Finnish National Committees of the International Flame Research Foundation.
4. Whitty, K., et al., *Influence of pressure on pyrolysis of black liquor: 2. Char yields and component release.* Bioresource Technology, 2008. **99**(3): p. 671-679.
5. Carlsson, P., et al., *Experimental investigation of an industrial scale black liquor gasifier. 1. The effect of reactor operation parameters on product gas composition.* Fuel, 2010. **89**(12): p. 4025-4034.
6. Higman, C. and M. van der Burgt, *Chapter 5 - Gasification Processes*, in *Gasification (Second Edition)*. 2008, Gulf Professional Publishing: Burlington. p. 91-191.
7. Lee, S.H., et al., *Gasification characteristics of coke and mixture with coal in an entrained-flow gasifier.* Energy, 2010. **35**(8): p. 3239-3244.
8. Murthy, B.N., et al., *Petroleum coke gasification: A review.* Canadian Journal of Chemical Engineering, 2013.
9. Qin, K., et al., *High-temperature entrained flow gasification of biomass.* Fuel, 2012. **93**(0): p. 589-600.
10. Xiao, R., et al., *Pyrolysis pretreatment of biomass for entrained-flow gasification.* Applied Energy, 2010. **87**(1): p. 149-155.
11. Zhou, J., et al., *Biomass–oxygen gasification in a high-temperature entrained-flow gasifier*. Biotechnology Advances, 2009. **27**(5): p. 606-611.
12. Samiran, N.A., et al., *Progress in biomass gasification technique – With focus on Malaysian palm biomass for syngas production.* Renewable and Sustainable Energy Reviews, 2016. **62**: p. 1047-1062.
13. Abdullah, H., et al., *Bioslurry as a Fuel. 3. Fuel and Rheological Properties of Bioslurry Prepared from the Bio-oil and Biochar of Mallee Biomass Fast Pyrolysis.* Energy & Fuels, 2010. **24**(10): p. 5669-5676.
14. Van der Drift, A., et al. (2004) *Entrained flow gasification of biomass*.
15. Dahmen, N., et al., *The bioliq® bioslurry gasification process for the production of biosynfuels, organic chemicals, and energy*. Energy, Sustainability and Society, 2012. **2**(1): p. 1-44.

16. Henrich, E., N. Dahmen, and E. Dinjus, *Cost estimate for biosynfuel production via biosyncrude gasification.* Biofuels, Bioproducts and Biorefining, 2009. **3**(1): p. 28-41.
17. Chhiti, Y., et al., *Wood Bio-Oil Noncatalytic Gasification: Influence of Temperature, Dilution by an Alcohol and Ash Content.* Energy & Fuels, 2010. **25**(1): p. 345-351.
18. Chhiti, Y., et al., *Thermal decomposition of bio-oil: Focus on the products yields under different pyrolysis conditions.* Fuel, 2012. **102**(0): p. 274-281.
19. Marda, J.R., et al., *Non-catalytic partial oxidation of bio-oil to synthesis gas for distributed hydrogen production.* International Journal of Hydrogen Energy, 2009. **34**(20): p. 8519-8534.
20. Chhiti, Y., M. Peyrot, and S. Salvador, *Soot formation and oxidation during bio-oil gasification: experiments and modeling.* Journal of Energy Chemistry, 2013. **22**(5): p. 701-709.
21. Creager, N. and R.C. Brown. *High pressure, oxygen blown entrained-flow gasification of bio-oil*. in *AIChE 2012 - 2012 AIChE Annual Meeting, Conference Proceedings*. 2012.
22. Chhiti, Y. and S. Salvador, *Gasification of Wood Bio-Oil*. Gasification for Practical Applications. 2012.
23. Abdoulmoumine, N., A. Kulkarni, and S. Adhikari, *Effects of Temperature and Equivalence Ratio on Pine Syngas Primary Gases and Contaminants in a Bench-Scale Fluidized Bed Gasifier.* Industrial & Engineering Chemistry Research, 2014. **53**(14): p. 5767-5777.
24. Williams, A., *Combustion of Liquid Fuel Sprays*. 1990, London: Butterworth & Co (Publishers) Ltd.
25. Karamarkovic, R. and V. Karamarkovic, *Energy and exergy analysis of biomass gasification at different temperatures.* Energy, 2010. **35**(2): p. 537-549.
26. Lide, D.R., *CRC Handbook of Chemistry and Physics 84th Edition*. 2004: CRC Press LLC.
27. Latifi, M., *Gasification of Bio-oils to Syngas in Fluidized Bed Reactors*, in *Department of Chemical and Biochemical Engineering*. 2012, University of Western Ontario: Ontario.
28. Ricketts, B., et al. *Technology status review of waste/biomass co-gasification with coal*. in *IChemE Fifth European Gasification Conference*. 2002.
29. Higman, C. and M. van der Burgt, *Chapter 2 - The Thermodynamics of Gasification*, in *Gasification (Second Edition)*, C. Higman and M.v.d. Burgt, Editors. 2008, Gulf Professional Publishing: Burlington. p. 11-31.
30. Kunze, C. and H. Spliethoff, *Modelling, comparison and operation experiences of entrained flow gasifier.* Energy Conversion and Management, 2011. **52**(5): p. 2135-2141.
31. Hernández, J.J., et al., *Effect of steam content in the air–steam flow on biomass entrained flow gasification.* Fuel Processing Technology, 2012. **99**(0): p. 43-55.

32. Basu, P., *Chapter 1 - Introduction*, in *Biomass Gasification and Pyrolysis*, P. Basu, Editor. 2010, Academic Press: Boston. p. 1-25.

7.4 Non-Slagging Entrained Flow Gasification of Biomass Pyrolysis Oil: Influence of Oxygen Flow Rate on Producer Gas Composition at Constant Equivalence Ratio

This section will be submitted as a research paper in the international journal Biomass and Bioenergy

Abstract:

This work investigated entrained flow gasification of biomass pyrolysis oil at atmospheric pressure and temperature up to 1100^{o}C. The pyrolysis oil was derived from New Zealand radiata pine wood chips via fast pyrolysis process. The pyrolysis oil was feed into the system as fine spray droplets after impact with oxygen gas as it exits an external mix twin-fluid atomizer. The equivalence ratios tested in this work were in the range between 0.1 and 0.9. This article presents important effect of oxygen flow rate on gasification producer gas composition at constant equivalence ratio. The results showed unique relationship between oxygen flow rate and producer gas composition where two distinctive trends were observed when oxygen flow rate were varied at low and high equivalence ratio values. Increase of oxygen flow rate was also found to drive the system closer to equilibrium, as observed from improved agreement between the experiment and equilibrium model producer gas compositions. Nevertheless there is a maximum oxygen flow rate value, above which, the system again shifts away from the equilibrium. Deviation from equilibrium in this condition could be advantageous as it generates producer gas with higher H_2 and CO concentrations than that given at equilibrium. This article ultimately shows advantage of conducting gasification at high feed flow rates in order to reach equilibrium as well as to maximize H_2 and CO yields in the producer gas.

Keywords: Entrained flow gasification, biomass pyrolysis oil, oxygen flow rate, equilibrium

7.4.1 Introduction

Challenges for using forest residues for renewable energy production are generally associated with the biomass low density and high moisture content. This situation makes the costs for transporting and storing the material in large scale uneconomical [1, 2], especially when long transportation distance is needed during the process. One of the solutions to this limitation is to pre-treat and densify the raw biomass into a lower moisture content and higher density intermediate product. This can be achieved by densifying the biomass into liquid form through fast pyrolysis using mobile pyrolysis reactors which are located near the biomass supplying sites. Then the liquid product, which is usually referred to as 'pyrolysis oil' or 'bio-oil' can be transported to a central gasification plant for subsequent conversion into producer gas.

Conversion of solid biomass into pyrolysis oil is also advantageous as this facilitates formation of very fine feed size [2, 3] as small as 10μm into subsequent gasification process; in most cases the entrained flow gasification. Woody biomass is difficult to be pulverized into fine particles due to its fibrous nature although extensive energy is consumed [1, 4]. In addition, feeding liquid into a pressurized system is also easier and simpler in comparison with feeding of solid particles [1, 2].

Entrained flow gasification has been used in petrochemical refineries as well as in black liquor and coal processing plants [5-12]. This gasification approach delivers high carbon conversion performance (almost 100% reported) and produces a product gas, termed as producer gas with low tar content due to the high operation temperature and short residence times [13-15]. Entrained flow gasification of biomass pyrolysis oil with steam have been reported in a few studies [16-18] where different operation conditions were examined for their influences on gasification performance (producer as yield, gas composition and tar content). Amongst parameters investigated in these studies include operation temperature, pyrolysis oil dilution with ethanol, heating rates and pyrolysis oil ash content.

Reports on gasification of pyrolysis oil with pure oxygen as the gasification agent, on the other hand, are scarce in literature. The lack of information on oxidative entrained flow gasification has left many aspects of its operation remain unexplored and effects of related operation conditions have not been evaluated for its true potential. Creager et al. [19], as an example, studied pyrolysis oil gasification at equivalence ratio and temperature of 2.5 and 850^{o}C, respectively, and operation pressures of 1 atm and 6.8 atm. The equivalence ratio (ER) is the ratio of oxygen feed into the system during gasification over that required for theoretical stoichiometric combustion of pyrolysis oil [20]. In this work, both pressure and oil atomization characteristics were found to have major impacts on producer gas composition. However, depth analysis and explanation of these impacts were not reported.

Marda et al. [21] also investigated entrained flow gasification of pyrolysis oil with oxygen at equivalence ratio between 0 to 0.35 and temperatures of 625 to 850^{o}C, respectively. The results showed improvements in carbon conversion values as gasification temperature increased, which is believed due to advance steam reforming reactions from high steam concentration in the system. It was also reported that the equivalence ratio had more dominant impact on carbon conversion in comparison with that caused by gasification temperature.

Following these findings, Chhiti et al. [16] investigated entrained flow gasification of pyrolysis oil with oxygen at much higher temperatures (1000-1400^{o}C) and equivalence ratio from 0.08 to 0.5. The results showed that H_2 concentration in the producer gas increased continuously with temperature. Results in this work are consistent with findings of Marda et al. [21] where the equivalence ratio had more significant impact on gasification producer gas compared to the impact of temperature. Separate study also found that the entrained flow gasification process was closer to equilibrium state at higher operation temperatures [17] while resulting producer gas of higher quality hence is desirable for gasification operations.

To date, no reports have been found in literature on effects of varying oxygen feeding rate on gasification products at given equivalence ratios and gasification temperatures. The feeding rate of oxygen is an important parameter to be explored considering its major influence on pyrolysis oil atomization characteristics; which has been shown to significantly affect producer gas compositions during gasification [19]. Therefore, this article aims to investigate effects of oxygen feeding rate on producer gas composition during entrained flow gasification of pyrolysis oil at constant equivalence ratios. The experimental results will then be compared with the predicted producer gas compositions from an equilibrium model, so thermodynamically stable operation of the entrained flow gasification of biomass pyrolysis oil could be analysed.

7.4.2 Materials and Methods

7.4.2.1 Feedstock

The pyrolysis oil used in this work was derived from radiata pine wood chips through fast pyrolysis process by a local company, Alternative Energy Solutions (AES) Ltd. Pyrolysis oil is a reasonably unstable product [22] where its properties change upon storage or when subjected to varying temperature. To monitor the changes in the properties of pyrolysis oil used in this work over time, measurements of the

oil properties were conducted periodically. Summary of the pyrolysis oil properties over a period of 7 weeks have been given the previous paper (Section 7.2) in Table 7-2.

7.4.2.2 Entrained flow gasification system

Pyrolysis oil and oxygen gas are feed into the system through a twin-fluid atomizer that disintegrates the oil stream into fine spray droplets in a flat spray pattern. The atomizer is an 'external mix' atomizer, thus, oxygen and pyrolysis oil flow separately in the atomizer and only come into contact when both streams exit the atomizer. The use of external mix atomizer in this study allows independent adjustments of oxygen and pyrolysis oil flow rates during atomization thus maximize control of the resulted spray characteristics by alteration of only one parameter at a time. The atomizer is integrated with a cooling jacket to prevent excessive heating of the atomizer body that could cause blockage to the oil feeding system due to pyrolysis oil polymerization.

In comparison to the more commonly used internal mixing atomizer, the external mixing atomization offers a much safer operation for pyrolysis oil and oxygen gas by lowering risk of flame flashback or internal combustion at high temperature [23].

The atomizer air cap used in this work has two dissimilar sides in order to enable formation of flat spray pattern during its operation. To differentiate between these two sides, one side is named as 'edge side' and the other as 'front side', respectively. Figure 7–18 illustrates the shape of the air cap used in this study and different images produced from both sides for comparison.

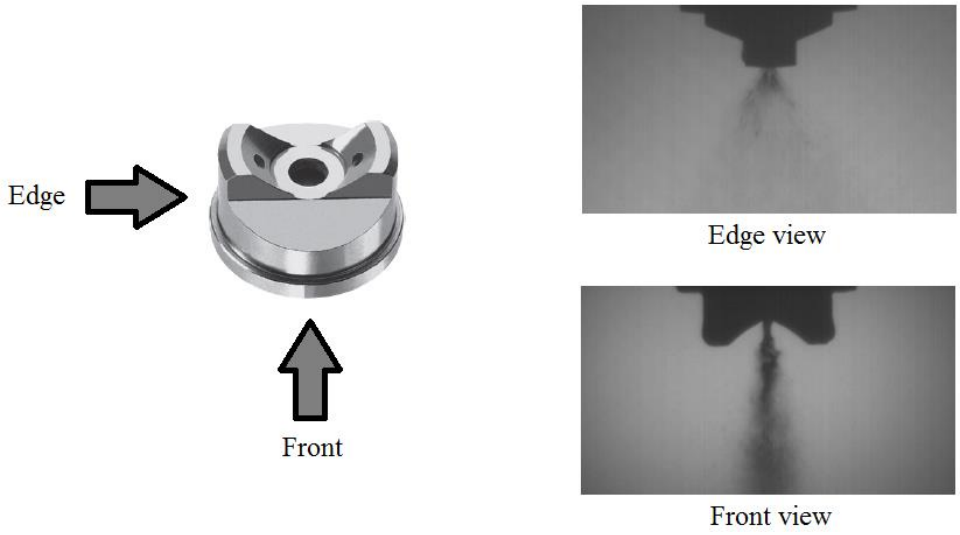

Figure 7–18: Different sides of atomizer air cap and examples of their corresponding spray views

More detailed information related to the entrained flow gasification system and its design has been reported in the previous paper (Section 7.2) in Section 7.2.2.2.

7.4.2.3 Experimental procedures, sampling method and producer gas analysis

Prior to any gasification run, the gasifier is pre-heat to the desired start-up temperature of 750^{o}C by two LPG burners. When the system stabilized at the start-up temperature, the LPG burners were switched off and supplies of pyrolysis oil and oxygen gas into the system were initiated. In this work, pyrolysis oil flow rate of up to 70 mL/min was used while oxygen gas feeding rate was varied between 600-3000 L/h depending on the objective of an individual gasification run. The equivalence ratio values were calculated based on flow rates of pyrolysis oil and oxygen gas feed into the system.

During any set of gasification run, the oxygen gas flow rate was kept constant while the pyrolysis oil flow rate was adjusted accordingly to give the desired equivalence ratio value. In all runs, the system was allowed to stabilize for 20-30 minutes before the first sample was taken for analysis. In order to minimize inconsistencies between results, intervals between two consecutive samples were maintained at 10-15 minutes. Gasification process is rapid with residence time of 1-5 seconds; therefore, production of producer gas at a new gasification condition should stabilize reasonably quickly.

Gasification products exit the gasifier through a port located at the bottom of the gasifier. The temperature of the product line is usually maintained between 450-600^{o}C to prevent condensation of products inside the line. During sampling, the gasification products were passed through two SPE columns with different packing materials to make sure the samples collected were free from condensable compounds such as water and tar. The concentrations of producer gas components was analysed using a Micro-GC. Detailed descriptions of the sampling method used in this work as well as information about the producer gas analysis have been given in the previous paper (Section 7.2) from Section 7.2.2.4 to Section 7.2.2.6.

7.4.2.4 Equilibrium model

In this work, an equilibrium model was developed to provide theoretical understanding of the entrained flow gasification operation as well as to predict producer gas composition at equilibrium. The model was developed by minimizing Gibbs free energy of the system based on major producer gas species expected from the gasification operation, which are H_2, CO, CO_2, CH_4, N_2 and H_2O. Detailed descriptions, list of assumptions and derivations of equations used during the model development have been reported in the previous paper (Section 7.3).

7.4.3 Results and Discussions

7.4.3.1 Effect of oxygen gas flow rate on producer gas composition (at high equivalence ratio)

To investigate the effect of oxygen feeding rate on producer gas composition, gasification results at four oxygen feeding rates of 600L/h, 900L/h, 1500L/h and 3000L/h were compared. Studies in Section 7.3 have discussed presence of critical equivalence ratio during gasification at constant oxygen flow rates, where equivalence ratio of 0.3 was the critical ER value for gasification at 900L/h oxygen feeding rate while equivalence ratio of 0.5 was the critical ER value for gasification at 1500L/h oxygen feeding rate.

Due to distinctive producer gas composition behaviour found before and after the critical ER, discussions on the influence of oxygen flow rate on the producer gas have to be separated into two sections. This section will compare the producer gas composition results at high equivalence ratio values, while effects of oxygen flow rates on the producer gas compositions at low equivalence ratio values will be discussed in Section 7.4.3.2 of this article.

Producer gas compositions during gasification at constant oxygen flow rates of 600L/h, 900L/h, 1500L/h and 3000L/h are shown in Figure 7–19. From the figure, it is found that H_2, CO and CH_4 concentrations decreased with equivalence ratio at a given oxygen feeding rate, however, at the same equivalence ratio, these concentrations were increased with oxygen feeding rate. The opposite trend was observed for CO_2 concentration.

The producer gas compositions observed in Figure 7–19 are different from those reported in literature from entrained flow gasification. Theoretically, producer gas composition is expected to remain unchanged during gasification when equivalence ratio is maintained constant, regardless of the pyrolysis oil or oxygen flow rates, as a result of constant molar ratio between oxygen and biomass feed supplied into the system. Results observed in Figure 7–19, therefore, indicate presence of other appreciable changes on the system's behaviour when oxygen flow rates were changed at a given equivalence ratio, which caused the changes in the final gasification products.

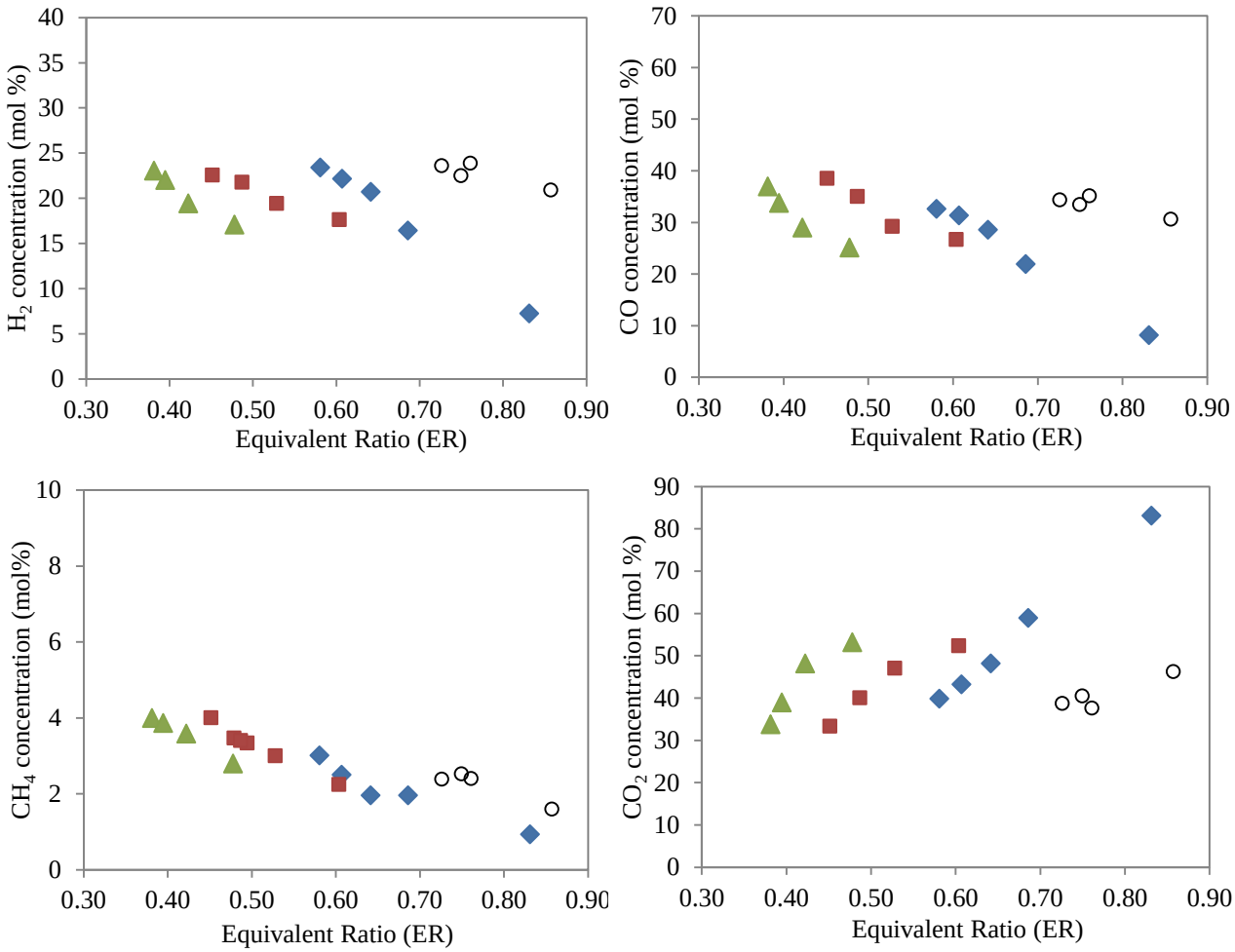

Figure 7–19: Producer gas compositions at different equivalence ratio and oxygen flow rates. Oxygen flow rates: ▲600L/h, ■ 900L/h, ◆1500L/h, ○ 3000L/h.

7.4.3.1.1 Effect of oxygen flow rate on spray characteristics

The effects of oxygen flow rate on producer gas composition observed in Figure 7–19 could be explained mainly by considering the consequences of varying oxygen flow rate on pyrolysis oil spray characteristics. In order to investigate the impact of gas feeding rate in the oil spray characteristics, separate experiments were conducted using the same atomizer assembly to spray the pyrolysis oil at room temperature. The setup consists of an enclosed spray chamber, with the front and back walls made of clear Perspex material to provide good light penetration for observation and sample collection.

In this work, air was used to represent the oxygen gas during atomization considering oxygen gas highly reactive nature. Three atomizer liquid caps namely 1650, 2050 and 2850 with varying liquid orifice

diameters (0.41 mm, 0.51 mm and 0.71mm respectively) were used in these experiments to verify consistencies of spray characteristics produced at different conditions. For this investigation, atomization was performed at various atomizing gas flow rates while the pyrolysis oil feeding rate was kept at a constant value. Spray images were captured using Mega Speed MS50K high speed camera which capable of capturing at least 1068 frames per second, thus freezes any objects in motion for highly accurate analysis. The images were then analysed using Image-J software to determine the resulted spray characteristics. Figure 7–20 shows examples of spray images captured from the cold model atomization.

<table>
<tr>
<td> 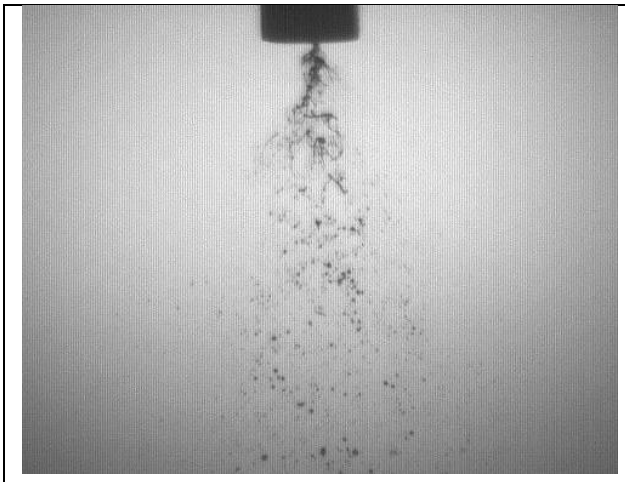
Atomizing gas flow rate: 800L/h
Pyrolysis oil flow rate: 76 mL/min
Liquid cap: 1650</td>
<td> 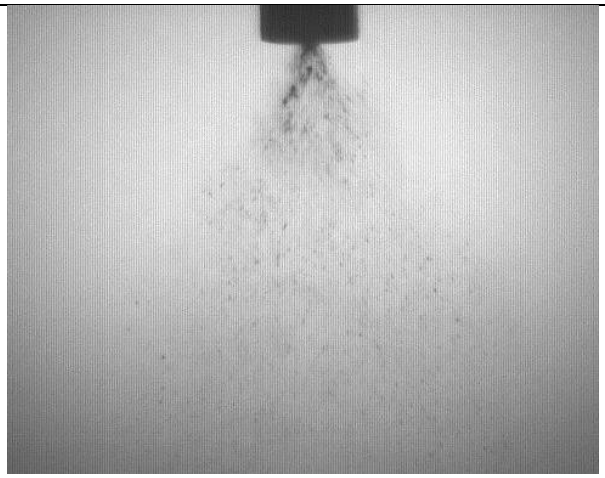
Atomizing gas flow rate: 1200L/h
Pyrolysis oil flow rate: 76 mL/min
Liquid cap: 1650</td>
</tr>
<tr>
<td> 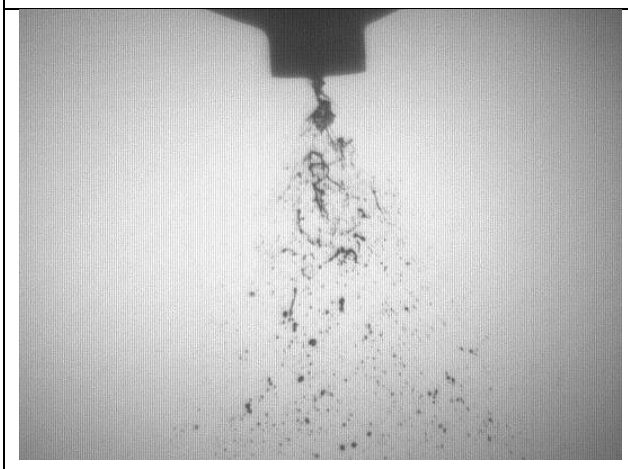
Atomizing gas flow rate: 800L/h
Pyrolysis oil flow rate: 93 mL/min
Liquid cap: 2050</td>
<td> 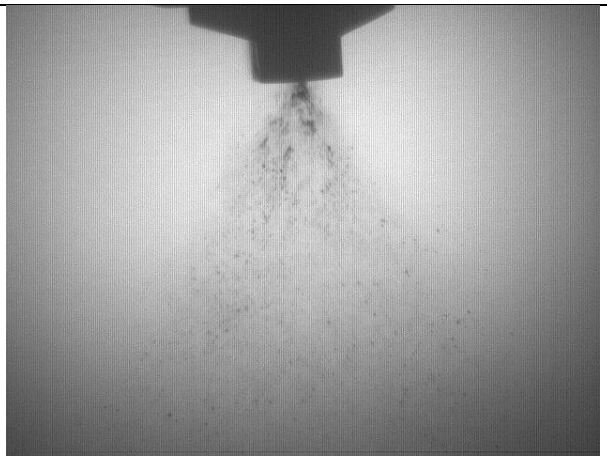
Atomizing gas flow rate: 1200L/h
Pyrolysis oil flow rate: 93 mL/min
Liquid cap: 2050</td>
</tr>
</table>

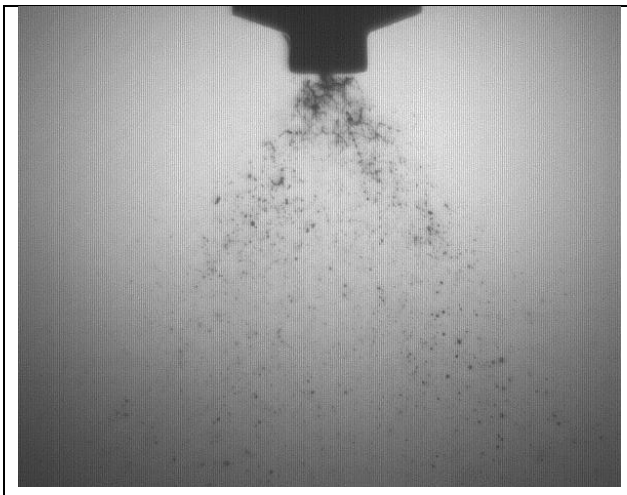

Atomizing gas flow rate: 800L/h
Pyrolysis oil flow rate: 93 mL/min
Liquid cap: 2850

Atomizing gas flow rate: 1200L/h
Pyrolysis oil flow rate: 93 mL/min
Liquid cap: 2850

Figure 7–20: Examples of spray images of pyrolysis oil in cold model atomization experiments at different gas flow rates.

From studies on cold model pyrolysis oil atomization, it has been found that the oil spray characteristics were improved when the atomizing gas flow rate increased progressively from 800L/h to 1200L/h; as a result of greater atomizing gas impact on the oil stream during spray formation process. Influence of oxygen flow rate on spray characteristics is well anticipated due to the external mix configuration of the atomizer used in this work; in which atomization performance depends strongly on collision impacts between oxygen and pyrolysis during its operation.

At sufficiently high oxygen flow rate values, the spray eventually turned into a thick ‘spray cloud’ that completely obscured the test rig. The thick spray cloud formation indicates an excellent atomization performance where the oil successfully atomized into very fine droplets (or mists) and distributed uniformly in the system. These improvements collectively result in desired pyrolysis oil spray characteristics at higher atomizing gas flow rate which is expected to boost the gasification reaction rates.

Moreover, the use of flat spray pattern in this work also contributed substantially to the improved spray distribution upon atomization. This is because in contrast to the more popular round spray pattern, the thin and wide geometry of the flat spray enhances transfers of heat and mass between the spray and gasification environment thus improved the overall reaction kinetics of the system. At higher oxygen flow rates, such interactions became more prominent since the spray pattern was found to grow wider while still maintaining its thinness, thus increasing the effective surface area for reactions to occur. Growth of pyrolysis oil spray pattern at increasing atomizing gas flow rate was determined based on the angle of

spray measured near the atomizer nozzle. The spray angle values measured during cold model atomization study for gas flow rates between 600-1500L/h are illustrated in Table 7-3.

Table 7-3: Pyrolysis oil spray angles at varying gas flow rates from different sides of the atomizer

Measurement Side	Atomizing gas flow rate (L/h)		
	600	900	1500
	Spray angle (°)		
Edge view	36	46	54
Front view	27	27	27

7.4.3.1.2 Theory of influence of oxygen flow rate on pyrolysis oil spray conversion

As pyrolysis oil spray characteristics are affected by the oxygen flow rate, it is then critical to understand how the oil spray characteristics are related to spray conversion and producer gas composition. Very little information has been found in the literature that explored pyrolysis oil spray conversion in gasification environment. In combustion applications, on the other hand, such information is readily available especially when traditional liquid fuel such as diesel and gasoline is used, following high demand for improved fuel combustion efficiency and emission reduction. There may be some similarities between combustion and gasification processes, for example, the liquid droplets are exposed to high temperatures in both processes. However, the most important difference between these two processes is that the availability of oxygen gas during gasification is much less than that in combustion system. Therefore, the reaction mechanisms involved during the fuel spray conversion between both systems are different.

In theory, combustion of fuel spray occurs as either homogeneous or heterogeneous combustions [23, 24]. Homogeneous combustion usually results from combustion of highly volatile fuels with sufficiently small initial droplet size to cause rapid evaporation of spray droplets into vapour clouds before combustion starts. In other words, homogeneous combustion takes place when the liquid fuel manages to completely vaporizes into vapour before reacting with oxygen. Heterogeneous combustion, on the other hand, takes place when spray droplets fails to vaporize completely before combustion starts. In this case, combustion occurs while the fuel present in two separate phases (liquid and vapour phases). Heterogeneous combustion flames are normally yellow in colour and could be further categorized into four different sub-modes as illustrated in Figure 7–21.

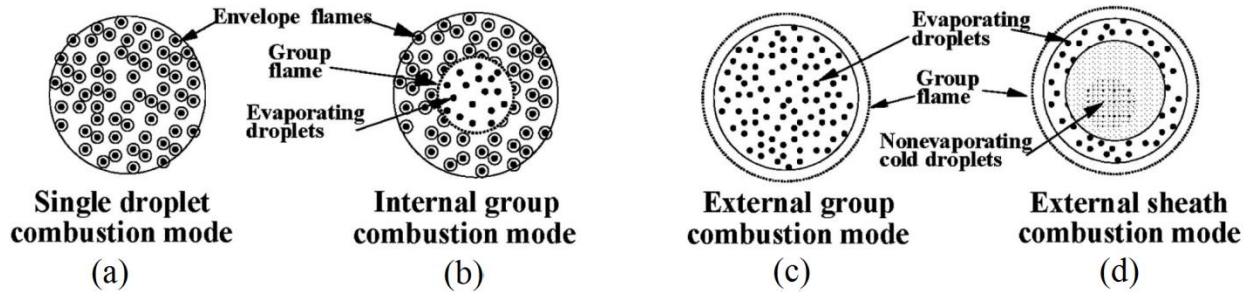

Figure 7–21: Four different modes of heterogeneous spray combustion [adapted from [24]].

It is clear from Figure 7–21 that the main difference between the combustion modes is related to how individual droplet burns and their contributions to the overall spray combustion. On one extreme case shown in Figure 7–21 (a), spray droplets distribute extremely well and burn individually, representing perfect spray combustion behaviour. With decrease in the spray combustion performance, the droplets form two groups, a core group in which the droplets evaporate and vapour moves outward; and an outer layer group in which the droplets and vapour combust (Figure 7–21 (b)). If the core group occupies the whole space, then the combustion of vapour occurs at the outer space as one large flame as shown in Figure 7–21 (c). On the other extreme case shown in Figure 7–21 (d), only a small fraction of the spray droplets manages to vaporize and participates in combustion, while major fraction of the fuel still remains in liquid form thus not contributing to the overall spray combustion.

In the last three cases of combustion of liquid fuel (Figure 7–21 (b) – (d)), the evaporated droplets release combustible vapour and, depending on the availability of oxygen around each droplet, the vapour burns either as individual envelope flame surrounding each droplet or collectively as a single group flame from combustion of vapour cloud. This justifies the strong dependence of combustion performance on fuel spray characteristics, where the droplets sizes, droplets distribution and oxygen-oil mixing within the spray play important roles in determining its conversion rate. In addition to spray characteristics, the fuel properties also have significant impact on spray combustion behaviour since these properties determine the fuel vaporization rate upon heating and ultimately affect whether the spray combust homogenously or heterogeneously.

Applying the above theory of fuel spray and combustion to entrained flow gasification of pyrolysis oil, spray characteristics also play an important role in gasification rate and producer gas composition, therefore, increasing oxygen flow rate leads to shift of conversion mode from ‘external sheath combustion/gasification’ towards ‘single combustion/gasification’ modes. This is because as the spray droplets become more distributed and smaller in size at higher oxygen flow rates, droplets vaporization

becomes more rapid and the fraction of droplets reacting individually is also expected to increase. Figure 7–22 shows the predicted spray combustion/gasification mode taking place during gasification in this work after taking into account the flat spray pattern and its growth from low to high oxygen flow rates.

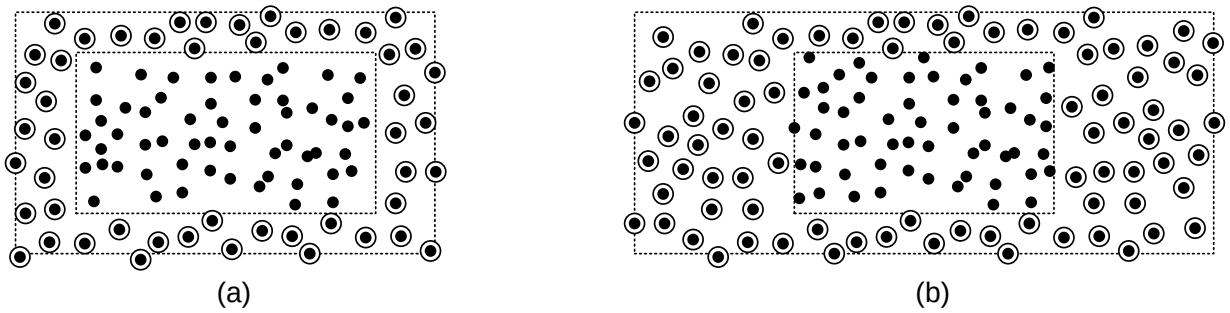

Figure 7–22: The expected heterogeneous spray combustion/gasification modes from flat spray pattern used in this study (a) at low oxygen flow rate (b) at high oxygen gas flow rate

With the increase of oxygen and pyrolysis oil feeding rates at constant equivalence ration, more small droplets have formed and burn individually. This means that efficient consumption of oxygen gas by smaller fractions of oil has been achieved, in comparison to the gasification of oil at lower oxygen and oil feeding rates. In this case, although the oxygen-oil ratio was constant at constant equivalence ratio, the percentage of oil involved in oxidation reaction is decreased which is advantageous for gasification as it allows a larger fraction of oil to involve in non-oxidation reactions to generate higher concentrations of H_2, CO and CH_4 in the product, as described in Reactions (1) and (2) [25].

Pyrolysis oil thermal decomposition:

$$C_xH_yO_z \rightarrow C_mH_nO_k + gases\left(H_2, CO, CO_2, CH_4, H_2O, C_xH_y\ etc\right) + C_{residues} \qquad \text{Reaction 1}$$

Pyrolysis oil steam gasification:

$$C_xH_yO_z + (x-z)H_2O \rightarrow x\ CO + \left(x - z + {}^{y}/_{2}\right) H_2 \qquad \text{Reaction 2}$$

In addition to the above two reactions, lack of available oxygen also promotes non-oxidation reactions amongst the gasification products which otherwise may undergo oxidation reactions. Major non-oxidation reactions among the gasification products are presented as follows [26-30]:

Boudouard reaction:

$C + CO_2 \leftrightarrow 2CO$ Reaction 3

Char-steam reforming:

$C + H_2O \leftrightarrow CO + H_2$ Reaction 4

$C + 2H_2O \leftrightarrow CO_2 + 2H_2$ Reaction 5

Steam/methane reforming

$CH_4 + H_2O \leftrightarrow CO + 3H_2$ Reaction 6

$CH_4 + CO_2 \leftrightarrow 2CO + 2H_2$ Reaction 7

The combustion and gasification process at different oxygen feeding rates can be transferred to an entrained flow gasifier as illustrated in Figure 7–23. At a constant equivalence ratio, when the oxygen and oil feeding rates are low as shown in Figure 7–23 (a), large combustion region forms and thus the non-oxidation reactions are reduced. In this condition, oxygen gas may react with useful gasification products such as H_2 and CO following Reactions (8) and (9) and consequently favours production of CO_2 and H_2O in the producer gas.

Combustion/Oxidation reactions:

$CO + {}^1/_2\, O_2 \rightarrow CO_2$ Reaction 8

$H_2 + {}^1/_2\, O_2 \rightarrow H_2O$ Reaction 9

With increase in oxygen and oil feeding rates, small combustion/oxidation region forms with more uniform spray and fine droplets (Figure 7–23(b)). In this case, consumptions of the oxygen gas by pyrolysis oil droplets are more rapid thus complete combustion of small fraction of the spray droplets are more favourable. In this condition, most of the pyrolysis oil droplets undergo non-oxidation reactions in the gasification region thus generating higher concentrations of H_2, CO and CH_4 in the producer gas.

Table 7-4 summarizes comparison of important parameters between high and low oxygen flow rates at constant equivalence ratio that can be used for improving the overall gasification performance.

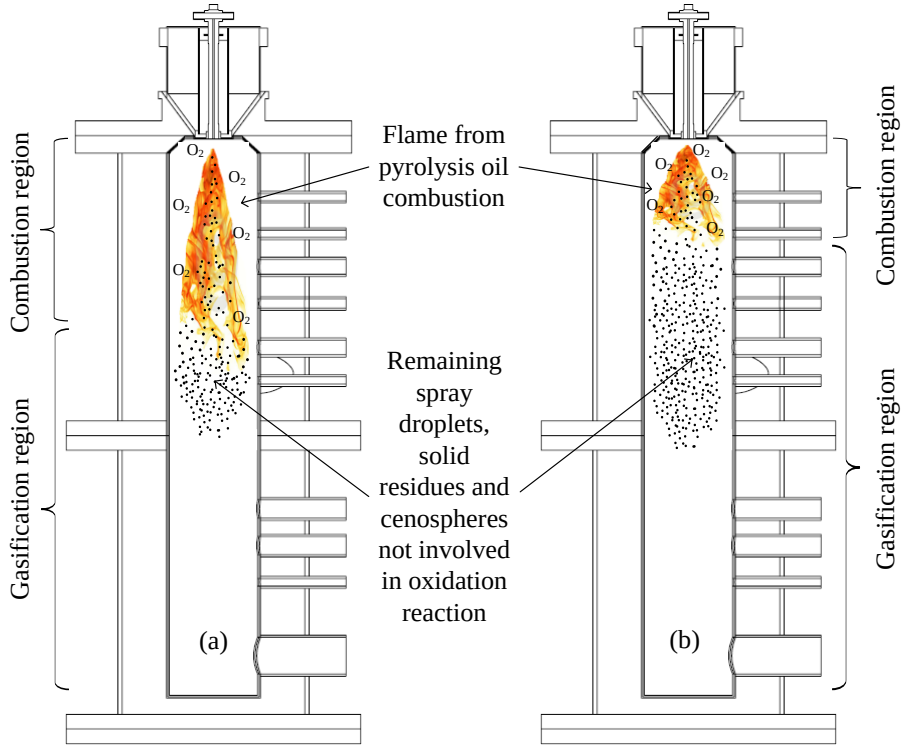

Figure 7–23: Differences between gasification operation at constant equivalence ratio and different oxygen gas flow rate (a) at low oxygen gas flow rate (b) at high oxygen gas flow rate

Table 7-4: Effect of oxygen flow rates on combustion and gasification of pyrolysis oil spray at constant equivalence ratio

Parameters	Low oxygen flow rate	High oxygen flow rate
Spray performance	Poor	Excellent
Combustion mode of pyrolysis oil spray droplets	Incomplete combustion	Complete combustion
Fraction of gasification gas (H_2, CO and CH_4) reacting with oxygen gas	Large	Small
Major final products	CO_2 and H_2O	H_2, CO and CH_4

The above discussion also confirms that that the decline in residence times as a result of increased pyrolysis oil and oxygen flow rates as discussed in the previous paper (Section 7.2) does not cause negative influence on the producer gas composition when the equivalence ratio is high during gasification operations. Findings from this section are important for optimisation of entrained flow gasification operation conditions.

7.4.3.2 Effect of oxygen flow rate on producer gas composition (at low equivalence ratio)

Investigation into effects of oxygen flow rate at low equivalence ratios revealed reverse trends from that discussed earlier at high equivalence ratios. Figure 7–24 shows that at low equivalence ratio values, gasification at 900 L/h oxygen flow rate resulted producer gas with higher concentrations of H_2 and CO compared to that generated by 1500 L/h gasification. As the equivalence ratio increased, H_2 and CO concentrations from 1500 L/h oxygen flow rate gasification increased more rapidly and eventually surpassed that produced by 900 L/h oxygen flow rate gasification. The opposite was found for CO_2 where its concentration at 1500 L/h oxygen flow rate reversed from being higher to lower than that at 900 L/h oxygen flow rate with increase in equivalence ratio. CH_4 on the other hand did not show any reverse trends as its concentrations at 900L/h oxygen flow rate remained consistently lower than that at 1500L/h throughout the equivalence ratio range tested.

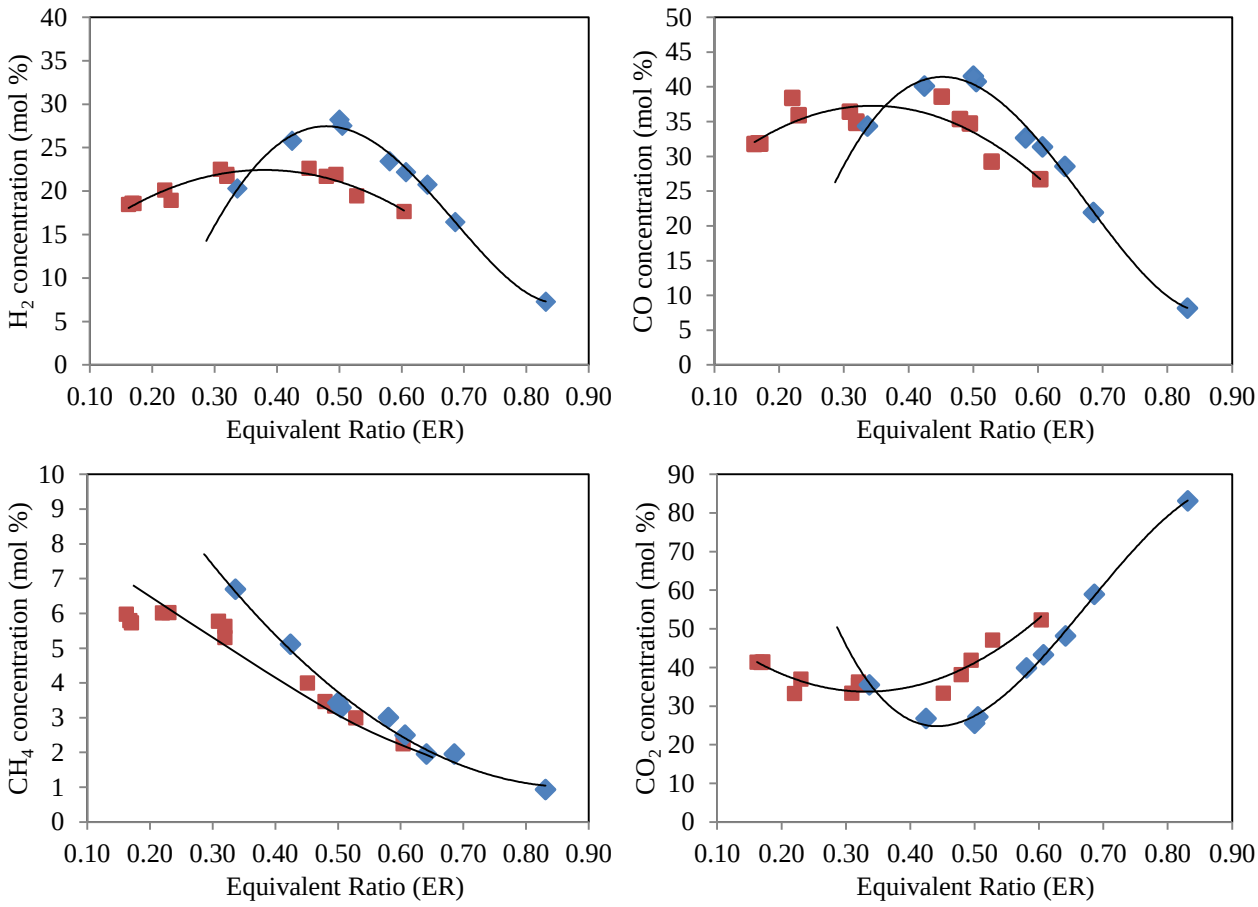

Figure 7–24: Producer gas compositions at varying equivalence ratio during gasification at (■) 900L/h and (◆) 1500L/h oxygen flow rates

The differences in the producer gas compositions between gasification at different oxygen flow rates could be explained by taking into account variations in the process residence time during operations at both conditions. Residence time has strong influence on pyrolysis oil conversion particularly during gasification at low equivalence ratio due to relatively poor spray characteristics (hence reaction kinetics) at this condition.

At a given equivalence ratio, increase in oxygen flow rate also reflects an increase in the oil feeding rate to maintain the equivalence ratio. Increase in the oil feeding rate generates higher producer gas flow (g/min) thus reduces the process residence time. Consequently gasification at higher oxygen flow rate (1500 L/h) corresponds to lower residence time in comparison to that given at lower oxygen flow rate (900 L/h). Therefore in Figure 7–24, it is possible that the decline in residence time during gasification at 1500 L/h oxygen flow rate was sufficient to significantly constrain pyrolysis oil conversion into producer gas, thus causing to the low H_2 and CO concentrations in the product.

Nevertheless, pyrolysis oil conversion during gasification at 1500 L/h oxygen flow rate improved rapidly when the residence time increased at increasing equivalence ratio. Although the H_2 and CO concentrations during gasification at 1500L/h were initially lower than that at 900L/h at low equivalence ratio values, the improvements in the oil-gas conversion at increasing equivalence ratio was more superior at higher oxygen flow rate thus resulting much faster growth in the H_2 and CO concentrations in the producer gas.

The variations in the rate of improvements for pyrolysis oil conversion during both gasification runs could be justified by considering the substantial differences in the pyrolysis oil spray characteristics at different gas flow rates as found during cold model pyrolysis oil atomization investigation, similar to that described earlier in Section 7.4.3.1. Analysis of spray images produced during this investigation, as shown in Figure 7–25, proved that at a given equivalence ratio, higher gas flow rates lead to much better spray characteristics thus promotes more significant advancements of relevant reactions progresses; and therefore explains the more rapid improvements in H_2 and CO concentrations at higher oxygen flow rate when residence time was increased at increasing equivalence ratio.

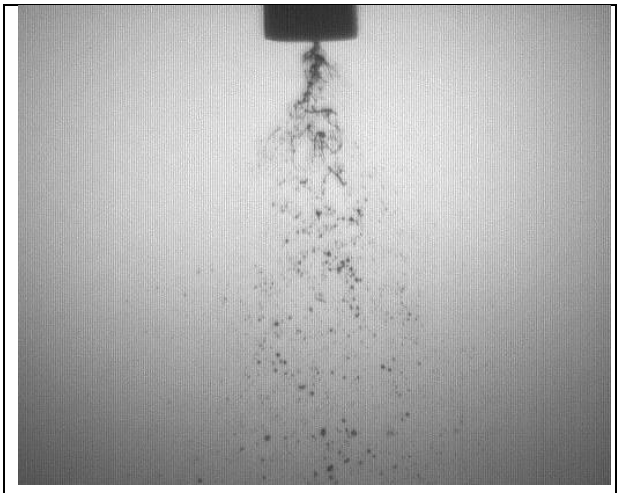	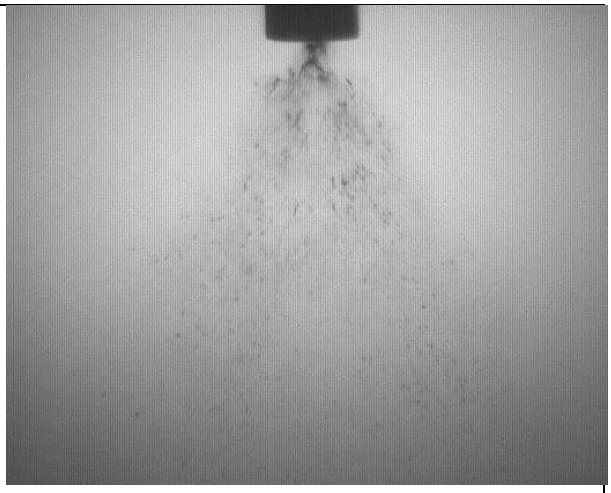
Equivalence Ratio (ER): 0.27 Atomizing gas flow rate: 800 L/h Pyrolysis oil flow rate: 80 mL/min Liquid cap: 1650	Equivalence Ratio (ER): 0.27 Atomizing gas flow rate: 1200 L/h Pyrolysis oil flow rate: 119 mL/min Liquid cap: 1650

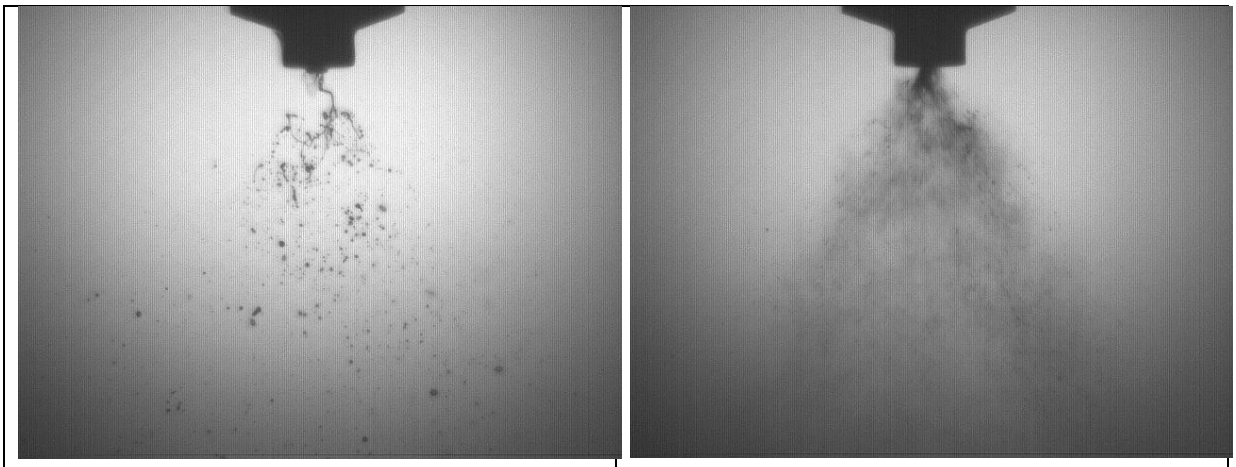

Equivalence Ratio (ER): 0.23 Atomizing gas flow rate: 400L/h Pyrolysis oil flow rate: 47 mL/min Liquid cap: 2850	Equivalence Ratio (ER): 0.23 Atomizing gas flow rate: 1600L/h Pyrolysis oil flow rate: 186 mL/min Liquid cap: 2850

Figure 7–25: Example of spray images from pyrolysis oil cold model atomization at constant equivalence ratio but higher gas flow rates

Other than reversing producer gas composition trends, increase of oxygen flow rate was also found to alter the critical ER value during gasification. It is clear from Figure 7–24 that the critical ER value shifted from 0.30 to 0.50 when the oxygen flow rate was increased from 900L/h to 1500L/h during gasification. In order to explain this change, it is important to acknowledge that the critical value represents balance between oxidation and non-oxidation reactions during gasification, which has been discussed in the previous paper (Section 7.3). Therefore, the increase of the critical ER value during gasification at higher oxygen flow rate indicates higher demand of oxygen for oxidation reactions to start dominating gasification reactions over non-oxidation reactions.

The increasing demand of oxygen from 900L/h to 1500L/h gasification is parallel to the theory presented earlier in Section 7.4.3.1 where during gasification at higher oxygen flow rate, non-oxidation reactions were highly dominant as a result of large percentages of pyrolysis oil droplets reacting in the gasification zone, as illustrated in Figure 7–23 (b). Therefore, the system demanded larger oxygen supply (hence equivalence ratio) before balance between the oxidation and non-oxidation reactions could be achieved.

The domination of non-oxidation reactions also justifies higher maximum concentrations of H_2 and CO recorded at 1500 L/h oxygen flow rate in comparison to that at 900 L/h. The maximum H_2 concentration increased from 22 vol% to 28 vol% while the maximum CO concentration increased from around 36 vol% to 41 vol% when oxygen flow rate was increased from 900 L/h to 1500 L/h during the operations.

7.4.3.3 Effect of oxygen flow rate on comparison between experimentally measured and model predicted producer gas compositions

Predictions of equilibrium producer gas compositions at different gasification conditions were performed using the equilibrium model developed in this study to analyse how far the gasification process deviates from the equilibrium state. Equilibrium producer gas compositions were calculated based on the same gasification conditions as in the experiments, which were recorded when gas samples were taken. This approach was taken to ensure compatibility and comparability between both results during comparison.

In this section, comparisons were made between experimental and equilibrium producer gas compositions during gasification at constant oxygen flow rates of 600L/h, 900L/h, 1500L/h and 3000L/h respectively. Results from these comparative analyses are shown in Figure 7–26.

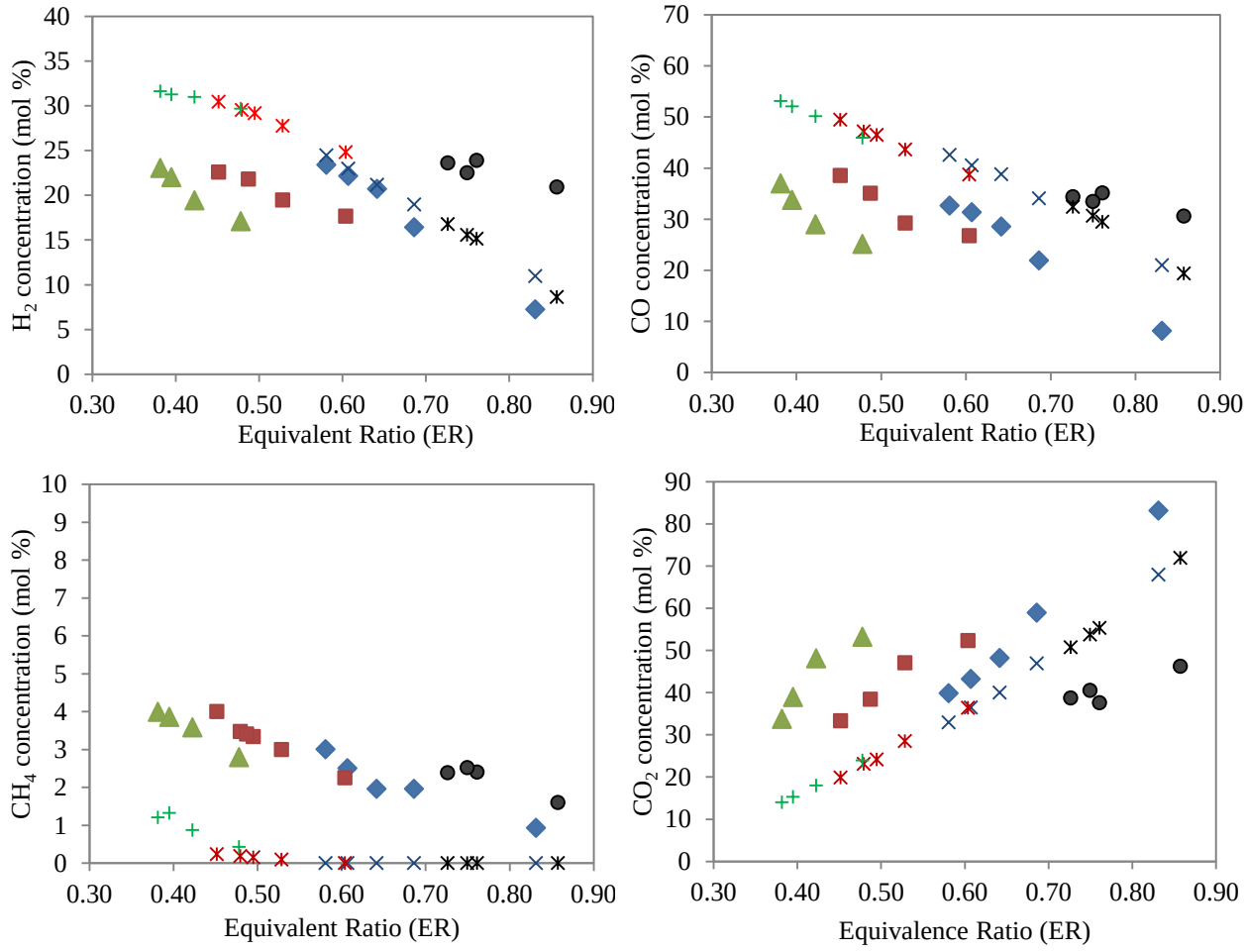

Figure 7–26: Experimental and equilibrium producer gas compositions at different oxygen flow rates (Experimental: ▲600L/h, ■ 900L/h, ◆1500L/h, ● 3000L/h. Equilibrium: + 600L/h, ✳ 900L/h, × 1500L/h, ✳ 3000L/h)

The figure shows that the producer gas compositions obtained from all conditions tested during the experiments were not at equilibrium. Nevertheless as the oxygen flow rate increased from 600 L/h to 1500 L/h, deviations between experimental and equilibrium producer gas compositions became smaller indicating the system's shift towards equilibrium. This behaviour could be explained by considering improvements in the system's kinetics as a result of better spray characteristics when oxygen flow rate was increased from low to higher values, as shown earlier in Section 7.4.3.2.

During gasification at low oxygen flow rate (600L/h), reaction kinetics was relatively low due to poor spray characteristics therefore the system was unable to reach equilibrium within the process residence time. As the oxygen flow rate increased to a 1500 L/h, improvements of spray characteristics contributed significantly to advancement of reaction kinetics which drives the system closer to equilibrium state hence giving better agreements between the experiments and equilibrium predictions. Given sufficiently high reaction kinetics and long residence time, the system will eventually favour products with minimum Gibbs energy and therefore reach equilibrium.

In addition to spray characteristics, gasification temperature also has major influence on whether or not a system is able to reach equilibrium. Equilibrium is likely to be achieved at high gasification temperature as reported by Chhiti et al. [17] who required gasification temperature as high as 1400^{o}C before equilibrium state was finally achieved. In this work, the average temperature during entrained flow gasification of pyrolysis oil at 600L/h, 900L/h and 1500L/h of oxygen flow rates were 720^{o}C, 760^{o}C to 850^{o}C respectively. Despite the relatively lower gasification temperature compared to many entrained flow gasification operations reported in the literature [13, 16, 17, 31, 32], the proximity between experimental and equilibrium producer gas compositions at high oxygen flow rates obtained in this work are promising as this proved the system's ability to reach equilibrium even during gasification at low temperatures.

The aforementioned relationship should hold as long as the system has sufficiently long residence time to allow the producer gas to reach equilibrium. In events when oxygen feeding rates were too high, such as that during gasification at 3000 L/h oxygen flow rate, increase of kinetics were insufficient to compensate the drastic decline of residence time, thus shifting the producer gas composition away from equilibrium composition. However it is interesting to note the higher concentrations of H_2, CO and CH_4 in the producer gas from gasification at 3000 L/h oxygen flow rate, compared to that expected at equilibrium.

This behaviour indicates possible advantages of conducting gasification at exceptionally high kinetics but low residence time, in order to generate producer gas with the highest H_2 and CO concentrations. The trend also suggests gasification at non-equilibrium condition is not necessarily unfavourable since it may

generate producer gas with higher quality if operated under the right operation conditions. Nevertheless, more comprehensive investigations are required to investigate other aspects of gasification performance at this condition such as the producer gas flow rate, tar content and gas yield before any conclusion could be drawn; thus is a subject of further investigations in the future.

7.4.4 Conclusion

In this work, effects of oxygen flow rate on producer gas composition and the system's ability to achieve equilibrium state have been investigated. These investigations prove strong influence of oxygen and pyrolysis oil flow rates in determining producer gas composition during gasification at constant equivalence ratio. This finding is unique because in theory producer gas composition is expected to remain unchanged during constant equivalence ratio gasification due to constant molar ratio between oxygen and pyrolysis oil supplies into the system.

The results show two distinctive trends when the oxygen flow rate is increased at low and high equivalence ratio values. During gasification at high equivalence ratios, increase in oxygen flow rate from 900 L/h to 1500 L/h is found to consistently increase H_2 and CO concentrations in the producer gas while the opposite is observed for CO_2. This relationship can be explained by considering significant improvements in the pyrolysis oil spray characteristics at higher oxygen flow rate, which result more efficient consumption of oxygen molecules by smaller fractions of oil during gasification. This situation consequently allows larger fraction of the oil to involve in non-oxidation reactions thus favouring higher concentrations of H_2, CO and CH_4 in the product.

On the other hand, comparison at low equivalence ratios show opposite trends where gasification at 900 L/h oxygen flow rate generates producer gas with higher concentrations of H_2 and CO than that produced by 1500 L/h gasification. The lower H_2 and CO concentrations in the producer gas at higher oxygen flow rate can be explained by taking into account combined effects of short residence time at high pyrolysis oil flow rate and relatively poor spray characteristics at low equivalence ratio; that may have constrained pyrolysis oil conversion into producer gas during the operation. However, as the residence time increases at increasing equivalence ratio, pyrolysis oil conversion improves more rapidly at 1500 L/h than that at 900 L/h thus giving more rapid growth in H_2 and CO concentrations in the producer gas. The variations in the rate of improvements for pyrolysis oil conversion also relates to the better pyrolysis oil spray characteristics at higher oxygen flow rates that promote more significant advancements of relevant reactions progresses when the residence time is increased.

Besides that, increase of oxygen flow rate from 900L/h to 1500L/h is also found to shift the critical ER value from 0.30 to 0.50 during the operation. The shift of the critical value represents higher demand for oxygen in the system to achieve balance between oxidation and non-oxidation reactions during gasification at higher oxygen flow rates.

Comparison between experimental and equilibrium model producer gas compositions indicates the system's tendency to shift towards equilibrium state when oxygen flow rate is higher during gasification operation. This behaviour could be explained by taking into account rapid improvement of the system's kinetics due to better spray characteristics, as well as increase in gasification temperature when the oxygen flow rate increases from low to higher values. It is also possible that when the oxygen feeding rate is set too high, improvement of reaction kinetics is insufficient to compensate the drastic decline of residence time, thus driving the system away from the equilibrium.

7.4.5 Acknowledgements

This work was funded by the Ministry of Business, Innovation and Employment New Zealand and Ministry of Higher Education Malaysia. The authors would like to thank the sponsors, Alternative Energy Solutions (AES) Ltd. for the pyrolysis oil supplies and technical staffs in the University of Canterbury, New Zealand for their support.

7.4.6 References

1. Van der Drift, A., et al. (2004) *Entrained flow gasification of biomass*.
2. Henrich, E., N. Dahmen, and E. Dinjus, *Cost estimate for biosynfuel production via biosyncrude gasification.* Biofuels, Bioproducts and Biorefining, 2009. **3**(1): p. 28-41.
3. Dahmen, N., et al., *The bioliq® bioslurry gasification process for the production of biosynfuels, organic chemicals, and energy.* Energy, Sustainability and Society, 2012. **2**(1): p. 1-44.
4. Abdullah, H., et al., *Bioslurry as a Fuel. 3. Fuel and Rheological Properties of Bioslurry Prepared from the Bio-oil and Biochar of Mallee Biomass Fast Pyrolysis.* Energy & Fuels, 2010. **24**(10): p. 5669-5676.
5. Whitty, K., *Investigation of Pressurized Entrained-Flow Kraft Black Liquor Gasification in an Industrially Relevant Environment - Annual Topical Report - Year 1*. 2006, University of Utah.
6. Whitty, K., R. Backman, and M. Hupa, *Influence of pressure on pyrolysis of black liquor: 1. Swelling.* Bioresource Technology, 2008. **99**(3): p. 663-670.

7. Kankkunen, A., et al., *Spraying characteristics of mixed black liquor - Two different spraying cases.* The Swedish and Finnish National Committees of the International Flame Research Foundation.
8. Whitty, K., et al., *Influence of pressure on pyrolysis of black liquor: 2. Char yields and component release.* Bioresource Technology, 2008. **99**(3): p. 671-679.
9. Carlsson, P., et al., *Experimental investigation of an industrial scale black liquor gasifier. 1. The effect of reactor operation parameters on product gas composition.* Fuel, 2010. **89**(12): p. 4025-4034.
10. Higman, C. and M. van der Burgt, *Chapter 5 - Gasification Processes*, in *Gasification (Second Edition)*. 2008, Gulf Professional Publishing: Burlington. p. 91-191.
11. Lee, S.H., et al., *Gasification characteristics of coke and mixture with coal in an entrained-flow gasifier.* Energy, 2010. **35**(8): p. 3239-3244.
12. Murthy, B.N., et al., *Petroleum coke gasification: A review.* Canadian Journal of Chemical Engineering, 2013.
13. Qin, K., et al., *High-temperature entrained flow gasification of biomass.* Fuel, 2012. **93**(0): p. 589-600.
14. Xiao, R., et al., *Pyrolysis pretreatment of biomass for entrained-flow gasification.* Applied Energy, 2010. **87**(1): p. 149-155.
15. Zhou, J., et al., *Biomass–oxygen gasification in a high-temperature entrained-flow gasifier.* Biotechnology Advances, 2009. **27**(5): p. 606-611.
16. Chhiti, Y., M. Peyrot, and S. Salvador, *Soot formation and oxidation during bio-oil gasification: experiments and modeling.* Journal of Energy Chemistry, 2013. **22**(5): p. 701-709.
17. Chhiti, Y., et al., *Wood Bio-Oil Noncatalytic Gasification: Influence of Temperature, Dilution by an Alcohol and Ash Content.* Energy & Fuels, 2010. **25**(1): p. 345-351.
18. Chhiti, Y. and S. Salvador, *Gasification of Wood Bio-Oil*. Gasification for Practical Applications. 2012.
19. Creager, N. and R.C. Brown. *High pressure, oxygen blown entrained-flow gasification of bio-oil*. in *AIChE 2012 - 2012 AIChE Annual Meeting, Conference Proceedings*. 2012.
20. Abdoulmoumine, N., A. Kulkarni, and S. Adhikari, *Effects of Temperature and Equivalence Ratio on Pine Syngas Primary Gases and Contaminants in a Bench-Scale Fluidized Bed Gasifier.* Industrial & Engineering Chemistry Research, 2014. **53**(14): p. 5767-5777.
21. Marda, J.R., et al., *Non-catalytic partial oxidation of bio-oil to synthesis gas for distributed hydrogen production.* International Journal of Hydrogen Energy, 2009. **34**(20): p. 8519-8534.

22. Svoboda, K., et al., *Pretreatment and feeding of biomass for pressurized entrained flow gasification.* Fuel Processing Technology, 2009. **90**(5): p. 629-635.
23. Williams, A., *Combustion of Liquid Fuel Sprays*. 1990, London: Butterworth & Co (Publishers) Ltd.
24. Nakamura, M., et al., *Combustion mechanism of liquid fuel spray in a gaseous flame.* Physics of Fluids, 2005. **17**(12): p. 123301.
25. Latifi, M., *Gasification of Bio-oils to Syngas in Fluidized Bed Reactors*, in *Department of Chemical and Biochemical Engineering*. 2012, University of Western Ontario: Ontario.
26. Ricketts, B., et al. *Technology status review of waste/biomass co-gasification with coal*. in *IChemE Fifth European Gasification Conference*. 2002.
27. Higman, C. and M. van der Burgt, *Chapter 2 - The Thermodynamics of Gasification*, in *Gasification (Second Edition)*, C. Higman and M.v.d. Burgt, Editors. 2008, Gulf Professional Publishing: Burlington. p. 11-31.
28. Kunze, C. and H. Spliethoff, *Modelling, comparison and operation experiences of entrained flow gasifier.* Energy Conversion and Management, 2011. **52**(5): p. 2135-2141.
29. Hernández, J.J., et al., *Effect of steam content in the air–steam flow on biomass entrained flow gasification.* Fuel Processing Technology, 2012. **99**(0): p. 43-55.
30. Basu, P., *Chapter 1 - Introduction*, in *Biomass Gasification and Pyrolysis*, P. Basu, Editor. 2010, Academic Press: Boston. p. 1-25.
31. Leijenhorst, E.J., et al., *Entrained flow gasification of straw- and wood-derived pyrolysis oil in a pressurized oxygen blown gasifier.* Biomass and Bioenergy, 2015. **79**: p. 166-176.
32. Qin, K., et al., *Biomass Gasification Behavior in an Entrained Flow Reactor: Gas Product Distribution and Soot Formation.* Energy & Fuels, 2012. **26**(9): p. 5992-6002.

7.5 Non-Slagging Entrained Flow Gasification of Biomass Pyrolysis Oil: Influence of Equivalence Ratio on Tar Species Distribution and Concentrations

This section will be submitted as a research paper in the international journal Biomass and Bioenergy

Abstract:

This work investigated entrained flow gasification of biomass pyrolysis oil at atmospheric pressure and temperatures up to 1100^{o}C. The actual gasification temperature depends on the feeding rates of pyrolysis oil and oxygen into the system. The pyrolysis oil was derived from New Zealand radiata pine wood chips via fast pyrolysis process. The pyrolysis oil was fed into the system as fine spray droplets after impact with oxygen gas as it exits an external mix twin-fluid atomizer. In this article performances of the methods used for tar sampling and analysis for the entrained flow gasification operation were evaluated. The experimental results showed high performance of LC-Si SPE column capturing up to 95 wt% of tar compounds in producer gas and was most effective for Class 2, 4 and 5 tars. LC-NH_2 SPE column, on the other hand, performed well as the second column to capture any tar breakthrough from the LC-Si SPE column. Effects of equivalence ratio on tar species distribution and concentrations were also investigated where the results showed that the overall tar concentrations in producer gas were decreased with increase in the equivalence ratio. The overall tar concentrations dropped from 6.2 g/m^3 to 4.2 g/m^3 when the equivalence ratio was increased from 0.42 to 0.67. In all cases, the tar mainly formed of light polyaromatic hydrocarbon (PAH) compounds (Class 4 tar) with naphthalene being the most abundant tar species. It has been noticed that results from tar analysis using GC could contain significant errors when large variation of tar species were present in the producer gas when pyrolysis oil conversion during the gasification operation was low. In these cases, the total tar concentrations in the producer gas tended to be underestimated; therefore appropriate measures are required to account for the errors.

Keywords: Entrained flow gasification, biomass pyrolysis oil, equivalence ratio, tar species

7.5.1 Introduction

Entrained flow gasification is a promising technology for converting renewable biomass into energy. This technology decomposes feedstock at significantly high temperature, up to 1500ºC, into gaseous products. Gas product from gasification is known as producer gas which contains combustible gas species such as H_2, CO, CH_4 and C_2H_4. Due to the high gasification temperature, conversion of feedstock is rapid and high in the entrained flow gasifier and the residence time is short [1-3]. Entrained flow gasification has been used widely in petrochemical refineries and coal gasification processes, however, its application on biomass feedstock is still relatively new.

One of the biggest challenges for using biomass for energy production is associated with its high moisture content and low density, which induces high costs for handling, storing and transporting the biomass feedstock [2, 4-7]. In addition, woody biomass is highly fibrous hence is difficult to be pulverised into small particles for entrained flow gasification. Pulverization of woody biomass also consumes extensive energy [5, 8].

In order to resolve these challenges, biomass can be pre-treated with torrefaction or densified through fast pyrolysis process [2, 4, 6, 9]. During the fast pyrolysis process, biomass is thermally decomposed into vapour products before being quenched rapidly into liquid form. The liquid product is commonly referred to as pyrolysis oil or bio-oil and its yield from optimised fast pyrolysis can be as high as 75 wt% [10-12].

The use of pyrolysis oil in entrained flow gasification is advantageous as this allows feeding of liquid as fine spray droplets [4, 13] with size as small as 10μm. Entrained flow gasification has also been reported to be capable of generating producer gas with low tar content [3], mainly due to the high gasification temperature. Tar can be defined as a complex mixture of compounds; mainly hydrocarbons that are condensable at reduced temperatures. Tar is usually made of compounds with aromatic rings and may also contain other complex organic compounds. In a more general term, all organic compounds in the producer gas with molecular weight larger than benzene can be categorized as tar [14, 15].

During gasification, biomass is thermally decomposed into both simple gases species such as H_2, CO, CO_2, CH_4, C_2H_4 and C_2H_6; as well as more complex compounds such as naphthalene, acenaphthylene, fluoranthene, pyrene and chrysene. The complex compounds are largely tars, and in some case, the tar concentrations in producer gas are significant which lead to fouling or blockage in downstream process equipment as a result of severe tar deposition upon condensation at lower temperatures.

Some studies have been reported in the literature that explored entrained flow gasification of biomass pyrolysis oil at different operating conditions [16-21]. Creager et al. [20] studied the entrained flow

gasification of pyrolysis oil at 850ºC, and pressures of 1 bar and 6.9 bar, respectively. Results from this study showed strong influence of atomization performance on the producer gas compositions. The study also showed that with increase in the gasification pressure, the H_2 concentration in the producer gas increased while the concentrations of CO, CO_2, CH_4, C_2H_4 and C_2H_6 were decreased.

Marda et al. [18] conducted entrained flow gasification of pyrolysis oil at temperatures between 625ºC to 850ºC. This study investigated effects of temperatures on carbon conversion and producer gas composition at equivalence ratio between 0-0.35. Equivalence ratio (ER) represents the fraction of oxygen used during gasification over that required for theoretical stoichiometric combustion [22], thus ER: 1 represents adequate oxygen for stoichiometric combustion while ER: 0 represents no oxygen supply into the system (pyrolysis condition). The results showed that high carbon conversion could be achieved at gasification temperatures from 700ºC, which is attributed to fast reactions at high temperatures. This study also proved that the equivalence ratio had more significant influence on carbon conversion compared to gasification temperature.

Chhiti et al. [19], on the other hand, studied entrained flow gasification of pyrolysis oil at higher operating temperatures (1000-1400ºC) and equivalence ratio between 0.08-0.5. The results from this study portrayed similar trends as those reported by Marda et al [18], where temperature and equivalence ratio significantly improved carbon conversion during gasification. Increase of gasification temperature was shown to enhance H_2 production while the H_2 concentration was decreased with increasing equivalence ratio. In addition, this work also showed that the soot content in the producer gas decreased with the equivalence ratio.

However, no research has been found in literature on influence of operation conditions on tar species and its concentrations in producer gas in entrained flow gasification of biomass pyrolysis oil. As discussed in separate papers, a new entrained flow gasification system has been developed in this study for gasifying biomass pyrolysis oil at low temperatures (700-1000°C), and effects of operation conditions on gasification performance have been investigated. In this article, influences of equivalence ratio on tar formation during gasification operation have been investigated. The effectiveness of tar sampling and analysis methods adopted in this work were also evaluated to determine their performance for this application. This research will contribute to fundamental understanding of tar formation during entrained flow gasification at various equivalence ratios as well as potential source of errors associated with tar analysis that may influence determination of tar concentrations in the producer gas.

7.5.2 Materials and Methods

7.5.2.1 Feedstock

The pyrolysis oil used in the experiments was produced from radiata pine wood chips through a fast pyrolysis reactor by a local company, Alternative Energy Solutions (AES) Ltd. Measurements of the oil properties were conducted periodically so changes of the oil properties due to ageing were recorded over time. Results from pyrolysis oil properties measurements are reported in previous paper (refer to Section 7.2 in Table 7-2).

7.5.2.2 Entrained flow gasification system

The entrained flow gasifier developed in this study is capable of operation at atmospheric pressure and maximum temperature of 1100ºC. LPG burners are used to pre-heat the system to the desired start-up temperature prior to any gasification run. Pyrolysis oil and oxygen gas are introduced into the system through an external mix twin-fluid atomizer of model 1/4J SUE15B, manufactured by Spraying Systems Co which capable of generating fine spray droplets in a flat spray pattern. The use of external mix atomizer allows for independent control of pyrolysis oil and oxygen flow rates during atomization thus enable maximum control of the desired spray characteristics by adjustment of only one parameter at a time. The atomizer is surrounded by a water cooling jacket so it remains at low temperature to prevent plugging of the oil feeding system due to pyrolysis oil polymerization.

Detailed information on the entrained flow gasification system and its design can be found in the previous paper (Section 7.2) in Section 7.2.2.2.

7.5.2.3 Experimental procedures

During experiments, the reactor was first heated up to 750ºC. When the system reached this temperature, pyrolysis oil was fed into the system using a peristaltic pump at flow rates up to 70 mL/min. The flow rate was measured using a positive displacement flow meter installed after the pump. Then oxygen gas was injected into the system in the range between 600-1500 L/h to start gasification. Once the system stabilized at the gasification conditions, samples of producer gas and tar were taken from the sampling line for analysis. In these experiments, only a small fraction of producer gas was sampled while the main stream of producer gas was combusted in an after-burner.

The gasification temperature was dependent on the heat generated from partial combustion of pyrolysis oil spray with oxygen upon leaving the atomizer thus the gasification temperature is related to the feeding rates of pyrolysis oil and oxygen. The equivalence ratio values were also calculated based on these flow rates. During a gasification run, the oxygen gas flow rate was set to a constant value while the pyrolysis oil flow rate was changed depending on the required equivalence ratio. In all runs, the system was allowed to stabilize for at least 20-30 minutes before the first sample was taken for analysis. The interval between two consecutive samplings was 10-15 minutes. It is expected that the gasification process is rapid with residence time of 1-5 seconds; therefore, the producer gas yield and composition at a new gasification condition should stabilize reasonably quickly.

7.5.2.4 Sampling method

All products of gasification exit the gasifier through a port located at the bottom of the gasifier. The temperature of the product line usually remains between 450-600^{o}C depending on the temperature of products flowing in it. To prevent condensation of tar compounds during the sampling, the probe used for sampling was positioned at the centre of producer gas flow so that the temperature difference between the probe and the flowing gas was insignificant. In addition, the sampling probe length was kept as short as possible to maximize adsorption of condensable products onto solid phase extraction (SPE) column packed bed. Two SPE columns with different packed materials were used in every sample to make sure the gas samples collected were free from condensable compounds such as water and tar.

The first SPE column used to capture condensable products in this study is a model of Supelclean LC-Si column with packing of a silica gel based material with no bonded phase hence is extremely hydrophilic. The second SPE column is a model of Supelclean LC-NH_2 column with packing of a silica gel based material bonded with aminopropyl active group. This column was aimed for strong adsorption of polar, weak anion and organic acid compounds.

Details of the product sampling assembly have been reported in the previous paper (Section 7.2.2.4). During each product sampling, a total of 200-300 mL of producer gas from the gasification system was passed through the SPE columns, aiming to trap as much tar compounds as possible. After sampling was completed, the sampling probe and the SPE columns containing tar were removed from the sampling assembly, sealed and stored in a refrigeration unit at temperature of 4°C ready for tar extraction and analysis.

7.5.2.5 Tar extraction and analysis

In order to extract the tar compounds trapped in the SPE columns, solvents with high solubility of tars and other required properties were used. The methods used to extract and analysis tar in this work were obtained from [23] and were modified accordingly to suit entrained flow gasification products and operations. Two extraction solvents of dichloromethane (DCM) and isopropanol (IPA) were used to extract most tar compounds adsorbed to the SPE column matrix. DCM is a non-polar solvent and was used to flush off less-polar compounds such as naphthalene, acenaphthalene, fluoranthene, pyrene and chrysene from the SPE column. On the other hand, polar IPA solvent was used to extract polar compounds such as phenol, toluene, xylene, cresol and styrene from the column. During tar extraction, weak polarity compounds like polycyclic aromatic hydrocarbons (PAH) were extracted by flushing the columns with 0.9 mL of the DCM solvent into a 2 mL vial. Meanwhile, more polar tar compounds were extracted by flushing the same SPE columns with 0.9 mL of the IPA solvent. In both approaches, 0.1 mL of 400 ppm of n-dodacane was added into the vials to act as an internal standard (IS) during tar analysis.

Species of tar present in the producer gas were determined using a gas chromatography (GC) of Varian CP-3800 model with a flame ionization detector (GC-FID). The GC column used for this analysis was a 50% phenyl and 50% dimethyl-polysiloxane fused silica capillary with dimensions of 30m x 0.25 µm x 0.25µm. Tar analysis was performed at temperature of 300^{o}C using Helium as the carrier gas (1 mL/min).

7.5.3 Results and Discussions

7.5.3.1 Tar adsorption and extraction performance

A complete list of all tar species analysed in this study along with their retention times are given in Table 7-5. Calibration of the tar species were obtained from two calibration standards containing mixture of various hydrocarbon compounds at 2000 µg/mL in DCM solvent. The first calibration standard was 8270 Calibration Mix #5 manufactured by Restek Co. containing PAH compounds such as naphthalene, acenaphthylene, fluorene, phenanthrene, fluoranthene, pyrene and chrysene. The second calibration standard, on the other hand was a custom mix calibration standard from Sigma Aldrich Co. containing various aromatic compounds such as benzene, toluene, pyridine, xylenes, styrene and phenol.

Table 7-5: List of tar species used in this study during tar analysis

Tar #	Retention Time (min)	Tar Species	Tar Class #
1	2.4	Toluene	3
2	2.7	Pyridine	2
3	3.4	p-xylene + Ethylbenzene	3
4	3.5	m-xylene	
5	3.9	o-xylene	
6	4.1	Styrene	
7	5.7	Phenol	2
8	6.4	Dodecane	N/A
9	6.7	Indene	4
10	6.9	o-cresol	2
11	7.2	m+p-cresol	
12	9.1	Naphthalene	4
13	10.4	Quinoline	2
14	10.6	2-Methylnaphthalene	4
15	10.7	Isoquinoline	2
16	10.9	1-Methylnaphthalene	4
17	11.9	Biphenyl	
18	13.2	Acenaphthylene	
19	13.5	Acenapthene	
20	14.7	Fluorene	
21	17.3	Phenanthrene	
22	17.3	Anthracene	
23	18.8	Fluoranthene	5
24	19.0	Pyrene	
25	19.9	Bens(a)anthracene	
26	19.9	Chrysene	
27	20.8	Benso(b)fluoranthene	
28	20.8	Benso(k)fluoranthene	
29	21.2	Benso(a)Pyrene	
30	22.6	Indeno(1,2,3-cd)pyrene	
31	22.7	Benso(g,h,i)perylene	
32	23.3	Dibenso(a,h)anthracene	

As observed in Table 7-5, tar components can be categorized into five major classes [15]. Such classification is important because not all tar classes condense into undesirable products and cause problems during operations. Therefore, priority should be given to tar classes and species which are

detrimental to gasification operations. Brief descriptions of each tar class used in this study are provided as in Table 7-6.

Table 7-6: Description of tar classes and example compounds [adapted from [15]]

Tar Class	Class Name	Major Descriptions
1	GC undetectable	This class consists of very large PAH molecules. Molecules in this class usually have very high dew points hence condense at high temperatures. As a result, these compounds cannot be detected by GC for analysis.
2	Heterocyclic aromatics (≥ 1 ring)	Molecules in this class are not classified as hydrocarbon. They contain atoms other than hydrogen and carbon such as oxygen and nitrogen in their molecules. Due to their relatively polar nature, molecules in this class are highly soluble in water, thus poses a significant threat to the environment.
3	Light aromatics hydrocarbons (1 ring)	Tars in this class are small hydrocarbons with single aromatic ring in its structure. Due to its nature, its condensation and solubility poses no major issue on process equipment during operations.
4	Light PAH (2-3 rings)	Tars in this class are hydrocarbons with 2-3 rings in its structure. The dew point of these molecules are low, thus poses risks of tar condensing at reasonably low temperatures.
5	Heavy PAH (4-7 rings)	Tars in this class consist of aromatic hydrocarbons with more than 3 rings in its structure. The dew point of these molecules are high thus favours condensation even at high operation temperatures. These tar class cause high risk of plugging during gasification operation.

Prior to any tar analysis, the two calibration standards were mixed and diluted into several low concentrations mixtures before being used by the GC to generate 31 calibration curves for individual tar components in the mixture. Note that in Table 7-5, dodecane is not a tar species rather it was added separately to act as an internal standard during calibration and tar measurements in order to minimize errors from solvent evaporation.

From the gasification results, it is found that 95% of the tar adsorbed to the SPE columns from producer gas was successfully captured by the first SPE column (Supelclean LC-Si). In all tar samples analysed in this study, heterocyclic aromatic compounds (Class 2) were captured completely by this column. PAH compounds (Class 4 and 5) were also mostly captured by this column with percentages of tar being captured between 91-100 wt%. Light aromatic hydrocarbon compounds (Class 3) was also captured in this column but accounted for only up to 52 wt% of the overall Class 3 tar in the producer gas.

The second SPE column (Supelclean LC-NH_2), on the other hand, captured the remaining tar after the first column most of which is Class 3 tar in the producer gas. In some cases, this column was recorded to have captured up to 91 wt% of Class 3 tar present in the producer gas. Nevertheless, the total tar captured in this column was relatively small, with the maximum of 7 wt% of the overall tar present in producer gas samples. Although the amount of tar captured in the second column was low, the presence of tar in this column proves compounds breakthrough from the first SPE column thus marking the importance of having a second SPE column during tar sampling, especially when tar concentration in producer gas is high.

Form the tar analysis results it is also found that during tar extraction, most tar compounds were extracted by the first flush with IPA solvent. Tar extracted by this solvent accounted for 65-94 wt% of the total tar compounds. The effective extraction of tar compounds by IPA applies to both LC-Si and LC-NH_2 columns regardless of their packing nature. The remaining tar which was not extracted by IPA solvent were flushed with DCM solvent, which accounted for 6-35 wt% of the total tar compounds. DCM is a suitable solvent for extracting less polar Class 5 tar compounds, particularly for the LC-NH_2 column, due to the tar molecules non-polar nature.

7.5.3.2 Influence of equivalence ratio on individual tar species distribution and concentrations

Figure 7–27 shows the overall tar concentrations in the producer gas from entrained flow gasification of pyrolysis oil as a function of equivalence ratio between 0.42 – 0.67.

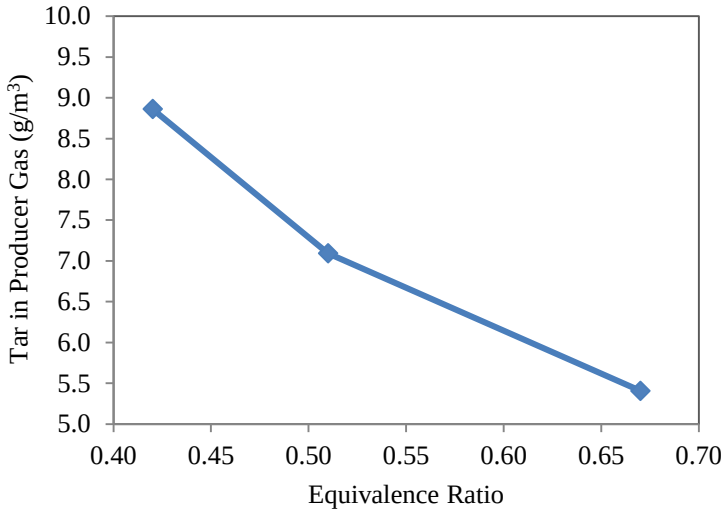

Figure 7–27: Overall tar concentration in the producer gas from pyrolysis oil entrained flow gasification as a function of equivalence ratio.

From Figure 7–27 it is observed that the tar concentrations in producer gas decreased with the equivalence ratio. This trend is consistent with that reported in literature as expected. With increase in the equivalence ratio at a given fuel flow rate, more oxygen was supplied into the system, therefore, gasification temperature was increased. In this way, some tar and other heavy molecules were oxidized and cracked into lighter hydrocarbon molecules and non-condensable gases. In this regard, Wu et al. [24] showed that the tar yield was significantly reduced with even small increase in equivalence ratio by 0.025 (from 0 to 0.025) during gasification, in which case, the tar content is the producer gas was reduced from 10 wt% to below 6 wt%. With further increases in the equivalence ratio to 0.34, the tar content in the producer gas reached a minimum value of 0.26 wt%.

Using tar classification presented in Table 7-6, concentrations of each class of tar in producer gas during entrained flow gasification of pyrolysis oil are shown in Figure 7–28.

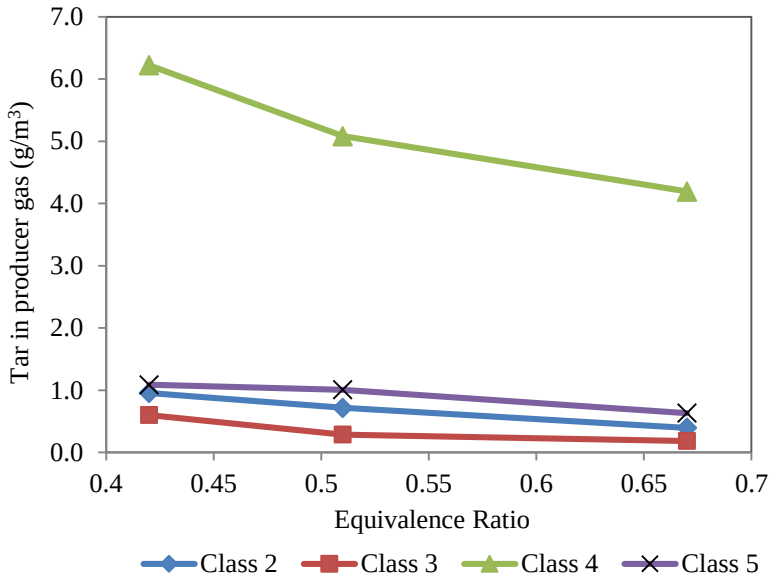

Figure 7–28: Concentrations of individual tar classes at different equivalence ratio

It is clear from the figure that with increase in the equivalence ratio, concentrations of all tar classes were decreased. In particular, the concentration of Class 4 tar decreased most rapidly from 6.2 g/m^3 to 4.2 g/m^3 when the equivalence ratio was increased from 0.42 to 0.67. Decrease in concentrations of Classes 2, 3 and 5 tars were also observed with increasing equivalence ratio, but reduction rates were much less in comparison with Class 4 tar.

Figure 7–28 also shows that Class 4 tar is the greatest contributor to overall tars in the producer gas during entrained flow gasification of biomass pyrolysis oil, accounting for 70% of the total tars at equivalence ratio of 0.42 and 78% at equivalence ratio of 0.67 respectively. This information indicates that light PAH compounds with 2-3 aromatic rings are the major components of tar in the producer gas. In order to explain the rapid formation of Class 4 tar compounds in the producer gas, information on individual tar species within this tar class were also analysed. Figure 7–29 summarizes concentration distribution of Class 4 tar species found in the producer gas at different equivalence ratios for comparisons.

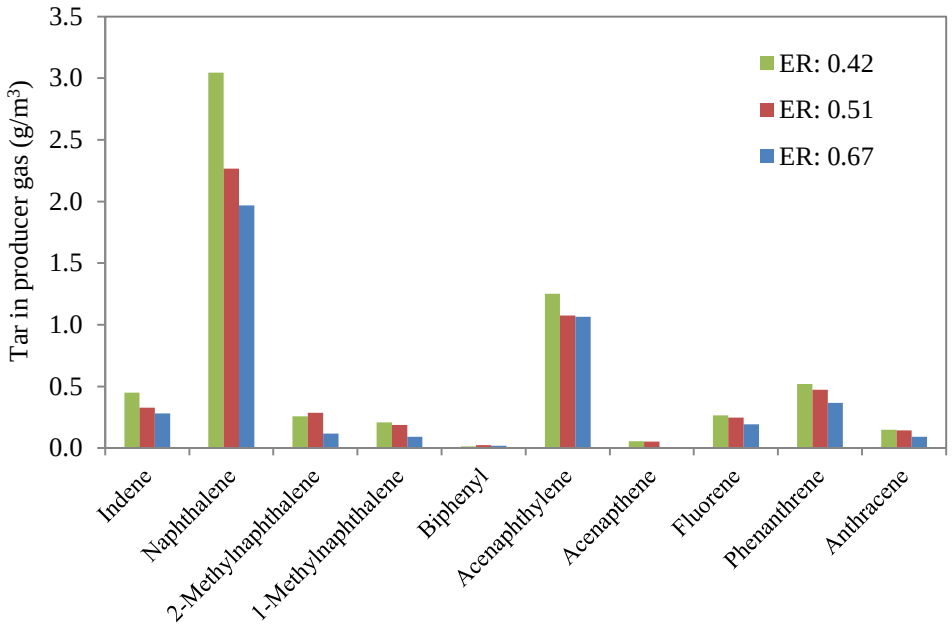

Figure 7–29: Individual concentrations of class 4 tar species in the producer gas at different equivalence ratios.

From the figure it is clear that naphthalene was the major compound in the Class 4 tar, varying from 3.05 g/m^3 at ER of 0.42 to 1.97 g/m^3 at ER of 0.67. In fact, the naphthalene concentration in the producer gas was consistently the highest among all of the tar species detected in the producer gas, regardless of the equivalence ratio. During entrained flow gasification at equivalence ratio 0.67 as an example, naphthalene alone contributed as much as 36 wt% of the overall tar in the producer gas, followed by acenaphthylene (20 wt%), phenanthrene (7 wt%) and indene (5 wt%).

The results from this study can be used for optimisation of gasification operation conditions in order to minimise the tar content in the producer gas. It is useful to understand the fundamentals on the formation of PAH compounds at high temperatures. It is reported by Kislov et al. [25] that the formation of large polyaromatic structures are most likely resulted from addition of cyclic ring on smaller tar structures during its conversion. Kislov et al. [25] showed addition of cyclopenta (five membered ring) on naphthalene as the more favourable pathway during formation of PAH with higher aromatic rings at high temperatures. The study found large production of cyclopenta-fused PAH products such as acenaphthylene, 4-ethynylacenaphthalene and 1-methylene-1H-cyclopenta[b]naphthalene from the initial naphthalene molecules, which accounted for up to 75% of the total yield; as opposed to the products of six membered ring (benzene) addition such as anthracene and phenanthrene, which only contributed to 6% of the total PAHs formed from naphthalene.

While direct conversion of naphthalene into anthracene and phenanthrene were not favoured, these species may still be formed at the presence of acetylene (C_2H_2) in the reaction environment. This reaction pathways was reported in [25] where acetylene was found to react with cyclopenta-fused PAH compounds such as acenaphthylene to form phenanthryl radical intermediate and eventually phenanthrene, as illustrated in Figure 7–30.

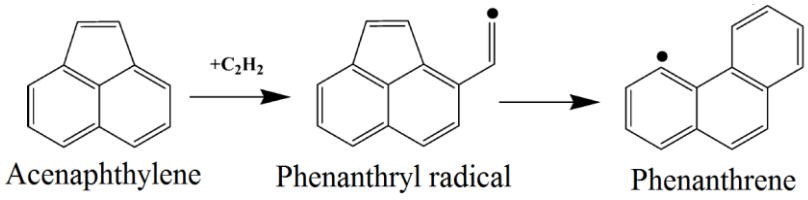

Figure 7–30: Multi-step formation of phenanthrene from acenaphthylene [adapted from Kislov et al. [25]]

The multi-step formation of PAH species provides a reasonable explanation to the concentration distribution of Class 4 tar major components as shown in Figure 7–29. The naphthalene was an important precursor for formation of acenaphthylene, which was then a precursor for formation of anthracene and phenanthrene in the producer gas.

Indene on the other hand is different from other Class 4 tar species since this compound contains only one six-member ring that fuses with a five membered cyclopentene ring in its structure. Production of indene was reported to be more favourable at low temperatures, which is opposite to formation of benzene and naphthalene [26] – thus explaining low concentration of indene but high concentration of naphthalene as tars species in the producer gas from entrained flow gasification at high temperatures.

If similar growth principle presented for larger PAH molecules applies to indene, this compound may also react with acetylene molecule to form naphthalene hence also contributed to high naphthalene concentrations in the producer gas.

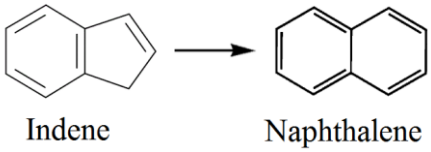

Figure 7–31: Formation of naphthalene from indene

The species and concentrations of tar formed in Class 4 also have strong influence on Class 5 tar concentrations during the entrained flow gasification of pyrolysis oil. Although concentrations of Class 5 tar species in most cases were much lower than those of Class 4 tar, there was a consistent correlation

between major tar species in both classes. Individual species concentrations for Class 5 tar as measured in this work were plotted in Figure 7–32.

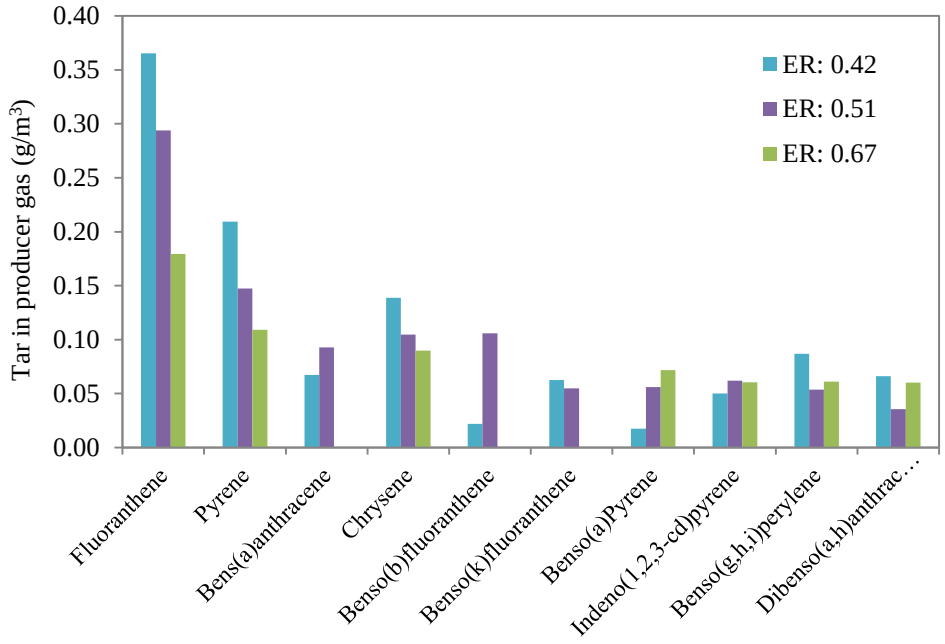

Figure 7–32: Individual concentrations of class 5 tar species at different equivalence ratio

Comparing the three major components of Class 5 tar (fluoranthene, pyrene and chrysene) with those of Class 4 tar (naphthalene, acenaphthalene and phenanthrene), it is likely that the Class 5 tar species were formed with cyclopenta ring addition to corresponding Class 4 tar compounds. According to this conversion pathway, formation of fluoranthene, pyrene and chrysene are formed from acenaphthalene and phenanthrene as illustrated in Figure 7–33.

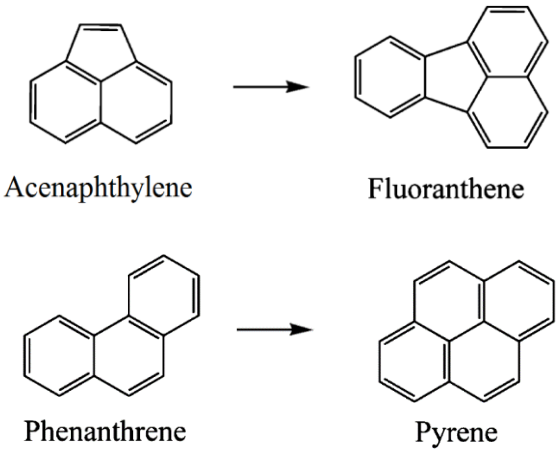

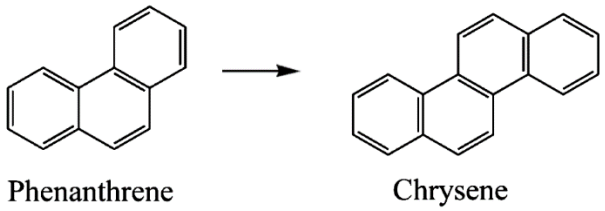

Figure 7–33: Proposed pathways for conversion of Class 4 tar major components into Class 5 tar major components during the entrained flow gasification of biomass pyrolysis oil.

Fluoranthene concentration was consistently the highest amongst all other Class 5 tar species due to its rapid formation from abundant acenaphthylene species in the producer gas. Similar pathway applies to pyrene and chrysene concentrations where their formations were relatively more favoured than other Class 5 species due to high concentrations of phenanthrene in the producer gas.

7.5.3.3 Potential sources of errors in measurement of tar concentrations in producer gas

While measurements of tar concentrations in producer gas by GC have acceptable accuracy in general, in certain circumstances, results from GC may have error level above expectation due to its dependency on the limited number of tar species defined during its calibration. In this work as an example, a mixture of 31 chemical compounds were used as the calibration standard to represent major tar species expected in the producer gas from entrained flow gasification of pyrolysis oil. However in some cases, wider range of tar species may present in the producer gas therefore some tar species may be unable to be identified hence were not accounted for towards the overall tar concentrations in the producer gas. Figure 7–34 shows an example of result from GC analysis with tar sample that contains wider range of tar species compared to that in the calibration standard.

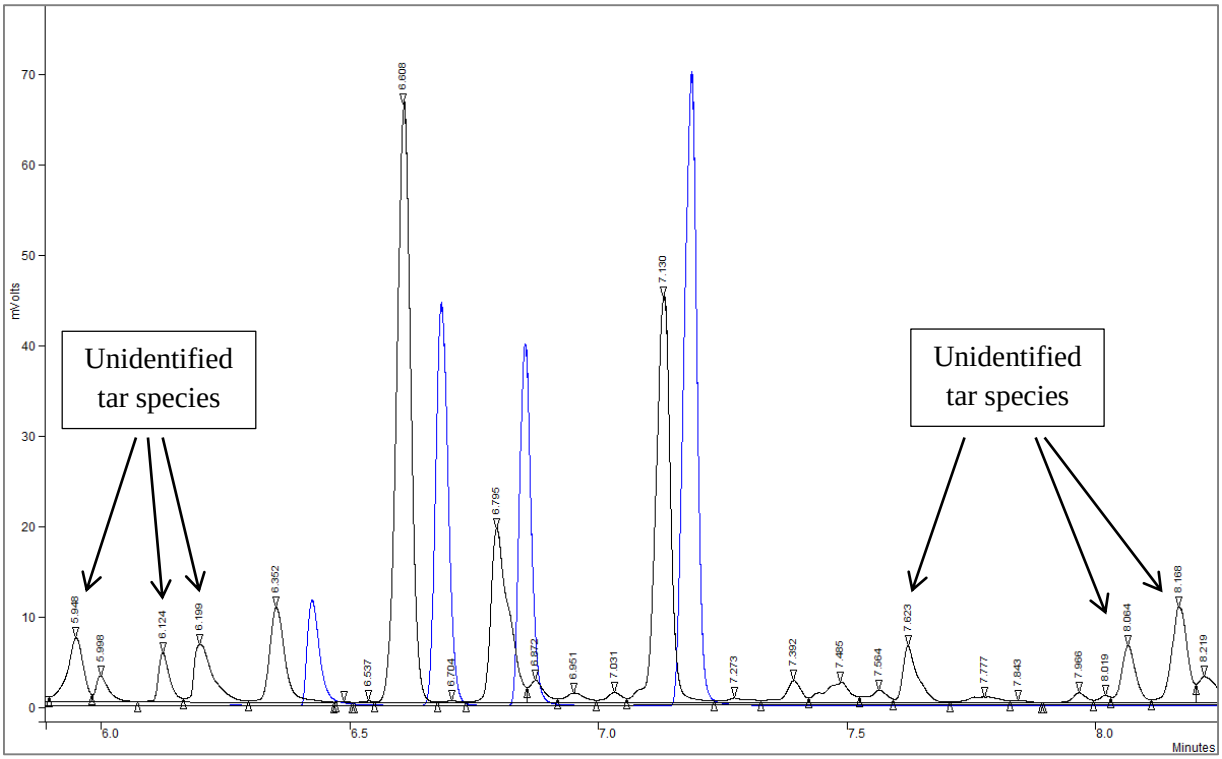

Figure 7–34: Example of GC signal plot showing unidentified tar species, where the blue curve represents calibrated tar species while the black curve represents the actual tar compounds in the producer gas

In order to improve this situation, calibration standards with more tar species are required during GC calibration so the unidentified peaks from GC analysis could be determined and ultimately analysed for their contributions.

Another major source of error found during tar determination in this work was associated with poor decomposition of pyrolysis oil chemical compounds, which resulted in remarkably high percentages of organic compounds directly transferred from the pyrolysis oil to the producer gas. Such condition could have taken place as a result of slow reaction kinetics or during gasification with extremely short residence time. These compounds, once formed, present as vapour at high temperatures, and were then adsorbed on SPE columns during sampling which could be extracted out during flushing with the appropriate solvents.

This error could be clearly identified from tar analysis plot generated by the GC, where the component signal peaks were too many and severely overlapping one another, as illustrated in Figure 7–35. In the figure, the actual tar picks as measured from tar samples are shown as the black curve while the known tar species used during calibration are shown as the purple curves tar picks.

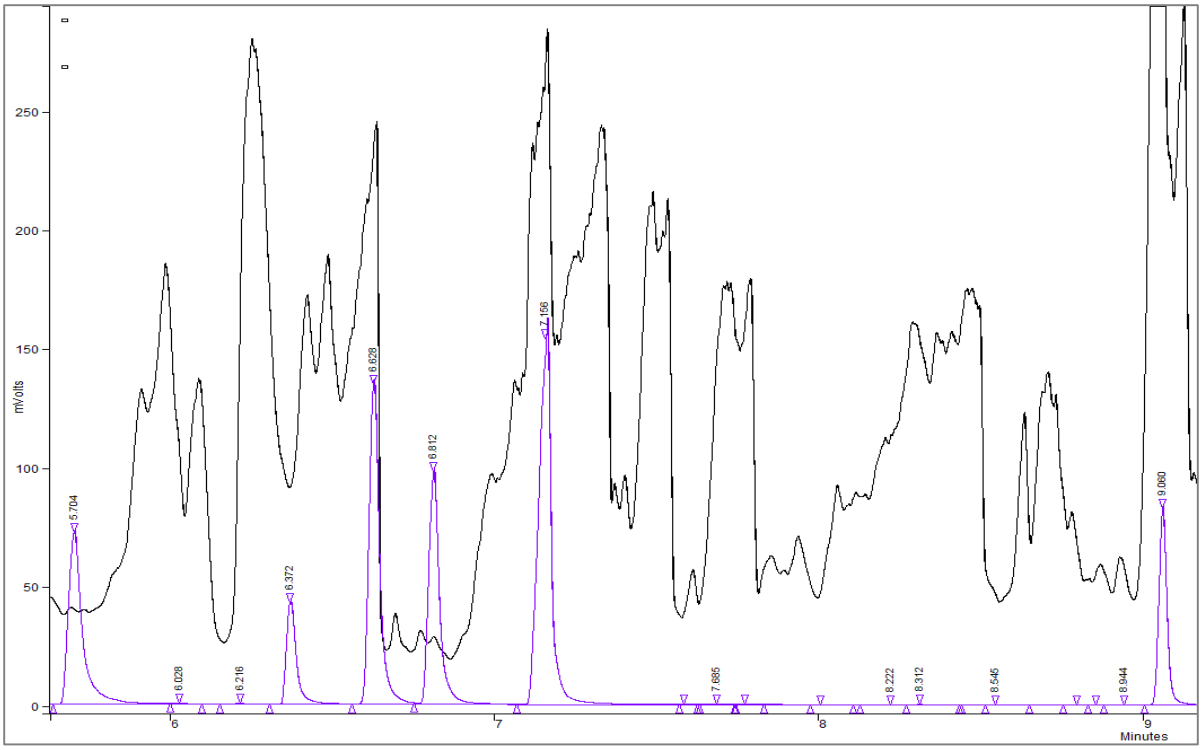

Figure 7–35: Example of GC signal plot from unsuccessful tar analysis, where the purple curve represents calibrated tar species while the black curve represents the actual tar compounds in the producer gas

It is important that such error is identified during analysis since it leads to major discrepancies in the tar concentration results. Tar samples showing such behaviour should not be used for GC analysis, unless appropriate tar standards that can identify every overlapping peak detected in the analysis is used. In addition, the settings, methods and capillary column used by the GC for the analysis may also have to be changed to improve separations between each individual peaks in the results. Considering the abundance of unidentified peaks and the severity of overlapping problem in the result, analysis of such tar samples are often not practical to be done using GC.

For accurate determination of overall tar concentrations, gravimetric method is useful. Gravimetric tar analysis is performed by accurately measuring the mass of SPE columns before and after sampling so weight differences caused by tar adsorption in the columns could be determined. This approach requires large producer gas samples considering the relatively small tar content in the producer gas expected from entrained flow gasification. In addition, effects of water condensation should be completely eliminated from the tar samples so accurate measurement of tar mass in the producer gas could be made.

Another alternative method for measurement of overall tar content is to use series of impinging bottles filled with solvents to trap tar which has been described in [15]. Major drawback associated with this

approach is that the sampling setup is generally more complicated and the setup can only be used for sampling one operation condition at a time. In addition, analysis of solvents used to trap the tar in producer gas are also performed using GC, hence there are similar limitations to this approach as discussed earlier in the paper.

In occasions where GC results such that in Figure 7–35 are still used without appropriate calibration standards, this will lead to severe underestimation of the tar content in the producer gas from its true values. Figure 7–36 illustrates comparisons between successful and unsuccessful GC analysis and deviations from the expected trend at varying equivalence ratio.

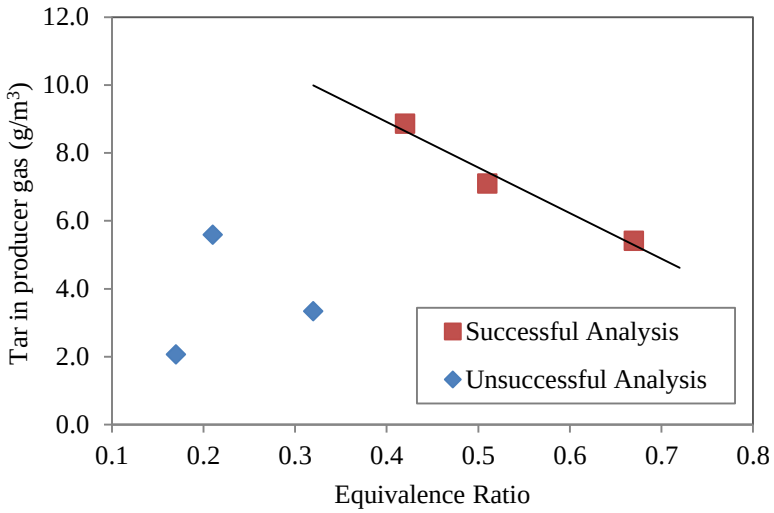

Figure 7–36: Underestimation of total tar concentration from unsuccessful tar analysis in comparison to the expected trend

7.5.4 Conclusion

In this article, effect of equivalence ratio on tar species distribution and concentrations in the producer gas from entrained flow gasification of biomass pyrolysis oil has been investigated. Performance of methods used during tar sampling and analysis were also tested. The results show the LC-Si SPE column is able to capture most tar compounds in producer gas, up to 95 wt% of the total tar. This column is most effective for Class 2, 4 and 5 tars. LC-NH_2 SPE column, on the other hand, performs well as the second column to capture any tar breakthrough from the first column and adsorb Class 3 tar in the producer gas. Class 3 tar can also be captured by the LC-Si column although the adsorption in LC-NH_2 column is most efficient.

For tar extraction from the solid phase extraction (SPE) column, isopropanol (IPA) is a suitable solvent and it can extract most tars (up to 94%) from both SPE columns regardless of the columns packing properties. On the other hand, dichloromethane (DCM) is effective for extraction of non-polar compounds from the columns. In addition, DCM is also capable of flushing any remaining tars in the SPE columns after the first flush with IPA.

The experimental results show that the overall tar content in producer gas decreases with increase in the equivalence ratio during entrained flow gasification of biomass pyrolysis oil. When the equivalence ratio is increased from 0.42 to 0.71, the tar concentrations dropped from 6.2 to 4.2 g/m^3. It is also found that, among the 5 classes of tars, Class 4 tar are the most abundant compounds accounting for 70-78% of the total tar concentrations at equivalence ratio between 0.42 and 0.68. The class 4 tar mainly consists of light PAH compounds in which naphthalene is the single most abundant tar compound found in the producer gas. The results of concentrations of major tar compounds in the producer gas are attributed to PAH formation through cyclopenta (five membered) ring addition where heavier PAH compounds are formed by cyclic ring addition on lighter PAH tar structures.

Although determination of tar contents in producer gas by GC are generally at satisfied accuracy, the results are dependent on the limited number of tar species defined during GC calibration. In cases where wider range of tar species is present in the producer gas, some tar species may not be able to be identified during tar analysis hence are not accounted for towards the final tar content calculations. Results of tar analysis may also be compromised when pyrolysis oil conversion in entrained flow gasification is poor as a result of slow reaction kinetics or short residence time. In both cases, the total tar content in producer gas measured by the GC will be underestimated; therefore appropriate measures are required to account for the errors.

7.5.5 Acknowledgements

This work was funded by the Ministry of Business, Innovation and Employment New Zealand and Ministry of Higher Education Malaysia. The authors would like to thank the sponsors, Alternative Energy Solutions (AES) Ltd. for the pyrolysis oil supplies and technical staffs in the University of Canterbury, New Zealand for their support.

7.5.6 References

1. Qin, K., et al., *High-temperature entrained flow gasification of biomass.* Fuel, 2012. **93**(0): p. 589-600.
2. Xiao, R., et al., *Pyrolysis pretreatment of biomass for entrained-flow gasification.* Applied Energy, 2010. **87**(1): p. 149-155.
3. Zhou, J., et al., *Biomass–oxygen gasification in a high-temperature entrained-flow gasifier*. Biotechnology Advances, 2009. **27**(5): p. 606-611.
4. Henrich, E., N. Dahmen, and E. Dinjus, *Cost estimate for biosynfuel production via biosyncrude gasification.* Biofuels, Bioproducts and Biorefining, 2009. **3**(1): p. 28-41.
5. Abdullah, H., et al., *Bioslurry as a Fuel. 3. Fuel and Rheological Properties of Bioslurry Prepared from the Bio-oil and Biochar of Mallee Biomass Fast Pyrolysis.* Energy & Fuels, 2010. **24**(10): p. 5669-5676.
6. Abdullah, H. and H. Wu, *Bioslurry as a Fuel. 4. Preparation of Bioslurry Fuels from Biochar and the Bio-oil-Rich Fractions after Bio-oil/Biodiesel Extraction.* Energy & Fuels, 2011. **25**(4): p. 1759-1771.
7. Manzer, L. *Recent developments in the conversion of biomass to renewable fuels and chemicals*. 2009.
8. Van der Drift, A., et al. (2004) *Entrained flow gasification of biomass*.
9. Sarkar, S. and A. Kumar, *Large-scale biohydrogen production from bio-oil.* Bioresource Technology, 2010. **101**(19): p. 7350-7361.
10. Johansson, D., P.T. Franck, and T. Berntsson, *Hydrogen production from biomass gasification in the oil refining industry - A system analysis.* Energy, 2012. **38**(1): p. 212-227.
11. Chhiti, Y., *Non catalytic steam gasification of wood bio-oil*. 2011.
12. Bridgwater, A.V., *Review of fast pyrolysis of biomass and product upgrading.* Biomass and Bioenergy, 2012. **38**(0): p. 68-94.
13. Dahmen, N., et al., *The bioliq® bioslurry gasification process for the production of biosynfuels, organic chemicals, and energy*. Energy, Sustainability and Society, 2012. **2**(1): p. 1-44.
14. Devi, L., K.J. Ptasinski, and F.J.J.G. Janssen, *A review of the primary measures for tar elimination in biomass gasification processes.* Biomass and Bioenergy, 2003. **24**(2): p. 125-140.
15. Li, C. and K. Suzuki, *Tar property, analysis, reforming mechanism and model for biomass gasification—An overview*. Renewable and Sustainable Energy Reviews, 2009. **13**(3): p. 594-604.
16. Chhiti, Y., et al., *Wood Bio-Oil Noncatalytic Gasification: Influence of Temperature, Dilution by an Alcohol and Ash Content.* Energy & Fuels, 2010. **25**(1): p. 345-351.

17. Chhiti, Y., et al., *Thermal decomposition of bio-oil: Focus on the products yields under different pyrolysis conditions.* Fuel, 2012. **102**(0): p. 274-281.
18. Marda, J.R., et al., *Non-catalytic partial oxidation of bio-oil to synthesis gas for distributed hydrogen production.* International Journal of Hydrogen Energy, 2009. **34**(20): p. 8519-8534.
19. Chhiti, Y., M. Peyrot, and S. Salvador, *Soot formation and oxidation during bio-oil gasification: experiments and modeling*. Journal of Energy Chemistry, 2013. **22**(5): p. 701-709.
20. Creager, N. and R.C. Brown. *High pressure, oxygen blown entrained-flow gasification of bio-oil*. in *AIChE 2012 - 2012 AIChE Annual Meeting, Conference Proceedings*. 2012.
21. Chhiti, Y. and S. Salvador, *Gasification of Wood Bio-Oil*. Gasification for Practical Applications. 2012.
22. Abdoulmoumine, N., A. Kulkarni, and S. Adhikari, *Effects of Temperature and Equivalence Ratio on Pine Syngas Primary Gases and Contaminants in a Bench-Scale Fluidized Bed Gasifier.* Industrial & Engineering Chemistry Research, 2014. **53**(14): p. 5767-5777.
23. Saw, W.L. and S. Pang, *The influence of calcite loading on producer gas composition and tar concentration of radiata pine pellets in a dual fluidised bed steam gasifier.* Fuel, 2012. **102**(0): p. 445-452.
24. Wu, W.-g., et al., *Experimental Investigation of Tar Conversion under Inert and Partial Oxidation Conditions in a Continuous Reactor*. Energy & Fuels, 2011. **25**(6): p. 2721-2729.
25. Kislov, V.V., A.I. Sadovnikov, and A.M. Mebel, *Formation Mechanism of Polycyclic Aromatic Hydrocarbons beyond the Second Aromatic Ring.* The Journal of Physical Chemistry A, 2013. **117**(23): p. 4794-4816.
26. Wang, D., et al., *Formation of Naphthalene, Indene, and Benzene from Cyclopentadiene Pyrolysis: A DFT Study.* The Journal of Physical Chemistry A, 2006. **110**(14): p. 4719-4725.

8 GENERAL CONCLUSIONS

In this work, a new non-slagging entrained flow (EF) gasifier for gasification of biomass pyrolysis oil was successfully developed and tested for different gasification conditions. The gasification runs were conducted at atmospheric pressure while the operation temperatures were dependent on the heat generated from partial combustion of pyrolysis oil with oxygen upon leaving the atomizer. The system used oxygen gas as the gasification agent and was proven to be capable of converting biomass pyrolysis oil into producer gas with high H_2 and CO concentrations.

In addition, cold model experiments were conducted to investigate the performance of the selected atomizer (external mix twin-fluid atomizer) and the factors affecting the spray characteristics. It is found that the external mix twin-fluid atomizer is advantageous than other types of atomizer as it allows superior control of atomization performance by independent adjustments of pyrolysis oil and oxygen flow rates. Results obtained in this study showed both flow rates of pyrolysis oil and oxygen gas have distinct influence on the resulted spray characteristics and consequently gasification performance. In addition, by using an external mix configuration, mixing between spray droplets and oxygen gas could also be altered by simple adjustment of pyrolysis oil and oxygen gas feeding rate into the system.

The experiments on EF gasification show that the producer gas flow rate was virtually linearly increased with the pyrolysis oil feeding rate which is expected. Oxygen feeding rate, on the other hand, has dominant impact on gasification temperature in comparison with the influence by pyrolysis oil feeding rate. At constant pyrolysis oil flow rate, the gasification temperature increases significantly with increase of oxygen feeding rate as a result of enhanced exothermic oxidation reactions.

At a given oxygen feeding rate, increase in pyrolysis oil flow rate has negative impact on pyrolysis oil atomization performance and generates larger droplet sizes. At higher oil feeding rate, more producer gas is generated and the gas velocity is increased during gasification, which consequently shortens the process residence time. Accordingly, when the oxygen feeding rate is fixed, selection of pyrolysis oil feeding rate requires considerations on both atomization performance and the resulted producer gas flow rate, so the optimum pyrolysis oil flow rate could be determined.

During gasification, the influence of combined effect of oxygen and pyrolysis oil feeding rates is reflected by the gas-to-fuel ratio (GFR). It is shown that increase in GFR value significantly improves the spray characteristics thus positively influences kinetics of reactions, oil-gas conversion and in certain

conditions, H_2 and CO concentrations in the producer gas. However, it needs to notice that changes of GFR can be a result of changing oxygen feeding rate at a constant pyrolysis oil feeding rate or of varying the pyrolysis feeding rate at a constant oxygen feeding rate. This study shows that changes in oxygen feeding rate at a constant pyrolysis oil feeding rate has more dominant role affecting gasification performance compared to that with changing pyrolysis oil feeding rate at a constant oxygen feeding rate. This is closely related to the relatively more significant improvements of the spray characteristics and mixing behaviour with changes in the oxygen flow rate values.

The experimental results also show that the equivalence ratio (ER) is an important parameter influencing the yield and composition of the producer gas. Effect of equivalence ratio on producer gas composition at constant oxygen flow rate was investigated and it is found that H_2, CO and CO_2 concentrations change in parabolic trends with increase in the equivalence ratio values. Below the critical ER value, the H_2 and CO concentrations increase while the CO_2 concentration decreases with increase in equivalence ratio. However, above the critical value, the opposite trends are observed. In all of the cases, the CH_4 concentration decreases with equivalence ratio. These trends are different from those reported in literature where linear relationships are reported.

The changes in producer gas trends with equivalence ratio indicate the direction for continuous improvements of the spray characteristics and increase in the process residence time during entrained flow gasification of biomass pyrolysis oil. During gasification at constant oxygen flow rate, low equivalence ratio value is obtained with high feeding rate of pyrolysis oil into the system which corresponds to low GFR value and therefore relatively poor spray characteristics. In this condition, conversion of oil into producer gas is not efficient and is significantly limited by kinetics. As the equivalence ratio increases, pyrolysis oil feeding into the system decreases accordingly corresponding to higher GFR value thus better spray characteristics. The decline in pyrolysis oil feeding also results production of less producer gas which reduces its velocity thus increases the process residence time. The improvements in spray characteristics and residence time enhance pyrolysis oil conversion during gasification thus promotes production of higher producer gas yield.

Due to limited amount of oxygen present in the system at equivalence ratio below the critical ER value, gasification is highly dominated by non-oxidation reactions thus justifies the increasing H_2 and CO concentrations in the producer gas as the equivalence ratio increases. However, when the equivalence ratio exceeds the critical value, oxidation reactions progressively become more dominant thus consumes H_2, CO, CH_4 and other combustible species in the product to produce higher concentrations of CO_2 and H_2O.

During gasification at constant equivalence ratio, operation with high oxygen flow rate is highly desirable due to the substantial improvements in the oil spray characteristics and mixing behaviour that consequently leads to higher overall reaction kinetics and consequently more rapid gasification reactions in the system. Moreover, increase of oxygen flow rate also drives the gasification system closer to equilibrium state which favours high concentrations of H_2 and CO in the producer gas.

In this work, increase of oxygen flow rate from 900 L/h to 1500L/h was found to alter the critical ER value from 0.30 to 0.50, indicating greater domination of non-oxidation reactions during gasification at higher oxygen flow rate; which therefore demands higher equivalence ratio before the system starts the be dominated by oxidation reactions. Besides that, the enhanced reaction kinetics during gasification at higher oxygen flow rate also favours higher H_2 and CO concentrations and lower CO_2 concentration at the critical ER value. The maximum H_2 concentration increased from 22 vol% to 28 vol% while the maximum CO concentration increased from 36 vol% to 41 vol% when oxygen flow rate was increased from 900 L/h to 1500 L/h during the operations. Furthermore, the growths in H_2 and CO concentrations in the producer gas with increasing equivalence ratio are also more rapid during gasification at higher oxygen flow rates; thus suggesting superior improvements in the pyrolysis oil conversion at this condition compared to that taking place at lower oxygen flow rates.

From the tar analysis, the tar content in the producer gas is also affected by the gasification operation. In overall, the tar content is reduced at higher equivalence ratio which is positively related to the gasification temperature. Detailed investigation into the tar individual species revealed light polyaromatic hydrocarbon (PAH) compounds as the major component of the tar, which alone contributed up to 78 wt% of the total tar in the producer gas. In all gasification conditions investigated in this work, naphthalene was the single most abundant tar species and accounted for as much as 36 wt% of the total tar in the producer gas.

Results from the tar analysis also confirm that the sampling method adopted in this work is capable of capturing tar compounds in the producer gas. Isopropanol (IPA) is the best solvent for tar extraction due to its ability to extract up to 94% of the total extractable tar from the columns in a single 1 mL flush. Dichloromethane (DCM) solvent works best extracting non-polar compounds from the columns while also capable of flushing any remaining tars in the SPE columns after the first wash with IPA. LC-Si SPE column is proven to be effective to capture up to 95 wt% of the total tars in the producer gas while LC-NH_2 SPE column can capture the remaining tars including any breakthrough tars from the first column.

The biggest challenge encountered during the entrained flow gasification operations relates to inconsistencies and interruptions in the pyrolysis oil feeding into the system, most commonly as a result

of complete blockage of the atomizer nozzle by pyrolysis oil. Although the pyrolysis oil has been pre-filtered to remove solid contaminants as small as 10μm prior to atomization; plugging of the atomizer still occurred during gasification thus suggesting inherent issues associated with pyrolysis oil flow through the atomizer's liquid outlet orifice for this application. The most likely cause of the atomizer blockage was concluded to result from pyrolysis oil complex multiphase structure where presence of waxy materials, fine char and heavy components of the oil may have form viscous agglomeration that clog the atomizer in the middle of gasification operations. Another common cause to the atomizer blockage was due to rapid polymerization of pyrolysis oil upon exposure to high gasification temperature.

This thesis, as a whole, contributes to the fundamental understanding of entrained flow gasification for biomass pyrolysis oil at different operation conditions, which is critical for optimization of the system. Findings in this thesis mainly highlight important influence of pyrolysis oil spray characteristics affecting gasification operation and ultimately the gasification products. With the use of external mix twin-fluid atomizer such as that in this work, high atomization performance can be achieved most efficiently with high oxygen flow rates. Findings in this thesis also proved the ability of the system to operate close to the equilibrium state with excellent spray characteristics and sufficient residence time, despite low gasification temperature.

Based on the information connecting influences of various parameters on gasification performances (temperature, producer gas composition, gas flow rate, gas yield, tar species distribution and tar content) presented in this thesis; optimization of the entrained flow gasification system can now be performed. This could be done by considering oxygen flow rate, pyrolysis oil flow rate and equivalence ratio that produce the best spray characteristics and gasification performance at which producer gas has the highest H_2 and CO concentrations and the lowest tar content. In this regard, the oxygen flow rate and the pyrolysis flow rate should be optimized so that the equivalence ratio is close to the critical ER value.

9 RECOMMENDATIONS

The development of the entrained flow gasification system for biomass pyrolysis oil has been challenging due to various issues associated with its operations as well as due to complex physicochemical properties of the pyrolysis oil. Following the observations, findings and discussions presented in this thesis, further investigations into various aspects of the entrained flow gasification operation could be undertaken, particularly in terms of pyrolysis oil feeding consistencies as well as optimization of important control parameters for improved gasification operation and performance in the future.

In this chapter, recommendations of potential areas of future works and improvements are proposed. These recommendations are presented in point forms and are listed as follows:

1. In order to improve conversion pyrolysis oil during gasification, it is highly recommended that the total height of the gasifier is increased so the process residence time can be extended. It is predicted that with longer residence time, better pyrolysis oil conversion will be obtained during gasification at low equivalence ratio that can improve the overall gasification performance thus shifting the critical ER to a lower value to favour producer gas with higher H_2 and CO concentrations.

2. Acknowledging the importance of pyrolysis oil spray characteristics on gasification performance, more comprehensive investigations into this relationship is therefore recommended. It is recommended that full quantitative analyses of the spray characteristics (such as in terms of droplet sizes, droplets spatial distributions and interactions between adjacent droplets in the spray) are conducted so more information on the oil spray characteristics at different operation conditions could be gathered.

3. Comprehensive analyses on the relationship between pyrolysis oil spray characteristics, spray combustion and gasification at different operating conditions are also recommended. These investigations may require advanced simulation of pyrolysis oil atomization at different flow rates of oxygen and pyrolysis oil, after which influence of gasification environment (such as temperature, mass and heat transfer as well as types of reactions) on conversions of individual droplets in the spray could be integrated to predict spray combustion behaviour during gasification at different conditions.

4. While the equilibrium model developed in this study has been proven capable of predicting producer gas composition at equilibrium, the model may be further improved by minimizing the number of assumptions made during the calculation. In this regard, it is recommended that more attention is given to how the model can best represent entrained flow gasification non-ideal operations in practice, in order to improve the comparability of results between the model and that produced during real gasification operations. The opposite approach may also be taken where the gasification operation could be improved towards ideal conditions; nevertheless this is generally difficult to be achieved in large scale gasification operations such as that used in this work.

5. Further considerations on the pyrolysis oil feeding system is recommended in order to obtain stable and consistent oil feeding during gasification operations with minimal interruptions. In order to achieve this, more investigations are required to study the influences of pyrolysis oil multiphase structure and possible agglomerations of waxy compounds, fine char and heavy components of the pyrolysis oil on the oil flow-ability through atomizer orifice at room and elevated temperatures.

6. Further analysis is recommended to investigate physicochemical properties of the pyrolysis oil used in this work and potential factors that contribute to its unique behaviour upon ageing. In particular, the decline in pyrolysis oil water content upon storage is highly advantageous and, if successfully explored, may uncover great potentials for pyrolysis oil applications in the future.

Additional information obtained from these areas of future works is expected to contribute significantly to development of entrained flow gasification for pyrolysis oil in the future, while at the same time provides in-depth understanding of the gasification operation and key parameters that contribute to its optimum performance.

10 APPENDICES

10.1 Appendix A: Hazard and Operability (HAZOP) Analysis

10.1.1 HAZOP Definition

Hazard and Operability (HAZOP) analysis is a tool to identify potential hazards in a system and unexpected problems that could take place during its operation. This assessment tool evaluates potential harm, occurrence and risks associated with the hazards and the operational problems so appropriate protective measures, corrective actions and safeguards could be assigned to prevent the expected harmful conditions from taking place.

10.1.2 HAZOP Team Members

1. Muhamad Fazly Abdul Patah	PhD student
2. Prof. Shusheng Pang	Senior Supervisor
3. Dr. Woei Saw	Associate Supervisor
4. Mr. Leigh Richardson	Mechanical Technician
5. Mr. Stephen Beuzenberg	Electrical Technician
6. Michael Sandridge	Analytical Technician
7. Mr. Tim Moore	Health and Safety officer

10.1.3 HAZOP Scoring Guidelines

Details of parameters, guide words, occurrence score [O], environmental impact score [E], impact on people score [P], safeguard score [SG] and final risk rating that were used to guide evaluations of relevant conditions during the HAZOP analysis are shown in Table 1 – 6 respectively. Other than that, Table 7 provides the normal operating conditions for the non-slagging entrained flow gasification system.

Table 10-1: Common parameters and guide words used in the HAZOP

Parameter	Guide words
Flow rate	Zero, Too High, Too Low, Reverse, Other than
Temperature	Too high, Too low
Pressure	Too high, Too low
Level	Zero, Too High, Too Low
Start-up/Shut-down	Too fast, Too slow, Other than =Actions missed
Reaction	Zero, Too fast, Too slow, Other than = unwanted reaction
Utility failure (power)	Failure

Table 10-2: Probability of occurrence score (Score O)

Score	Order of magnitude Frequency or Likelihood	Qualitative
+1	About once per month (10^{1})	Expected to occur frequently or regularly
0	Once per year (10^{0})	Likely to occur occasionally/several times during plant lifetime
-1	10% chance per year (10^{-1}) (once every 10 years)	Probably will happen more than once during plant lifetime
-2	1% chance per year (10^{-2}) (once every 100 years) (100 plant, once/year)	Not expected to occur but could occur during plant lifetime
-3	1 in 1,000 chance per year (10^{-3})	Would be very surprising if happened during plant lifetime
-4	1 in 10,000 chance per year (10^{-4})	Extremely remote, or not expected to be possible

Table 10-3: Environmental impact score (Score E)

Score	Effects expected to occur exclusively On-Site	Effects expected to occur Off-site
6		• Catastrophic release to environment • Long term effects • Substantial fines/penalties expected
5	• Catastrophic release to facility • Long term effects • Substantial fines/penalties expected	• Major release to environment • Long term impact likely • Fines/penalties likely
4	• Major release to facility • Long term impact likely • Fines/penalties likely	• Minor release to facility/outside help needed • Short term impact likely • Legal/public relation consequences
3	• Minor release to facility/outside help needed • Short term impact likely • Legal/public relation consequences	• Major release handled with internal resources • No legal/public relation consequences
2	• Major release handled with internal resources • No legal/public relation consequences	• Minor release handled with internal resources • No legal/public relation consequences
1	• Minor release handled with internal resources • No legal/public relation consequences	• Environmental impact unlikely
0	• Environmental impact unlikely	none

Table 10-4: Impact on people score (Score P)

Score	Unlikely but might affect one person On-site (10% of time)	Likely to affect 1-2 people On-site	Likely to affect 5-20 people On-site or Off-site
6			Fatality

5		Fatality	Immediate impairment, Permanent health effects
4	Fatality	Immediate impairment, Permanent health effects	Severe injury, Lost time
3	Immediate impairment, Permanent health effects	Severe injury, Lost time	Injury requiring medical treatment
2	Severe injury, Lost time	Injury requiring medical treatment	Minor injury
1	Injury requiring medical treatment	Minor injury	Probably none
0	Minor injury	Probably none	None

Table 10-5: Probability of safeguard failure score (Score SG)

Score	Probability of safeguard failure	Example
0	100%	• No safeguards • Operator in difficult position
1	10%	• Single operator with adequate time (> 5 min) fails to do correct thing 1 out of 10 times
2	1%	• Single set of hardware, functionally tested • Automatic shutdown procedure
3	0.1%	• Passive protection (explosion disk) • Combination of Score 1 & 2
4	0.01%	• Two independent sets of hardware

Table 10-6: Risk rating and prioritization

Risk level	Risk rating score	Descriptions
1	-4 to -1	Low risk, existing safeguards are adequate
2	0 to 3	Low risk, but risk control measures are required
3	4 to 8	High risk, risk control measures and additional protective measures are needed
4	9 to 13	Very high risk, this part or process cannot be operated unless risk control measures and additional protective measures have been conducted to reduce the risk and hazard

Table 10-7: Normal operating conditions for non-slagging entrained flow gasification

Parameters	Normal Operating Range
Gasifier temperature	600-1100^{o}C
Gasifier pressure	1 atm
Pyrolysis oil mass flow rate	≤ 150 g/min
Oxygen gas flow rate	≤ 50 L/min
Burner LPG flow rate	~ 4 L/min
Burner compressed air flow rate	~ 56 L/min
Nitrogen purge flow rate	$1 - 5$ L/min

10.1.4 Hazard and Operability Study (HAZOP)

Node/Stream	Parameter	Guide Word	Deviation	Causes	Score O	Consequences	Score E	Score P	Safeguards	Score SG	Risk Rating	Risk Level	Comments/Actions
Assign each entry a unique tracking number	Describe parameter that the guide word relates to	Insert deviation guide word used	Describe the deviation	Describe how the deviation may occur	Key in score from Table 2	Describe what may happen if the deviation occurs	Key in score from Table 3	Key in score from Table 4	List controls (preventive or reactive) that reduce deviation likelihood or severity	Key in score from Table 5	Calculate from equation	Key in level from Table 6	Identify any hazard mitigation or control actions required
(1) Burner compressed air supply	(A) Flow rate	(i) Zero	No air supply into burner	Regulator not open	0	No flame Accumulation of LPG within reactor which could lead to explosion	1	0	**Ionization probe** to detect absence of flame and sends signal to **cut LPG solenoid valve** **Alarm** to alert operator that flame extinguished	2	-1	1	Follow procedure to make sure the regulator is turned ON
				Main compressor is turned off	0		1	0		2	-1	1	
				Complete blockage on compressed air pipe	-3		1	0		2	-4	1	
		(ii) Too high	Excess air supply into burner	Malfunction air regulator/rotameter	-2	Flame extinguishes	0	0	**Ionization probe** to detect absence of flame and sends signal to **cut LPG solenoid valve** **Alarm** to alert operator that flame extinguished	2	-4	1	
				Rotameter reading is set too high	1		0	0		2	-1	1	
		(iii) Too low	Reduce air supply into burner	Malfunction air regulator/rotameter	-2	Incomplete combustion of LPG thus producing high CO concentration in flue gas	3	5	**Extraction fan** must be turned ON at all time. If extraction fan is OFF, **peristaltic pump and solenoid valves (LPG and oxygen)** could not switched on/activated **CO sensor** to detect release of CO into surrounding (portable sensor) and **alarm** **Pressure sensor** on the compressed air line to detect low supply pressure and trigger **alarm**.	4	2	2	
				Rotameter reading is set too low	1		3	5		4	**5**	**3**	There must be at least 2 operators during operation
				Partial blockage on air supply tubing	0		3	5		4	**4**	**3**	There must be at least 2 operators during operation
	(B) Temperature	(i) Too high	Increase in air temperature	Hot compressed air supply	-2	No harm	0	0		0	-2	1	

Node/Stream	Parameter	Guide word	Deviation	Causes	Score O	Consequences	Score E	Score P	Safeguards	Score SG	Risk Rating	Risk level	Actions
		(ii) Too low	Decrease in air temperature	Cold compressed air supply	-2	No harm	0	0		0	-2	1	
	(C) Pressure	(i) High	Increase in compressed air supply pressure	Increase in compressed air flow *Refer to Node 1A (ii) i.e. too high air flow*		*Refer to Node 1A (ii) i.e. too high air flow*							
		(ii) Low	Pressure drop in compressed air supply line	Decline in compressed air flow *Refer to Node 1A (iii) i.e. too low air flow*		*Refer to Node 1A (iii) i.e. too low air flow*							
(2) Burner LPG supply	(A) Flow rate	(i) Zero	No LPG supply into burner	Regulator/rotameter needle valve not open	0	No flame No harm Compress air supply will cool down the gasifier *Also refer to Node 6B (ii) i.e. gasifier low temperature*	0	0		0	0	1	
				Complete blockage on LPG pipe	-3		0	0		0	0	1	
				LPG tank is empty	1		0	0		0	0	1	In procedure, weigh the LPG tank before and after the experiment to ensure sufficient LPG for each run
		(ii) Too high	Excess LPG supply into burner	Malfunction LPG regulator/rotameter	-2	Incomplete combustion could produces high toxic CO concentration in flue gas Flame extinguish Risk of explosion from high LPG accumulation in flue gas	3	5	**Ionization probe** to detect absence of flame and sends signal to **cut LPG solenoid valve** **Extraction fan** must be turned ON at all time. If extraction fan is OFF, **peristaltic pump and solenoid valves (LPG and oxygen)** could not switched on/activated **CO sensor** to detect release of CO into surrounding (portable sensor) and **alarm**	4	2	2	
				Rotameter reading is set too high	1		3	5		4	**5**	**3**	2 operators are required LPG regulator is required to limit the maximum allowed pressure
				Sudden increase in LPG tank pressure (mainly when tank is about to empty)	0		0	0		1	-1	1	Make sure the LPG content is well above the desired operating amount. Use spare LPG bottle if

													its content is less than required for a run
Node/Stream	**Parameter**	**Guide word**	**Deviation**	**Causes**	**Score O**	**Consequences**	**Score E**	**Score P**	**Safeguards**	**Score SG**	**Risk Rating**	**Risk level**	**Actions**
		(iii) Too low	Decrease of LPG supply into burner	Malfunction LPG regulator/rotameter	-2	Flame extinguish Decrease of temperature inside the outer reactor *Also refer to Node 6B (ii) i.e. gasifier low temperature*	0	0	**Ionization probe** to detect absence of flame and sends signal to **cut LPG solenoid valve** **Extraction fan** must be turned ON at all time. If extraction fan is OFF, **peristaltic pump and solenoid valves (LPG and oxygen)** could not switched on/activated	1	-3	1	
				Rotameter reading is set too low	1		0	0		1	0	1	
				Partial blockage in LPG supply tubing	-3		0	0		1	-4	1	
	(B) Temperature	(i) Too high	Increase in LPG temperature	Direct contact of LPG tank or supply tube with EFG body	-2	No harm							Ensure the LPG tank is not located next to the reactor
		(ii) Too low	Decrease in LPG temperature	Cold LPG supply	-3	Low LPG supply as it turns into liquid. Refer to Node 2A (iii) i.e. low LPG flow rate.							
	(C) Pressure	(i) Too high	Increase in LPG supply pressure	Increase in LPG tank temperature or/and pressure (especially when tank is about to empty)	-2	No harm							
				Regulator set too high	1	High LPG supply into the burner *Refer to Node 2A (ii) i.e. high LPG flow rate.*							
		(ii) Too low	Pressure decline in LPG supply line	Decline in LPG tank pressure (could be tank is empty)	0	No harm *Refer to Node 2A (i) and Node 2A (iii) i.e. LPG no/low flow rate.*							

Node/Stream	Parameter	Guide word	Deviation	Causes	Score O	Consequences	Score E	Score P	Safeguards	Score SG	Risk Rating	Risk level	Actions
(3) Nitrogen purge	(A) Flow rate	(i) Zero	No nitrogen purge into sight glass	Nitrogen regulator valve is completely closed	0								Follow operating procedure to ensure N_2 regulator is turned ON at the beginning of each run
				Needle valve is closed completely	1	No harm Condensate formation on sight-glass							Follow operating procedure to make sure needle valve is opened Ensure the reactor has been cooled before dissembled.
				Complete blockage in nitrogen supply tube or sight glass purge port	-3								
		(ii) Too high	Excess nitrogen supply into the system	Supply valve is opened too wide	1	No harm							
				Increase in nitrogen tank pressure (when tank is about to empty)	0								
		(iii) Too low	Lack of nitrogen supply through the sight glass	Partial blockage in nitrogen supply tube or sight glass purge port	-2	No harm							
	(B) Temperature	(i) Too high	Increase in nitrogen temperature	Direct contact of nitrogen tank with EFG body	-2	No harm							Ensure the N_2 tank is not located next to the reactor
		(ii) Too low	Decrease in nitrogen temperature	Cold nitrogen supply	-3	No harm							
	(C) Pressure	(i) Too high	Increase in nitrogen supply pressure	Increase in nitrogen tank temperature or/and pressure	-3	No harm							

Node/Stream	Parameter	Guide word	Deviation	Causes	Score O	Consequences	Score E	Score P	Safeguards	Score SG	Risk Rating	Risk level	Actions
		(ii) Too low	Pressure decline in nitrogen supply line	Decline in nitrogen tank pressure/ empty tank	-2	No harm							
(4) Oxygen supply into gasifier through atomizer	(A) Flow	(i) Zero	No oxygen supply into gasifier	Oxygen regulator valve is completely closed	0	No harm Decrease in gasifier temperature since there will be no pyrolysis oil combustion Accumulation of pyrolysis oil at the bottom of gasifier	1	1	**Pressure sensor** sends signal to controller thus **cut peristaltic pump power** (when there is **no pressure or high pressure** due to blockage) **Temperature sensor** monitor gasifier temperature decline. Below gasifier minimum temperature limit, **alarm** will sound and **oxygen and pyrolysis oil supply will be cut** Note: There should be delay on the oxygen solenoid valve after the peristaltic pump has been turned ON	2	0	1	Check procedure to prevent this from happening
				Needle valve is completely closed	1		1	1		2	1	1	
				Check valve malfunction or blocked (fail closed)	-3		1	1		2	-3	1	
				Complete blockage in oxygen supply tube or atomizer	0		1	1		2	0	1	
				Oxygen tank is empty	0		1	1		2	0	1	
		(ii) Too high	Excess oxygen supply into the system	Needle valve is opened too wide	1	Increase in gasifier temperature from complete combustion High oxygen concentration in product gas (excess from combustion) Potential risk of explosion Inner chamber may melt; resulting O2 and oil leak into the outer chamber and further combust.	1	5	**Oxygen sensor** to detect excess oxygen in product gas and sends signals to **cut oxygen solenoid valve.** If gasifier **temperature** exceeds its maximum temperature limit, **alarm** will sound. And signal will be sent to **cut oxygen and LPG solenoid valves** and **peristaltic pump power**.	4	3	2	Oxygen regulator is required to limit the maximum allowed pressure
				Sudden increase in oxygen tank pressure (especially when tank is about to empty)	0		1	5		4	2	2	Follow operating procedure to make sure oxygen amount is sufficient before experiment

Node/Stream	Parameter	Guide word	Deviation	Causes	Score O	Consequences	Score E	Score P	Safeguards	Score SG	Risk Rating	Risk level	Actions
		(iii) Too low	Decrease of oxygen supply through the atomizer	Needle valve is opened less than required	1	Less pyrolysis oil could combust Decline in gasifier temperature Accumulation of pyrolysis oil at the bottom of gasifier	1	1	**Temperature sensor** monitor gasifier temperature decline. Below gasifier minimum temperature limit, **alarm** will sound and **oxygen and pyrolysis oil supply will be cut** Extraction fan need to be turned ON all the time	2	1	2	
				Partial blockage in oxygen supply tube or in atomizer	1		1	1		2	1	2	
				Leak or rupture of oxygen supply tube	-2		1	1		2	-2	1	Copper tube will be used
		(iv) Reverse	Oxygen flows in reverse direction	Pressure increase in the gasifier (through the atomizer)	-3	Risk of flash back fire Risk of explosion	0	0	**Check valve** on oxygen supply line to stop reverse flow **Safety valve** to release sudden increase in gasifier pressure **Flame arrester** to stop backfire from reaching oxygen tank	4	-7	1	
	(B) Temperature	(i) High	Increase in oxygen temperature	Direct contact of oxygen tank with EFG body	-3	No harm	0	0		0	-3	1	
		(ii) Low	Decrease in oxygen temperature	Cold oxygen supply	-2	No harm	0	0		0	-2	1	
	(C) Pressure	(i) High	Increase in oxygen supply pressure	Increase in oxygen tank temperature or/and pressure	0	*See Node 4A (ii) i.e. high oxygen flow*							
				Blockage in atomizer or oxygen supply tube	0	*See Node 4A (i) i.e. no oxygen flow*	0	0		1	-1	1	Operating procedure
		(ii) Low	Pressure decline in oxygen supply line	Decline in oxygen tank pressure	0	*See Node 4A (iii) i.e. low oxygen flow*	0	0					

Node/Stream	Parameter	Guide word	Deviation	Causes	Score O	Consequences	Score E	Score P	Safeguards	Score SG	Risk Rating	Risk level	Actions
	(D) Reaction	(i) Unwanted	Unwanted combustion/ reaction in oxygen supply tube	Sudden increase in gasifier back-pressure or when explosion occur	-3	Flame travel back to oxygen tank *Refer Node 4A (iv) i.e. reverse oxygen flow*	0	0					
(5) Pyrolysis oil feed into gasifier through atomizer	(A) Flow	(i) Zero	No pyrolysis oil supply into gasifier	Peristaltic pump is not ON	1	No combustion within the gasifier	0	0	**Oxygen sensor** detects un-combusted oxygen in product gas, **alarm** and sends signals to **shut oxygen solenoid valve and cut power to pump.** **Pressure sensor** on pyrolysis oil supply line detect increase in pressure (due to blockage), **alarm** and send signal to **cut peristaltic pump power and close oxygen solenoid valve** **2 alarms depending on which event occur first**	4	-3	1	
				Ash filter or/and tank filter is completely blocked	1		0	0		4	-3	1	
				Pyrolysis oil supply tube is completely blocked	1		0	0		4	-3	1	
				Complete blockage in atomizer	1		0	0		4	-3	1	
				Pyrolysis oil tank is empty	0		0	0		4	-4	1	Operating procedure: Monitor oil level in tank
				Serious rupture of pyrolysis oil supply tube	-1	Danger to aquatic life if enter drain	1	0	Bunk/container underneath pyrolysis oil feeding system	1	-1	1	Clean any spill as soon as possible to prevent any prolonged exposure on operator
		(ii) Too high	Excess pyrolysis oil supply into the system	Peristaltic pump rpm setup is too high	1	Decline of gasifier temperature Accumulation of pyrolysis oil at the bottom of gasifier	1	1	**Pressure sensor** and **alarm** to alert significant increase in pipe pressure (due to increase in flow) **Temperature sensor** monitor gasifier temperature decline. Below gasifier minimum temperature limit, **alarm** will sound and **oxygen and pyrolysis oil supply will be cut**				Operator's reaction: Either lower the oil supply flow rate or increase O_2 flow to maintain the ratio

Node/Stream	Parameter	Guide word	Deviation	Causes	Score O	Consequences	Score E	Score P	Safeguards	Score SG	Risk Rating	Risk level	Actions
		(iii) Too low	Lack of pyrolysis oil supply through the atomizer	Peristaltic pump rpm setup is too low	1	Complete combustion of pyrolysis oil Risk of explosion due to excess oxygen accumulation inside EFG Similar effect to too high O2 flow Node 4A (ii) but expected to be less severe as this is under limited fuel supply	1	5	**Oxygen sensor** to detect excess oxygen in product gas and sends signals to **cut oxygen solenoid valve.** If gasifier **temperature** exceeds its maximum temperature limit, **alarm** will sound. And signal will be sent to **cut oxygen and LPG solenoid valves** and **peristaltic pump power**.	4	3	2	
				Partial blockage in pyrolysis oil supply tube	0		1	5		4	2	2	
				Partial blockage of ash filter or/and tank filter	1		1	5		4	3	2	
				Partial blockage in atomizer	1		1	5		4	3	2	
				Leak of pyrolysis oil supply tube	-1	Danger to aquatic life if enter drain	1	0	Bunk/container underneath pyrolysis oil feeding system	1	-1	1	
Not applicable	(B) Temperature	(i) Too High	Pyrolysis oil temperature is too high	Pyrolysis oil is pre-heated to a very high temperature	-2	Pyrolysis oil become viscous very rapidly Refer to Node 5A(i) and 5A(iii)			Temperature probe for pyrolysis oil inside tank and connected to alarm				
		(ii) Too Low	Pyrolysis oil temperature is too low	Surrounding temperature is too low	-1	Risk of blockage due to increase in pyrolysis oil viscosity Refer to Node 5A(i) and 5A(iii)			Temperature probe for pyrolysis oil inside tank and connected to alarm				
	(C) Pressure	(i) Too High	Increase in pyrolysis oil tube pressure	Blockage in atomizer or pyrolysis oil supply tube	1	Risk of transfer tube rupture/leak	1	0	**Pressure sensor** to monitor pyrolysis oil transfer tube pressure and send signals to **cut peristaltic pump power** (if pressure is over its maximum limit)	2	0	2	
				Peristaltic pump rpm is too high	1	Slip on the pump	1	0	Bunk/tray under the feeding system **Alarm** to alert operator	2	0	2	

Node/Stream	Parameter	Guide word	Deviation	Causes	Score O	Consequences	Score E	Score P	Safeguards	Score SG	Risk Rating	Risk level	Actions
		(ii) Too Low	Pressure decline in pyrolysis oil supply tube	Significant leak or rupture on pyrolysis oil supply tube	-1	Danger to aquatic life if enter drain	1	0	Bunk/container underneath pyrolysis oil feeding system	1	-1	1	
(6) Entrained flow gasifier	(A) Flow	(i) Zero	No flow within gasifier	*Refer to Node 4A (i) and Node 5A (i) i.e. no oxygen and pyrolysis oil flow*		No harm							
				Refer to Node 1A (i) and Node 2A (i) i.e. no combustion air and LPG flow		No harm							
		(ii) Too High	Flow rate within the gasifier is too high	Too high supply of oxygen *Refer to Node 4A(ii)*		Refer to Node 4A(ii)							
				Too high supply of pyrolysis oil *Refer to Node 5A(ii)*		Refer to Node 5A(ii)							
				Too high supply of LPG *Refer to Node 2A(ii)*		Refer to Node 2A(ii)							
				Too high supply of combustion air *Refer to Node 1A(ii)*		Refer to Node 1A(ii)							
				High LPG AND combustion air supply (outer reactor)		Rapid increase in gasifier temperature			If gasifier **temperature** exceeds its maximum temperature limit, **alarm** will sound. And signal will be sent to **cut oxygen and LPG solenoid valves** and **peristaltic pump power**.				
				High O2 AND pyrolysis oil supply (inner reactor)									

Node/Stream	Parameter	Guide word	Deviation	Causes	Score O	Consequences	Score E	Score P	Safeguards	Score SG	Risk Rating	Risk level	Actions
		(iii) Too Low	Flow rate within the gasifier is too low	Too low supply of oxygen *Refer to Node 4A(iii)*		Decline in gasifier temperature No harm			**Temperature sensor** monitor gasifier temperature decline. Below gasifier minimum temperature limit, **alarm** will sound and **oxygen and pyrolysis oil supply will be cut**				
				Too low supply of pyrolysis oil *Refer to Node 5A(ii)*									
				Too low supply of LPG *Refer to Node 2A(iii)*									
				Too low supply of combustion air *Refer to Node 1A(iii)*									
	(B) Temperature	(i) Too high	Gasifier temperature is too high	Excess/too high supply of oxygen into gasifier *Refer Node 4A (ii) i.e. high oxygen flow*		Overheating of the gasifier Melting of the gasifier wall			If gasifier **temperature** exceeds its maximum temperature limit, **alarm** will sound. And signal will be sent to **cut oxygen and LPG solenoid valves** and **peristaltic pump power**				
				Uncontrolled/too high LPG into gas burner *Refer Node 2A (ii) i.e. high LPG flow*									
		(ii) Too low	Gasifier temperature is too low	Lack of oxygen supply into gasifier *Refer Node 4A (iii) i.e. low oxygen flow*		No harm			**Temperature sensor** monitor gasifier temperature decline. Below gasifier minimum temperature limit, **alarm** will sound and **oxygen and pyrolysis oil supply will be cut**				
				Excess supply of pyrolysis oil into gasifier *Refer Node 5A (ii) i.e. high pyrolysis oil flow*		No harm							

				Ineffective pre-heating by gas burner or burner shut down before reaching the desired start-up temperature		No harm							
	(C) Pressure	(i) Too high	Gasifier pressure is too high	Blockage on product gas exit port (from tar/ash)	-1	Risk of explosion	2	3	**Pressure sensor** connected to **alarm** to alert operator of significant pressure increase Safety valve and rupture disc to release sudden increase in reactor	4	0	2	In procedure, clean the exit port after each run.
		(ii) Too low	Gasifier pressure too low	Fume extraction is too powerful	-3	No harm Not possible							
				Online GC vacuum pump is too strong	-3	No harm and impossible Only micro-liter range							
	(D) Reaction	(i) Too fast	Reactions in gasifier are too rapid	Supply of oxygen is too high which leads to mainly combustion of pyrolysis oil *Refer to Node 4A (ii) i.e. O2 flow too high*		Rapid increase in gasifier temperature *Refer to Node 6B (i) i.e. gasifier temp too high*			If gasifier **temperature** exceeds its maximum temperature limit, **alarm** will sound. And signal will be sent to **cut oxygen and LPG solenoid valves** and **peristaltic pump power**				
		(ii) Too slow	Reactions in gasifier are too slow	Supply of oxygen is too low *Refer to Node 4A (iii) i.e. O2 flow too low*		No harm							
				Gasifier pre-heating temperature is too low *Refer Node 2A (iii) i.e. LPG flow too low*		*Refer to 6B (ii) i.e. low gasifier temperature*							
(7) Product gas stream	(A) Flow	(i) Zero	No flow of product gas from the gasifier	No supply of oxygen and pyrolysis oil into gasifier		*Refer to Node 6A(i) i.e. no flow in gasifier*							
		(ii) Too fast	Flow rate of product stream is too high	Flow rate of pyrolysis oil and/or oxygen feed supply is too high		No harm							

				Refer to Node 6A (ii) i.e. too high flow rates in gasifier									
Node/Stream	**Parameter**	**Guide word**	**Deviation**	**Causes**	**Score O**	**Consequences**	**Score E**	**Score P**	**Safeguards**	**Score SG**	**Risk Rating**	**Risk level**	**Actions**
		(iii) Too low	Flow rate of product stream is too high	Flow rate of pyrolysis oil and/or oxygen feed supply is too low *Refer to Node 6A (iii) i.e. too low flow rates in gasifier*		No harm Potential condensation in the exit pipe							
	(B) Temperature	(i) Too high	Temperature within product pipe is too high	Gasifier temperature is too high *Refer to Node 6B (i) i.e. gasifier temperature too high*		No harm The pipe material melting point is very similar to that of gasifier wall							
		(ii) Too low	Temperature within product pipe is too low	Gasifier temperature is too low *Refer to Node 6B (ii) i.e. gasifier temperature too low*		No harm Condensation of water and/or tar on oxygen sensor (operational issue)							
	(C) Pressure	(i) Too high	Pressure within product pipe is too high	Gasifier pressure is too high *Refer to Node 6C (i) i.e. gasifier pressure too low*		No harm							
		(ii) Too low	Pressure within product pipe is too low	Gasifier pressure is too low *Refer to Node 6C (ii) i.e. gasifier pressure too low*		No harm							
(8) Exit to pressure safety valve	(A) Flow	(i) No	No flow when pressure is high	Safety valve malfunction/blocked	-2	Pressure build up inside reactor *Refer to Node 6C (i) i.e. too high pressure inside reactor*							
		(ii) Unexpected flow	Gas leak at low pressure	Safety valve leaks or fails open	-2	Producer gas exhaust to fume hood	1	0		1	-2	1	

10.1.5 List of Safety Device

#	Safety Device	Location	Function(s)
1	Alarm	Gasifier room	Alert operator for any deviation from intended operating conditions when: 1. Preheater gas burner flame extinguished – signal from **ionization probe** 2. High CO concentration is detected by **CO sensor** 3. Too high pressure in pyrolysis oil supply stream (due to high flow or blockage) – signal from **pressure sensor** 4. High oxygen concentration in product gas – signal from **oxygen sensor** 5. **Pressure** of gasifier is above its **maximum limit** – signal from **pressure sensor** 6. **Gasifier temperature exceeds minimum temperature limit** – signal from **temperature probe** 7. **Gasifier temperature drops below minimum temperature limit** – signal from **temperature probe**
2	Ionization probe	Inside gas pre-heater burner	Detect presence/absence of gas burner flame and trigger **alarm** when there is no flame in gas burner Send signal to controller to **shut LPG solenoid valve** when there is no flame

3	Fume hood/ Extraction fan	Above the whole system	Draw combustion flue gas, producer gas and any possible toxic gas release from the system. If extraction fan is OFF, **peristaltic pump and solenoid valves (LPG and oxygen)** could not switched on/activated
4	Carbon Monoxide (CO) sensor	Portable CO sensor with operator	Detect CO concentration in the surrounding. Trigger **alarm** if the concentration is too high
5	Pressure sensor	Oxygen supply line before check valve	Sends signal to cut **peristaltic pump power** when: 1. There is **increase** in pressure in oxygen supply line (due to flow too high or blockage). 2. There is **no pressure** (0kPa gauge), indicating no oxygen flow. *Note: There should be delay on the oxygen solenoid valve after the peristaltic pump has been turned ON*
		Pyrolysis oil supply line after peristaltic pump	Sends signal to controller (PLC) to: 1. **Alarm** and **cut peristaltic pump power and shut oxygen solenoid valve** when there is **INCREASE** in pressure in pyrolysis oil supply line due to blockage.
		Inside gasifier (to measure reactor pressure)	Measure pressure inside gasifier while connected to **alarm** to alert operator of any significant increase. Calibration should be made to determine normal operating pressures along gasifier (and set the alarm slightly higher).
		Compressed air supply line	Measure pressure and trigger **alarm** to alert operator when there is: 1. **Low pressure** in air supply line which could cause incomplete combustion and release of CO

6	Oxygen sensor	On product gas exit stream	Detect excess/unreacted oxygen in product gas and trigger **alarm** – indication whether combustion is taking place or oxygen is excessive Send signals to PLC to **shut oxygen solenoid valve and peristaltic pump power** when **high oxygen concentration** is detected in product gas
7	Temperature sensor	Within the gasifier inner reactor	Measure inner reactor temperature and sends signals to **alarm** and: 1. **Close oxygen solenoid valve** and **cut peristaltic pump power** when gasifier temperature is below its **minimum limit** 2. **Close oxygen and LPG solenoid valves and cut peristaltic pump power** when gasifier temperature is above its **maximum limit**
8	Pressure relief valve	On safety pressure relief line	Release pressure builds up inside the gasifier inner reactor when it exceeds a safe operating pressure
9	Flame arrester	On oxygen supply line	Prevent unexpected flashback flame from travelling in reverse direction towards oxygen tank
10	Emergency button	Close to operator	Immediately **stops the whole operation** in the event of emergency shut-down by: **1. Closing solenoid valve for oxygen supply** **2. Closing solenoid valve for LPG supply** **3. Disconnecting peristaltic pump power** But allowing continuous flow of nitrogen purge and combustion air

11	Peristaltic pump switch	Before peristaltic pump	Switch OFF peristaltic pump power when: 1. **Extraction fan is OFF** 2. **Temperature** of gasifier is above the **maximum limit** 3. **Temperature** of gasifier is below the **minimum limit** 4. **Pressure of pyrolysis oil supply line is too high** (due to blockage or high flow)
12	Regulator	Oxygen and LPG tank	Indicate the content of gas tanks for safe operation. Restrict the maximum operating pressure in the event of unexpected tank pressure increase
13	Solenoid valve	LPG supply line	**Cut LPG solenoid valve** when there is: 1. **Extraction fan is OFF** 2. **No flame** is detected from ionization probe (no/high flow of compressed air into burner) 3. **Temperature of gasifier is above maximum temperature limit**
		Oxygen supply line	**Cut oxygen solenoid valve** when there is: 1. **Extraction fan is OFF** 2. **High oxygen content** in product gas – detected by oxygen sensor 3. **Temperature** of gasifier is above the **maximum limit** 4. **Temperature** of gasifier is below the **minimum limit**
14	Check valve	Oxygen and nitrogen supply stream	Prevent reverse flow of gas
15	Container/bunk	Underneath system	Prevent spill or leak of pyrolysis oil from entering drain

10.1.6 Safety Checklist

Days before gasifier run:

1) There must always be at least 2 operators for running the system
2) Weigh LPG tank before and after the experiment to ensure sufficient LPG for each run. Use spare LPG bottle if its content is less than required for a run
3) Check (and clean) inner reactor bottom before every run to make sure there is no unconverted residues remains from previous experiments
4) Make sure there is sufficient oxygen in tank before starting an experiment.
5) There should be a bunk underneath pyrolysis oil feeding system to avoid oil spill or leak into drain

During gasifier run:

1. Extraction fan must be turned ON all the time. Otherwise, no LPG, oxygen or pyrolysis oil supply could be made.
2. Make sure the compressed air regulator is turned ON before starting experiment
3. Make sure N_2 regulator is turned ON at the beginning of each run
4. Make sure O_2 regulator is turned ON before each run
5. Ensure peristaltic pump is not operated when there is no pressure in the O_2 line
6. To stop experiment, first cut pyrolysis oil followed by oxygen, LPG and air for safe operation. Do not skip procedure. Can we use emergency button?
7. Bleed small amount of N_2 into the system during pre-heating before introducing O_2 and pyrolysis oil to burn and purge any leftover residues in the reactor.
8. Pressure decrease in pressure sensor between peristaltic pump and ash filter indicates the severity of blockage on ash filter
9. Monitor pyrolysis oil level in tank

After gasifier run:

1. Ensure the gasifier is cooled sufficiently before taking the gasifier apart. This is important to prevent burn or release of un-purged producer gas to the operator.
2. Clean gasifier exit port after each run.

10.2 Appendix B: Technical Drawings and Item Register

10.2.1 Piping and Instrumentation Diagram (P&ID)

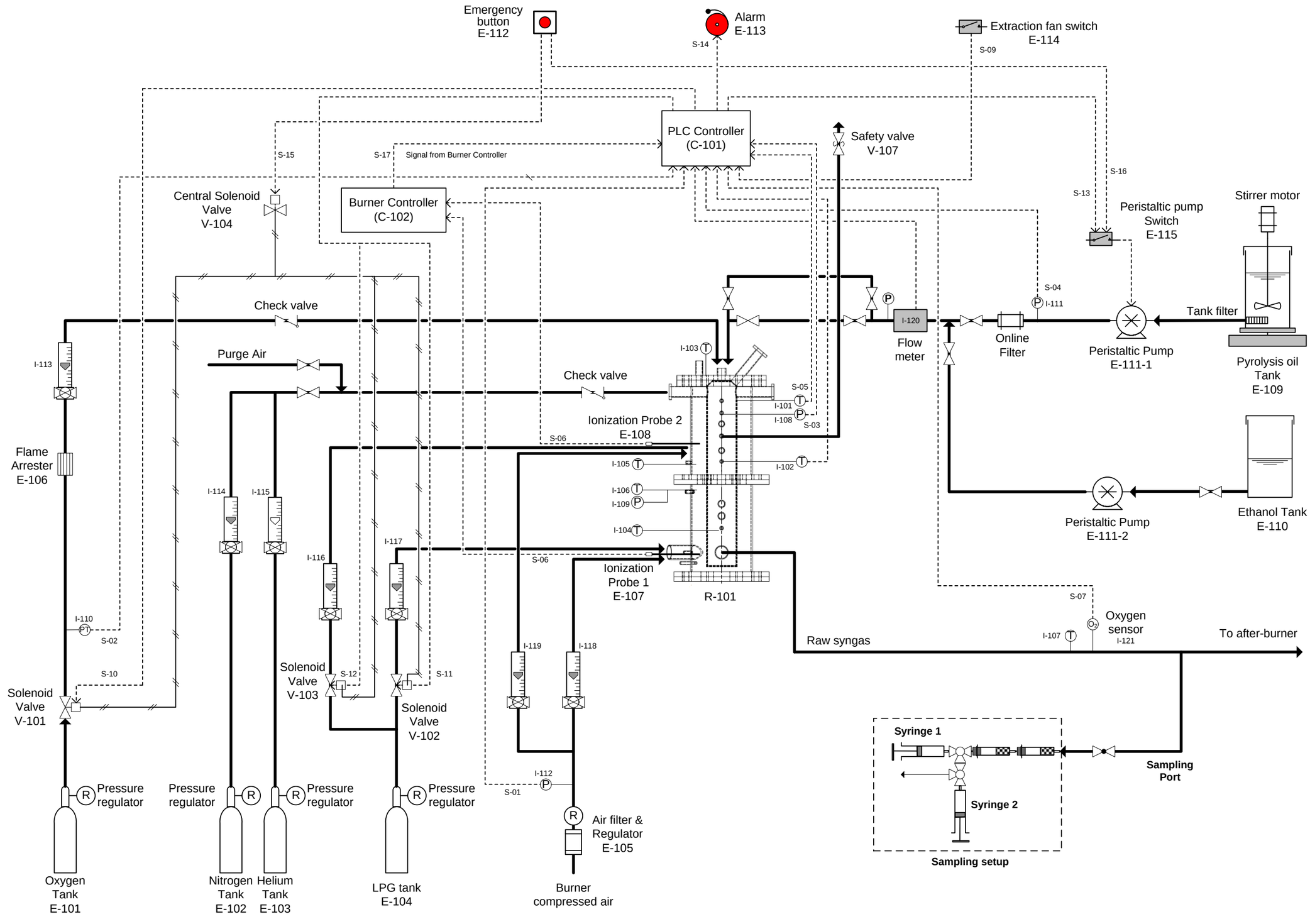

10.2.2 Electrical Diagram

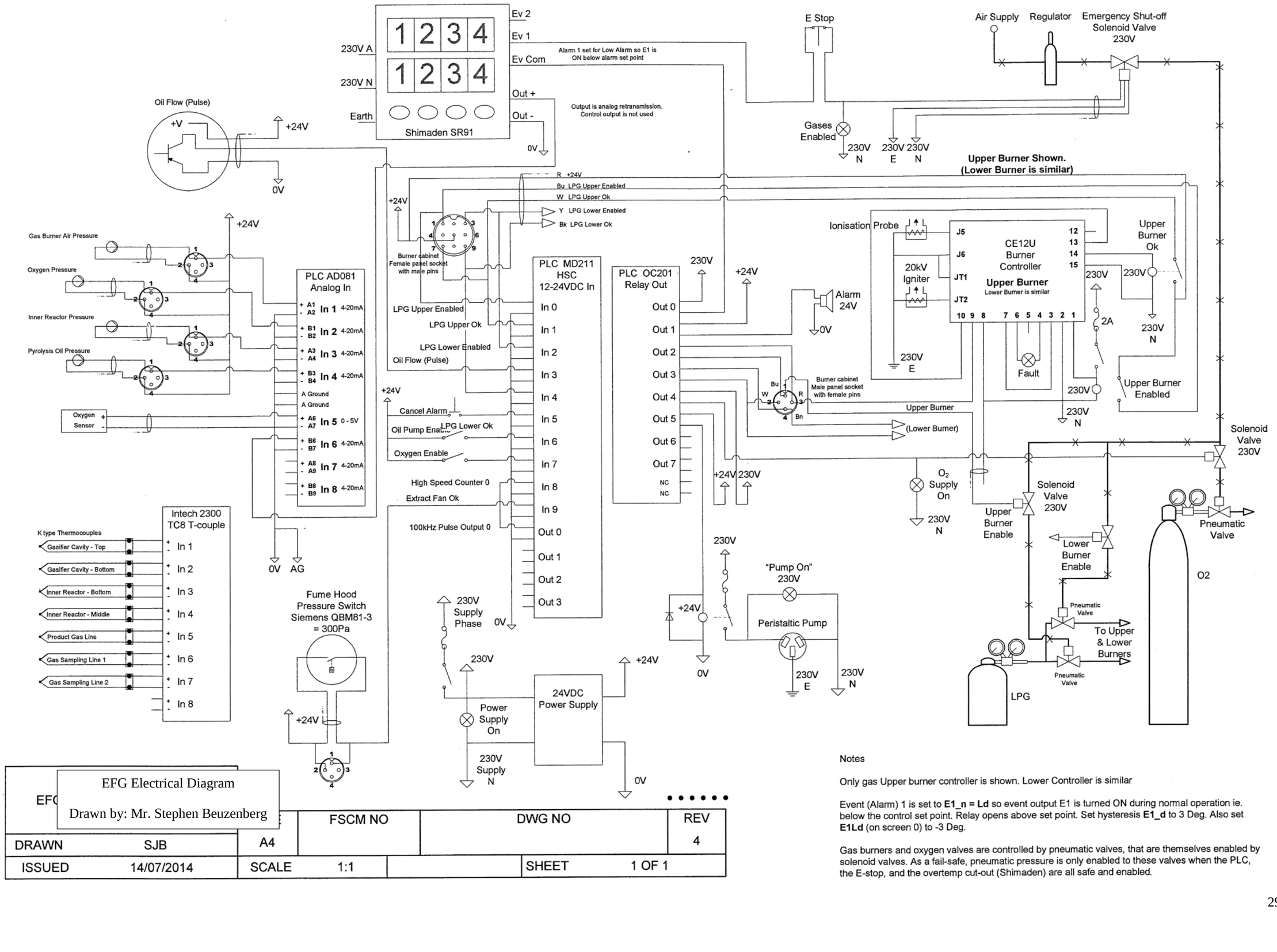

EFG Electrical Diagram

Drawn by: Mr. Stephen Beuzenberg

EFG		FSCM NO	DWG NO	REV
DRAWN	SJB	A4		4
ISSUED	14/07/2014	SCALE 1:1	SHEET	1 OF 1

Notes

Only gas Upper burner controller is shown. Lower Controller is similar

Event (Alarm) 1 is set to **E1_n = Ld** so event output E1 is turned ON during normal operation ie. below the control set point. Relay opens above set point. Set hysteresis **E1_d** to 3 Deg. Also set **E1Ld** (on screen 0) to -3 Deg.

Gas burners and oxygen valves are controlled by pneumatic valves, that are themselves enabled by solenoid valves. As a fail-safe, pneumatic pressure is only enabled to these valves when the PLC, the E-stop, and the overtemp cut-out (Shimaden) are all safe and enabled.

10.2.3 Item Register

10.2.3.1 PLC (C-101) Inlet Register

#	Inlet	Stream Number	Physical Range	Signal Range
1	Signal from burner air supply line pressure sensor (I-112)	S-01	0 - 5 bar	4 - 20mA
2	Signal from oxygen line pressure sensor (I-111)	S-02	0 - 5 bar	4 - 20mA
3	Signal from gasifier pressure sensor (I-108)	S-03	0 - 5 bar	4 - 20mA
4	Signal from pyrolysis oil line pressure sensor (I-111)	S-04	0 - 5 bar	4 - 20mA
5	Temperature signal from gasifier (I-101)	S-05	0 - 1100^{o}C	0 - 45 mV
6	Signal from ionization probe (E-107 & E-108)	S-06	Flame ON/OFF	Digital (ON/OFF)
7	Signal from oxygen sensor (I-121)	S-07	0 - 21 %	0 - 10 mV
8	Signal from extraction fan switch (E-114)	S-09	Switch ON/OFF	Digital (ON/OFF)
9	Signal from burner controller (C-102)	S-17	Flame ON/OFF	Digital (ON/OFF)

10.2.3.2 PLC (C-101) Outlet Register

#	Outlet	Stream Number	Input Signal Stream
1	Feedback to oxygen tank solenoid valve (V-101)	S-10	S-09 S-07 S-05

2	Feedback to LPG tank solenoid valve (V-102 & V-103)	S-11 S-12	S-09 S-06 S-05 S-17
3	Signal to peristaltic pump switch (E-115)	S-13	S-09 S-05 S-04
4	Signal to alarm (E-113)	S-14	S-06 S-08 S-04 S-07 S-03 S-05 S-01

10.2.3.3 Emergency Button Outlet Register

#	Outlet	Stream Number
1	Feedback to central solenoid valve to simultaneously cut supplies of LPG and oxygen gas (V-104)	S-15
2	Signal to peristaltic pump switch (E-114)	S-16

10.2.3.4 List of Equipment

#	Location	Device Code
1	Entrained Flow Gasifier	R-101
2	Oxygen tank	E-101
3	Nitrogen tank	E-102
4	Helium tank	E-103

5	LPG tank	E-104
6	Compressed air filter and regulator	E-105
7	Flame arrester	E-106
8	Ionization probe 1	E-107
9	Ionization probe 2	E-108
10	Pyrolysis oil tank	E-109
12	Ethanol tank	E-110
13	Peristaltic pump	E-111
14	'Emergency Stop' button	E-112
15	Alarm	E-113
16	Extraction fan switch	E-114
17	Peristaltic pump switch	E-115

10.2.3.5 List of Thermocouples

#	Location	Device Code	Physical Range	Signal Range	TC Type	Auto Logging?
1	EFG inner reactor 1	I-101	0 - 1100ºC	0 - 45 mV	K	Y
2	EFG inner reactor 2	I-102	0 - 1100ºC	0 - 45 mV	K	Y
3	Cooling jacket floor	I-103	0 - 1100ºC	0 - 45 mV	K	Y
4	EFG inner reactor 3	I-104	0 - 1100ºC	0 - 45 mV	K	Y
5	EFG cavity (top)	I-105	0 - 1100ºC	0 - 45 mV	K	Y
6	EFG cavity (bottom)	I-106	0 - 1100ºC	0 - 45 mV	K	Y
7	Product gas line	I-107	0 - 1100ºC	0 - 45 mV	K	Y

10.2.3.6 List of Pressure Devices

#	Location	Device Code	Physical Range	Signal Range	Signal Type	Auto Logging?
1	EFG inner reactor	I-108	0 - 2.1 bar	4-20 mA	Analog	Y
2	EFG cavity	I-109	0 - 2.5 bar	N/A	Pressure Gauge	N

3	Oxygen line	I-110	0 - 6.9 bar	4-20 mA	Analog	Y
4	Pyrolysis oil line	I-111	0 - 6.9 bar	4-20 mA	Analog	Y
5	Burner air line	I-112	0 - 6.9 bar	4-20 mA	Analog	Y

10.2.3.7 List of Rotameters

#	Location	Device Code	Physical Range	Signal Range	Signal Type	Auto Logging?
1	Oxygen line	I-113	0 - 4000 L/h	N/A	N/A	N
2	Nitrogen line	I-114	0 - 10 L/min	N/A	N/A	N
3	Helium line	I-115	0.3 – 5.8 L/min	N/A	N/A	N
4	LPG line 1	I-116	0 - 11 L/min	N/A	N/A	N
5	LPG line 2	I-117	0 - 11 L/min	N/A	N/A	N
6	Burner air line 1	I-118	0 – 170 L/min	N/A	N/A	N
7	Burner air line 2	I-119	0 – 170 L/min	N/A	N/A	N

10.2.3.8 List of other devices

#	Location	Device Code	Physical Range	Signal Range	Signal Type	Auto Logging?
1	Pyrolysis oil line	I-120	0 - 2000 L/min	1050 pulses/L	Digital pulse	Y
2	Oxygen sensor on product gas line	I-121	0 - 21%	0 - 10 V	Analog	Y
3	CO sensor	I-122	0 - 250 ppm	N/A	N/A	N

10.3 Appendix C: Operation Procedures and Checklist

SAFETY NOTE: Make sure appropriate Personal Protection Equipment (PPE) is used before starting operation. This includes lab coat, heat resistant apron, safety glasses and closed sturdy shoes. When handling of hot parts/materials are required, use appropriate heat resistant gloves and face shield to prevent burn.

Prior to Gasifier Operation

1. Check the availability of electricity, compressed air and low pressure water.
2. Prepare product sampling components and assembly (Micro-GC, SPE columns, sampling probes, syringes and 3-way valve).
3. Check there is **sufficient amount of pyrolysis oil, ethanol, LPG gas, oxygen gas, nitrogen gas and helium gas** for the planned run. Use new gas bottles if the gas contents are less than the required amount.
4. Check operation of CO sensor, particularly the battery level.
5. Assemble the atomizer and cooling jacket so that they are ready to be used for gasification.
6. Using torchlight, inspect the condition inside gasifier to make sure no significant amount of residues remains from previous experiments. Also make sure all its ports are not blocked. If required, clean the gasifier.
7. Make sure there is a bunk underneath pyrolysis oil tank and peristaltic pump to avoid oil spill or leak into drain.
8. Make sure the LPG, oxygen and nitrogen cylinders are not located close to the gasifier or any hot surface.
9. As part of safety requirement, there must always be at least 2 operators to run the system.

During Gasifier Operation

Start-up procedure:

1. Switch ON the Micro-GC.
2. Switch ON the main Extraction Fan above the entrained flow gasification system. The switch is located inside *Gasifier Control Room* on the main control panel. ***SAFETY NOTE:*** *Extraction fan must be turned ON at all time. Otherwise, LPG, oxygen or pyrolysis oil supplies will be blocked.*

3. Turn ON the *Main Compressed Air* supply valve.
4. Activate portable carbon monoxide (CO) sensor. Keep the sensor close to operator at all times.
5. Switch ON power to the *Main Control Box* located on the front of gasifier trolley.
6. Check all *Safety Alarm Set Values* in the Programmable Terminal (PT) LCD Display to make sure they are right. The values should be as follows:

#	Name	Alarm Value	#	Name	Alarm Value
1	P LPG Air 1	150 kPa	7	P Pyrolysis Oil Max	200 kPa
2	P LPG Air 2	150 kPa	8	P Oxygen Max	350 kPa
3	T Reactor Warning	1000^{o}C	9	P Oxygen Min	5 kPa
4	T Reactor Max	1050^{o}C	10	Oxygen % Max	5 %
5	T Reactor Min	500^{o}C	11	LPG Ignition Time	10 sec
6	P Reactor Max	10 kPa			

7. Make sure atomizer and cooling jacket assembly is placed on the dedicated ring holder mounted on the wall next to the gasifier (NOT on the gasifier body). This is critical so that the atomizer is not excessively heated during gasifier pre-heating period.
8. Cover cooling jacket slot on the main gasifier body with the dedicated metal cover. Add extra insulation over the metal cover.

9. Make sure the LPG rotameter needle valves are completely closed to avoid uncontrolled release of LPG when burners are switched ON. This is particularly critical if the burners are to be restarted at high gasifier temperature to prevent sudden LPG purge into the hot environment, which could potentially lead to serious explosion.
10. Open *Burner Air* regulator and set the outlet pressure to 160 kPa.
11. Adjust the air flow rate into *Bottom Burner* to 5cm on respective rotameters.
12. Open LPG cylinder valve. Regulate the gas outlet pressures to 100 kPa.
13. Turn ON *Bottom Burner* switch on the *Burner Controller Box*. Automatic ignition will take place.
14. Slowly adjust LPG gas flow rates into *Bottom Burner* to 2 L/h using respective rotameter. Listen to successful ignition (flame) sound.

SAFETY NOTE: *If ignition fails to take place, burner will automatically switched to LOCK-OUT condition for 10 seconds; for safety. This ensures sufficient purge of accumulated LPG in the gasifier before re-ignition.*

SAFETY NOTE: *Always start gas burners at low flow rates (i.e. at 2 L/h for LPG) to avoid sudden release of LPG gas into combustion chamber during ignition attempts. Low air and LPG flow rates also increase the chance of success ignition for the burners.*

15. When ignition is successful, gradually increase air and LPG flow rates to the desired set values (4 L/h LPG and 11cm on air rotameter). This must be done simultaneously to keep the right ratio for combustion.
16. Adjust the air flow rate into *Top Burner* to 5cm on respective rotameters.
17. Turn ON *Top Burner* switch on the *Burner Controller Box.* Similar ignition mechanism as for the *Bottom Burner* will take place.
18. Slowly adjust LPG gas flow rates into *Top Burner* to 2 L/h using respective rotameter.
19. When ignition success, gradually increase air and LPG flow rates to the desired set values (4 L/h LPG and 12cm on air rotameter). Similar to the *Bottom Burner*, this must be done simultaneously to keep the right ratio for combustion.

20. Monitor pressure change inside the gasifier cavity. There should not be any significant pressure build-up (above 0.05 kPa gauge) in the gasifier cavity during pre-heating.
21. When the gasifier temperatures reach 500^{o}C, open *Purge Air* regulator to allow small flow of fresh air into the gasifier to burn-off any remaining char or pyrolysis oil residues in the gasifier from previous experiments.
22. Leave the purge air to flow for at least 5-10 minutes. Then close *Purge Air* regulator to stop purging air into gasifier.
23. Let the temperatures continue to increase.
24. While waiting for gasifier temperature to increase, remove the lid of DEACON 8875 high temperature sealant container and mix the content thoroughly.

25. Using putty knife, apply a thin layer of DEACON 8875 sealant around the cooling jacket slanted surfaces to provide gas-tight seal between the cooling jacket and gasifier body.

During gasification operation:

1. When gasifier temperatures reach 700^{o}C and the operators are ready, switch OFF *Top and Bottom Burner* switches on the *Burner Controller Box*.
2. Stop compressed air supplies into both burners by closing their rotameters.
3. Turn ON cooling water inlet valve for the cooling jacket. Make sure water exiting the cooling jacket is directed into drain.
4. When ready, remove the metal cover from the cooling jacket slot. Place the hot metal cover on the dedicated area (on the gasifier trolley) and leave it to cool. ***SAFETY NOTE:*** *Heat resistance glove, heat resistance apron and face shield must be used for this step. Due to narrow space available on the platform, do not step down the platform or move backwards when removing the metal cover.*
5. Use a special ring holder to move and drop the cooling jacket and atomizer assembly onto the slot. Make sure the jacket fits perfectly in the slot to avoid gas leak. ***SAFETY NOTE:*** *Mind your steps when stepping down the platform.*
6. Take the hot metal cover and replace it at far end corner of the laboratory room – away from operator. Leave it to cool to ambient.

7. Ignite producer gas after-burner
8. Open *Purge Air* regulator to allow small flow of fresh air into the gasifier to create an oxygen-rich environment. ***NOTE:*** *This is important to combust oil injected into gasifier before atomizing air is introduced (during start-up) to avoid oil accumulation in the system.*
9. Open oxygen cylinder valve. Regulate the gas outlet pressure to 250 kPa.
10. Switch ON '*Pyrolysis Oil Supply'* switch on the *Main Control Box.*
11. Adjust peristaltic pump RPM value corresponding to the desired oil feed flow rate. ***SAFETY NOTE:*** *It is advisable to start with a low RPM values.*
12. Press 'START' button on the peristaltic pump to start feeding oil into gasifier. ***NOTE:*** *It may take few minutes for the oil to reach atomizer from the pump. As soon as the oil flows out the atomizer, gasifier temperature is expected to decline rapidly due to liquid evaporation.*
13. Monitor the oil flow rate, making sure its value continuously changing hence indicating oil flow through the meter. ***NOTE:*** *If the oil flow rate reading on PT remains constant at a fix value, this indicates no flow. Switch OFF 'Pyrolysis Oil Supply'* switch on the *Main Control Box. Fix blockage before restarting peristaltic pump.*
14. Switch ON '*Oxygen Gas Supply'* switch on the *Main Control Box.*

15. Gradually adjust oxygen rotameter to control oxygen feed rate into the gasifier following the desired Equivalence ratio (ER) value. ***SAFETY NOTE:*** *Strictly, plan and perform ER calculations prior to each operation.*

16. Monitor decrease in oxygen concentration in the product gas line. ***NOTE:*** *Oxygen concentration alarm will be activated when the concentration drops below the set value (5%) for the first time. The alarm could be reset by switching OFF oxygen supply switch and until oxygen gas supply pressure has dropped below the set 'P Oxygen Min' value (5 kPa).*
17. Monitor the gasifier temperature so that it does not fall below the minimum operating temperature limit (600^{o}C).

18. Open helium gas regulator and adjust rotameter to 2.5 L/min. ***NOTE:*** *Helium acts as a tracer gas during gasification while at the same time keeping the side glass clean from soot and char deposit.*
19. Wait for at least 30-45 minutes until gasifier temperatures stabilize. Monitor temperatures changes so that they remain within the allowable minimum and maximum operating range.
20. When gasifier middle and bottom temperatures stabilize, take gas samples from the system. Refer to *Gas Sampling Procedure* section for detailed sampling procedures.
21. Increase oil feed rate into the gasifier as required, by changing RPM setting on the peristaltic pump.

Product Sampling Procedure:

NOTE: *TRACER GAS needs to be injected into the system to determine the total product gas flow rate from gasification. In this study, Helium gas is the most appropriate tracer.*

1. Open the gas sampling valve.
2. Insert the sampling rod through the sampling port.
3. Switch the 3-way valve on direction where product gas could flow through SPE columns into the 100 mL syringe.
4. Pull 100 mL product gas into the syringe. Repeat this step three times to obtain 300 mL of gas sample in total.
5. Switch the 3-way valve to off position. Then switch the 3 way valve to the 60 mL syringe.

6. Inject around 30-60 mL of producer gas sample from the 100 mL syringe into the 60 mL syringe to be used for Micro-GC analysis. Dispose the remaining gas in the 100 mL syringe.
7. Remove the sampling assembly from the port. Then close the gas sampling valve.
8. Inject gas sample in the 60 mL syringe into the Micro-GC
9. Follow Micro-GC operating procedures.
10. Keep the used SPE columns in a clean and labelled plastic bag. Store the bag in a refrigerator to avoid compounds evaporation. These columns will be later used for tar analysis by GC.

Shut-down procedure:

1. Switch OFF '*Oxygen Gas Supply'* switch on the *Main Control Box.*
2. Close oxygen gas cylinder regulator.
3. Switch OFF '*Pyrolysis Oil Supply'* on the *Main Control Box.*
4. Close LPG cylinder valve to isolate supply.
5. Open *Purge Air* regulator. ***NOTE:*** *Purge air functions to purge accumulated producer gas and burns-off leftovers char and residues in the gasifier from the experiment.*

6. Close pyrolysis oil supply valve located right after ash filter. Then open ethanol supply valve located on ethanol cleaning system to allow ethanol feeding.
7. Swap 'double Y tubing' fitted inside the peristaltic pump head with the one dedicated for ethanol.
8. Now switch ON '*Pyrolysis Oil Supply'* switch on the *Main Control Box.*
9. Adjust peristaltic pump RPM value to 5RPM.
10. Press 'START' button on the peristaltic pump to start feeding ethanol into gasifier. Ethanol will dilute and clean pyrolysis oil residues in flow meter and atomizer assembly to prevent clogging or blockage resulted from oil ageing.
11. Leave ethanol to flow for 5-10 minutes. Ethanol exiting the atomizer will vaporize at high temperature and combust with the presence of purge air in the gasifier.
12. Press 'STOP' button on peristaltic pump to stop ethanol flow.
13. Release tubing track from peristaltic pump head assembly by lifting the two levers at either side of the pump head to relief pressure on transfer tubes. This helps to increase tube lifespan. Make sure the track is re-assembled before next operation.
14. Close *Purge Air* regulator.

15. Lift atomizer and cooling jacket from the main gasifier body to avoid it from getting trapped or jammed in its slot due to uneven contractions as well as solidifying cooled sealant. ***SAFETY NOTE:*** *Heat resistance glove, heat resistance apron, respirator and face shield must be used for this step.*
16. Place the hot cooling jacket on the allocated ring holder mounted on the wall next to the gasifier.
17. Place 'CAUTION: HOT' warning sign on the gasifier and allow the system to cool.

After Gasifier Operation

1. Ensure the gasifier is cooled sufficiently before conducting any inspection, analysis or before it is taken apart.
2. Clean the gasifier body particularly the cooling jacket slot from dried DEACON sealant.
3. Clean cooling jacket surfaces particularly the area covered by dried DEACON sealant. Soak the cooling jacket in water so that any residues on it could be easily removed.
4. Clean all sight glasses from soot and char deposit
5. Clean atomizer outlet from char deposit. Usually the atomizer
6. Check solid filter and sampling port, making sure no blockage
7. Clean oxygen sensor from any deposit
8. Analyse tar captured in the SPE columns using GC.

9. The entrained flow gasification system needs to be inspected and maintained every 6 months

10.4 Appendix D: Methods for Pyrolysis oil Properties Analysis

The analysis methods used to measure properties of pyrolysis oil relevant in this study are summarized in Table 10-8. This chapter will provide detailed procedures for each analysis methods for future reference. The procedures were developed by Ms. Jingge Li during her appointment as a research associate at the Chemical and Process Engineering Department, University of Canterbury. Various sections of the procedures have been modified and revised to suit pyrolysis oil application in this work.

Table 10-8: Summary of pyrolysis oil properties measured in this work and the relevant analysis methods

Physical Property	Analysis Method
Water content	ASTM E203, Karl-Fischer titration
Viscosity	ASTM D445, Cannon-Fenske Routine capillary viscometer, No. 100
Acidity (pH)	pH meter, Eutech pH 510
Density	ASTM D4052, Anton Paar DMA60 digital density meter

10.4.1 Water Content

Pyrolysis liquids contain low-boiling (below 100 °C) compounds and hence any drying method cannot be used (Oasmaa et al, 1997). There are two standard methods for Karl Fischer titration: in ASTM D1744, the titration solvent is a mixture of chloroform and methanol (3:1) and in ASTM E203 (2008) a mixture of pyridine and ethyleneglycol monomethylether (1:4). The latter method is suitable for determining moisture in samples containing aldehydes and ketones. For radiata pine pyrolysis oil, Marosky (2008) suggested to use the ASTM E203.

The fundamental principle of Karl Fischer titration in ASTM E203 is based on the reaction between iodine and sulphur dioxide in an aqueous medium. The basic reaction is modified, so that water in a non-aqueous system with an excess of sulphur dioxide can be determined. The Karl Fischer reaction (Equation 1) uses a primary alcohol as solvent and a base as buffering agent (ASTM E203).

The general reactions behind Karl Fischer titration are as follows:

$CH_3 OH + SO_2 + RN \rightarrow [RNH] SO_3 CH_3$

Methanol + sulphur dioxide + organic base → intermediate

$[RNH]\,SO_3\,CH_3 + H_2O + I_2 + 2\,RN \rightarrow [RNH]\,SO_4\,CH_3 + 2\,[RNH]\,I$

Intermediate + water + iodine + organic base → hydro-iodic acid salt + alkyl-sulphate salt

* *Learn more at:* http://www.sigmaaldrich.com/technical-documents/articles/analytical/basic-principles-of-karl-fischer-titration.html#sthash.bRoLAOhT.dpuf

The alcohol reacts with sulphur dioxide and the base to form an intermediate alkylsulfite salt, which is oxidised by iodine to an alkylsulfate salt. Water is consumed during this oxidation reaction. Typically methanol is used as reactive alcohol. The base used to be pyridine, a noxious carcinogen, which is nowadays replaced by less harmful imidazole or primary amines. Water and iodine are consumed in a ratio of 1:1 (see Equation 1). If all the present water in the sample is consumed, the excess iodine is detected voltametrically by the titrator's indicator electrode, which signals the end-point of titration. The water amount in the sample is then calculated based on the concentration of iodine (Marosky 2008). The Karl-Fischer Titrator dose the calculation automatically and gives the result of water content directly.

3.2.1 Equipment and reagent

- Volumetric Karl-Fischer Titrator: TitraLab TIM 550 of Radiometer-analytical in CAPE as shown in Figure1. It should be setup and ready to go with new reagent, new solvent, empty container for used solvent, and regenerated molecular sieve.
- Titration reagent: Sigma Aldrich HYDRANAL Composite 5, 4.5-5.5mg H_2O/ mL, which contains all required chemicals including iodine, sulphur dioxide and the base, dissolved in alcohol.
- Solvent: Dry methanol.
- Molecular sieve: regenerated in two stages 1) wash with deionised water 4-5 times to eliminate SO, and 2) dry it in an oven at 250-300°C overnight.
- Water standard: 15.66% H_2O
- Scale: 4 digit
- Syringe: 10 mL for water standard and 1 mL for pyrolysis sample.
- Needle for syringe: 23-25 gauge

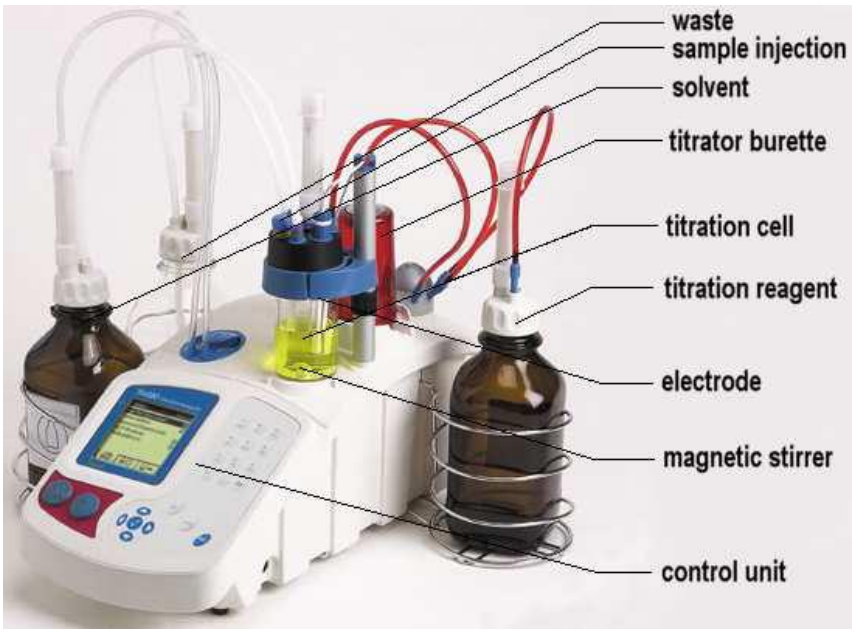

Figure 10–1: Volumetric Karl Fischer Workstation at the University of Canterbury

3.2.2. Procedure

The titrator is turned on using the switch on the back of the instrument (<Run method> is shown), and operated according to the TIM550 User's Manual or the procedure with parameters setup below. The cell and burette can be emptied or filled, and stirring speed can be adjusted using the cell and burette functions as shown in the manual.

Setup

Burette, press for 3 s

↓KF reagent No. 5

↓Reageant 5 <Edit>

↓KF reagent ID: Stand (typed using the keyboard A-Z)

↓KF reagent titre <Calibrate> (search using →)

↓Autostart <No>

↓Cal. Every 7 days

→Edit <Parameters>

↓Drift threshold: 60μg/min

↓Max. burette speed: 150%/min (default)

↓Min. titration time: 00:30 (min:s)

↓Max titration time: 00:10 (h:min)

↓Max volume: 20 mL (in case that injection volume is larger than planned)

↓Quality control: yes

↓Min titre: 0.001mg/mL (default)

↓Max titre: 9999.999mg/mL (default)

---end of menu---↓

→Edit<Standard>

↓Standard ID: No

↓Standard unit: g

↓Advised amount: 0.10g (ideally inject amount similar to sample)

↓H_2O in stand: 15.66 ±0.05%

---end of menu---

Titration method

Method, press for 3 s

Method <7> <Edit>

↓Method ID: Jingge

↓Use Oven: <No>

↓Autostart: <No>

↓Blank: <No>

→Edit <Parameters>

↓drift threshold: 60µg/min (default)

↓Max. burette speed: 150%/min (default)

↓Min. titration time: 00:30 (min:s)

↓Max titration time: 00:10 (h:min)

↓Max volume: 20 mL

---end of menu---

→Edit<Sample>

↓Sample ID: yes

↓Sample unit: g

Advised amount: 0.05g

(Note: This is the targeted sample amount. To introduce sample, inject approximately 0.5 mL sample into the titration cell using syringe)

↓Sample factor: 1.000

↓Result unit: %

↓Number of digit: 5

↓Quality control: yes

↓Min titre: 0.001% (default)

↓Max titre: 9999.999% (default)

---end of menu---

Measurement

Reagent calibration (repeat 3 or 5 times)

Press Burette

Burette <Reagent Cal.> √

↓Standard No: 1

↓Drift: ST==60 µg/min

(Note: This reading may start with up to 5 figures if using new solvent and/or if the system is not used for a long time. This situation will lead to significant burette reagent consumption. Let it go for a while to neutralize the water in the system, the drift will reach to the setup value eventually. If the drift takes unreasonably long time to stabilize, this may indicate leak or consistent source of H_2O somewhere in the system. In this case, stop the titration immediately and clean the system before continue).

Warning: Avoid leaving the system to drift for too long since this will rapidly use the titration reagent!

↓Introduce std: 0.1g press √ (Titration starts automatically. Ideally this amount is similar to sample amount)

↓Std. amount: exact g by weighing, type in using the A-Z √

↓Result shown

↓Accept result: yes if reasonable, no otherwise

↓Mean xxx mg/mL

KF titration of sample

Press Method

Method: Jingge <7>

Press Run

Sample ID: PyOil (typed using the A-Z) √

↓Sample no: 1√

↓Drift: ST== 60 µg/min (see above, may take long time to reach this value)

↓Introduce sample 0.05g √

↓Sample amount: Enter the exact sample weight from weighing balance √

↓Result shown

↓Accept result: yes if reasonable, no otherwise.

To verify the calibration, 0.1 grams of 15.66% water standard is injected into the cell (as sample) and the general water content analysis is performed. The derivation from 15.66% water content is recorded and the analysis is repeated several times. Based on the average derivation, a correction factor is formulated. Different pyrolysis oil samples are now ready to be analyzed. Each sample is tested 3 times, the value is corrected and the average is taken.

10.4.2 Viscosity

Viscosity describes a fluid's internal resistance to flow and may be thought of as a measure of fluid friction (Wikipedia 2012). There are two types of viscosity: dynamic viscosity, also called absolute viscosity, the ratio between the applied shear stress and the rate of shear of a liquid; and kinematic viscosity, the resistance of a fluid to flow under gravity (Marosky 2008). Kinematic viscosity can be determined by measuring the time for a volume of liquid to flow under gravity through a calibrated glass capillary viscometer as specified in ASTM D445. It usually expressed as Centistoke (cSt) (1cSt = 1 mm^2/second). The dynamic viscosity in mPa.s can be obtained by multiply the kinematic viscosity (mm^2/s) by the density (kg/m^3) of the liquid (ASTM D445). The operation instruction is given in ASTM D446 for glass capillary kinematic viscometers. Kinematic viscosity is a product of the measured flow

time and the calibration constant of the viscometer. Tow such determinations are needed from which to calculate a kinematic viscosity result that is the average of two acceptable values.

3.3.1. Equipment and reagent

- Water bath: with temperature being controlled at 20 and 50°C, in sufficient water depth to immerse the sample in the viscometer;
- Stop watch: with accuracy of 0.1 second;
- Viscometer holder;
- Ethanol: technical grade for cleaning the viscometer as ethanol is completely miscible with the pyrolysis oil;
- De-ionised water: for final cleaning the viscometer;
- Syringe: 100 mL for sucking and drawing the pyrolysis oil in the viscometer;
- Viscometer:

There is a range of viscometers that could be used for this purpose. In this experiment, five viscometers chosen to used are:

Viscometer Type	Cannon-Flask Routine			BS/IP/RF	BS/U
Viscometer Size	150	200	300	5	F
Range (cSt)	7-35	20-100	50-250	60-300	200-1000

Example of viscometer setup for pyrolysis oil viscosity measurement in this work is shown in Figure 10–2. Calibration of viscometer was performed by using viscosity calibration standards with known liquid viscosity at different temperatures to determine viscosity constants (cSt/s) for each capillary viscometer.

The only function of the upper bulb on the capillary arm is to serve as an accurate loading device in conjunction with the end capillary and efflux bulb. Laboratory experiments show that the instrument and liquid contents reach a bath temperature of 37.78°C in 4 minutes and a temperature of 98.8°C in about 10 minutes (Cannon and Fenske 1938).

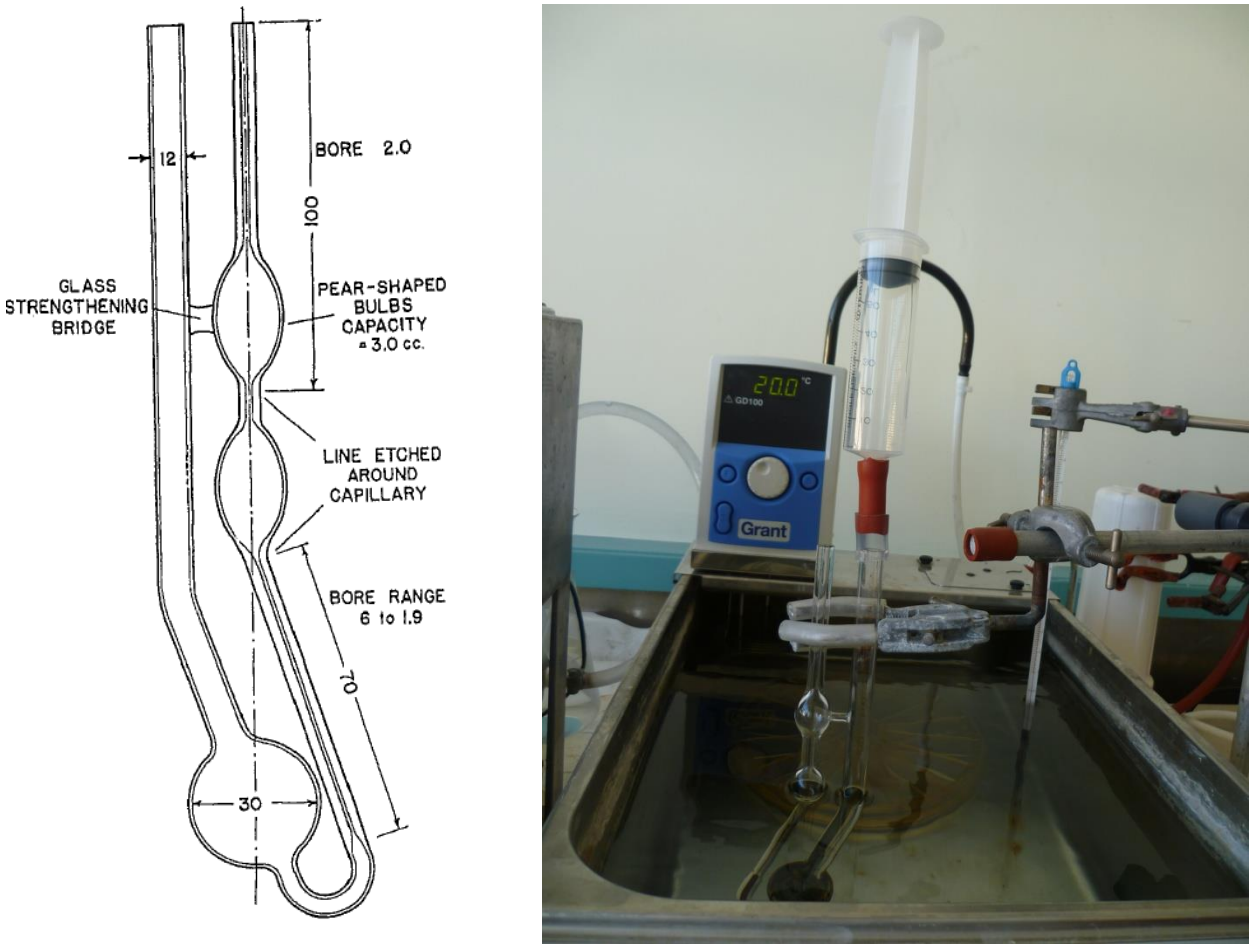

Figure 10–2: Cannon-Fenske Routine viscometer and its set up in a water bath

3.3.2 Procedure

1. The water bath is filled with water and heated to a constant temperature of 20°C.
2. Procedures to fill pyrolysis oil into the viscometer type may vary significantly from one viscometer type to another. Therefore, appropriate procedures for the selected viscometer have to be followed.
3. Then the viscometer was fixed in the constant-temperature water bath with a viscometer holder for 10 minutes.
4. The efflux time is obtained by drawing the liquid up to the mark between the bulbs and measuring the time required for the meniscus to pass from the mark between the bulbs and the mark below the lower bulb on the capillary.
5. The viscosity (ν, cSt) of the pyrolysis oil is then calculated by multiplying the efflux time t (s) by the viscosity constant C (cSt/s) using the equation of $v = Ct$.

10.4.3 Acidity (pH)

The pH of pyrolysis liquids is low (2 - 3) due to high amounts (8 - 10 wt%) of volatile acids, mainly acetic and formic acids (Oasmaa et al 1997). The pH is measured with a pH meter.

3.5.1 Equipment and reagent

- pH meter: EUTECH pH510 as shown in Figure 10–3 with an accuracy of pH measurement about ±0.02.
- Ethanol: ≥ 97%, technical grade for cleaning.
- Deionised water: for cleaning.

3.5.2 Procedure

Calibration

A two-point calibration is performed with certified traceable standard reference material.

• 4.01 ± 0.01 (red);

• 7.00 ± 0.01 (green);

Measurement

A pyrolysis oil sample of 50 mL is taken from the container and measured for its pH by reading the value.

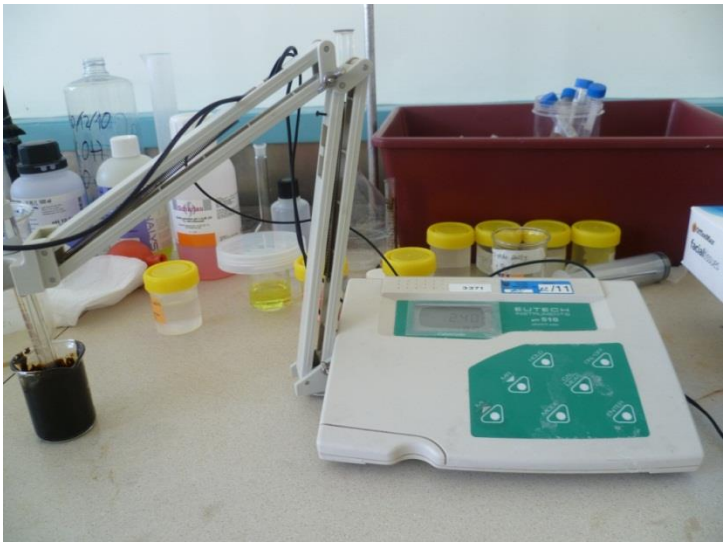

Figure 10–3: pH meter of EUTECH pH 510

10.4.4 Density

Density is known as mass per unit volume of a substance at a certain temperature and pressure. For a petroleum distillates and viscous oils, density can be determined according to ASTM D4052 by digital density meter using either manual or automated sample injection equipment. A small volume (1-2 mL) of liquid sample is introduced into an oscillating sample U-tube and the change in oscillating frequency caused by the change in the mass of the tube is used in conjunction with calibration data to determine the density. The laws of physics state that the period of spring is directly proportional to the square root of the mass. Thus with a constant volume U-tube the mass or density is linearly related to the square of the period of oscillation.

3.4.1 Equipment and reagent

- Digital density meter: Anton Paar DMA60 as shown inFigure 10–4. It gives a read of the period of oscillation for the U-tube.
- Ethanol: ≥ 97%, technical grade for cleaning the U-tube.
- Deionised water: for cleaning and calibration.

Figure 10–4: Anton Paar DMA60 digital density meter

3.4.2 Procedure

1. Plug in the unit and turn on the solvent bath heater (Julabo F10), temperature controllers JulaboC and Fluke 2200. Set the temperature to 20°C at the both temperature controllers.
2. Swith on both DMA60 and DMA 602 (switches should be up), set oscillation counter on the DMA60 to 1K and input selector to cell 1.
3. Press start on the DMA60 and counter should start cycling.
4. Remove the cover (labelled Top) of the DMA602.
5. Ensure the cell is clean and dry out the cell by connecting the plastic tube from the pump to the top syringe connection and turn on the air pump on DMA602. When the period has settled turn off the pump.
6. Record the period for air. The value should be between 0.259572 and 0.259579. A value higher than this indicates the tube is wet or dirty.
7. Fill 1 mL a syringe with deionised water; inject it through the bottom connection. A plastic tube is inserted into the upper connection to allow sample to come out without spilling.
8. Record the period of deionised water. It was 0.338719 on 30 Sep. 05 by unknown, 0.338741on 31 Jan 2012 and 0.338740 on 21 Sep 2012 by Jingge. A lower value can indicate air bubbles are present.
9. Remove the water using the syringe and flush the remaining water out with the air pump.
10. Insert 1 mL pyrolysis oil with a syringe into the bottom connection, record the period.
11. Remove the sample, clean the tube by injecting and removing ethanol a few times until the ethanol is colourless, then flush with deionised water and dry with the air pump. If there is any chance that it is not complete clean don't dry any contaminant onto the U-tube.
12. Duplicates were measured.

3.4.3 Calculation

The density (ρ, kg/m³) is calculated from:

$$\rho = \rho_w + \left[\frac{\rho_w - \rho_a}{\tau_w^2 - \tau_a^2}\right](\tau^2 - \tau_w^2)$$

Where at 20°C:

ρ_w is water density, 998.2 kg/m³;

ρ_a is air density, 1.21 kg/m³;

τ is oscillation period of the pyrolysis oil;

τ_w is oscillation period of the water, 0.338741;

τ_a is oscillation period of air, 0.259572.

10.5 Appendix E: Solution Preparation, Tar Extraction and Analysis Procedures

Tips on Using Pipette for DCM and Other Volatile Samples

DCM is a volatile solution hence its measurement using pipette is considerably technical. It readily vaporizes at room temperature and consequently causes significant measurement errors if not handled cautiously. These are few basic procedures that could be followed to minimize errors when using pipette for such samples:

i. Always use pipette plunger to the second stop. This allows extraction of extra liquid into pipette tip so that evaporation of some sample off the tip could be compensated

ii. Flush sample in pipette for 5-6 times (using the first stop). This is important so that excessive DCM evaporation could be avoided besides slowing down liquid dripping speed to a more manageable rate

iii. When pipetting, avoid even a single extra droplet from the pipette since this could significantly affect the final amount. To accomplish this, quickly move pipette tip away from vial/flask mouth as soon as pipette head come to the first stop. This require some practice before every pipetting so that a more consistent transfers could be made

$1\ ppm = 1\mu l/L = 1ml/m^3 = 1mg/L = 1mg/kg$

IMPORTANT: Rinse all apparatus required for this analysis using DCM and leave to dry. This removes any contaminants from the apparatus which may affect results.

10.5.1 Solution Preparations for Tar Calibration and Tar Extractions

10.5.1.1 Overall Instructions for Internal Standard and Tar Standard Preparation

1. Prepare stock internal standard solution of approximately 400 ppm. Separate the solution in as many 2 mL vials as required, ready to be used for tar standard calibration and tar sample extraction. The complete procedures for this are given in Section 10.5.1.2.
2. Use GC to check consistency of Internal Standard peaks. Discard deviated standards if required.
3. Dilute Light Tar and Heavy Tar standards (2000 ppm) into concentrations of 1000 ppm. Similarly separate the solution in several 2 mL vials, ready to be used for tar standard calibration. The complete procedures for this are given in Section 10.5.1.3.
4. Prepare the pre-determined tar standard concentrations by mixing required volume of 1000 ppm Light Tar and Heavy Tar solutions into 2 mL vials. The complete procedures for this are given in Section 10.5.1.4. *NOTE: DO NOT add Internal Standard to the mixture until when ready to be used. Make sure the same internal Standard is used for tar calibration and tar sample extraction.*

10.5.1.2 Internal Standard Preparation

1. Pipette 0.1 mL of dodecane into a 25 mL volumetric flask using 20-200µl pipette.
2. Then weigh dodecane mass using a balance. The weight should be 0.0765 ± 0.0005 grams.
1. Fill DCM into the volumetric flask until the marked line. This should make a 25 mL of 4000 ppm dodecane solution. Label the volumetric flask.
2. Transfer 10 mL of 4000 ppm solution into a 10 mL volumetric flask i.e. until marked line.
3. Then transfer the 10 mL solution into a 100 mL volumetric flask. Fill DCM into the volumetric flask until marked line to produce 100 mL of 400 ppm internal standard. Label the volumetric flask.
4. Transfer 1 mL of the 400 ppm Internal Standard into a 2 mL vial. Then replace its lid. Repeat this to as many vials as required.
5. Label and store the prepared standard in a fridge for used during tar extraction and analysis.

10.5.1.3 Tar Standard Preparation for Calibration

Tar calibration is required every time a new Internal Standard solution is prepared.

This calibration aims to obtain calibration curve of known tar species and their concentrations relative to that of the internal standard. To achieve this, Tar Standard solutions are required. There are 2 types of Tar

Standards which are Light Tar Standard (LT) and Heavy Tar Standard (HT). List of tar standard concentrations required for the calibration is as follows:

NOTE: In this case, it is not possible to use pipette until the 2nd stop due to limited volume of tar standard available. Therefore normal forward pipetting method needs to be used in this case. Other than that tip of pipette must not be submerged too deep in the sample as this could cause precious samples to overflow from its container.

10.5.1.3.1 Dilution of Light Tar (LT) Standard Mix

1. Break LT Standard Mix ampule containing 2 mL of 2000 ppm light tar components.
2. Using disposable pipette, quickly transfer ampule content into a 3 mL centrifuge tube and replace its cap. Label and store the centrifuge tube in fridge if required.
3. When ready, use a 1000µl pipette to transfer 900µl of LT standard into a 2 mL vial. Then replace its lid. Repeat this to a second 2 mL vial to use 1800µl of the LT standard. Note: The remaining 200µl of the standard may not be utilized as it is impossible to extract the ampule completely.
4. Pipette 900µl of DCM into each vial to dilute the tar standard mix to 1000 ppm; ready to be used for Calibration Set samples.
5. Label and store the prepared standard in a fridge.

10.5.1.3.2 Dilution of Heavy Tar (HT) Standard Mix

1. Break HT Standard Mix ampule containing 1 mL of 2000 ppm heavy tar components.
2. Using the 1000µl pipette, transfer 400µl of HT standard into a 2 mL vial. Then replace its lid. Repeat this to another vial to use 800µl of the HT standard. Note: The remaining 200µl of the standard may not be utilized as it is impossible to extract the ampule completely.
3. Pipette 400µl of DCM into each vial to dilute the tar standard mix to 1000 ppm; ready to be used for Calibration Set preparation.
4. Label and store the prepared standard in a fridge.

10.5.1.4 Solution Preparation Steps for Tar Calibration

1. **0.1 mL 1000 ppm LT standard + 0.1 mL 1000 ppm HT standard + 0.8 mL DCM = 1 mL of 100 ppm LT-HT solution**
2. 0.1 mL of 100 ppm LT-HT solution + 0.1 mL IS + 0.8 mL DCM = 1 mL of 10 ppm LT-HT-IS solution
3. 0.2 mL of 100 ppm LT-HT solution + 0.1 mL IS + 0.7 mL DCM = 1 mL of 20 ppm LT-HT-IS solution

4. 0.5 mL of 100 ppm LT-HT solution + 0.1 mL IS + 0.4 mL DCM = 1 mL of 50 ppm LT-HT-IS solution

5. **0.1 mL of 100 ppm LT-HT solution + 0.9 mL DCM = 1 mL of 10 ppm LT-HT solution**
6. 0.1 mL of 10 ppm LT-HT solution + 0.1 mL IS + 0.8 mL DCM = 1 mL of 1 ppm LT-HT-IS solution
7. 0.5 mL of 10 ppm LT-HT solution + 0.1 mL IS + 0.4 mL DCM = 1 mL of 5 ppm LT-HT-IS solution

10.5.2 GC Column Conditioning

The aim of column conditioning is to clean the column from any residues and contaminants from previous experiments. Column conditioning generally takes at least 80 minutes to complete and is performed in three stages:

Step	Temperature (°C)	Temperature Rate (°C/min)	Hold Time (minutes)	Total Time (minutes)
1	50	-	1	1
2	210	10	0	17
3	340	50	60	79.6

The procedures for column conditioning are as follows:

1. Fill one 2 mL vial with pure DCM and close the lid
2. Place the vial in Gas Chromatography (GC) sample holder
3. In the GC software, change the analysis method to ‘Column Conditioning’
4. Complete other information required and press START SAMPLE

10.5.3 Tar Calibration in GC

Tar calibration is conducted to extract important information related to each tar species present in the tar standard so this information can be used during analysis of tar samples from entrained flow gasification experiments. The calibration is performed by analysing known concentrations of the tar in the GC to

determine retention times of each tar species and signal counts that correspond to various tar concentrations.

To minimize errors due to rapid solvent evaporation during tar extraction and analysis, an internal standard is used. In this work, dodecane is used as the internal standard and the concentration is fixed at 40 ppm. The internal standard is added to the solvent during both calibration and tar sample analysis. With the use of internal standard, ratios of signal counts between each tar component and the internal standard are used to construct calibration curves that can be used to estimate concentrations of tar in the producer gas during gasification. Examples of information gathered during tar calibration as well as the resulted calibration curves used in this work are illustrated in Table 10-9 and Figure 10–5 respectively.

Table 10-9: Key information gathered during tar calibration (Note in this example, tar standard concentrations of 4 ppm, 12 ppm, 16 ppm and 40 ppm were used)

#	Ret Times	Tar Species	Signal Count				Ratio to Internal Standard			
			Species Concentration (µg/mL)				Species Concentration (µg/mL)			
			4	12	16	40	4	12	16	40
1	2.44	Toluene	8563	29406	36752	80013	0.39	1.30	1.79	3.74
2	2.76	Pyridine	4059	19356	25002	57122	0.18	0.85	1.22	2.67
3	3.41	p-xylene + Ethylbenzene	8103	28652	35650	78171	0.37	1.26	1.73	3.65
4	3.47	m-xylene	17790	60517	75822	164383	0.81	2.67	3.69	7.67
5	3.88	o-xylene	8607	29909	37472	81370	0.39	1.32	1.82	3.80
6	4.07	Styrene	8805	30405	38080	82740	0.40	1.34	1.85	3.86
7	5.72	Phenol	6763	22753	28985	62901	0.31	1.00	1.41	2.94
8	6.42	Dodecane (Internal Standard)	22053	22704	20568	21422	1.00	1.00	1.00	1.00
9	6.69	Indene	8685	28935	36261	78576	0.39	1.27	1.76	3.67
10	6.85	o-cresol	7152	24028	30713	66172	0.32	1.06	1.49	3.09
11	7.17	m+p-cresol	13915	46050	59728	128027	0.63	2.03	2.90	5.98
12	9.14	Naphthalene	3605	12000	15332	33106	0.16	0.53	0.75	1.55
13	10.43	Quinoline	6900	24079	32020	69369	0.31	1.06	1.56	3.24
14	10.60	2-Methylnaphthalene	3783	12144	15810	33798	0.17	0.53	0.77	1.58
15	10.76	Isoquinoline	5945	21044	29863	64763	0.27	0.93	1.45	3.02
16	10.95	1-Methylnaphthalene	3555	10940	14780	31492	0.16	0.48	0.72	1.47
17	11.88	Biphenyl	9641	30560	39966	84797	0.44	1.35	1.94	3.96
18	13.20	Acenaphthylene	3562	11284	14939	31988	0.16	0.50	0.73	1.49
19	13.51	Acenapthene	3653	11280	14895	32052	0.17	0.50	0.72	1.50
20	14.73	Fluorene	3544	10894	14680	31290	0.16	0.48	0.71	1.46
21	17.29	Phenanthrene	3596	10179	14198	29837	0.16	0.45	0.69	1.39
22	17.35	Anthracene	3460	9854	13865	29341	0.16	0.43	0.67	1.37
23	18.76	Fluoranthene	4474	12961	17463	32234	0.20	0.57	0.85	1.50

24	19.00	Pyrene	4749	15506	40333	67239	0.22	0.68	1.96	3.14
25	19.87	Bens(a)anthracene	6351	11387	15706	29498	0.29	0.50	0.76	1.38
26	19.93	Chrysene	9666	15253	18686	111834	0.44	0.67	0.91	5.22
27	20.73	Benso(b)fluoranthene	9424	12522	15959	29813	0.43	0.55	0.78	1.39
28	20.78	Benso(k)fluoranthene	7316	11913	16138	29863	0.33	0.52	0.78	1.39
29	21.22	Benso(a)Pyrene	14694	17969	19606	36852	0.67	0.79	0.95	1.72
30	22.60	Indeno(1,2,3-cd)pyrene	10316	16835	19853	34159	0.47	0.74	0.97	1.59
31	22.65	Benso(g,h,i)perylene	10423	16545	19747	33244	0.47	0.73	0.96	1.55
32	23.26	Dibenso(a,h)anthracene	13461	19740	22707	37505	0.61	0.87	1.10	1.75

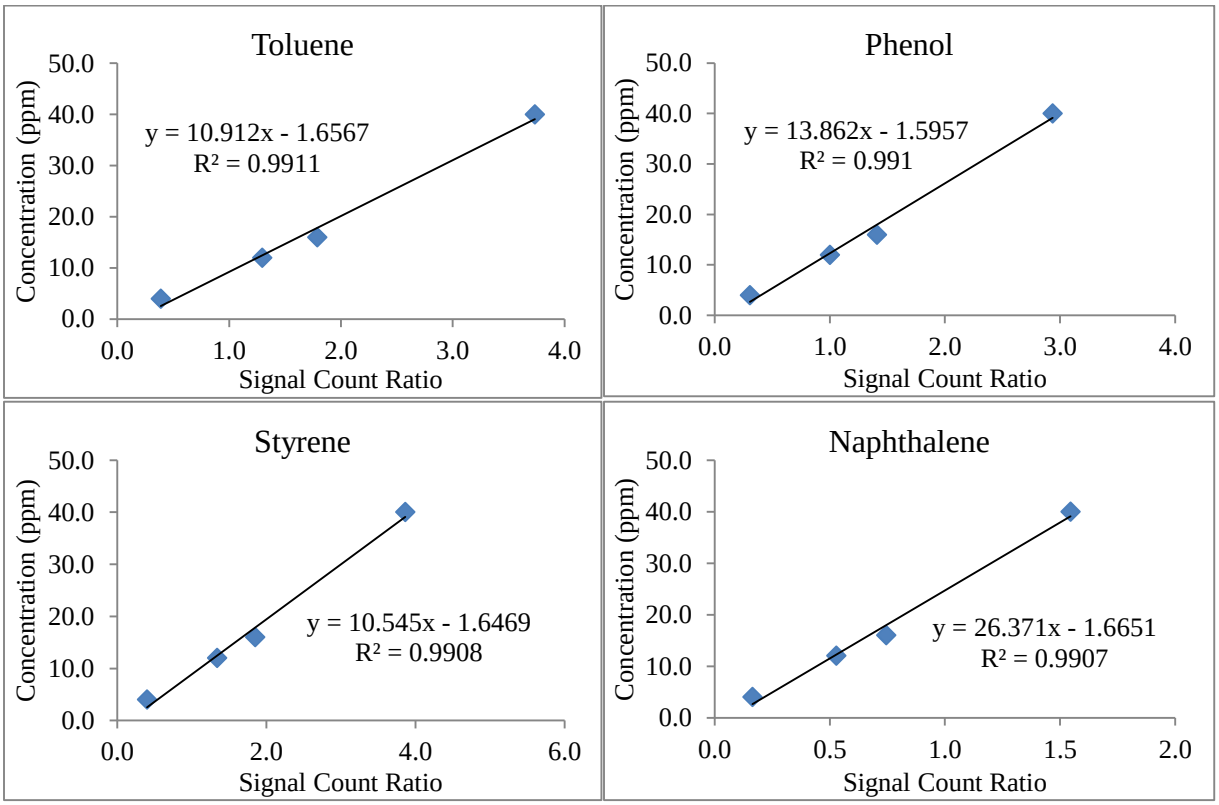

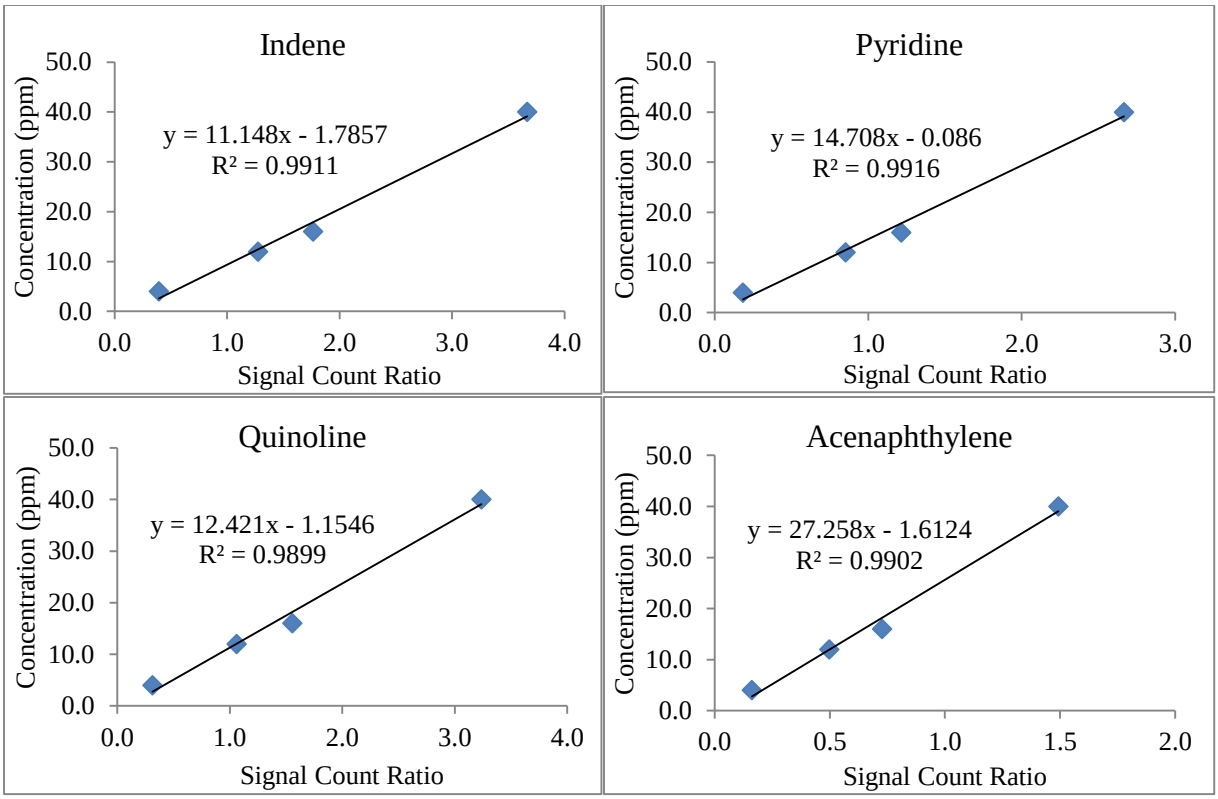

Figure 10–5: Examples of calibration curves created during tar calibration to relate tar concentrations with signal count ratio from GC analysis

10.5.4 Tar Extraction and Analysis Method

1. Weight the mass of two empty 2 mL vials with their lid. Record the values.
2. Clamp the SPE column on a retort stand.
3. Clamp the sampling rod used in sampling on a second retort stand. The sampling rod should be positioned right above the SPE column.
4. Place the first 2 mL vial under the SPE column, ready for sample extraction.
5. Now, draw 0.1 mL of the prepared 400 ppm Internal Standard using 200µl pipette and inject into the sampling rod hole. The Internal Standard will flow through the rod (hence flush it) and gathered inside the SPE column.
6. Then, inject another 0.9 mL of DCM using 1 mL pipette into the SPE column through the sampling rod.

7. Connect a syringe to the SPE column using a connector and force the solution in the SPE column through the packed bed into the 2 mL vial. *Note: Do this ONLY ONCE to minimize evaporation of DCM which could contribute to error*.
8. Close the vial using its lid.
9. Repeat steps 4 -8 using 0.9 mL 50:50 DCM-IPA solvent (instead of DCM) into the second vial.
10. Shake the two vials rigorously to mix.
11. Weight the mass of both vials containing liquid sample. Record its final mass. *Note: The mass of liquid sample is required to estimate the amount of tar extracted from the SPE column i.e. Extracted Mass of Tar = 1 mL Solution with Tar – 1 mL Solution without Tar.*
12. Place the vials in Gas Chromatography (GC) sample holder. Turn on the GC and follow the instruction for its operation.
13. Analyse the samples using GC and record the resulted signal area count.

10.6 Appendix F: Positive Displacement Flow Meter Cleaning and Assembly Guide

In some occasions, the positive displacement flow meter used in this work may be required to be fully disassembled for maintenance works. In this situation, it is important that the internal parts are handled and re-assembled appropriately to prevent damage to the meter, as well as to make sure the meter is able to work again. In order to achieve this, some important guidelines that should be followed were outlined in this section.

1. Gear with magnet must be located nearest to dimple mark on flow meter body
2. Carefully inspect gears for sides with smooth edges. This side must face down during assembly to ensure smooth gear rotations
3. Gears must be fitted 90^{o} to each other
4. Oil inlet must be from the side where there is a machine mark on meter body i.e. the right hole when dimple mark is at the top
5. Cover the meter body with clear Perspex and tighten screws around it. Feed water into the flow meter and check for smooth gear rotations

Note: Failing to follow these guidelines will cause gears to move roughly and jammed frequently during operation.

6. When fitting the electronic block of flow meter, make sure dimple marks are aligned. When this is fitted right, the metal label in meter body should be situated on the left side of meter. Ignore the fact that writings on electric board inside flow meter is upside down.
7. The hole on the metal label side is the liquid outlet hole.
8. Tighten the screws to hold both flow meter blocks together. Do not over-tighten the screws as this may reduce the life span of seal in between the two blocks.

10.7 Appendix G: Equilibrium Model

ENTRAINED FLOW GASIFICATION MASS BALANCE

PROCESS BLOCK DIAGRAM

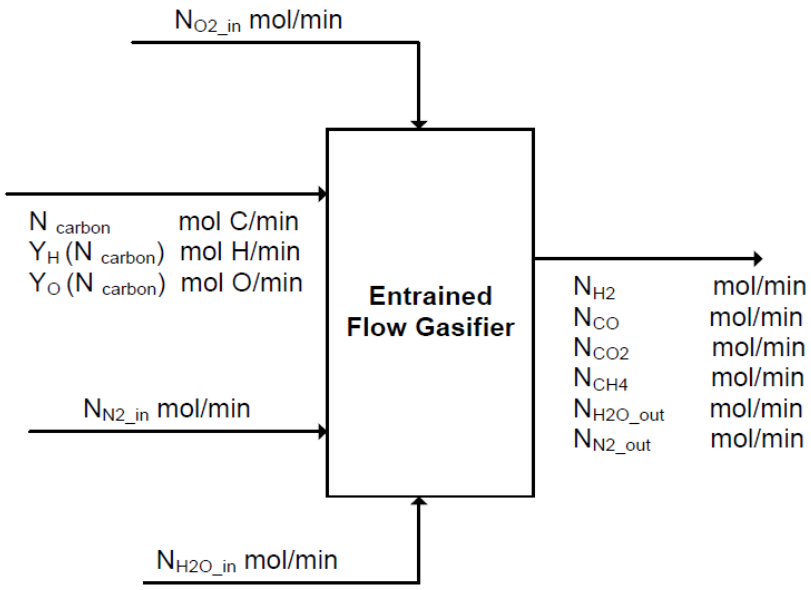

PYROLYSIS OIL ULTIMATE ANALYSIS AND EMPIRICAL FORMULA

Element	Atomic weight	Weight %	Mass flow (g/min)	Molar flow (mol/min)	Molar ratio (%)	Ratio to C (y_i)	Mol Weight (g/mol)
C	12.01	42.9%	49.8	4.14	26.0%	1.0	28.0
H	1.01	7.1%	8.2	8.17	51.3%	2.0	
N	14.01	0.1%	0.1	0.01	0.05%	0.002	
S	32.07	0.01%	0.0	0.00	0.002%	0.0001	
O	16.00	49.9%	57.9	3.62	22.7%	0.9	
TOTAL		100.0%	116.0	15.94	100.0%		

GASIFICATION OPERATING CONDITIONS

Gasification Temperature	1000	°C	=	1273 K
Gasification Pressure	1	atm/bar	=	100 kPa
Pyrolysis oil combustion SR (molar)	1.06	mol O_2/mol oil		
Pyrolysis oil combustion SR (mass)	1.21	g O_2/g oil		

FEED & INPUT CONDITIONS

Pyrolysis oil feed rate	100	ml/min		
	116.0	g/min	=	6.96 kg/hr
	4.15	mol/min		
Pyrolysis oil density	1160	g/L		

	A	B	C	D	E	F	G	H
53								
54	Oxygen-Oil Equivalent Ratio			0.45	g/g basis			
55								
56								
57	Oxygen gas feed rate			63.1	g/min	=	3.8	kg/hr
58				49	L/min	=	2913	L/hr
59				2.0	mol/min	=	0.12	kmol/hr
60								
61								
62	Oxygen to Fuel Ratio (AFR)			485	L/L basis			
63	Oxygen to Carbon Ratio (O:C)			0.48				
64								
65								
66	Steam to Carbon ratio (S:C) ratio			8.30				
67								
68	Water/Steam feed rate			34.4	mol/min			
69				619.5	g/min	(calculated from S:C ratio OR from L/min)		
70				0.620	L/min			
71								
72								
73	Nitrogen gas feed rate			2	L/min			
74				2.33	g/min	=	0.140	kg/hr
75				0.08	mol/min			
76								
77								
78	Helium gas feed rate			2.5	L/min			
79				0.45	g/min			
80				0.11	mol/min			
81								
82								
83	**ELEMENTAL BALANCE FOR EF GASIFICATION SYSTEM FROM EQUILIBRIUM MODEL**							
84								

85	Element	INPUT	OUTPUT	Mass Flow	Difference
86		*mol/min*	mol/min	(g/min)	
87	*C*	4.14	4.14	49.76	0.0%
88	*H*	76.95	76.95	77.56	0.0%
89	*N*	0.17	0.17	2.45	0.0%
90	*S*	0.00	0.00	0.01	0.0%
91	*O*	41.95	41.95	1345.12	0.0%
92	He	0.11	0.11	0.45	0.0%
93	**Total**	**123.3**	**123.3**	**1475.3**	**0.0**

CHEMICAL EQUILIBRIUM MODELING CALCULATIONS

Summary of Feed/Input to the EF gasification:

N_{carbon}	4.14	mol/min
N_{O2_in}	1.97	mol/min
$N_{N2\ in}$	0.08	mol/min
$N_{H2O\ in}$	34.39	mol/min
N_{He}	0.11	mol/min

Molecules molecular weights:

H_2O	18.0 g/mol
CH_4	16.0 g/mol
H_2	2.0 g/mol
CO_2	44.0 g/mol
CO	28.0 g/mol
N_2	28.0 g/mol
He	4.0 g/mol

STEP 1: Enter initial guess for Solver

%mol CH_4	0.0%	(y_{CH4})
%mol H_2O	80.2%	(y_{H2O})
Solver target cell	0.0000	

STEP 2: Calculate molar flows of producer gas products **mol% = vol%**

#	Species	Species flow rate mol/min	Species flow rate g/min	Species molar concentration y_i (%mol) Total	N_2 free	N_2 & H_2O free	He, N_2 & H_2O free	Concentration (wt%) Total	H_2O free	N_2 & H_2O free	Gas yield g_{gas}/g_{oil}
1	N_{H2O}	34.35	618.8	80.2%	80.4%			77.2%			5.33
2	N_{CH4}	0.00	0.0	0.0%	0.0%	0.0%	0.0%	0.0%	0.00%	0.0%	0.00
3	N_{H2}	4.12	8.3	9.6%	9.7%	48.7%	49.9%	1.0%	4.55%	4.6%	0.07
4	N_{CO2}	3.46	152.1	8.1%	8.1%	40.8%	41.8%	19.0%	83.33%	84.5%	1.31
5	N_{CO}	0.69	19.2	1.6%	1.6%	8.1%	8.3%	2.4%	10.52%	10.7%	0.17
6	$N_{C\_residues}$	0.00	0.00	0.0%	0.0%	0.0%	0.0%	0.0%	0.00%	0.0%	0.00
7	N_{S_out}	0.00	0.01	0.0%	0.0%	0.0%	0.0%	0.0%	0.01%	0.0%	0.00
8	N_{N2_out}	0.09	2.45	0.2%				0.3%	1.34%		0.02
9	N_{He_out}	0.11	0.45	0.3%	0.3%	1.3%		0.1%	0.25%	0.2%	0.00
TOTAL	N_{gas}	42.82	801.4	100.0%	100.0%	99.0%	100.0%	100%	100.0%	100%	6.91

Further Product Analysis:

Mass flow of dry producer gas:	182.6	g/min
Molar flow of dry producer gas:	8.47	mol/min
Volumetric flow of dry producer gas:	203	N L/min
Content of water in producer gas:	3.04	kg water/m^3 gas
Pyrolysis oil conversion %:	100%	
Condensate yield:	618.8	g/min
Dry producer gas yield:	182.6	g/min (dry basis)
Char yield:	0.0	g/min
Total	801.4	g/min

STEP 3: Consider Steam Reforming and Water-Gas Shift reactions to complete Degree of Freedom (DOF)

Homogenoues Gas-Gas Reactions

Reaction 1	Steam Reforming	CH4 + H2O <--> CO +3H2
Reaction 2	Water-Gas Shift	CO + H2O <--> CO2 + H2

Stoichoimetry Chart Table

REACTION #	C	CO	CO2	CH4	H2	H2O
Reaction 1	0	1	0	-1	3	-1
Reaction 2	0	-1	1	0	1	-1

STEP 4: Calculate standard Gibbs Energy of each element at operating temperature

Elements	Standard Gibbs energy, G° kJ/kmol	
	TRC, 1994	HYSYS Correlation
C	0	0
CO	-223900	-223368
CO2	-396100	-395753
CH4	49300	48430
H2	0	0
H2O	-177200	-177701

CHECK VALUE!

HYSYS Gibbs Energy Parameters:
$\Delta G° = aT^2 + bT + C$

HYSYS	CO	CO2	CH4	H2O
a	9.74E-04	1.02E-03	8.60E-03	4.96E-03
b	-89.51	-3.461	87.74	43.41
c	-1.1E+05	-3.9E+05	-7.72E+04	-2.4E+05

STEP 5: Calculate Equilibrium Constants (K) from elements Standard Gibbs Energy of Reactions:

			ΔG°	ln K	K	1/K
Reaction 1	Steam Reforming	CH4 + H2O <--> CO +3H2	-94096	8.89065	7263.73	0.00014
Reaction 2	Water-Gas Shift	CO + H2O <--> CO2 + H2	5316.17	-0.5023	0.60514	1.65251

STEP 6: Calculate %mol CH_4 (y_{CH4}) and %mol H_2O (y_{H2O}) from calculated Chemical Equilibrium constants, K:

Calculated values:			Errors from guessed values:	Error^2:
%mol CH_4	0.00%	(y_{CH4})	0.00%	6.04E-18
%mol H_2O	80.22%	(y_{H2O})	0.00%	9.75E-19

Solver target cell: 0.0000

Solver Add-In Prompt:

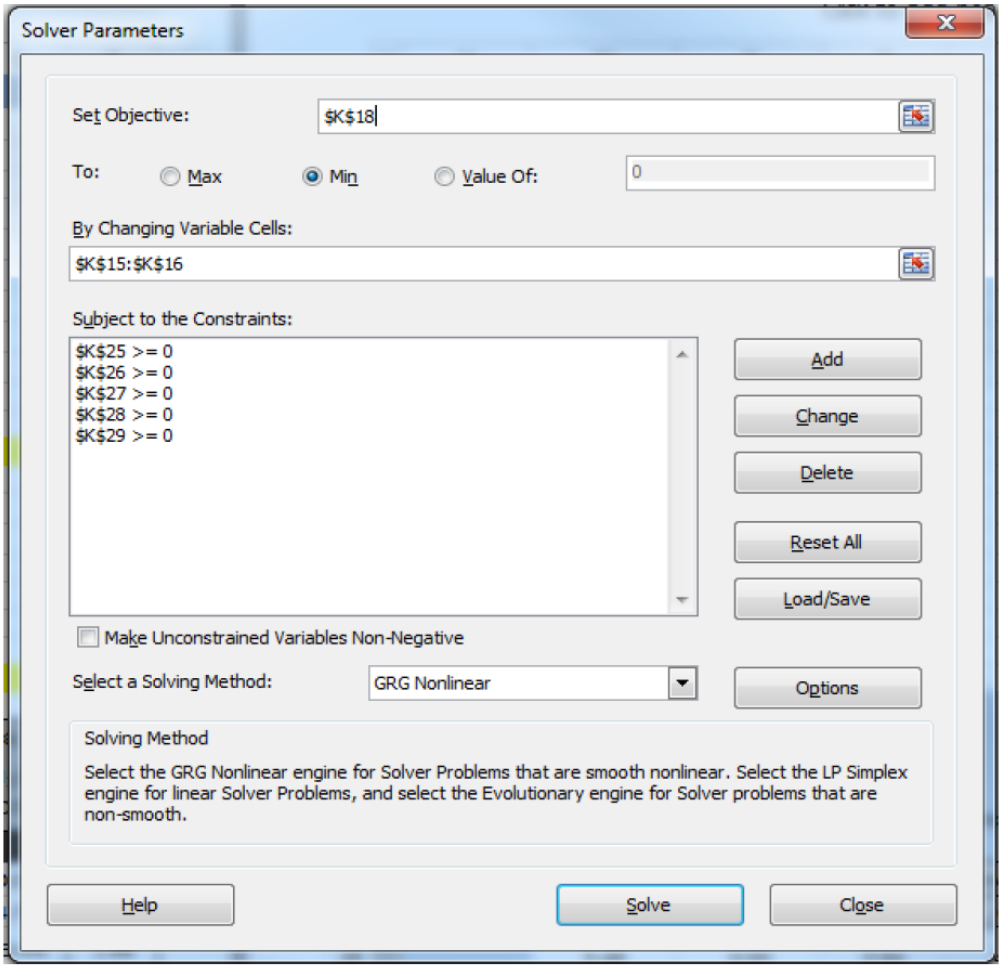

Solver Result Prompt:

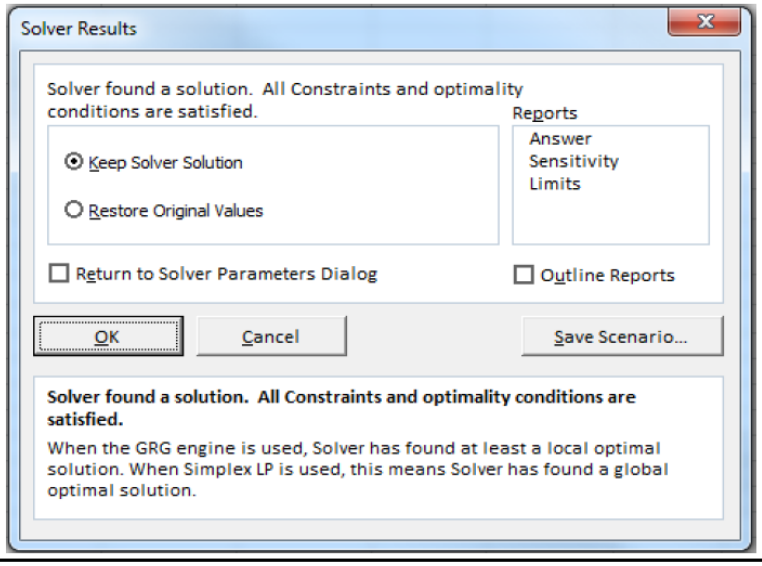

10.8 Appendix H: Distributions of Pyrolysis Oil Properties Used in this Work

Run #	Pyrolysis Oil ID	Viscosity (cSt)	Moisture Content (wt %)	pH	Density (kg/m^3)	Elemental Composition (wt %)		
						C	H	O
-	PyOil #1	16	39	N/A	N/A	27.2	± 7.7	64.9
-	PyOil #2	8	29 – 39	N/A	1165	N/A	N/A	N/A
1	PyOil #3	N/A	23	N/A	1165	38-40	± 7.7	52-54
2								
3	PyOil #4	30-690	15	2.9	1180	40.0	± 7.7	50.3
4						40.0	± 7.7	50.3
5						42.0	± 7.7	50.3
6	PyOil #5	330	19	3.3	1170	46.7	± 7.7	45.6
7		17	39	3.2	1220	46.7	± 7.7	45.5
8		15	37	3.2	1160	36.7	± 7.7	55.6

*** N/A = Not Available. This term is used to specify pyrolysis oil properties not measured prior to gasification experiments due to various technical reasons*

NOTE: Some of the pyrolysis oil batches received in this work were analysed but not used for gasification experiments